Microbiology Monographs

Series Editor: Alexander Steinbüchel

Michael Hippler *Editor*

Chlamydomonas: Biotechnology and Biomedicine

Springer

Microbiology Monographs

Volume 31

Series editor
Alexander Steinbüchel
Münster, Germany

More information about this series at http://www.springer.com/series/7171

Michael Hippler
Editor

Chlamydomonas: Biotechnology and Biomedicine

Springer

Editor
Michael Hippler
Institute of Plant Biology and Biotechnology
University of Münster
Münster, Germany

ISSN 1862-5576 ISSN 1862-5584 (electronic)
Microbiology Monographs
ISBN 978-3-319-66359-3 ISBN 978-3-319-66360-9 (eBook)
DOI 10.1007/978-3-319-66360-9

Library of Congress Control Number: 2017955540

Printed on acid-free paper

This Springer imprint is published by Springer Nature
The registered company is Springer International Publishing AG
The registered company address is: Gewerbestrasse 11, 6330 Cham, Switzerland

Contents

Chlamydomonas Photoreceptors: Cellular Functions and Impact on Physiology

Dimitris Petroutsos

Abstract *Chlamydomonas reinhardtii* accurately senses the information provided by light and regulates important cellular functions, including gene expression, sexual life cycle, phototaxis, photosynthesis, and photoprotection, using a network of specialized photoreceptors. It is equipped with a single-copy phototropin, four cryptochromes (one animal-type, one plant, and two DASH cryptochromes), and eight rhodopsin-like proteins (two animal-type rhodopsins, two microbial-type channelrhodopsins that act as light-gated cation-selective ion channels, and four histidine-kinase rhodopsins), as well as the UV-B photoreceptor UVR8. This review summarizes knowledge and recent findings on Chlamydomonas photoreceptors with a focus on their known cellular and physiological functions.

1 Introduction

Given the tremendous amount of solar energy reaching the Earth, estimated at 120,000 TW annually (Liao et al. 2016), there is no surprise that when thinking of light, energy comes naturally in mind. It is through photosynthesis that light energy is converted to chemical energy, in the form of ATP and NADPH, fueling this way the transformation of inorganic CO_2 into organic carbon metabolites. At the same time, light, composed of different wavelengths from ultraviolet to infrared, is an important environmental stimulus that directs the development, morphogenesis, and physiology of photosynthetic organisms. This is achieved by specialized proteins, the photoreceptors that detect and respond to changes in light intensity, quality, direction, and duration.

These light-responsive proteins typically contain a prosthetic cofactor or chromophore that enables them to perceive and respond to specific wavelengths of light

D. Petroutsos (✉)
Laboratoire de Physiologie Cellulaire et Végétale, UMR 5168, Centre National de la Recherche Scientifique (CNRS), Commissariat à l'Energie Atomique et aux Energies Alternatives (CEA), Université Grenoble Alpes, Institut National Recherche Agronomique (INRA), Institut de Biosciences et Biotechnologies de Grenoble, (BIG), CEA Grenoble, 17 rue des Martyrs, 38054 Grenoble cedex 9, France
e-mail: dimitris.petroutsos@cea.fr

M. Hippler (ed.), *Chlamydomonas: Biotechnology and Biomedicine*, Microbiology Monographs 31, DOI 10.1007/978-3-319-66360-9_1

(Christie et al. 2015) ranging from UV-B to far-red illumination. Light perception is particularly important as the spectra and intensity of solar radiation change depending on factors like the geographical location, the time of the day or season, the weather conditions, and the presence of phototrophs (Fortunato et al. 2015). Photoperception spans several orders of magnitude of light intensity (Briggs 2014) ranging from far below the threshold for photosynthetic biomass production to values beyond the capacity of photosynthetic CO_2 assimilation. Besides its beneficial effects, light can also be toxic. The UV components of sunlight can damage DNA, mainly by inducing the formation of pyrimidine dimers (Fortunato et al. 2015), whereas excess light causes oxidative damage and cell death. These destructive for the cell processes can be prevented by enhanced thermal dissipation via a high-energy quenching photoprotective response (Li et al. 2009) with the blue light playing a prominent role in the activation of this response (Petroutsos et al. 2016). In this chapter current knowledge on Chlamydomonas photoreceptors will be presented with an emphasis on how they regulate important cellular functions and their impact on the physiology of this green alga.

2 Cryptochromes

For 110 years following the observation of Darwin that heliotropic plants show tropism specifically toward the blue light (phototropism), the nature of the responsible photoreceptor(s) remained cryptic, and this was captured with the name cryptochrome (Van Gelder 2002). It was not until 1993 that the first blue-light photoreceptor, the cryptochrome CRY1, was discovered in *Arabidopsis thaliana* (Ahmad and Cashmore 1993).

Cryptochromes (CRY) are receptors for blue and ultraviolet (UV-A) light with significant amino acid sequence similarity to DNA photolyases in their N termini that have lost or reduced DNA repair activity and have gained novel roles in signaling. In addition, cryptochromes contain a C-terminal extension that appears to be unique for each cryptochrome in size and amino acid sequence (Lin and Shalitin 2003; Chaves et al. 2011). The photolyases together with the cryptochromes make up the photolyase/cryptochrome superfamily. According to their sequence similarities, cryptochromes met in various organisms can be roughly clustered into three subfamilies: plant cryptochromes, animal cryptochromes, and cryptochrome-DASH proteins (DASH: Drosophila, Arabidopsis, Synechocystis, Homo) (Lin and Todo 2005; Chaves et al. 2011).

Cryptochromes are flavoprotein receptors. In the dark, Arabidopsis cryptochromes are in the inactive state (C-terminal domain folded against the protein, flavin in the oxidized redox state, FADox). Upon illumination with blue light (wavelengths below 500 nm), flavin undergoes photoreduction to the $FADH^o$ redox form leading to the activation of the receptor. Subsequent illumination of $FADH^o$ with an additional photon of either blue or green light (wavelengths below 600 nm) can induce further reduction to the (FADH) inactive redox form.

Reoxidation of $FADH^{o}$ to FADox occurs spontaneously in the presence of molecular oxygen (please refer to (Chaves et al. 2011; Ahmad 2016) for comprehensive review on the CRY photocycle).

In plants cryptochromes control many aspects of growth and development including seedling de-etiolation, elongation growth, the initiation of flowering, and entrainment of the circadian clock (Ahmad 2016). In animals, cryptochromes can act as light-responsive circadian photoreceptors (in Drosophila and other insects; type I cryptochromes) or as transcription-repressors without photoreceptor function (in mouse, human, and other vertebrates; type II cryptochromes) although some animal species (zebrafish and monarch butterfly) possess both types of cryptochromes (Chaves et al. 2011). Both type I and II animal cryptochromes can additionally act as magnetoreceptors (Gegear et al. 2010).

The genome of Chlamydomonas encodes for a plant cryptochrome (known as CPH1; Cre06.g295200.t1.2; Reisdorph and Small 2004), an animal-type CRY (aCRY; Cre06.g278251.t1.1; Beel et al. 2012), and two DASH-CRYs (CRY-DASH1; Cre02.g078939.t1.1 and CRY-DASH2; Cre01.g030650.t1.2; Beel et al. 2012, 2014). The domain organization of these proteins can be seen in Fig. 1.

Chlamydomonas CPH1 protein accumulates in the dark and rapidly degrades after exposure to blue or red light because of proteasome-dependent protein degradation in a photosynthesis-independent manner (Reisdorph and Small 2004). Till now the function of CPH1 remains unknown. Similarly, the roles of the two Chlamydomonas CRY-DASH remain to date unexplored. More insights are expected from the characterization of recently generated insertional mutants of CPH1, CRY-DASH1, and CRY-DASH2, available at Chlamydomonas Library Project (CLiP) collection of mutants (Li et al. 2016). Much more is known for the animal-type CRY in Chlamydomonas thanks to the joint efforts of the research groups of Maria Mittag and Tilman Kottke (Beel et al. 2012). Specifically, for the in vivo function of aCRY in Chlamydomonas, an insertional *acry* mutant was isolated in which the APHVIII cassette was inserted into intron 7 of *aCRY* gene. The *acry* mutant accumulated 20% of the WT aCRY protein levels. Dark-adapted acry cells exposed for 2 h to low-fluence blue light (10 μmol photons m^{-2} s^{-1}) showed altered expression of genes encoding proteins involved in chlorophyll and carotenoid biosynthesis (magnesium chelatase subunit D; CHLD, phytoene desaturase; PDS, glutamate-1-semialdehyde aminotransferase; GSA), light-harvesting complexes (chlorophyll a/b binding protein of LHCII type; LHCBM6), nitrogen metabolism (cytosolic Gln synthetase; GLN1), and the circadian clock (C3 subunit of the RNA-binding protein CHLAMY1; CRB3) as compared to WT cells, suggesting that these genes are directly or indirectly regulated by aCRY. Unexpectedly the acry mutant showed altered expression of these genes also after exposure to red light, while other genes like the light-dependent protochlorophyllide reductase (POR, involved in chlorophyll biosynthesis) and the cyclin-dependent kinase B1 (CDKB1, involved in cell cycle control) were altered only after red and not after blue-light exposure (Beel et al. 2012).

How can a blue-light photoreceptor respond to red or yellow light? These in vivo effects can be explained by the fact that Chlamydomonas aCRY can exist in three

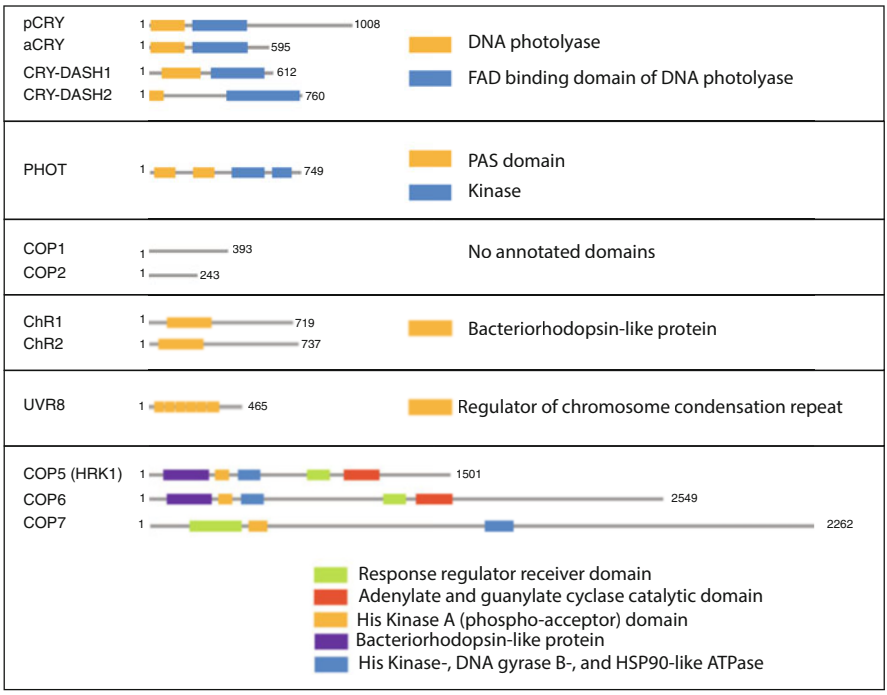

Fig. 1 Schematic representation of the conserved domains of different Chlamydomonas photoreceptors, as indicated by Phytozome 11.0

redox states: in the dark, aCRY is at the oxidized inactive form which is converted to the inactive neutral radical upon blue illumination. The inactive neutral radical can be further converted to the active form of the photoreceptor (anionic fully reduced flavin) after illumination by blue, yellow, or red (but not far-red) light (Beel et al. 2012) playing at that state the role of a blue-, yellow-, and red-light-absorbing photoreceptor. In line with these suggestions, a recent infrared difference spectroscopy study showed that the blue-light reaction of the oxidized flavin to the neutral radical is not accompanied by any detectable changes in secondary structure, observation which is in agreement with a nonphysiological pre-activation role in vivo. In contrast, the conversion by red light of the neutral radical to the anionic fully reduced state proceeds with conformational changes in turn elements, which most probably constitute a part of the signaling process (Spexard et al. 2014). At variance with higher plants CRYs, the decay of the reduced aCRY to the inactive oxidized aCRY is independent of oxygen concentration (Spexard et al. 2014).

The degradation of the blue-light photoreceptor CPH1 by red light has led to the suggestion that a red-light photoreceptor may exist in Chlamydomonas (Reisdorph and Small 2004). It remains to be tested if the broad spectral response aCRY could fulfill this role (i.e., by checking if red light can trigger CPH1 degradation in the

acry mutant) or if another red-light photoreceptor exists as suggested by Beel et al. (2014). Indeed, blue-light and red-light treatment of dark-adapted cells cause reduced transcript levels of the clock-relevant component ROC15 in wild type. In the acry mutant, blue-light treatment also reduces ROC15 levels; however, under red light, ROC15 transcript levels are strongly increased, indicating the existence of a red-light photoreceptor that acts in the absence of aCRY (Beel et al. 2012).

3 Phytochromes

Phytochromes are a widespread family of red/far-red responsive photoreceptors first discovered in plants. All plant phytochromes so far known utilize covalently attached bilin chromophores that enable photoconversion between red-absorbing (Pr) and far-red-absorbing (Pfr) forms. Plant phytochromes are therefore photoswitchable red/far-red photoreceptors that allow competition with neighboring plants for photosynthetically active red light (Rockwell et al. 2006). In aquatic environments, red and far-red light are rapidly attenuated with depth, and blue light is dominant (Depauw et al. 2012). Nevertheless, phytochrome-related proteins are found in recently sequenced genomes of many eukaryotic algae from aquatic environments which surprisingly are not limited to red and far-red responses, but they rather cover the entire visible spectrum (Rockwell et al. 2014).

Despite the absence of phytochromes (Merchant et al. 2007), Chlamydomonas genome retains cyanobacterial-derived genes for the two key enzymes required for bilin biosynthesis: a heme oxygenase (HMOX1) that converts heme to biliverdin (BV) and a ferredoxin-dependent bilin reductase (PCYA) that converts BV to phycocyanobilin (PCB). Both HMOX1 and BV are active in Chlamydomonas and synthesize PCB in vivo. The hmox1 mutant that cannot produce bilins cannot grow phototrophically unless supplemented with exogenous BV (Duanmu et al. 2013). Interestingly, genome-wide transcriptome analyses revealed that the expression of several genes typically induced by high light (e.g., encoding LHCSR1, PSBS1, ELI3, HSP22, GPX, HSP70) was suppressed by BV. At the same time, BV specifically upregulated a subset of nuclear genes in darkness. Overall these data suggest that plastid-derived bilins function in the light as negative signals to suppress photosynthesis-associated nuclear gene expression in Chlamydomonas, a network largely promoted by phytochromes in plants (Duanmu et al. 2013).

4 Phototropin

Phototropins (PHOT) are blue-light-activated kinases that belong to the AGC-type kinase superfamily, a group of serine/threonine protein kinases that based on sequence alignments of their catalytic kinase domain show high similarity to cAMP-dependent protein kinase A (PKA), cGMP-dependent protein kinase G

(PKG), and phospholipid-dependent protein kinase C (PKC) (Pearce et al. 2010). PHOTs possess two flavin mononucleotide (FMN) chromophores (LOV1 and LOV2) at the N-terminus and a C-terminal Ser/Thr kinase domain (Christie 2007) (Fig. 1). The LOV (light, oxygen, voltage) domain is largely spread among archaea, bacteria, fungi, and plants (Losi and Gärtner 2011) and is a subgroup of the PAS superfamily of domains, which are thought to be sensory motifs that are involved in detecting diverse stimuli ranging from light or oxygen to redox state and small ligands (Taylor and Zhulin 1999).

Although the action spectrum for phototropism was the guiding force in the hunt for a blue-light receptor in higher plants, the identification of the first cryptochrome (Ahmad and Cashmore 1993) preceded the identification of the first phototropin (Christie et al. 1998). Higher plants have two phototropins, PHOT1 and PHOT2, that exhibit distinct but overlapping roles (reviewed in Christie 2007) in regulating phototropism, opening, and closure of stomatal pores and movement of chloroplasts in response to different light intensities. A screen of an expressed sequence tag (EST) Chlamydomonas database for clones with sequence homology to PHOTs of higher plants led to the identification of a single-copy gene of PHOT encoding for a protein distinctly smaller (ca. 80 KDa) than the homologous proteins of higher plants with molecular masses of around 120 KDa (Huang et al. 2002).

Blue light induces covalent adduct formation between the FMN and a cysteine residue of each LOV domain and subsequent conformational changes in the LOV domains and the conserved amphipathic a-helix that is located downstream of LOV2. These structural changes result in the activation of the kinase, which is inhibited in the dark by association with LOV2 (Christie et al. 1999; Crosson et al. 2003; Kottke et al. 2003; Fedorov et al. 2003; Harper et al. 2003; Tokutomi et al. 2008). The onset of the PHOT-dependent signal transduction requires additionally autophosphorylation of PHOT which is induced upon activation of the LOV domains (Christie et al. 2002; Salomon et al. 2003; Kinoshita 2003; Matsuoka and Tokutomi 2005; Sullivan et al. 2008). Chlamydomonas PHOT shows different levels of in vitro autophosphorylation as compared with PHOTs of higher plants (Onodera et al. 2005), while the N-terminus and the hinge region between LOV1 and LOV2 of Chlamydomonas PHOT are shorter than those of Arabidopsis PHOT1 and PHOT2 (Onodera et al. 2005; Christie 2007). Detailed information on PHOT photochemistry can be found in the comprehensive reviews of Losi and Gärtner (2011, 2012).

Using immunofluorescent localization techniques, Chlamydomonas PHOT was found to localize in the plasma membrane and in the flagella (Huang et al. 2004). A proteomic analysis of isolated flagella of Chlamydomonas identified PHOT as one of the three hundred sixty (360) flagella-localized proteins, ninety (90) of which were putative signal transduction proteins, underscoring the importance of signaling in the function of this organelles (Pazour et al. 2005). PHOT was also found to be present in the eyespot of Chlamydomonas as indicated by a proteomic analysis (Schmidt et al. 2006).

The first investigation of the role of PHOT in the physiology of Chlamydomonas became possible with the generation of knockdown lines of PHOT using the RNA interference method. Several independent phot knockdown lines were partially

impaired in the following three steps of the life cycle: in gametogenesis, in the maintenance of mating ability, and in the germination of zygotes (Huang and Beck 2003) and also in the chemotactic behavior of gametes from this alga (Ermilova et al. 2004). Using the phot knockdown (RNAi) line described previously (Huang and Beck 2003; Ermilova et al. 2004), the possible role of PHOT in expression of light-regulated genes in Chlamydomonas was tested in microarray experiments (Im et al. 2006). Expression of genes involved in chlorophyll and carotenoid biosynthesis, namely, the glutamate-1-semialdehyde aminotransferase (GSA), phytoene desaturase (PDS), and a light-harvesting polypeptide (LHCBM6), was induced in a transition from darkness to very low intensity of blue light (1 μmol photons m^{-2} s^{-1} or lower) in a WT strain, and this induction was largely suppressed in the *phot-kd* lines. This difference in expression between WT and phot-kd was no longer observed however at higher light intensities (25 μmol photons m^{-2} s^{-1}). Interestingly, expression of GSA and LHCBM6 was also induced by low-fluence red light, and again this induction was suppressed in the *phot-kd* suggesting the possibility of interactions between blue- and red-light-signaling pathways (Im et al. 2006). This red-light-dependent signal was photosynthesis-independent (Im et al. 2006) raising the question whether a red-light photoreceptor is involved in the regulation of GSA and LHCBM6 in synergy with PHOT. The role of such a red-light photoreceptor could be fulfilled by the broad spectral response of aCRY. Indeed, the acry mutant shows compromised induction of GSA and LHCBM6 in both blue and red illumination (Beel et al. 2012) allowing for a speculation that a PHOT-aCRY signaling synergism may exist.

Besides the role of PHOT on gene expression under very low-intensity blue light, PHOT is also actively involved in the light regulation of the eyespot size. Using a homologous recombination strategy, a Chlamydomonas PHOT knockout mutant (*phot*) was generated (Zorin et al. 2009). The *phot* mutant together with phot-complemented lines with different fragments of the PHOT gene (full-length, LOV1 + LOV2, kinase) was used in a comprehensive study that established a link between PHOT and the regulation of the eyespot size (Trippens et al. 2012). More specifically, it was found that the size of the eyespot of Chlamydomonas is light regulated, and this regulation is under control of PHOT. At the same time, in a transition from darkness to light channelrhodopsin-1 (the dominant primary receptor for phototaxis within the eyespot; CHR1), protein levels diminish in a PHOT-dependent manner. Complementation of *phot* with the kinase fragment of PHOT resulted in reduced eyespot size, independent of light and in reduced levels of CHR1. PHOT was therefore suggested to be a regulator of phototaxis that desensitizes the eyespot when blue-light intensities increase (Trippens et al. 2012). The proposed role of PHOT in phototaxis is supported by the fact that PHOT is present both in the flagella and in the eyespot, but the generation of a motile phot mutant is still needed to directly address this hypothesis, since the phot mutant (Zorin et al. 2009) has been generated in a flagella-less genetic background (*cw15-302*). Based on experimental data, it has been suggested that aside from activation of the kinase domain, the photosensory domains LOV1 + LOV2 alone have an independent signaling function

in the cell because overexpression of LOV1 + LOV2 affected eyespot size and phototaxis (Trippens et al. 2012).

All abovementioned PHOT-dependent phenotypes were observed at very low (1 μmol photons m^{-2} s^{-1} or lower; Huang and Beck 2003; Ermilova et al. 2004; Im et al. 2006) or relatively low light intensities (60 μmol photons m^{-2} s^{-1} or lower; Trippens et al. 2012). However, algae are frequently exposed to much higher light intensities that may exceed their photosynthetic capacity. This excess light can be toxic causing oxidative damage or even cell death. This is prevented by a sophisticated photoprotective mechanism that has evolved in photosynthetic organisms, called NPQ (non-photochemical quenching). NPQ mostly consists of qE (quenching of energy), the pH-dependent thermal dissipation of excess energy (Li et al. 2009). In Chlamydomonas, qE requires LHCSR3 (Peers et al. 2009) (light-harvesting complex stress related), a nuclear-encoded, high-light (HL) inducible, chloroplast-localized protein, encoded by the genes LHCSR3.1 and LHCSR3.2. Besides HL, induction of the LHCSR3 requires Ca^{2+} signaling and active photosynthesis (Petroutsos et al. 2011). The view in the field has long been that qE induction is a retrograde response stemming from photosynthetic stress perception in the chloroplast. Recent findings challenge this dogma, showing direct anterograde regulatory links of the blue-light photoreceptor phototropin (PHOT) with photoprotection in Chlamydomonas (Petroutsos et al. 2016). The action spectrum of LHCSR3 accumulation and qE showed that blue light was especially effective in inducing LHCSR3 and qE. This was because PHOT controls qE by inducing the expression of the qE effector protein LHCSR3 in high light. This control requires blue-light perception by LOV domains, LHCSR3 induction through PHOT kinase, and active photosynthesis, while cAMP/cGMP are also involved in the PHOT-dependent LHCSR3 regulation signaling cascade. The *phot* mutant and the *phot* complemented by the LOV1 + LOV2 domains display severely reduced fitness under excessive light conditions, due to the low LHCSR3 and qE induction. The *phot* mutant complemented by the kinase fragment of PHOT has restored qE, LHCSR3, and photosensitivity phenotypes and induced LHCSR3 in a color-independent and photosynthesis-dependent manner (Petroutsos et al. 2016).

Although several PHOT-interacting proteins have been identified in higher plants (summarized in Christie et al. 2015), no direct interacting partner of PHOT has been currently identified in Chlamydomonas, and the PHOT-dependent signaling pathways resulting in the so far described phenotypes remain elusive. Equally complex and certainly more elusive is how the single-copy PHOT in Chlamydomonas can respond differently to the low- and high-light-intensity responses described above. A plausible explanation could be that Chlamydomonas PHOT can trigger high-light intensity signaling when acting in synergy with a photosynthetic signal (Petroutsos et al. 2016). Nevertheless further investigation is needed for the elucidation of the PHOT-dependent signaling cascades under low and high-light intensities. Higher plants contain PHOT1, responding to low-intensity blue-light signals, and PHOT2, triggering high-intensity blue-light responses. Chlamydomonas PHOT gene, orthologue of Arabidopsis PHOT2 (Galván-Ampudia and Offringa 2007), could restore phototropin-mediated responses in the *phot1phot2* double mutant of Arabidopsis,

behaving more like PHOT2 than PHOT1, but its biological activity was different from that of authentic PHOT2 (Onodera et al. 2005).

5 UVR8

Even though the ozone layer absorbs most UV-B (wavelengths from 280 to 315 nm) from sunlight, there is still 0.5% that reaches the surface of earth. UV-B has the highest energy of any part of the light spectrum and has the potential to damage DNA and the photosynthetic apparatus, to generate reactive oxygen species (ROS) and to impair cellular processes. Not surprisingly UV-B is a key environmental signal that regulates diverse processes in a range of organisms. In plants, UV-B modifies plant biochemical composition, influences plant morphology, and stimulates the expression of genes involved in UV protection and damage repair (Jenkins 2009; Mach 2016).

UV-B activates the photoreceptor UV RESISTANCE LOCUS8 (UVR8) that dissociates into monomers which interact with CONSTITUTIVELY PHOTOMORPHOGENIC1 (COP1), an E3 ubiquitin ligase (Rizzini et al. 2011). UVR8-COP1 interaction induces UV-B signaling governed by the bZIP transcription factor ELONGATED HYPOCOTYL5 (HY5) and its homologue which leads to UV-B acclimation. The COP1-UVR8 interaction also induces the expression of negative regulators that interact directly with UVR8 to help it transition back into a homodimer and to downregulate UV-B signaling, as reviewed in Heijde and Ulm (2012) and (Jenkins 2014). At variance to many photoreceptors that make use of bound cofactors as chromophores (e.g., FMN for PHOT, FAD for CRY), in the case of UVR8, an intrinsic tryptophan functions as a chromophore for UV-B perception (Rizzini et al. 2011; Christie et al. 2012).

A Chlamydomonas UVR8 (Cre05.g230600) has been recently identified together with an ortholog of Arabidopsis COP1 (Cre02. g085050) (Tilbrook et al. 2016). The domain organization of UVR8 protein is shown in Fig. 1. Like in the case of Arabidopsis, Chlamydomonas UVR8 is a homodimer in the absence of UV-B and monomerizes in response to UV-B irradiation, while in a yeast two-hybrid assay, Chlamydomonas UVR8 interacted with both Chlamydomonas and Arabidopsis COP1 in a UV-B-dependent manner. Notably, complementation of an Arabidopsis *uvr8* null mutant with the Chlamydomonas *UVR8* restored UV-B perception and signaling (Tilbrook et al. 2016). Treating Chlamydomonas cultures with low-level narrowband UV-B slowed down their growth rate during exponential phase only slightly, without any impact on their steady-state cell density, but did offer a significant acclimation to UV-B stress. UV-B acclimated cells previously grown under low-level narrowband UV-B displayed significantly higher survival rate and less UV-B-induced photoinhibition following broadband UV-B stress than non-acclimated cultures, assessed by colony survival assays and by photosynthetic efficiency measurements and D1 and D2 immunoblotting (Tilbrook et al. 2016). Genome-wide transcriptomic analyses (RNAseq) of Chlamydomonas cells after 1-hour exposure to low-level narrowband UV-B were accompanied by broad changes

in gene expression. Among the upregulated genes, there are two genes identified by the authors (Tilbrook et al. 2016) as putative orthologs of the Arabidopsis genes HY5 (a bZIP transcription factor activated by the UVR8-COP1 interaction; Cre06.g310500) and RUP1/RUP2 (negative regulators that interact directly with UVR8 to help it transition back into a homodimer and to downregulate UV-B signaling; Cre01.g053850). Interestingly, genes associated with photosynthesis and photoprotection (*PSBS1*, *PSBS2*, *LHCSR1*, *LHCSR3.1*, *LHCSR3.2*, and *ELIP1,4,5*) were also found to be significantly upregulated (Tilbrook et al. 2016). The Elip (early light-inducible protein) family in photosynthetic organisms consists of more than hundred (100) different stress proteins that accumulate in photosynthetic membranes in response to light stress (Heddad and Adamska 2002). Chlamydomonas genome encodes for ten *ELIP* genes (Elrad and Grossman 2004; Zones et al. 2015). In Arabidopsis the induction of *ELIP1* and *ELIP2* was found to be UVR8-dependent (Favory et al. 2009), and similarly three *ELIP* genes (*ELIP1*, *ELIP5*, and *ELIP6*) were induced by irradiation of Chlamydomonas cells by UV-B (Tilbrook et al. 2016). At a different study, high temporal resolution genome-wide transcriptomic analyses of diurnal gene expression of synchronized cultures of Chlamydomonas identified a gene cluster containing 280 genes whose expression is sharply induced during the very onset of the light period (Zones et al. 2015). This "light-stress" cluster contains five out of the ten *ELIP* Chlamydomonas genes, and interestingly none of the UV-B-responsive *ELIP* genes identified in Tilbrook et al. (2016), suggesting that high light and UV-B stress target different subset of genes. On the other hand, *LHCSR3.1* and *LHCSR3.2* genes, whose expression is under control of PHOTOTROPIN and photosynthesis (Petroutsos et al. 2016), are also under control of UV-B-dependent signaling (Tilbrook et al. 2016) raising the question of the existence of overlapping UVR8/PHOTOTROPIN signaling pathways that regulate LHCSR3 expression (reviewed in Allorent and Petroutsos, 2017). The other member of *LHCSR* genes of Chlamydomonas, the *LHCSR1*, encoding for the LHCSR1 protein with a rather limited role in high-light-induced qE (Peers et al. 2009) is also included in the UV-B inducible list of genes identified by the research group of Roman Ulm (Tilbrook et al. 2016).

Higher plants do not have LHCSR proteins. There the effector protein for the qE component of NPQ is the PSBS which is constitutively expressed (Li et al. 2000). The genome of Chlamydomonas encodes for two PSBS genes, PSBS1 (Cre01.g016600.t1.2) and PSBS2 (Cre01.g016750.t1.2). PSBS1 and PSBS2 gene expression has been documented under conditions of nitrogen deprivation (Miller et al. 2010), and PSBS2 is included in the "light-stress" cluster of genes described few lines above (Zones et al. 2015). It was for long believed that no PSBS protein expression occurs in Chlamydomonas (Bonente et al. 2008). Recent studies however show that PSBS protein is expressed in this green alga after exposure to high-intensity white light (Tibiletti et al. 2016; Correa-Galvis et al. 2016) or to UV-B irradiation (Allorent et al. 2016) and that PSBS induction is photosynthesis-independent (Allorent et al. 2016; Tibiletti et al. 2016) contrary to the photosynthesis-dependent induction of LHCSR3 (Petroutsos et al. 2011; Maruyama et al. 2014). The UV-B-dependent expression of PSBS is based on direct UV-B reception by UVR8 which, together with COP1, initiates anterograde signaling and the accumulation of LHCSR1 and PSBS proteins.

The UV-B signal appears to act as a proxy for high light, priming the cells for photoprotection (Allorent et al. 2016).

The recent findings that PSBS and LHCSR1 under control of UV-B/UVR8 (Tilbrook et al. 2016) and that PHOTOTROPIN controls induction of LHCSR3 (Petroutsos et al. 2016) open new perspectives in the interconnection of photoperception, photosynthesis and photoprotection (reviewed in Allorent and Petroutsos, 2017), that deserve further investigation.

6 Rhodopsins

Chlamydomonas is one of the smallest organisms which possess eyes. Each cell contains one light-sensing eyespot, a primitive visual organelle of 1 μm in diameter, located approximately at the equator of the cell. The eyespot allows sensing the direction and intensity of continuous light and swimming toward the light to maximize photosynthesis (positive phototaxis) or away from it to avoid photodamage (negative phototaxis). The response to bright flashes of light is transient backward swimming named photophobic response (Hegemann 1997; Kreimer 2008). Swimming in Chlamydomonas is achieved using its two motile organelles, the flagella. The flagellar pair typically works in a breast-swimming-like fashion for forward motion. Due to the flagellar beating, the cell rotates at the same time counterclockwise (Häder and Lebert 2009).

The molecular mechanisms underlying these light-dependent movements remained largely unclear until recent years, when the analysis of genome and transcriptome sequencing data allowed for the identification of many rhodopsin-like photoreceptors (Kateriya et al. 2004; Kianianmomeni and Hallmann 2013).

Rhodopsins consist of a protein moiety, an opsin, and a nonprotein moiety, the chromophore retinal (derived from vitamin A in animals and from cleavage of β-carotene in Chlamydomonas). They belong to a family of membrane proteins found in all life domains. All members of the family bind a retinal chromophore and display either light-sensing, light-powered ion-pumping, or light-gated ion-channeling activities. These functions are carried out by a common protein architecture featuring seven α-helices forming a cavity with a chromophore-binding lysine located in the middle of the seventh helix. Type I rhodopsins are typically microbial, whereas type II are found in the eyes of animals (Sharma et al. 2006; Terakita and Nagata 2014; Luk et al. 2015). The dark state of microbial and animal rhodopsins possesses all-*trans*- and 11-*cis*-retinal as its chromophore, respectively. Usually, photoactivation isomerizes microbial rhodopsin selectively at the C13=C14 double bond and animal rhodopsin at the C11=C12 double bond (Ernst et al. 2014).

The first direct demonstration that a rhodopsin mediates phototaxis in Chlamydomonas came from the work of K.W. Foster and coworkers (Foster et al. 1984). They used the *fn68* mutant, later found to be devoid of PSY1 gene encoding phytoene synthase (McCarthy et al. 2004), which cannot perform phototaxis as it is

carotenoid- and therefore retinal-deficient. By complementation of *fn68* cells with all-trans retinal or analogous compounds, it was demonstrated that phototaxis was restored in the mutant, and the action spectrum maximum was dependent on the retinoid used (Foster et al. 1984). Next, it was shown that electrical responses, namely, the photoreceptor current and the flagellar current, as they occur after stimulation with a bright light flash are mediated by rhodopsin (Harz and Hegemann 1991). Two animal-type rhodopsins were identified in Peter Hegemann's group, Chlamyrhodopsin1 (COP1) and COP2, both localized in the eyes (Deininger et al. 1995), but later phototactic characterization of knockdown RNAi lines showed that neither COP1 nor COP2 is the primary photoreceptor for phototaxis (Fuhrmann et al. 2001). Instead, COP2 has been suggested to function as a sensory photoreceptor that regulates the biogenesis of photosystem I (PSI) complex under varying light conditions (Ozawa et al. 2009). This suggestion was based on the fact that COP2 forms a 1:1 complex with Ycf4, a thylakoid protein essential for the accumulation of PSI in Chlamydomonas. However, a decrease in COP2 to 10% of wild-type levels by RNAi did not affect the accumulation of PSI, suggesting that COP2 is not essential for PSI assembly (Ozawa et al. 2009).

Three research groups independently of each other identified two sequences in the Chlamydomonas cDNA database hypothetically encoding large microbial rhodopsins. The encoded proteins were named channelrhodopsin 1 and 2 (ChR1 and ChR2), Chlamydomonas sensory rhodopsin A and B (CSRA and CSRB), or archaeal-related sensory rhodopsin 1 and 2 (ASR1 and ASR2), also named as chlamyopsin 3 and 4 (COP3 and COP4) (Hegemann 2008). Sineshchekov and coworkers demonstrated the direct involvement of both proteins in photoperception (Govorunova et al. 2004). Hegemann and Nagel have shown that these two Chlamydomonas rhodopsins are light-gated ion channels (Nagel et al. 2002, 2003). Upon light stimulation, the all-*trans*-retinal chromophore of ChR isomerizes into 13-*cis* and activates a photoreceptor channel which leads to a rapid proton and Ca^{2+} influx into the eyespot region (Braun and Hegemann 1999; Nagel et al. 2003). At low light levels, the depolarization activates small flagellar currents which induce small but slightly different beating changes in the cis-flagellum (the one closest to the eyespot) and the trans-flagellum resulting in distinct directional changes. In continuous light, Ca^{2+} fluxes serve as the molecular basis for phototaxis. In response to flashes of higher energy, the larger photoreceptor currents trigger a massive Ca^{2+} influx into the flagella which causes the phobic response (Hegemann 1997).

Besides the physiological implications of ChR1 and ChR2 in photomovement responses of Chlamydomonas, the functional analyses of those two channelrhodopsins marked the foundation of optogenetics, a brand-new scientific field. Cloning, heterologous expression, and functional characterization of ChR1 and ChR2 in *Xenopus* oocytes led to the discovery that those rhodopsins are light-gated cation-selective ion channels (Nagel et al. 2002, 2003). Not much later ChR2 was successfully expressed in mammalian neurons, and it could be demonstrated that blue light triggers robust firing of action potentials (Boyden et al. 2005; Li et al. 2005; Ishizuka et al. 2006). The spread of optogenetics with microbial opsins has been fast and spectacular and allowed for real-time control of neuronal activity and advancement of our understanding of brain

function (reviewed in Deisseroth 2015; Govorunova and Koppel 2016). After cation-conducting channelrhodopsins of green algae were converted by engineering into chloride-conducting channelrhodopsins (Berndt et al. 2014; Wietek et al. 2014), a whole group of anion-conducting channelrhodopsins (ACRs) were identified in Cryptomonades (Govorunova et al. 2015).

In bacteria and archaea, but also in some eukaryotic organisms, two-component systems (TCS) comprising sensor histidine kinases and response regulator proteins are among the most important players in signal transduction (Zschiedrich et al. 2016). Interestingly, the genome of Chlamydomonas encodes for four rhodopsin-like proteins, provisionally named COP5–8, whose sequences had previously escaped identification and show homology to TCS proteins (Kateriya et al. 2004; Awasthi et al. 2016). COP5 and COP6 consist of a rhodopsin, a histidine kinase, a response regulator, and an enzymatic output (effector) domain in the form of adenyl- or guanylyl-cyclase, whereas the function of the terminal enzyme domain of COP7 remains unclear (see Fig. 1). The unusual feature of the algal sequences is that all the elements, from the photoreceptor to the effector domain, are assembled in one protein (Hegemann 2008). COP5 (or HKR1; histidine-kinase rhodopsin-1) is a 170 KDa protein, localized in the eyespot of Chlamydomonas (Luck et al. 2012). The spectroscopic study of the rhodopsin domain of COP5 revealed that upon exposure to UV-A light (380 nm), it is photoconverted to a stable blue-light-absorbing state with an absorption maximum at 490 nm that switches back to the UV-A-absorbing state upon exposure to blue light (Luck et al. 2012). The functional role of COP5, as well as of COP6, COP7, and COP8, remains to be identified. COP8 is the most recently identified rhodopsin-like Chlamydomonas protein, a 302 KDa multidomain protein, which along with the domains of rhodopsin, histidine kinase, response regulator, and cyclase also contains a potassium channel and a cyclic nucleotide-binding domain at the N-terminus (Awasthi et al. 2016). Immunolocalization studies showed that COP8 is present in both the eyespot and the flagella of Chlamydomonas and that its distribution is light-dependent and intraflagellar transport (IFT) machinery-dependent, homologous to the mammalian rhodopsins trafficking in the outer segment of the photoreceptor cells (Awasthi et al. 2016). An IFT-dependent transport of a photoreceptor to Chlamydomonas flagella has been also suggested for the case of phototropin (Huang et al. 2004).

7 Outlook

With the biological function of many Chlamydomonas photoreceptors remaining unknown, generation and phenotypic characterization of Chlamydomonas knock-out lines of photoreceptors is a key requirement for their functional characterization that will advance the knowledge on the in vivo roles of photoreception. The newly acquired insertional library CLiP (Li et al. 2016) and the recent developments in targeted gene silencing in Chlamydomonas (Baek et al. 2016; Shin et al. 2016) can be useful tools to this direction.

The rhodopsin-like cyclases COP5,COP6, and COP8 together with the 71 adenylyl/guanylyl cyclases and 31 cyclic nucleotide phosphodiesterases (catalyzing cAMP/cGMP synthesis and degradation, respectively), which Chlamydomonas genome encodes for Merchant et al. (2007), highlight the importance of cyclic nucleotides in this microalga; they are critical for mating (Pasquale and Goodenough 1987) and for the regulation of flagellar beating (Hasegawa et al. 1987; Gaillard et al. 2006) and are involved in the regulation of phototaxis [via cAMP (Boonyareth et al. 2009)] and photoprotection via LHCSR3 (Petroutsos et al. 2016). The functional role of the COP5, COP6, and COP8 is therefore a research question of high interest.

The newly established link between photoreception and photoprotection (Tilbrook et al. 2016; Petroutsos et al. 2016) opens new questions on the signaling pathways that link PHOTOTROPIN and UVR8 in regulating genes involved in Chlamydomonas photoprotection, while the investigation of the role of the flagella-localized photoreceptors, COP8 and PHOTOTROPIN (Huang et al. 2004; Awasthi et al. 2016), is another interesting question that needs to be addressed.

Acknowledgments This work was supported by The French National Agency for Research through the GRAL Labex (grant number ANR-10-LABX-49-01).

References

Ahmad M (2016) Photocycle and signaling mechanisms of plant cryptochromes. Curr Opin Plant Biol 33:108–115. doi:10.1016/j.pbi.2016.06.013

Ahmad M, Cashmore AR (1993) HY4 gene of A. thaliana encodes a protein with characteristics of a blue-light photoreceptor. Nature 366:162–166. doi:10.1038/366162a0

Allorent G, Lefebvre-Legendre L, Chappuis R et al (2016) UV-B photoreceptor-mediated protection of the photosynthetic machinery in *Chlamydomonas reinhardtii*. Proc Natl Acad Sci U S A 113:14864–14869

Allorent G, Petroutsos D (2017). Photoreceptor-dependent regulation of photoprotection. Current Opinion in Plant Biology 37:102–108. doi:10.1016/j.pbi.2017.03.016

Awasthi M, Ranjan P, Sharma K et al (2016) The trafficking of bacterial type rhodopsins into the Chlamydomonas eyespot and flagella is IFT mediated. Sci Rep 6:34646. doi:10.1038/srep34646

Baek K, Kim DH, Jeong J et al (2016) DNA-free two-gene knockout in *Chlamydomonas reinhardtii* via CRISPR-Cas9 ribonucleoproteins. Sci Rep 6:30620. doi:10.1038/srep30620

Beel B, Prager K, Spexard M et al (2012) A flavin binding cryptochrome photoreceptor responds to both blue and red light in *Chlamydomonas reinhardtii*. Plant Cell 24:2992–3008. doi:10.1105/tpc.112.098947

Beel B, Müller N, Kottke T, Mittag M (2014) News about cryptochrome photoreceptors in algae. Plant Signal Behav 8:e22870. doi:10.4161/psb.22870

Berndt A, Lee SY, Ramakrishnan C, Deisseroth K (2014) Structure-guided transformation of channelrhodopsin into a light-activated chloride channel. Science 344:420–424. doi:10.1126/science.1252367

Bonente G, Passarini F, Cazzaniga S et al (2008) The occurrence of the *psbS* gene product in *Chlamydomonas reinhardtii* and in other photosynthetic organisms and its correlation with energy quenching. Photochem Photobiol 84:1359–1370. doi:10.1111/j.1751-1097.2008.00456.x

Boonyareth M, Saranak J, Pinthong D et al (2009) Roles of cyclic AMP in regulation of phototaxis in *Chlamydomonas reinhardtii*. Biologia 64:1058–1065. doi:10.2478/s11756-009-0194-4

Boyden ES, Zhang F, Bamberg E et al (2005) Millisecond-timescale, genetically targeted optical control of neural activity. Nat Neurosci 8:1263–1268. doi:10.1038/nn1525

Braun FJ, Hegemann P (1999) Direct measurement of cytosolic calcium and pH in living *Chlamydomonas reinhardtii* cells. Eur J Cell Biol 78:199. doi:10.1016/S0171-9335(99)80099-5

Briggs WR (2014) Phototropism: some history, some puzzles, and a look ahead. Plant Physiol 164:13–23. doi:10.1104/pp.113.230573

Chaves I, Pokorny R, Byrdin M, Hoang N, Ritz T, Brettel, K et al (2011) The cryptochromes: blue light photoreceptors in plants and animals. Annu Rev Plant Biol 62:335–364

Christie JM (2007) Phototropin blue-light receptors. Annu Rev Plant Biol 58:21–45. doi:10.1146/annurev.arplant.58.032806.103951

Christie JM, Reymond P, Powell GK et al (1998) Arabidopsis NPH1: a flavoprotein with the properties of a photoreceptor for phototropism. Science 282:1698–1701

Christie JM, Salomon M, Nozue K et al (1999) LOV (light, oxygen, or voltage) domains of the blue-light photoreceptor phototropin (nph1): binding sites for the chromophore flavin mononucleotide. Proc Natl Acad Sci U S A 96:8779–8783

Christie JM, Swartz TE, Bogomolni RA, Briggs WR (2002) Phototropin LOV domains exhibit distinct roles in regulating photoreceptor function. Plant J 32:205–219

Christie JM, Arvai AS, Baxter KJ et al (2012) Plant UVR8 photoreceptor senses UV-B by tryptophan-mediated disruption of cross-dimer salt bridges. Science 335:1492–1496. doi:10.1126/science.1218091

Christie JM, Blackwood L, Petersen J, Sullivan S (2015) Plant flavoprotein photoreceptors. Plant Cell Physiol 56:401–413. doi:10.1093/pcp/pcu196

Correa-Galvis V, Redekop P, Guan K et al (2016) Photosystem II subunit PsbS is involved in the induction of LHCSR protein-dependent energy dissipation in *Chlamydomonas reinhardtii*. J Biol Chem 291:17478–17487. doi:10.1074/jbc.M116.737312

Crosson S, Rajagopal S, Moffat K (2003) The LOV domain family: photoresponsive signaling modules coupled to diverse output domains. Biochemistry 42:2–10. doi:10.1021/bi026978l

Deininger W, Kroger P, Hegemann U et al (1995) Chlamyrhodopsin represents a new type of sensory photoreceptor. EMBO J 14:5849–5858

Deisseroth K (2015) Optogenetics: 10 years of microbial opsins in neuroscience. Neurosci 18:1213–1225. doi:10.1038/nn.4091

Depauw FA, Rogato A, d'Alcala MR, Falciatore A (2012) Exploring the molecular basis of responses to light in marine diatoms. J Exp Bot 63:1575–1591

Duanmu D, Casero D, Dent RM et al (2013) Retrograde bilin signaling enables Chlamydomonas greening and phototrophic survival. Proc Natl Acad Sci U S A 110:3621–3626. doi:10.1073/pnas.1222375110

Elrad D, Grossman AR (2004) A genome's-eye view of the light-harvesting polypeptides of *Chlamydomonas reinhardtii*. Curr Genet 45:61–75. doi:10.1007/s00294-003-0460-x

Ermilova EV, Zalutskaya ZM, Huang K, Beck CF (2004) Phototropin plays a crucial role in controlling changes in chemotaxis during the initial phase of the sexual life cycle in Chlamydomonas. Planta 219:420–427. doi:10.1007/s00425-004-1241-6

Ernst OP, Lodowski DT, Elstner M et al (2014) Microbial and animal rhodopsins: structures, functions, and molecular mechanisms. Chem Rev 114:126–163. doi:10.1021/cr4003769

Favory J-J, Stec A, Gruber H et al (2009) Interaction of COP1 and UVR8 regulates UV-B-induced photomorphogenesis and stress acclimation in Arabidopsis. EMBO J 28:591–601. doi:10.1038/emboj.2009.4

Fedorov R, Schlichting I, Hartmann E et al (2003) Crystal structures and molecular mechanism of a light-induced signaling switch: the phot-LOV1 domain from *Chlamydomonas reinhardtii*. Biophys J 84:2474–2482. doi:10.1016/S0006-3495(03)75052-8

Fortunato AE, Annunziata R, Jaubert M et al (2015) Dealing with light: the widespread and multitasking cryptochrome/photolyase family in photosynthetic organisms. J Plant Physiol 172:42–54. doi:10.1016/j.jplph.2014.06.011

Foster KW, Saranak J, Patel N et al (1984) A rhodopsin is the functional photoreceptor for phototaxis in the unicellular eukaryote Chlamydomonas. Nature 311:756–759

Fuhrmann M, Stahlberg A, Govorunova E et al (2001) The abundant retinal protein of the Chlamydomonas eye is not the photoreceptor for phototaxis and photophobic responses. J Cell Sci 114:3857–3863

Gaillard AR, Fox LA, Rhea JM et al (2006) Disruption of the A-kinase anchoring domain in flagellar radial spoke protein 3 results in unregulated axonemal cAMP-dependent protein kinase activity and abnormal flagellar motility. Mol Biol Cell 17:2626–2635. doi:10.1091/mbc.E06-02-0095

Galván-Ampudia CS, Offringa R (2007) Plant evolution: AGC kinases tell the auxin tale. Trends Plant Sci 12:541–547. doi:10.1016/j.tplants.2007.10.004

Gegear RJ, Foley LE, Casselman A, Reppert SM (2010) Animal cryptochromes mediate magnetoreception by an unconventional photochemical mechanism. Nature 463:804–807. doi:10.1038/nature08719

Govorunova EG, Koppel LA (2016) The road to optogenetics: microbial rhodopsins. Biochem Mosc 81:928–940. doi:10.1134/S0006297916090029

Govorunova EG, Jung K-H, Sineshchekov OA, Spudich JL (2004) Chlamydomonas sensory rhodopsins a and B: cellular content and role in photophobic responses. Biophys J 86:2342–2349. doi:10.1016/S0006-3495(04)74291-5

Govorunova EG, Sineshchekov OA, Janz R et al (2015) NEUROSCIENCE. Natural light-gated anion channels: a family of microbial rhodopsins for advanced optogenetics. Science 349:647–650. doi:10.1126/science.aaa7484

Häder D-P, Lebert M (2009) Photoorientation in photosynthetic flagellates. Methods Mol Biol 571:51–65. doi:10.1007/978-1-60761-198-1_3

Harper SM, Neil LC, Gardner KH (2003) Structural basis of a phototropin light switch. Science 301:1541–1544. doi:10.1126/science.1086810

Harz H, Hegemann P (1991) Rhodopsin-regulated calcium currents in Chlamydomonas. Nature 351:489–491. doi:10.1038/351489a0

Hasegawa E, Hayashi H, Asakura S, Kamiya R (1987) Stimulation of in vitro motility of Chlamydomonas axonemes by inhibition of cAMP-dependent phosphorylation. Cell Motil Cytoskeleton 8:302–311. doi:10.1002/cm.970080403

Heddad M, Adamska I (2002) The evolution of light stress proteins in photosynthetic organisms. Comp Funct Genomics 3:504–510. doi:10.1002/cfg.221

Hegemann P (1997) Vision in microalgae. Planta 203:265–274. doi:10.1007/s004250050191

Hegemann P (2008) Algal sensory photoreceptors. Annu Rev Plant Biol 59:167–189. doi:10.1146/annurev.arplant.59.032607.092847

Heijde M, Ulm R (2012) UV-B photoreceptor-mediated signalling in plants. Trends Plant Sci 17:230–237. doi:10.1016/j.tplants.2012.01.007

Huang K, Beck CF (2003) Phototropin is the blue-light receptor that controls multiple steps in the sexual life cycle of the green alga *Chlamydomonas reinhardtii*. Proc Natl Acad Sci U S A 100:6269–6274

Huang K, Merkle T, Beck CF (2002) Isolation and characterization of a Chlamydomonas gene that encodes a putative blue-light photoreceptor of the phototropin family. Physiol Plant 115:613–622

Huang K, Kunkel T, Beck CF (2004) Localization of the blue-light receptor phototropin to the flagella of the green alga *Chlamydomonas reinhardtii*. Mol Biol Cell 15:3605–3614

Im CS, Eberhard S, Huang K et al (2006) Phototropin involvement in the expression of genes encoding chlorophyll and carotenoid biosynthesis enzymes and LHC apoproteins in *Chlamydomonas reinhardtii*. Plant J 48:1–16. doi:10.1111/j.1365-313X.2006.02852.x

Ishizuka T, Kakuda M, Araki R, Yawo H (2006). Kinetic evaluation of photosensitivity in genetically engineered neurons expressing green algae light-gated channels. Neuroscience Research 54(2):85–94. doi:10.1016/j.neures.2005.10.009

Jenkins GI (2009) Signal transduction in responses to UV-B radiation. Annu Rev Plant Physiol Plant Mol Biol 60:407–431. doi:10.1146/annurev.arplant.59.032607.092953

Jenkins GI (2014) Structure and function of the UV-B photoreceptor UVR8. Curr Opin Struct Biol 29:52–57. doi:10.1016/j.sbi.2014.09.004

Kateriya S, Nagel G, Bamberg E, Hegemann P (2004) "Vision" in single-celled algae. News Physiol Sci 19:133–137

Kianianmomeni A, Hallmann A (2013) Algal photoreceptors: in vivo functions and potential applications. Planta 239:1–26. doi:10.1007/s00425-013-1962-5

Kinoshita T (2003) Blue-light- and phosphorylation-dependent binding of a 14-3-3 protein to phototropins in stomatal guard cells of broad bean. Plant Physiol 133:1453–1463. doi:10.1104/pp.103.029629

Kottke T, Heberle J, Hehn D et al (2003) Phot-LOV1: photocycle of a blue-light receptor domain from the green alga *Chlamydomonas reinhardtii*. Biophys J 84:1192–1201. doi:10.1016/S0006-3495(03)74933-9

Kreimer G (2008) The green algal eyespot apparatus: a primordial visual system and more? Curr Genet 55:19–43. doi:10.1007/s00294-008-0224-8

Li XP, Björkman O, Shih C et al (2000) A pigment-binding protein essential for regulation of photosynthetic light harvesting. Nature 403:391–395. doi:10.1038/35000131

Li X, Gutierrez DV, Hanson MG et al (2005) Fast noninvasive activation and inhibition of neural and network activity by vertebrate rhodopsin and green algae channelrhodopsin. Proc Natl Acad Sci U S A 102:17816–17821. doi:10.1073/pnas.0509030102

Li Z, Wakao S, Fischer BB, Niyogi KK (2009) Sensing and responding to excess light. Annu Rev Plant Biol 60:239–260. doi:10.1146/annurev.arplant.58.032806.103844

Li X, Zhang R, Patena W et al (2016) An indexed, mapped mutant library enables reverse genetics studies of biological processes in *Chlamydomonas reinhardtii*. Plant Cell 29:129–143. doi:10.1105/tpc.16.00465

Liao JC, Mi L, Pontrelli S, Luo S (2016) Fuelling the future: microbial engineering for the production of sustainable biofuels. Nat Rev Microbiol 14:288. doi:10.1038/nrmicro.2016.32

Lin C, Shalitin D (2003) Cryptochrome structure and signal transduction. Annu Rev Plant Biol 54:469–496. doi:10.1146/annurev.arplant.54.110901.160901

Lin C, Todo T (2005) The cryptochromes. Genome Biol 6:220. doi:10.1186/gb-2005-6-5-220

Losi A, Gärtner W (2011) Old chromophores, new photoactivation paradigms, trendy applications: flavins in blue light-sensing photoreceptors. Photochem Photobiol 87:491–510. doi:10.1111/j.1751-1097.2011.00913.x

Losi A, Gärtner W (2012) The evolution of flavin-binding photoreceptors: an ancient chromophore serving trendy blue-light sensors. Annu Rev Plant Physiol Plant Mol Biol 63:49–72

Luk HL, Melaccio F, Rinaldi S, Gozem S, Olivucci M (2015). Molecular bases for the selection of the chromophore of animal rhodopsins. Proceedings of the National Academy of Sciences, 112 (50):15297–15302. doi:10.1073/pnas.1510262112

Luck M, Mathes T, Bruun S et al (2012) A photochromic histidine kinase rhodopsin (HKR1) that is bimodally switched by ultraviolet and blue light. J Biol Chem 287:40083–40090. doi:10.1074/jbc.M112.401604

Mach J (2016) How plants take the bad with the good: conserved UV-B perception and signaling in Chlamydomonas. Plant Cell 28:tpc.00279.2016. doi:10.1105/tpc.16.00279

Maruyama S, Tokutsu R, Minagawa J (2014) Transcriptional regulation of the stress-responsive light harvesting complex genes in *Chlamydomonas reinhardtii*. Plant Cell Physiol 55:1304–1310. doi:10.1093/pcp/pcu068

Matsuoka D, Tokutomi S (2005) Blue light-regulated molecular switch of Ser/Thr kinase in phototropin. Proc Natl Acad Sci U S A 102:13337–13342. doi:10.1073/pnas.0506402102

McCarthy SS, Kobayashi MC, Niyogi KK (2004) White mutants of *Chlamydomonas reinhardtii* are defective in phytoene synthase. Genetics 168:1249–1257. doi:10.1534/genetics.104.030635

Merchant SS, Prochnik SE, Vallon O et al (2007) The Chlamydomonas genome reveals the evolution of key animal and plant functions. Science 318:245–250. doi:10.1126/science.1143609

Miller R, Wu G, Deshpande RR et al (2010) Changes in transcript abundance in *Chlamydomonas reinhardtii* following nitrogen deprivation predict diversion of metabolism. Plant Physiol 154:1737–1752. doi:10.1104/pp.110.165159

Nagel G, Ollig D, Fuhrmann M et al (2002) Channelrhodopsin-1: a light-gated proton channel in green algae. Science 296:2395–2398. doi:10.1126/science.1072068

Nagel G, Szellas T, Huhn W et al (2003) Channelrhodopsin-2, a directly light-gated cation-selective membrane channel. Proc Natl Acad Sci U S A 100:13940–13945. doi:10.1073/pnas.1936192100

Onodera A, Kong S-G, Doi M et al (2005) Phototropin from *Chlamydomonas reinhardtii* is functional in Arabidopsis thaliana. Plant Cell Physiol 46:367–374. doi:10.1093/pcp/pci037

Ozawa S-I, Nield J, Terao A et al (2009) Biochemical and structural studies of the large Ycf4-photosystem I assembly complex of the green alga *Chlamydomonas reinhardtii*. Plant Cell 21:2424–2442. doi:10.1105/tpc.108.063313

Pasquale SM, Goodenough UW (1987) Cyclic AMP functions as a primary sexual signal in gametes of *Chlamydomonas reinhardtii*. J Cell Biol 105:2279–2292

Pazour GJ, Agrin N, Leszyk J, Witman GB (2005) Proteomic analysis of a eukaryotic cilium. J Cell Biol 170:103–113. doi:10.1083/jcb.200504008

Pearce LR, Komander D, Alessi DR (2010) The nuts and bolts of AGC protein kinases. Nat Rev Mol Cell Biol 11:9–22. doi:10.1038/nrm2822

Peers G, Truong TB, Ostendorf E et al (2009) An ancient light-harvesting protein is critical for the regulation of algal photosynthesis. Nature 462:518–521. doi:10.1038/nature08587

Petroutsos D, Busch A, Janssen I et al (2011) The chloroplast calcium sensor CAS is required for photoacclimation in *Chlamydomonas reinhardtii*. Plant Cell 23:2950–2963. doi:10.1105/tpc.111.087973

Petroutsos D, Tokutsu R, Maruyama S et al (2016) A blue-light photoreceptor mediates the feedback regulation of photosynthesis. Nature 537:563–566. doi:10.1038/nature19358

Reisdorph NA, Small GD (2004) The CPH1 gene of *Chlamydomonas reinhardtii* encodes two forms of cryptochrome whose levels are controlled by light-induced proteolysis. Plant Physiol 134:1546–1554. doi:10.1104/pp.103.031930

Rizzini L, Favory J-J, Cloix C et al (2011) Perception of UV-B by the Arabidopsis UVR8 protein. Science 332:103–106. doi:10.1126/science.1200660

Rockwell NC, Su Y-S, Lagarias JC (2006) Phytochrome structure and signaling mechanisms. Annu Rev Plant Biol 57:837–858. doi:10.1146/annurev.arplant.56.032604.144208

Rockwell NC, Duanmu D, Martin SS et al (2014) Eukaryotic algal phytochromes span the visible spectrum. Proc Natl Acad Sci U S A 111:3871–3876. doi:10.1073/pnas.1401871111

Salomon M, Knieb E, Zeppelin von T, Rüdiger W (2003) Mapping of low- and high-fluence autophosphorylation sites in phototropin 1. Biochemistry 42:4217–4225. doi:10.1021/bi027324f

Schmidt M, Geßner G, Luff M et al (2006) Proteomic analysis of the eyespot of *Chlamydomonas reinhardtii* provides novel insights into its components and tactic movements. Plant Cell 18:1908–1930

Sharma AK, Spudich JL, Doolittle WF (2006) Microbial rhodopsins: functional versatility and genetic mobility. Trends Microbiol 14:463–469. doi:10.1016/j.tim. 2006.09.006

Shin S-E, Lim J-M, Koh HG et al (2016) CRISPR/Cas9-induced knockout and knock-in mutations in *Chlamydomonas reinhardtii*. Sci Rep 6:27810. doi:10.1038/srep27810

Spexard M, Thöing C, Beel B et al (2014) Response of the sensory animal-like cryptochrome aCRY to blue and red light as revealed by infrared difference spectroscopy. Biochemistry 53:1041–1050. doi:10.1021/bi401599z

Sullivan S, Thomson CE, Lamont DJ et al (2008) In vivo phosphorylation site mapping and functional characterization of Arabidopsis phototropin 1. Mol Plant 1:178–194. doi:10.1093/mp/ssm017

Taylor BL, Zhulin IB (1999) PAS domains: internal sensors of oxygen, redox potential, and light. Microbiol Mol Biol Rev 63:479–506

Terakita A, Nagata T (2014) Functional properties of opsins and their contribution to light-sensing physiology. Zool Sci 31:653–659. doi:10.2108/zs140094

Tibiletti T, Auroy P, Peltier G, Caffarri S (2016) *Chlamydomonas reinhardtii* PsbS protein is functional and accumulates rapidly and transiently under high light. Plant Physiol 171:2717. doi:10.1104/pp.16.00572

Tilbrook K, Dubois M, Crocco CD et al (2016) UV-B perception and acclimation in Chlamydomonas reinhardtii. Plant Cell 28:tpc.00287.2015–tpc.00287.2983. doi:10.1105/tpc.15.00287

Tokutomi S, Matsuoka D, Zikihara K (2008) Molecular structure and regulation of phototropin kinase by blue light. Biochim Biophys Acta 1784:133–142. doi:10.1016/j.bbapap.2007.09.010

Trippens J, Greiner A, Schellwat J et al (2012) Phototropin influence on eyespot development and regulation of phototactic behavior in *Chlamydomonas reinhardtii*. Plant Cell 24:4687–4702

Van Gelder RN (2002) Tales from the crypt(ochromes). J Biol Rhythm 17:110–120

Wietek J, Wiegert JS, Adeishvili N et al (2014) Conversion of channelrhodopsin into a light-gated chloride channel. Science 344:409–412. doi:10.1126/science.1249375

Zones JM, Blaby IK, Merchant SS, Umen JG (2015) High-resolution profiling of a synchronized diurnal transcriptome from *Chlamydomonas reinhardtii* reveals continuous cell and metabolic differentiation. Plant Cell 27:2743–2769. doi:10.1105/tpc.15.00498

Zorin B, Lu Y, Sizova I, Hegemann P (2009) Nuclear gene targeting in Chlamydomonas as exemplified by disruption of the PHOT gene. Gene 432:91–96. doi:10.1016/j.gene.2008.11.028

Zschiedrich CP, Keidel V, Szurmant H (2016) Molecular mechanisms of two-component signal transduction. J Mol Biol 428:3752–3775. doi:10.1016/j.jmb.2016.08.003

Chlamydomonas: Hydrogenase and Hydrogen Production

Anne Sawyer, Julian Esselborn, Martin Winkler, and Thomas Happe

Abstract An important aspect of *Chlamydomonas reinhardtii's* metabolism is its ability to produce molecular hydrogen (H_2) from protons and electrons. Hydrogen production is catalysed by two [FeFe]-hydrogenases, HYDA1 and HYDA2, although HYDA1 is the main isoform, accounting for ~75% of the H_2 produced. Hydrogen production can be light dependent, with the hydrogenase receiving electrons from the photosynthetic electron transport chain via the ferredoxin PETF, or light independent, where H_2 is produced via fermentation in the dark. Hydrogen production was first reported in microalgae in the early 1940s; however, due to *HYDA* gene expression being induced by anaerobiosis and the extreme oxygen sensitivity of the enzyme, this process only occurred transiently at low levels when the algae were subjected to anaerobic or hypoxic conditions. It was thus considered nothing more than a biological curiosity until the early 2000s, when a method temporally separating oxygenic photosynthesis and H_2 production was developed, which allowed sustained H_2 production in the light over the course of a few days. Light-driven H_2 production has the highest theoretical photon conversion efficiency and is thus of considerable biotechnological interest. However, the calculated theoretical efficiencies are still not achievable in practice, despite the implementation of a wide range of engineering strategies. For an improved H_2 production, a better understanding of the underlying biology is needed. *C. reinhardtii* is the ideal organism in which to study H_2 production, due to the many molecular tools available and the simplicity and long history of study of its hydrogenase.

A. Sawyer • J. Esselborn • M. Winkler • T. Happe (✉)
Faculty of Biology and Biotechnology, Department of Plant Biochemistry, Workgroup Photobiotechnology, Ruhr-University of Bochum, Universitätsstr. 150, 44801 Bochum, Germany
e-mail: thomas.happe@rub.de

M. Hippler (ed.), *Chlamydomonas: Biotechnology and Biomedicine*, Microbiology Monographs 31, DOI 10.1007/978-3-319-66360-9_2

1 Introduction

Rising global population growth and concomitant increases in demand for food, water and energy, as well as renewed efforts by governments to reduce carbon emissions, have all heightened interest in hydrogen (H_2) as a renewable fuel. The main attraction of H_2 is that the only by-product of its combustion is water, meaning that it can be carbon neutral or even carbon negative when produced renewably. Hydrogen also has an $\sim 3\times$ higher energy density compared to hydrocarbon fuels (Gupta et al. 2013). Currently, H_2 is produced via expensive energy-intensive fossil fuel-based methods such as steam reformation of natural gas, industrial oil and naphtha reforming, coal gasification and fossil fuel-driven water electrolysis (Gupta et al. 2013). However, it can also be produced under less energy-intensive conditions in cyanobacterial or microalgal systems, which use sunlight as their energy source (Oey et al. 2016).

To date, high bio-H_2 production efficiencies have been reported for eukaryotic microalgae. This is partly due to the high efficiency of the algal [FeFe]-hydrogenase, which is 100-fold higher than that of cyanobacterial hydrogenases, having a turnover rate of up to 10^4 H_2 molecules s^{-1} (Lubitz et al. 2014; Volgusheva et al. 2013). *Chlamydomonas reinhardtii* has emerged as the model organism for the study of photobiological H_2 production in green microalgae. This is likely due to the fact that the *C. reinhardtii* [FeFe]-hydrogenase HYDA1 was the first eukaryotic hydrogenase to be isolated (Roessler and Lien 1984; Happe and Naber 1993) but is also due to the large knowledge base and molecular toolset available for this organism. Since the initial purification of HYDA1, much progress has been made characterising the enzyme and elucidating its maturation, as well as in understanding the underlying regulatory pathways and improving H_2 production efficiencies. The structure, catalysis and oxygen (O_2) sensitivity of the enzyme have all been analysed, and many hydrogen mutants and higher H_2-producing algal strains have been created (see reviews Kruse et al. 2005; Ghirardi et al. 2007; Dubini and Ghirardi 2015; Antal et al. 2015; Torzillo et al. 2015; Oey et al. 2016). In this chapter, we review H_2 production in *C. reinhardtii* with a focus on HYDA1. We detail the induction, structure, maturation and catalytic mechanism of this enzyme and summarise strategies that have been used to improve microalgal H_2 production efficiencies.

2 Microalgal Hydrogen Metabolism

Microalgal H_2 production was first reported for *Scenedesmus* sp. in 1942 (Gaffron and Rubin) and later for *C. reinhardtii* and other species (Stuart and Gaffron 1972). Hydrogen evolution was observed at low levels under dark anaerobiosis and at higher levels in the light (Gaffron and Rubin 1942). Photosystem I (PSI) was identified as being essential for light-dependent H_2 production, whereas

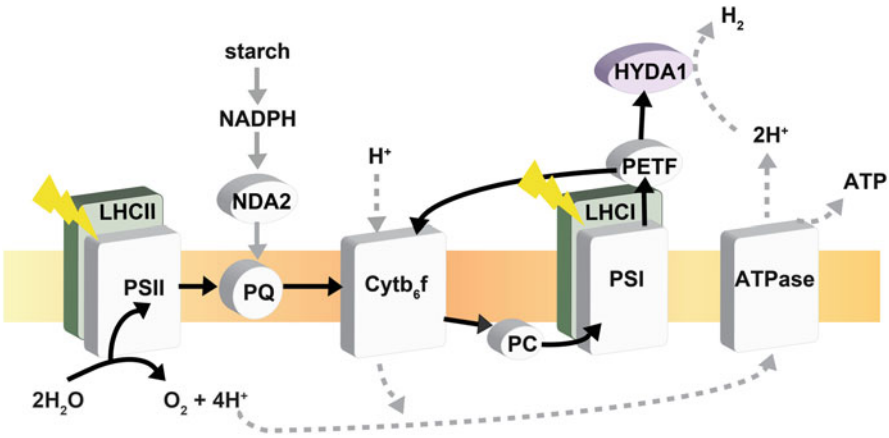

Fig. 1 Overview of the direct and indirect light-dependent hydrogen (H_2) production pathways. In the direct pathway, electrons are derived from the water-splitting reaction at photosystem II (PSII), while in the indirect pathway, electrons are derived from starch catabolism. Both pathways involve the capture of light, either by both light-harvesting complexes I and II (LHCI and LHCII, respectively) or by LHCI, and the transfer of electrons to the hydrogenase HYDA1 through the electron transport chain via the plastoquinone pool (PQ), cytochrome b_6f ($Cytb_6f$), plastocyanin (PC), PSI and the ferredoxin PETF. The indirect pathway additionally involves the NADPH-dehydrogenase NDA2

photosystem II (PSII), although a contributor of electrons, was found to be dispensable (Stuart and Gaffron 1972).

Three H_2 production pathways have since been identified in green microalgae: two that produce H_2 in the light and a third, dark fermentation pathway. The two light-dependent pathways (Fig. 1) include a direct pathway and an indirect pathway. In the direct pathway, HYDA1 receives electrons generated by the splitting of water at PSII via the photosynthetic electron transfer (PET) pathway. This involves the light-dependent excitation of electrons by PSI, the reduction of the ferredoxin PETF and the subsequent transfer of electrons from PETF to the hydrogenase (Melis and Happe 2001; Melis et al. 2000). In the indirect pathway, which is independent of PSII, electrons are also received via PETF but are derived from the catabolism of starch. In this pathway, the plastoquinone pool is reduced by NAD(P)H in a reaction mediated by the type II NADH dehydrogenase NDA2 (Desplats et al. 2009; Fouchard et al. 2005; Godde and Trebst 1980; Maione and Gibbs 1986; Chochois et al. 2009; Baltz et al. 2014; Jans et al. 2008; Mignolet et al. 2012; Mus et al. 2005). However, in this pathway, H_2 production is $\sim 10\times$ lower than in the direct pathway (Chochois et al. 2009). In the dark fermentation metabolism, electrons are also derived from the catabolism of starch but do not enter the PET pathway. Instead, it is thought that they are transferred to pyruvate, which can be oxidised by a pyruvate ferredoxin oxidoreductase and which can then reduce PETF in a process similar to H_2-producing fermentation pathways found in other microorganisms (Grossman et al. 2011; Atteia et al. 2013; van Lis et al. 2013; Noth et al. 2013).

It would appear slightly paradoxical that oxygenic green algae contain fermentative pathways such as the H_2 production pathway, which are more typical of strictly anaerobic microbes. However, green microalgae such as *C. reinhardtii* are in fact frequently exposed to anaerobic or hypoxic conditions and therefore need to be able to readily adapt their metabolisms (Mus et al. 2007; see chapter "Chlamydomonas: Anoxic Acclimation and Signaling" of Volume 1). Although the exact physiological role of H_2 production in microalgae remains unclear, it likely functions as a protection mechanism against the over-reduction of the chloroplast (Hemschemeier et al. 2008a). Under aerobic conditions, photosynthesis produces the carbohydrates that are required for respiration and cell growth. However, under anaerobiosis in the light, oxidative phosphorylation in the mitochondria is largely inhibited by a lack of O_2, leading to the over-reduction of the chloroplast and a reduced electron transfer, which ultimately results in photodamage and decreased levels of ATP. Under these conditions, the protons and electrons derived from water by the remaining PSII in the direct pathway or from starch in the indirect pathway can be fed to the hydrogenase via the PET chain, which recombines the protons and electrons to produce H_2. Therefore the hydrogenase is thought to act as a proton/electron release valve, removing excess protons and electrons by recombining them to produce H_2 gas, which can be easily released from the cells.

3 The *Chlamydomonas reinhardtii* Hydrogenase HYDA1

3.1 Hydrogenases

Three phylogenetically distinct classes of hydrogenases have been identified to date in H_2-consuming and H_2-evolving prokaryotes: [NiFe]-hydrogenases, which contain a nickel (Ni) and an iron (Fe) atom in their active site; [FeFe]-hydrogenases, which contain two Fe atoms; and [Fe]-hydrogenases, which have a mononuclear Fe active site but which are only found in a few methanogenic archaea (Vignais et al. 2001; Meyer 2007). Eukaryotic green microalgae have only been found to contain [FeFe]-hydrogenases, while cyanobacteria only contain [NiFe]-hydrogenases (Ludwig et al. 2006). However, [FeFe]-hydrogenases have also been found in eubacteria such as *Clostridium* sp. and *Desulfovibrio* sp., as well as in anaerobic protozoa such as *Trichomonas* sp. and *Nyctotherus* sp. (Vignais et al. 2001).

3.2 HYDA1 Gene

Two [FeFe]-hydrogenase genes have been identified in *C. reinhardtii: HYDA1* (Happe and Kaminski 2002) and *HYDA2* (Forestier et al. 2003). HYDA1 appears to be the primary isoform as it produces ~75% of the H_2 in the light (Meuser et al. 2012).

Both genes are nuclear encoded; however HYDA1 contains a transit peptide that facilitates its translocation to the chloroplast (Happe and Kaminski 2002). HYDA2 is also predicted to contain a chloroplast transit peptide and is thus also likely to function in the chloroplast (Forestier et al. 2003). Expression of *HYDA1* and *HYDA2*, as well as the hydrogenase specific maturase genes *HYDEF* and *HYDG*, is induced by anaerobiosis (Happe and Kaminski 2002; Happe and Naber 1993; Posewitz et al. 2004; Mus et al. 2007; Hemschemeier et al. 2013). *HYDA1* transcript abundance also increases after copper deprivation (Castruita et al. 2011), and the *HYDA1* promoter has been found to contain two GTAC motifs that are recognised by the *copper response regulator* 1 (CRR1) transcription factor (Pape et al. 2012), which regulates several genes under both copper deprivation and hypoxia/anaerobiosis (Kropat et al. 2005). In fact, anaerobiosis and copper deprivation appear to be linked, with many genes being expressed under both conditions (Castruita et al. 2011; see chapter "Chlamydomonas: Anoxic Acclimation and Signaling" of Volume 1).

3.3 HYDA1 Structure

The *C. reinhardtii* hydrogenase is a small (~48 kDa) monomeric soluble [FeFe]-hydrogenase located in the chloroplast (Happe and Naber 1993; Happe et al. 1994). Its structure consists of two lobes, each containing a beta-sheet surrounded by several alpha-helices, with the active site located between the lobes and interacting with amino acids from seven different protein stretches (Mulder et al. 2010) (Fig. 2b). The structure of HYDA1 and nearly all known [FeFe]-hydrogenases from microalgae features only this one domain, known as the H-domain, which is conserved in all [FeFe]-hydrogenases (Peters et al. 2015). Since additional N-terminal domains with further electron transporting FeS-clusters are present in all non-eukaryotic [FeFe]-hydrogenases, the relative simplicity of HYDA1 contributes to it being one of the model enzymes for hydrogenase research (Lubitz et al. 2014).

Protons can reach the active site of the hydrogenase from the surface by a phylogenetically conserved proton transfer pathway through the H-domain consisting of an arginine, two glutamates, a serine, a water molecule and a cysteine (Peters et al. 1998). Variations of these amino acids were shown to drastically alter both the catalytic competence and the pH optimum of bacterial [FeFe]-hydrogenases (Cornish et al. 2011; Morra et al. 2012). Channels for the diffusion of H_2 and O_2 through the protein towards the active site were discovered in the central domain of the bacterial [FeFe]-hydrogenase CPI from *Clostridium pasteurianum* by *in silico* approaches (Hong and Pachter 2012; Cohen et al. 2005). A complex [6Fe6S]-cluster, known as the H-cluster, forms the active site of [FeFe]-hydrogenases (Fig. 2a). It comprises a standard [4Fe4S]-cluster (the $4Fe_H$-subcluster) coordinated by four cysteine residues, which is linked to a unique [2Fe]-cluster (the $2Fe_H$-subcluster) through one of the cysteines (Peters et al. 1998, 2015; Nicolet et al. 1999). The iron atoms of this $2Fe_H$-subcluster are bridged by both thiolates of a singular aza-dithiolate (adt) ligand with further ligands being one CN^- and one CO molecule per iron, as well as another CO

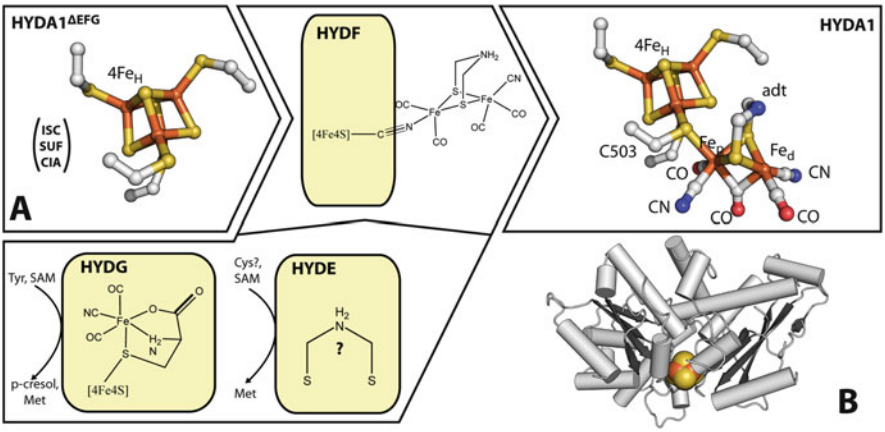

Fig. 2 Structure and maturation of the H-cluster. (**a**) HYDA1 expressed in a background devoid of specific maturases yields protein with the $4Fe_H$-subcluster only, which is supplied by the ISC, SUF or CIA systems. The maturases HYDG and HYDE synthesise parts of the $2Fe_H$-subcluster, which is probably assembled on HYDF. Transfer of the preassembled $2Fe_H$-subcluster from HYDF to HYDA1 completes the H-cluster. (**b**) Structure of HYDA1$^{\Delta EFG}$ in cartoon representation with the beta-sheets in *dark grey* and the $4Fe_H$-subcluster as spheres in *yellow* (S) and *orange* (Fe), respectively (PDB ID 3lx4) (Mulder et al. 2011)

in a bridged coordination between the two Fe atoms (Fig. 2a). While a number of amino acids are well positioned to form stabilising hydrogen bonds with the CN^- ligands in an otherwise hydrophobic active site pocket, the thiolate bond to the cysteine linking the two subsites is the only covalent connection between the $2Fe_H$-subcluster and the protein (Peters et al. 1998) (Fig. 4). In the case of the iron atom located proximal to the $4Fe_H$-subcluster (Fe_p), the linking cysteine is the sixth ligand in an octahedral coordination geometry, while the more distal iron (Fe_d), although restrained by the surrounding amino acids to the same octahedral geometry, is missing one of the axial ligands (Peters et al. 2015). This open coordination site and the amine group of the adt ligand pending above it have been identified as the key reasons for the striking difference in activity between the H-cluster within the protein and chemical compounds of similar composition (Berggren et al. 2013; Simmons et al. 2014; Esselborn et al. 2016).

3.4 Enzyme Maturation

The assembly of the H-cluster of [FeFe]-hydrogenases takes place in two stages. The $4Fe_H$-subcluster is assembled first by the standard FeS-cluster assembly machinery (Broderick et al. 2014), and then the $2Fe_H$-subcluster is added by the specific maturation enzymes HYDEF and HYDG (Posewitz et al. 2004) (Fig. 2). Recently, it became evident that the source of both CO and CN^- is tyrosine, which is

split by radical SAM chemistry in HYDG on a [4Fe4S]-cluster (Peters et al. 2015). The products are then assembled on the other end of a beta-barrel in HYDG to an Fe $(CO)_2(CN)$-cysteine-cluster at a second [4Fe4S]-cluster, turning it transiently into a [5Fe5S]-cluster (Suess et al. 2016; Pagnier et al. 2016). HYDE (in most organisms HYDE and HYDF are separate genes) also relies on radical SAM chemistry and is believed to contribute the aza-dithiolate ligand, as its substrate was shown to be a small sulphur compound (Betz et al. 2015). The product of HYDE appears to come together with two of the mono-iron clusters from HYDG onto HYDF, which serves as a scaffold for the complete [2Fe]-cluster. The interaction between the three maturases is not yet fully understood, but most likely involves GTP hydrolysis, as HYDF has been reported to have GTPase functionality (Peters et al. 2015). Once the [2Fe]-cluster is assembled on HYDF linked to a [4Fe4S]-cluster, the transfer of the [2Fe]-subcluster into the hydrogenase and assembly of the complete H-cluster takes place without additional energy input. However, it requires the $4Fe_H$-subcluster to be present within the hydrogenase (Shepard et al. 2010).

Importantly for hydrogenase research, the specific maturation machinery can be bypassed, as synthetic [2Fe]-clusters can be incorporated spontaneously into [FeFe]-hydrogenases in vitro once the $4Fe_H$-subcluster is formed either by the standard machinery in vivo or by reconstitution in vitro (Berggren et al. 2013; Esselborn et al. 2013). This yields semi-synthetic enzymes, which are indiscernible from their completely in vivo maturated counterparts.

Although much progress has been made using recombinant proteins in in vitro assays (Peters et al. 2015), neither the exact cellular mechanism, nor the cellular compartment in which the incorporation of either subcluster occurs, is known. In eukaryotic microalgae, proteins involved in the assembly of proteins with standard FeS-clusters are located in all cellular compartments, i.e. in the cytosol, plastid stroma and mitochondrial matrix (Balk and Schaedler 2014). Each plant cell compartment is able to synthesise FeS-clusters, but the machineries employed differ: the mitochondria and cytosol contain the FeS-cluster (ISC) and cytosolic FeS-protein assembly (CIA) systems, respectively, while the chloroplast utilises the sulphur mobilisation (SUF)-like machinery (Balk and Schaedler 2014). However, it is likely that the chloroplast-localised HYDA1 enzyme is assembled in the plastid compartment, as current knowledge indicates that only unfolded proteins are transported across the chloroplast outer membranes (Paila et al. 2015). Also, both HYDEF and HYDG contain putative chloroplast transit peptides, and HYDG was detected in the chloroplast in a proteomics study (Terashima et al. 2010), suggesting that at least the addition of the [2Fe]-cluster occurs in the chloroplast.

3.5 HYDA1 Catalysis

A comparative electrochemical analysis of representative [FeFe]- and [NiFe]-hydrogenases concluded that the catalytic competence of the H-cluster is inherently superior to the one from the [NiFe]-cofactor (Hexter et al. 2012). Mössbauer

spectroscopy and pulsed ENDOR/HYSCORE experiments with ^{57}Fe-enriched [FeFe]-hydrogenase showed that both subsites of the H-cluster are electronically coupled and show strong exchange interactions. Substrate binding (H^+/H_2) occurs at the open coordination site at the distal Fe centre (Fe_d) of $2Fe_H$ while being in the most oxidised "active ready" state denoted as H_{ox} (Fig. 3,1). The catalytic cycle, which either oxidatively degrades H_2 to H^+ or reductively converts two protons into H_2, presumably comprises three further catalytic main states (Fig. 3,1–4) while successively taking up or releasing two protons and electrons. The exact sequence of electron and proton transfer steps occurring during catalysis is unknown and has only been speculated to follow an ECEC mechanism in which ***e***lectron- and ***c***hemical proton-transfer steps alternate. However, electron paramagnetic

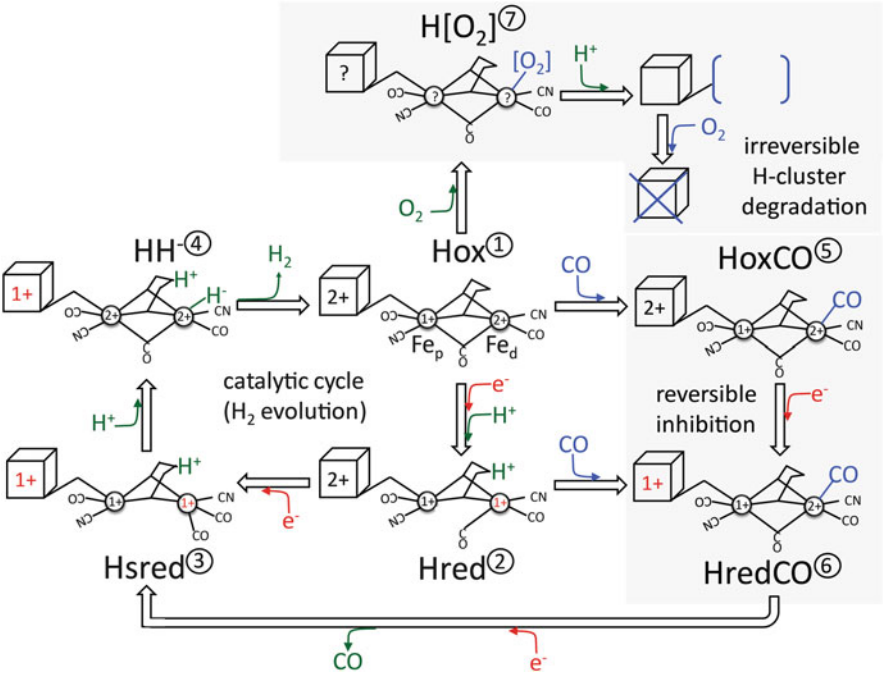

Fig. 3 Catalytic cycle of hydrogen (H_2) evolution and inhibitors of [FeFe]-hydrogenases. **1–4** Schematic working model of the reversible catalytic cycle of H_2 evolution at the H-cluster. Local redox states are indicated in *black* and *red numbers* (transiently lowered redox state). Proton transfer steps are presented according to the favoured ECEC mechanism. The *dotted line* indicates a transition of μCO from the bridging coordination to a terminally bound state. **5–6** Reversible inhibition of the two H-cluster states H_{ox} and H_{red} by CO binding to the open coordination site. Reductive reactivation is achieved via $H_{red}CO$ resulting in H_{sred} after another reduction step. **7** The irreversible process of oxygen (O_2)-induced H-cluster degradation starts with the binding of O_2 to the substrate coordination site, yielding a transient O_2 adduct which presumably requires a protonation step to induce the degradative process. Although the sequence of steps during H-cluster degradation is still under debate, recent experimental data support an initial loss of the $2Fe_H$-site before the oxidative degradation of the remaining $4Fe_H$-cluster occurs.

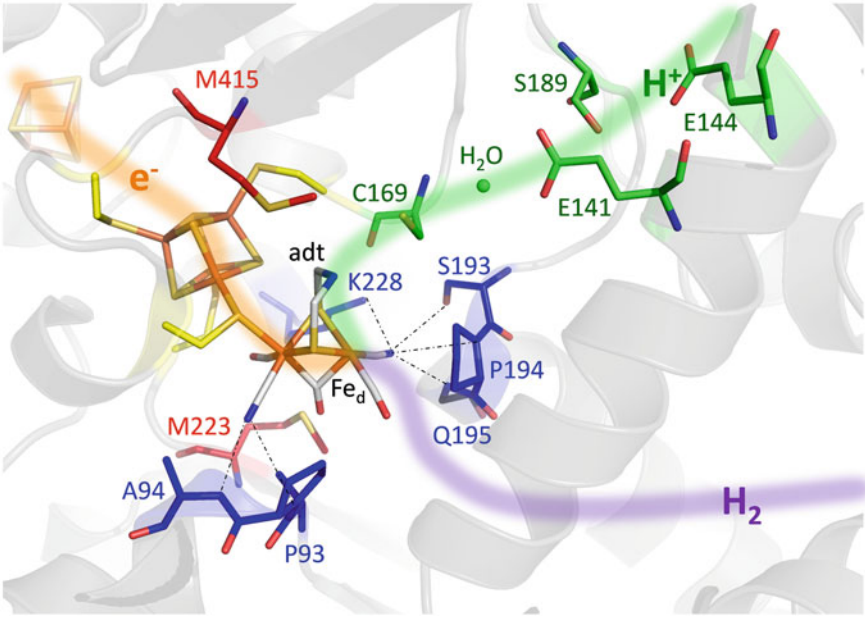

Fig. 4 First and second ligand sphere of the H-cluster in the active site of [FeFe]-hydrogenases. The model was generated using the CPI [FeFe]-hydrogenase holoprotein crystal structure (PDB ID 3C8Y) and depicts the H-cluster, as well as the most important polypeptide positions which provide the necessary environment for catalytic function (stick structures). The labelling corresponds to the homologous positions in HYDA1. Substrate/product pathways for electrons, protons and hydrogen (H_2), leading to or coming from the site of catalytic turnover at Fe_d, are indicated by an *orange*, *green* or *purple glow*, respectively. Amino acid positions contributing to the H-bond networks that stabilise the CN^- ligands are depicted in *blue*; those involved in proton transfer are presented in *green*, while the two methionine residues which allow catalytically relevant ligand movements are shown in *red*.

resonance (EPR) spectroscopy and Fourier transform infrared (FTIR) spectroscopy have enabled the detailed characterisation of the redox and spin state properties for states 1–3 (H_{ox}, H_{red} and H_{sred}). Monitoring H_2 evolution, the first reduction step occurs at the $2Fe_H$-site, thus transforming the paramagnetic H_{ox} state ($4Fe_H$(II)-Fe(I)-Fe(II)) into the EPR silent H_{red} state ($4Fe_H$(II)-Fe(I)-Fe(I)). The second reduction step is restricted to the $4Fe_H$-site, yielding the super-reduced $4Fe_H$(I)-Fe(I)-Fe(I) state (H_{sred}), which accumulates under redox potentials below −500 mV. While H_{sred} has not been found as an active state for the bacterial [FeFe]-hydrogenase DDH and is rather assumed to be an instable artificial product of over-reduction (Roseboom et al. 2006), this state has been demonstrated to be stable and catalytically relevant for the small M1-type enzymes of green algae (Adamska-Venkatesh et al. 2014; Adamska et al. 2012). The final state carrying the hydride intermediate of the heterosynthetic H_2-evolution mechanism (Fig. 3,4) has been presupposed but not yet experimentally verified for any wild-type [FeFe]-hydrogenase. However,

for the virtually inactive HYDA1 variant C169S, which displays a severely compromised proton transfer efficiency, two slightly deviating unknown states have been reported which might correspond to the protonated and unprotonated derivative of the hydride state (HH^-) (Mulder et al. 2014).

The two types of diatomic ligands at the $2Fe_H$-site (CO and CN^-) participate in adjusting its redox chemistry and spin distribution and further provide individual qualities to the H-cluster which are essential for catalytic competence (Winkler et al. 2013).

The CN^- ligands, which are coordinated in a trans orientation to each other, are embedded in strong H-bond networks on either side of the cofactor (Fig. 4, dotted lines), thereby stabilising the orientation and hexacoordinated configuration of the two Fe-sites in the $2Fe_H$-cluster (Winkler et al. 2013).

The latter aspect ensures a terminal coordination of the catalytically generated hydrido species (Fig. 3,4), which would otherwise swap to a kinetically stabilised and thus disadvantageous bridging coordination between the two Fe centres (Winkler et al. 2013). As they do not support H-bond interactions to the environment, CO ligands exhibit a higher degree of configurational flexibility, which is of significance for the role of the third CO ligand (μCO). In the oxidised state, μCO is located in a bridging configuration between both Fe sites (Fig. 3,1), while in the more reduced states (H_{red}; H_{sred}), it stabilises the higher electron density at Fe_d by switching to a terminally bound coordination (Adamska et al. 2012) (Fig. 3,2–3).

The close protein environment of the $2Fe_H$-site provides a second ligand sphere which further participates in the fine-tuning of catalytic features. Apart from the above-mentioned role of the H-bond networks in coordinating the two CN^- ligands, the second ligand sphere provides an efficient coupling to the proton transfer pathway (Fig. 4, green) and with precisely positioned methionine residues (Fig. 4, red), provides a suitable environment for structurally guided and reversible movements of individual ligands such as the proton-shuttling aza-dithiolate ligand or μCO (Knörzer et al. 2012).

Like the active sites of many enzymes, the ligand binding site on Fe_d can also be occupied by small inhibitor molecules such as formaldehyde (FA) or carbon monoxide (CO). While formaldehyde preferably binds to H_{sred} (Bachmeier et al. 2015), CO only interacts with H_{ox} or H_{red}, yielding the catalytically inactive states $H_{ox}CO$ or $H_{red}CO$ (Fig. 3,5–6), which can be reductively reactivated to yield H_{sred} (Fig. 3,3) (Adamska-Venkatesh et al. 2014).

3.6 *Oxygen Sensitivity*

The reversible inhibitory effect of CO and the irreversibly destructive influence of O_2 on the activity of algal hydrogenases were first described for whole cell extracts of *C. reinhardtii* in the late 1970s. It was further demonstrated that the destructive influence of O_2 is antagonised by pre-exposing the cell extract to CO (Erbes et al. 1979). The protective effect of CO gassing prior to O_2 exposure was later

systematically examined by protein film voltammetry, where *C. reinhardtii* HYDA1 was compared to different bacterial-type [FeFe]-hydrogenases (Goldet et al. 2009; Stripp et al. 2009). In contrast to [NiFe]-hydrogenases, all known [FeFe]-hydrogenases exhibit extraordinary high levels of O_2 sensitivity; however different enzyme subtypes show different nuances of sensitivity resulting from differing accessibilities of the gas channel system for O_2 and slight differences in the binding affinities of Fe_d for O_2. The authors further concluded that CO competitively occupies the initial binding site of O_2, thus preventing the following destructive process from being initiated.

Freeze drying renders [FeFe]-hydrogenases surprisingly insensitive towards O_2 (Noth et al. 2015). X-ray absorption spectroscopy demonstrates that exposure of lyophilized [FeFe]-hydrogenase to O_2 results in a stable O_2 adduct which might correspond to a trapped version of the otherwise highly transient initial reaction product between Fe_d and O_2. As proton transfer activity of hydrogenases has been demonstrated to be severely hampered in the freeze dried state, it can be speculated that protonation of the first O_2 adduct is essential for initiating the destructive downstream processes that lead to the irreversible loss of both H-cluster components (Fig. 3,7) (Noth et al. 2015).

While the formation of an initial O_2 adduct is uniformly accepted, the following sequence of events leading to the irreversible degradation of both H-cluster components is still under debate. XAS spectroscopy suggests the production of a reactive oxygen species which detaches from Fe_d and attacks the $4Fe_H$-site before a loss of the $2Fe_H$-cluster can be demonstrated (Stripp et al. 2009; Lambertz et al. 2011). A more recent examination instead favours a loss of the $2Fe_H$-cluster prior to the oxidative degradation of the $4Fe_H$-cluster (Fig. 3,7). The latter model is strongly supported by the fact that a large fraction of the O_2-inactivated enzyme can be reactivated by supplying synthetic [2Fe]-cofactor as a substitute for the lost H-cluster component (Swanson et al. 2015).

4 Photobiological H_2 Production in Practice

As O_2 gradually accumulates during photosynthesis, photobiological H_2 production requires the balancing of oxygenic photosynthesis and cell growth with anaerobic H_2 production. The standard approach for this involves first growing the algae aerobically, to allow for carbon fixation, cell growth and the build-up of carbohydrates, before inducing anaerobiosis and therefore H_2 production via nutrient deprivation. The most common induction method is sulphur deprivation (Melis et al. 2000). Sulphur deprivation results in anaerobiosis due to a reduction in the rate of repair of the PSII reaction centre protein, D1, as a result of a limitation in the sulphur-containing amino acids methionine and cysteine, which are required for D1 protein synthesis. This reduces the level of O_2 production below respiration, resulting in anaerobiosis and *HYDA1* gene expression. Sulphur deprivation also

results in the build-up of starch (Zhang et al. 2002), which is subsequently degraded during H_2 production (Hemschemeier et al. 2008a).

Anaerobiosis can also be achieved through the deprivation of other nutrients. This is possible as the limitation of any macronutrient results in a number of general nutrient deficiency responses in *C. reinhardtii*, many of which are conducive for H_2 production, such as the accumulation of starch and a reduction in photosynthetic O_2 evolution (Ball et al. 1990; Gonzalez-Ballester et al. 2015; Grossman et al. 2010; Zhang et al. 2002; Wykoff et al. 1998). The deprivation of nitrogen (Philipps et al. 2012), phosphorous (Batyrova et al. 2012) and magnesium (Volgusheva et al. 2015) have all been shown to induce H_2 production. Nitrogen and phosphorous deprivation resulted in lower levels of H_2 production compared to sulphur deprivation. In contrast, magnesium deprivation resulted in higher levels of H_2 production (Volgusheva et al. 2015). This was thought to be due to a prolonged H_2 production period of over 7 days, an increased respiration and starch accumulation and a smaller decrease in functional PSII [PSII was only reduced by 20% instead of 80% as in sulphur deprivation (Volgusheva et al. 2013)], resulting in a higher electron availability to the hydrogenase (Volgusheva et al. 2015).

5 Targets for Improved Microalgal H_2 Production

The major problem with nutrient deprivation is that H_2 production cannot be sustained for more than a few days. This is because the algae eventually die due to the lack of the respective nutrient. Therefore, the prolongation of photobiological H_2 production via other strategies has been the focus of much research. Significantly higher H_2 production efficiencies are required in order for biological H_2 production to be commercially viable. Microalgae systems currently only have photon conversion efficiencies of 3%, while the theoretical maximum is ~12–14% (Scoma et al. 2012; Volgusheva et al. 2013). The highest efficiency strains will therefore require a combination of strategies and involve significant re-engineering of the H_2 production process. The ultimate goal is continuous H_2 production where O_2 production and consumption are in balance and the water-splitting reaction is active at the same time as the hydrogenase.

However, there are a few major factors currently limiting sustained H_2 production. These include proton and electron supply to the hydrogenase and the extreme oxygen sensitivity of the hydrogenase enzyme. Factors limiting the growth of the algae and photosynthetic efficiency, such as light capture, also limit H_2 production. In attempts to overcome these bottlenecks, extensive genetic engineering has been performed. A number of high H_2-producing mutants with improvements in one or more of these bottlenecks have been generated and are detailed below. A tabular summary of the various mutants and their H_2 production efficiencies can also be found in the recent review by Dubini and Ghirardi (2015).

5.1 Electron Supply to the Hydrogenase

Electron flow to the hydrogenase is one of the main bottlenecks for sustainable H_2 production. This is due to the large number of other pathways competing for electrons from PETF (Winkler et al. 2011). For example, ferredoxin-$NADP^+$ reductase (FNR), sulphite reductase, nitrate reductase, glutamate synthase and fatty acid desaturases all compete with HYDA1 for electrons (Hemschemeier and Happe 2011). To improve electron flow to the hydrogenase, PETF, FNR and the hydrogenase itself have all been engineered (Long et al. 2009; Yacoby et al. 2011; Wittenberg et al. 2013; Lubner et al. 2011; Rumpel et al. 2014; Sun et al. 2013). For example, a PETF variant with a reduced affinity for FNR has been developed (Rumpel et al. 2014), and PETF and PSI have both been fused to the hydrogenase (Yacoby et al. 2011; Lubner et al. 2011). However, all of the above work has so far only been performed in vitro and remains to be tested in vivo.

Engineering has also focused on various indirect targets. For example, small and large subunit Rubisco mutants (Pinto et al. 2013; Hemschemeier et al. 2008b), cyclic electron flow (CEF) mutants (Kruse et al. 2005; Johnson et al. 2014; Steinbeck et al. 2015; Tolleter et al. 2011), starch degradation mutant strains (Chochois et al. 2009) and respiration mutants (Ruehle et al. 2008) have all been reported to display increased H_2 production levels. In fact, the cyclic electron flow mutants *state transition 6 (Stm6)* (Kruse et al. 2005) and the *proton gradient regulation like 1 (pgrl1)* (Tolleter et al. 2011) and *pgr5* mutants (Steinbeck et al. 2015) have been reported to have the highest H_2 production rates, producing between 540 and 840 mL of H_2 per litre of culture, which is $\sim$10$\times$ that produced by wild-type *C. reinhardtii*. Interestingly, these high H_2-producing mutants all display similar phenotypes: they have an enhanced oxygen consumption capacity and thus increased PSII stability and electron supply to the hydrogenase. The mutant cultures also become anaerobic earlier than the wild type following sulphur deprivation, which is thought to result in an increase in PSII stability due to a reduction in photo-oxidative damage (Steinbeck et al. 2015; Volgusheva et al. 2013). It is important to note that *Stm6* also has increased starch reserves compared to the wild type and thus more available substrate (Kruse et al. 2005).

The effect of adding extra components to the photosynthetic electron transfer pathway has also been tested. The expression of plastid-expressed NAD(P)H dehydrogenase (Baltz et al. 2014) and native and exogenous hydrogenases (Reifschneider-Wegner et al. 2014; Chien et al. 2012) has all been reported.

5.2 Proton Supply to the Hydrogenase

Proton supply to the hydrogenase is another bottleneck for H_2 production. This is because the ATP requirement drops during H_2 production (Das et al. 2014), resulting in a reduced electron transport at cytochrome b_6f (Burgess et al. 2011;

Antal et al. 2009) and an impaired dissipation of the proton gradient and therefore decreased proton availability for the hydrogenase. One strategy to improve H_2 production is to artificially dissipate the proton gradient to increase H_2 production transiently in the presence of the chemical uncoupler carbonyl cyanide *m*-chlorophenyl hydrazine (CCCP), which causes an efflux of protons from the thylakoid lumen into the stroma (Lee 2013; Kruse et al. 2005; Lee and Greenbaum 2003). This suggests that the integration of a proton channel into the thylakoid membrane could more permanently restore proton and electron flow to the hydrogenase. Such a proton channel however would need to be inducibly expressed, as the addition of the uncoupler prior to anaerobiosis was found to abolish hydrogenase activity, suggesting that the proton gradient is important for initial hydrogenase expression (Lee 2013) and aerobic growth. A similar strategy involves the development of a leaky ATPase to increase proton flow and reduce ATP production (Das et al. 2014; Robertson et al. 1990). Reduced ATP production caused by the introduction of a proton channel or mutated ATPase may additionally reduce reactions competing for reducing equivalents and therefore increase electron supply to the hydrogenase (Kumar and Das 2013).

5.3 Oxygen Sensitivity of the Hydrogenase

Sustained H_2 production under standard growth conditions remains a major challenge. The O_2 sensitivity of the hydrogenase is a multifaceted problem due to the fact that O_2 not only inhibits the activity of the hydrogenase enzyme, but also transcription and protein maturation (Cohen et al. 2005). However, to produce H_2 from water using photosynthesis, O_2 will be released; hence O_2 production (photosynthesis) needs to be balanced with O_2 consumption (respiration). Approaches have focused on developing O_2-tolerant hydrogenases or changing the balance between O_2 production and O_2 consumption. As detailed in Sect. 5.1, the highest reported H_2-producing mutants all display increased respiration rates and reach anaerobiosis earlier than the wild type following sulphur deprivation (Kruse et al. 2005; Steinbeck et al. 2015; Schonfeld et al. 2004), thus obtaining the correct balance between oxygen evolution and oxygen consumption appears to be of vital importance for further improvements in H_2 production efficiencies.

Several genetic engineering approaches have been utilised to reduce the O_2 sensitivity of the hydrogenase (reviewed in Ghirardi 2015), including random mutagenesis (Flynn et al. 2002) and targeted mutagenesis of the catalytic site to restrict O_2 access (Stiebritz and Reiher 2012). While engineering approaches have been successful for a bacterial [NiFe]-hydrogenase (Dementin et al. 2009), there has so far been no success for the microalgal [FeFe]-hydrogenase. However, two algae strains were recently reported to be able to express the hydrogenase in the presence of more than 21% O_2 and to produce low levels of H_2 at 15% atmospheric O_2 (Hwang et al. 2014). One problem with an O_2-tolerant hydrogenase however, is

that H_2 would be produced alongside O_2, which would make gas separation difficult and potentially lead to a dangerous gas mixture.

Balancing O_2 production and consumption is perhaps a better, more feasible approach and has already been demonstrated in a number of studies. Photosystem II itself has been the target of engineering. For example, mutant strains with downregulated PSII subunits (Surzycki et al. 2007; Lin et al. 2013) and a mutant containing amino acid substitutions in the D1 protein (Scoma et al. 2012; Torzillo et al. 2009) all displayed increased H_2 production efficiencies. The repression of *psbD* translation (Surzycki et al. 2007) and the downregulation of *psbO* in *Chlorella* sp. *DT* (Lin et al. 2013) both resulted in a lower O_2 evolution. A double amino acid substitution in the D1 protein resulted in an increase in the quantum yield of photosynthesis, a higher respiration rate, a higher carbohydrate accumulation following sulphur deprivation and a higher synthesis of xanthophyll cycle pigments, which was proposed to result in an improved photoprotection (Torzillo et al. 2009, 2015). A mutant with an inactivated Calvin-Benson cycle also displayed a higher respiration rate and higher H_2 evolution compared to the sulphur-deprived wild type (Ruehle et al. 2008).

Alternative approaches have also been tested to control the balance between oxygen evolution and consumption. Leghemoglobins, which are able to sequester O_2, have been expressed in *C. reinhardtii* (Wu et al. 2010, 2011), as has a pyruvate oxidase from *E. coli*, which was found to lower O_2 evolution (Xu et al. 2011). A sulphate permease mutant was also developed, which allowed a greater control over sulphur deprivation (Chen et al. 2005). Another approach targeting controlled sulphur deprivation implemented sulphur microdosing (Kosourov et al. 2005), whereby the sulphur in a sulphur-deprived culture was replaced in small amounts, allowing the repair of PSII and renewed production of protons and electrons to drive H_2 production. Finally, cocultivation of algae and bacteria was reported to result in algal anaerobiosis due to an increased bacterial respiration (Lakatos et al. 2014).

5.4 Indirect Targets

Hydrogen production can be improved further by optimising the general culture conditions. For example, light capture can be optimised so that the photosystems function to their maximal capacities. The LHC antennae systems function to capture photons and dissipate excess light energy to provide photoprotection (Takahashi et al. 2006; Niyogi 1999; Pascal et al. 2005; Oey et al. 2013). Biomass production efficiency, at least in the laboratory, can be improved by reducing LHC antenna size, as this enhances light distribution through the bioreactors and enables the use of increased operational cell concentrations, resulting in improved overall photosynthetic efficiencies (Melis et al. 1999; Mussgnug et al. 2007; Polle et al. 2003; Oey et al. 2013; Beckmann et al. 2009). A number of *C. reinhardtii* antenna mutants have been developed, including *Stm6Glc4T7*, a mutant expressing a permanently active LHC translational repressor NAB1, which resulted in a 10–17%

reduction in LHC antenna size and a ~50% increase in photosynthetic efficiency (Beckmann et al. 2009); *tla1 (truncated light-harvesting Chl antenna)*, an insertional mutant with a reduced LHCI and LHCII antenna complex (50% and 65% of the wild type, respectively) (Polle et al. 2003; Kosourov et al. 2011); and *LO1*, an RNAi knockdown of LHCBM1, 2 and 3 (21%, 81% and 41% expression of *LHCBM1*, *2* and *3*, respectively) (Oey et al. 2013).

6 Conclusion

Microalgal H_2 production is not only a fascinating biological phenomenon but is also of enormous biotechnological significance, as it offers a carbon neutral or even carbon negative approach for renewable energy production. In the more than 20 years since HYDA1 was isolated, remarkable progress has been made in elucidating this protein's structure, catalytic mechanism, induction and regulation. This in vitro groundwork has provided us with a detailed understanding of the enzyme and has paved the way for its in vivo engineering. Considerable work has also been carried out at the physiological level, and a large number of mutants displaying enhanced H_2 productions have now been created. To date, the mutants with the highest reported H_2 production rates have been the CEF mutants, which share the phenotype of an increased oxygen consumption, earlier onset of anaerobiosis and more stable PSII in common. However, further improvements are needed if microalgal H_2 production is to become a commercial reality, particularly in regards to limitations in electron transport, competition for reductants from ferredoxin and the O_2 sensitivity of the enzyme. The most successful approach is likely the combination of a number of different strategies. Solar conversion efficiency also needs to be improved. However, unresolved questions regarding, for example, the underlying regulation of HYDA1 in algae, need to be understood before such improvements can be made. Despite this, we are in a good position to solve these questions, and hopefully a H_2 economy is no longer a distant dream but a future reality.

References

Adamska A, Silakov A, Lambertz C, Rudiger O, Happe T, Reijerse E, Lubitz W (2012) Identification and characterization of the "super-reduced" state of the H-cluster in [FeFe] hydrogenase: a new building block for the catalytic cycle? Angew Chem Int Ed Engl 51 (46):11458–11462. doi:10.1002/anie.201204800

Adamska-Venkatesh A, Krawietz D, Siebel J, Weber K, Happe T, Reijerse E, Lubitz W (2014) New redox states observed in [FeFe] hydrogenases reveal redox coupling within the H-cluster. J Am Chem Soc 136(32):11339–11346. doi:10.1021/ja503390c

Antal TK, Volgusheva AA, Kukarskih GP, Krendeleva TE, Rubin AB (2009) Relationships between H_2 photoproduction and different electron transport pathways in sulfur-deprived *Chlamydomonas reinhardtii*. Int J Hydrog Energy 34(22):9087–9094. doi:10.1016/j.ijhydene.2009.09.011

Antal TK, Krendeleva TE, Tyystjarvi E (2015) Multiple regulatory mechanisms in the chloroplast of green algae: relation to hydrogen production. Photosynth Res 125(3):357–381. doi:10.1007/s11120-015-0157-2

Atteia A, van Lis R, Tielens AGM, Martin WF (2013) Anaerobic energy metabolism in unicellular photosynthetic eukaryotes. Biochim Biophys Acta Bioenerg 1827(2):210–223. doi:10.1016/j.bbabio.2012.08.002

Bachmeier A, Esselborn J, Hexter SV, Kramer T, Klein K, Happe T, McGrady JE, Myers WK, Armstrong FA (2015) How formaldehyde inhibits hydrogen evolution by [FeFe]-hydrogenases: determination by (1)(3)C ENDOR of direct Fe-C coordination and order of electron and proton transfers. J Am Chem Soc 137(16):5381–5389. doi:10.1021/ja513074m

Balk J, Schaedler TA (2014) Iron cofactor assembly in plants. Annu Rev Plant Biol 65:125–153. doi:10.1146/annurev-arplant-050213-035759

Ball SG, Dirick L, Decq A, Martiat JC, Matagne RF (1990) Physiology of starch storage in the monocellular alga *Chlamydomonas reinhardtii*. Plant Sci 66(1):1–9. doi:10.1016/0168-9452(90)90162-h

Baltz A, Kieu-Van D, Beyly A, Auroy P, Richaud P, Cournac L, Peltier G (2014) Plastidial expression of type II NAD(P)H dehydrogenase increases the reducing state of Plastoquinones and hydrogen photoproduction rate by the indirect pathway in *Chlamydomonas reinhardtii*. Plant Physiol 165(3):1344–1352. doi:10.1104/pp.114.240432

Batyrova KA, Tsygankov AA, Kosourov SN (2012) Sustained hydrogen photoproduction by phosphorus-deprived *Chlamydomonas reinhardtii* cultures. Int J Hydrog Energy 37(10):8834–8839. doi:10.1016/j.ijhydene.2012.01.068

Beckmann J, Lehr F, Finazzi G, Hankamer B, Posten C, Wobbe L, Kruse O (2009) Improvement of light to biomass conversion by de-regulation of light-harvesting protein translation in *Chlamydomonas reinhardtii*. J Biotechnol 142(1):70–77. doi:10.1016/j.jbiotec.2009.02.015

Berggren G, Adamska A, Lambertz C, Simmons TR, Esselborn J, Atta M, Gambarelli S, Mouesca JM, Reijerse E, Lubitz W, Happe T, Artero V, Fontecave M (2013) Biomimetic assembly and activation of FeFe-hydrogenases. Nature 499(7456):66–69. doi:10.1038/nature12239

Betz JN, Boswell NW, Fugate CJ, Holliday GL, Akiva E, Scott AG, Babbitt PC, Peters JW, Shepard EM, Broderick JB (2015) [FeFe]-hydrogenase maturation: insights into the role HydE plays in dithiomethylamine biosynthesis. Biochemistry 54(9):1807–1818. doi:10.1021/bi501205e

Broderick JB, Byer AS, Duschene KS, Duffus BR, Betz JN, Shepard EM, Peters JW (2014) H-cluster assembly during maturation of the [FeFe]-hydrogenase. J Biol Inorg Chem 19(6):747–757. doi:10.1007/s00775-014-1168-8

Burgess SJ, Tamburic B, Zemichael F, Hellgardt K, Nixon PJ (2011) Solar-driven hydrogen production in green algae. In: Laskin AI, Sariaslani S, Gadd GM (eds) Advances in applied microbiology, vol 75, pp 71–110. doi:10.1016/b978-0-12-387046-9.00004-9

Castruita M, Casero D, Karpowicz SJ, Kropat J, Vieler A, Hsieh SI, Yan W, Cokus S, Loo JA, Benning C, Pellegrini M, Merchant SS (2011) Systems biology approach in *Chlamydomonas* reveals connections between copper nutrition and multiple metabolic steps. Plant Cell 23(4):1273–1292. doi:10.1105/tpc.111.084400

Chen HC, Newton AJ, Melis A (2005) Role of *SulP*, a nuclear-encoded chloroplast sulfate permease, in sulfate transport and H_2 evolution in *Chlamydomonas reinhardtii*. Photosynth Res 84(1–3):289–296. doi:10.1007/s11120-004-7157-y

Chien LF, Kuo TT, Liu BH, Lin HD, Feng TY, Huang CC (2012) Solar-to-bio H_2 production enhanced by homologous overexpression of hydrogenase in green alga *Chlorella sp*. DT. Int J Hydrog Energy 37(23):17738–17748. doi:10.1016/j.ijhydene.2012.09.068

Chochois V, Dauvillee D, Beyly A, Tolleter D, Cuine S, Timpano H, Ball S, Cournac L, Peltier G (2009) Hydrogen production in *Chlamydomonas*: photosystem II-dependent and -independent pathways differ in their requirement for starch metabolism. Plant Physiol 151(2):631–640. doi:10.1104/pp.109.144576

Cohen J, Kim K, Posewitz M, Ghirardi ML, Schulten K, Seibert M, King P (2005) Molecular dynamics and experimental investigation of H_2 and O_2 diffusion in Fe-hydrogenase. Biochem Soc Trans 33:80–82

Cornish AJ, Gaertner K, Yang H, Peters JW, Hegg EL (2011) Mechanism of proton transfer in [FeFe]-hydrogenase from *Clostridium pasteurianum*. J Biol Chem 286(44):38341–38347. doi:10.1074/jbc.M111.254664

Das D, Khanna N, Dasgupta CN (2014) Biohydrogen production: fundamentals and technology advances. CRC Press, London

Dementin S, Leroux F, Cournac L, de Lacey AL, Volbeda A, Leger C, Burlat B, Martinez N, Champ S, Martin L, Sanganas O, Haumann M, Fernandez VM, Guigliarelli B, Fontecilla-Camps JC, Rousset M (2009) Introduction of methionines in the gas channel makes NiFe hydrogenase aero-tolerant. J Am Chem Soc 131(29):10156–10164. doi:10.1021/ja9018258

Desplats C, Mus F, Cuine S, Billon E, Cournac L, Peltier G (2009) Characterization of Nda2, a plastoquinone-reducing type II NAD(P)H dehydrogenase in *Chlamydomonas* chloroplasts. J Biol Chem 284(7):4148–4157. doi:10.1074/jbc.M804546200

Dubini A, Ghirardi ML (2015) Engineering photosynthetic organisms for the production of biohydrogen. Photosynth Res 123(3):241–253. doi:10.1007/s11120-014-9991-x

Erbes DL, King D, Gibbs M (1979) Inactivation of hydrogenase in cell-free extracts and whole cells of *Chlamydomonas reinhardi* by oxygen. Plant Physiol 63(6):1138–1142

Esselborn J, Lambertz C, Adamska-Venkatesh A, Simmons T, Berggren G, Nothl J, Siebel J, Hemschemeier A, Artero V, Reijerse E, Fontecave M, Lubitz W, Happe T (2013) Spontaneous activation of FeFe-hydrogenases by an inorganic 2Fe active site mimic. Nat Chem Biol 9 (10):607–609. doi:10.1038/nchembio.1311

Esselborn J, Muraki N, Klein K, Engelbrecht V, Metzler-Nolte N, Apfel UP, Hofmann E, Kurisu G, Happe T (2016) A structural view of synthetic cofactor integration into [FeFe]-hydrogenases. Chem Sci 7(2):959–968. doi:10.1039/c5sc03397g

Flynn T, Ghirardi ML, Seibert M (2002) Accumulation of O_2-tolerant phenotypes in H_2-producing strains of *Chlamydomonas reinhardtii* by sequential applications of chemical mutagenesis and selection. Int J Hydrog Energy 27(11–12):1421–1430. doi:10.1016/s0360-3199(02)00117-9

Forestier M, King P, Zhang LP, Posewitz M, Schwarzer S, Happe T, Ghirardi ML, Seibert M (2003) Expression of two [Fe]-hydrogenases in *Chlamydomonas reinhardtii* under anaerobic conditions. Eur J Biochem 270(13):2750–2758. doi:10.1046/j.1432-1033.2003.03656

Fouchard S, Hemschemeier A, Caruana A, Pruvost K, Legrand J, Happe T, Peltier G, Cournac L (2005) Autotrophic and mixotrophic hydrogen photoproduction in sulfur-deprived *Chlamydomonas* cells. Appl Environ Microbiol 71(10):6199–6205. doi:10.1128/aem.71.10.6199-6205.2005

Gaffron H, Rubin J (1942) Fermentative and photochemical production of hydrogen in algae. J Gen Physiol 26(2):219–240. doi:10.1085/jgp.26.2.219

Ghirardi ML (2015) Implementation of photobiological H_2 production: the O_2 sensitivity of hydrogenases. Photosynth Res 125(3):383–393. doi:10.1007/s11120-015-0158-1

Ghirardi ML, Posewitz MC, Maness P-C, Dubini A, Yu J, Seibert M (2007) Hydrogenases and hydrogen photoproduction in oxygenic photosynthetic organisms. Annu Rev Plant Biol 58:71–91. doi:10.1146/annurev.arplant.58.032806.103848

Godde D, Trebst A (1980) NADH as electron donor for the photosynthetic membrane of *Chlamydomonas reinhardtii*. Arch Microbiol 127(3):245–252. doi:10.1007/bf00427200

Goldet G, Brandmayr C, Stripp ST, Happe T, Cavazza C, Fontecilla-Camps JC, Armstrong FA (2009) Electrochemical kinetic investigations of the reactions of FeFe-hydrogenases with carbon monoxide and oxygen: comparing the importance of gas tunnels and active-site electronic/redox effects. J Am Chem Soc 131(41):14979–14989. doi:10.1021/ja905388j

Gonzalez-Ballester D, Luis Jurado-Oller J, Fernandez E (2015) Relevance of nutrient media composition for hydrogen production in Chlamydomonas. Photosynth Res 125(3):395–406. doi:10.1007/s11120-015-0152-7

Grossman AR, Gonzalez-Ballester D, Shibagaki N, Pootakham W, Moseley J, Pootakham W (2010) Responses to macronutrient deprivation. In: Abiotic stress adaptation in plants: physiological, molecular and genomic foundation. Springer, Dordrecht. doi:10.1007/978-90-481-3112-9_15

Grossman AR, Catalanotti C, Yang W, Dubini A, Magneschi L, Subramanian V, Posewitz MC, Seibert M (2011) Multiple facets of anoxic metabolism and hydrogen production in the unicellular green alga *Chlamydomonas reinhardtii*. New Phytol 190(2):279–288. doi:10.1111/j.1469-8137.2010.03534.x

Gupta SK, Kumari S, Reddy K, Bux F (2013) Trends in biohydrogen production: major challenges and state-of-the-art developments. Environ Technol 34(13–14):1653–1670. doi:10.1080/09593330.2013.822022

Happe T, Kaminski A (2002) Differential regulation of the Fe-hydrogenase during anaerobic adaptation in the green alga *Chlamydomonas reinhardtii*. Eur J Biochem 269(3):1022–1032. doi:10.1046/j.0014-2956.2001.02743.x

Happe T, Naber JD (1993) Isolation, characterization and N-terminal amino acid sequence of hydrogenase from the green alga *Chlamydomonas reinhardtii*. Eur J Biochem 214(2):475–481. doi:10.1111/j.1432-1033.1993.tb17944.x

Happe T, Mosler B, Naber JD (1994) Induction, localization and metal content of hydrogenase in the green alga *Chlamydomonas reinhardtii*. Eur J Biochem 222(3):769–774. doi:10.1111/j.1432-1033.1994.tb18923.x

Hemschemeier A, Happe T (2011) Alternative photosynthetic electron transport pathways during anaerobiosis in the green alga *Chlamydomonas reinhardtii*. BBA-Bioenergetics 1807(8):919–926. doi:10.1016/j.bbabio.2011.02.010

Hemschemeier A, Fouchard S, Cournac L, Peltier G, Happe T (2008a) Hydrogen production by *Chlamydomonas reinhardtii*: an elaborate interplay of electron sources and sinks. Planta 227(2):397–407. doi:10.1007/s00425-007-0626-8

Hemschemeier A, Jacobs J, Happe T (2008b) Biochemical and physiological characterization of the pyruvate Formate-Lyase Pfl1 of *Chlamydomonas reinhardtii*, a typically bacterial enzyme in a eukaryotic alga. Eukaryot Cell 7(3):518–526. doi:10.1128/ec.00368-07

Hemschemeier A, Casero D, Liu BS, Benning C, Pellegrini M, Happe T, Merchant SS (2013) Copper response regulator1-dependent and -independent responses of the *Chlamydomonas reinhardtii* Transcriptome to dark anoxia. Plant Cell 25(9):3186–3211. doi:10.1105/tpc.113.115741

Hexter SV, Grey F, Happe T, Climent V, Armstrong FA (2012) Electrocatalytic mechanism of reversible hydrogen cycling by enzymes and distinctions between the major classes of hydrogenases. Proc Natl Acad Sci U S A 109(29):11516–11521. doi:10.1073/pnas.1204770109

Hong G, Pachter R (2012) Inhibition of biocatalysis in [Fe–Fe] hydrogenase by oxygen: molecular dynamics and density functional theory calculations. ACS Chem Biol 7(7):1268–1275. doi:10.1021/cb3001149

Hwang J-H, Kim H-C, Choi J-A, Abou-Shanab RAI, Dempsey BA, Regan JM, Kim JR, Song H, Nam I-H, Kim S-N, Lee W, Park D, Kim Y, Choi J, Ji M-K, Jung W, Jeon B-H (2014) Photoautotrophic hydrogen production by eukaryotic microalgae under aerobic conditions. Nat Commun 5. doi:10.1038/ncomms4234

Jans F, Mignolet E, Houyoux P-A, Cardol P, Ghysels B, Cuine S, Cournac L, Peltier G, Remacle C, Franck F (2008) A type II NAD(P) H dehydrogenase mediates light-independent plastoquinone reduction in the chloroplast of *Chlamydomonas*. Proc Natl Acad Sci U S A 105(51):20546–20551. doi:10.1073/pnas.0806896105

Johnson X, Steinbeck J, Dent RM, Takahashi H, Richaud P, Ozawa SI, Houille-Vernes L, Petroutsos D, Rappaport F, Grossman AR, Niyogi KK, Hippler M, Alric J (2014) Proton gradient regulation 5-mediated cyclic electron flow under ATP- or redox-limited conditions: a study of Δ*ATPase pgr5* and Δ*rbcL pgr5* mutants in the green alga *Chlamydomonas reinhardtii*. Plant Physiol 165(1):438–452. doi:10.1104/pp.113.233593

Knörzer P, Silakov A, Foster CE, Armstrong FA, Lubitz W, Happe T (2012) Importance of the protein framework for catalytic activity of [FeFe]-hydrogenases. J Biol Chem 287(2):1489–1499. doi:10.1074/jbc.M111.305797

Kosourov S, Makarova V, Fedorov AS, Tsygankov A, Seibert M, Ghirardi ML (2005) The effect of sulfur re-addition on H_2 photoproduction by sulfur-deprived green algae. Photosynth Res 85 (3):295–305. doi:10.1007/s11120-005-5105-0

Kosourov SN, Ghirardi ML, Seibert M (2011) A truncated antenna mutant of *Chlamydomonas reinhardtii* can produce more hydrogen than the parental strain. Int J Hydrog Energy 36 (3):2044–2048. doi:10.1016/j.ijhydene.2010.10.041

Kropat J, Tottey S, Birkenbihl RP, Depege N, Huijser P, Merchant S (2005) A regulator of nutritional copper signaling in *Chlamydomonas* is an SBP domain protein that recognizes the GTAC core of copper response element. Proc Natl Acad Sci U S A 102(51):18730–18735. doi:10.1073/pnas.0507693102

Kruse O, Rupprecht J, Bader KP, Thomas-Hall S, Schenk PM, Finazzi G, Hankamer B (2005) Improved photobiological H_2 production in engineered green algal cells. J Biol Chem 280 (40):34170–34177. doi:10.1074/jbc.M503840200

Kumar K, Das D (2013) CO_2 sequestration and hydrogen production using cyanobacteria and green algae. In: Natural and artificial photosynthesis. Wiley, New York, pp 173–215. doi:10.1002/9781118659892.ch6

Lakatos G, Deak Z, Vass I, Retfalvi T, Rozgonyi S, Rakhely G, Oerdoeg V, Kondorosi E, Maroti G (2014) Bacterial symbionts enhance photo-fermentative hydrogen evolution of *Chlamydomonas* algae. Green Chem 16(11):4716–4727. doi:10.1039/c4gc00745j

Lambertz C, Leidel N, Havelius KGV, Noth J, Chernev P, Winkler M, Happe T, Haumann M (2011) O_2 reactions at the six-iron active site (H-cluster) in [FeFe]-hydrogenase. J Biol Chem 286(47):40614–40623. doi:10.1074/jbc.M111.283648

Lee J (2013) Designer transgenic algae for photobiological production of hydrogen from water. In: Lee JW (ed) Advanced biofuels and bioproducts. Springer, New York, pp 371–404. doi:10.1007/978-1-4614-3348-4_20

Lee JW, Greenbaum E (2003) A new oxygen sensitivity and its potential application in photosynthetic H_2 production. Appl Biochem Biotechnol 105:303–313

Lin H-D, Liu B-H, Kuo T-T, Tsai H-C, Feng T-Y, Huang C-C, Chien L-F (2013) Knockdown of PsbO leads to induction of HydA and production of photobiological H_2 in the green alga *Chlorella* sp. DT. Bioresour Technol 143:154–162. doi:10.1016/j.biortech.2013.05.101

Long H, King PW, Ghirardi ML, Kim K (2009) Hydrogenase/Ferredoxin charge-transfer complexes: effect of hydrogenase mutations on the complex association. J Phys Chem A 113(16):4060–4067. doi:10.1021/jp810409z

Lubitz W, Ogata H, Rudiger O, Reijerse E (2014) Hydrogenases. Chem Rev 114(8):4081–4148. doi:10.1021/cr4005814

Lubner CE, Applegate AM, Knoerzer P, Ganago A, Bryant DA, Happe T, Golbeck JH (2011) Solar hydrogen-producing bionanodevice outperforms natural photosynthesis. Proc Natl Acad Sci U S A 108(52):20988–20991. doi:10.1073/pnas.1114660108

Ludwig M, Schulz-Friedrich R, Appel J (2006) Occurrence of hydrogenases in cyanobacteria and anoxygenic photosynthetic bacteria: implications for the phylogenetic origin of cyanobacterial and algal hydrogenases. J Mol Evol 63(6):758–768. doi:10.1007/s00239-006-0001-6

Maione TE, Gibbs M (1986) Association of the chloroplastic respiratory and photosynthetic electron transport chains of *Chlamydomonas reinhardtii* with photoreduction and the oxyhydrogen reaction. Plant Physiol 80(2):364–368. doi:10.1104/pp.80.2.364

Melis A, Happe T (2001) Hydrogen production. Green algae as a source of energy. Plant Physiol 127(3):740–748

Melis A, Neidhardt J, Benemann J (1999) *Dunaliella salina* (Chlorophyta) with small chlorophyll antenna sizes exhibit higher photosynthetic productivities and photon use efficiencies than normally pigmented cells. J Appl Phycol 10(6):515–525. doi:10.1023/a:1008076231267

Melis A, Zhang LP, Forestier M, Ghirardi ML, Seibert M (2000) Sustained photobiological hydrogen gas production upon reversible inactivation of oxygen evolution in the green alga *Chlamydomonas reinhardtii*. Plant Physiol 122(1):127–135. doi:10.1104/pp.122.1.127

Meuser JE, D'Adamo S, Jinkerson RE, Mus F, Yang WQ, Ghirardi ML, Seibert M, Grossman AR, Posewitz MC (2012) Genetic disruption of both *Chlamydomonas reinhardtii* [FeFe]-hydrogenases: insight into the role of HYDA2 in H_2 production. Biochem Biophys Res Commun 417(2):704–709. doi:10.1016/j.bbrc.2011.12.002

Meyer J (2007) [FeFe] hydrogenases and their evolution: a genomic perspective. Cell Mol Life Sci 64(9):1063–1084. doi:10.1007/s00018-007-6477-4

Mignolet E, Lecler R, Ghysels B, Remacle C, Franck F (2012) Function of the chloroplastic NAD(P)H dehydrogenase Nda2 for H_2 photoproduction in sulphur-deprived *Chlamydomonas reinhardtii*. J Biotechnol 162(1):81–88. doi:10.1016/j.jbiotec.2012.07.002

Morra S, Giraudo A, Di Nardo G, King PW, Gilardi G, Valetti F (2012) Site saturation mutagenesis demonstrates a central role for cysteine 298 as proton donor to the catalytic site in CaHydA [FeFe]-Hydrogenase. Plos One 7(10):e48400. doi:10.1371/journal.Pone.0048400

Mulder DW, Boyd ES, Sarma R, Lange RK, Endrizzi JA, Broderick JB, Peters JW (2010) Stepwise [FeFe]-hydrogenase H-cluster assembly revealed in the structure of $HydA^{DEFG}$. Nature 465(7295):248–251. doi:10.1038/nature08993

Mulder DW, Shepard EM, Meuser JE, Joshi N, King PW, Posewitz MC, Broderick JB, Peters JW (2011) Insights into [FeFe]-hydrogenase structure, mechanism, and maturation. Structure 19(8):1038–1052. doi:10.1016/j.str.2011.06.008

Mulder DW, Ratzloff MW, Bruschi M, Greco C, Koonce E, Peters JW, King PW (2014) Investigations on the role of proton-coupled electron transfer in hydrogen activation by [FeFe]-hydrogenase. J Am Chem Soc 136(43):15394–15402. doi:10.1021/ja508629m

Mus F, Cournac L, Cardettini W, Caruana A, Peltier G (2005) Inhibitor studies on non-photochemical plastoquinone reduction and H_2 photoproduction in *Chlamydomonas reinhardtii*. Biochim Biophys Acta Bioenerg 1708(3):322–332. doi:10.1016/j.bbabio.2005.05.003

Mus F, Dubini A, Seibert M, Posewitz MC, Grossman AR (2007) Anaerobic acclimation in *Chlamydomonas reinhardtii* – anoxic gene expression, hydrogenase induction, and metabolic pathways. J Biol Chem 282(35):25475–25486. doi:10.1074/jbc.M701415200

Mussgnug JH, Thomas-Hall SR, Rupprecht J, Foo A, Klassen V, McDowall A, Schenk PM, Kruse O, Hankamer B (2007) Engineering photosynthetic light capture: impacts on improved solar energy to biomass conversion. Plant Biotechnol J 5(6):802–814. doi:10.1111/j.1467-7652.2007.00285.x

Nicolet Y, Piras C, Legrand P, Hatchikian CE, Fontecilla-Camps JC (1999) Desulfovibrio desulfuricans iron hydrogenase: the structure shows unusual coordination to an active site Fe binuclear center. Struct Fold Des 7(1):13–23. doi:10.1016/s0969-2126(99)80005-7

Niyogi KK (1999) Photoprotection revisited: genetic and molecular approaches. Annu Rev Plant Physiol Plant Mol Biol 50(1):333–359. doi:10.1146/annurev.Arplant.50.1.333

Noth J, Krawietz D, Hemschemeier A, Happe T (2013) Pyruvate: ferredoxin oxidoreductase is coupled to light-independent hydrogen production in *Chlamydomonas reinhardtii*. J Biol Chem 288(6):4368–4377. doi:10.1074/jbc.M112.429985

Noth J, Kositzki R, Klein K, Winkler M, Haumann M, Happe T (2015) Lyophilization protects [FeFe]-hydrogenases against O_2-induced H-cluster degradation. Sci Rep 5:13978. doi:10.1038/srep13978

Oey M, Ross IL, Stephens E, Steinbeck J, Wolf J, Radzun KA, Kuegler J, Ringsmuth AK, Kruse O, Hankamer B (2013) RNAi knock-down of LHCBM1, 2 and 3 increases photosynthetic H_2 production efficiency of the green alga *Chlamydomonas reinhardtii*. Plos One 8(4):e61375. doi:10.1371/journal.Pone.0061375

Oey M, Sawyer AL, Ross IL, Hankamer B (2016) Challenges and opportunities for hydrogen production from microalgae. Plant Biotechnol J 14(7):1487–1499. doi:10.1111/pbi.12516

Pagnier A, Martin L, Zeppieri L, Nicolet Y, Fontecilla-Camps JC (2016) CO and CN- syntheses by [FeFe]-hydrogenase maturase HydG are catalytically differentiated events. Proc Natl Acad Sci U S A 113(1):104–109. doi:10.1073/pnas.1515842113

Paila YD, Richardson LGL, Schnell DJ (2015) New insights into the mechanism of chloroplast protein import and its integration with protein quality control, organelle biogenesis and development. J Mol Biol 427(5):1038–1060. doi:10.1016/j.jmb.2014.08.016

Pape M, Lambertz C, Happe T, Hemschemeier A (2012) Differential expression of the *Chlamydomonas* [FeFe]-hydrogenase-encoding *HYDA1* gene is regulated by the copper response regulator1. Plant Physiol 159(4):1700–1712. doi:10.1104/pp.112.200162

Pascal AA, Liu Z, Broess K, van Oort B, van Amerongen H, Wang C, Horton P, Robert B, Chang W, Ruban A (2005) Molecular basis of photoprotection and control of photosynthetic light-harvesting. Nature 436(7047):134–137

Peters JW, Lanzilotta WN, Lemon BJ, Seefeldt LC (1998) X-ray crystal structure of the Fe-only hydrogenase (Cpl) from *Clostridium pasteurianum* to 1.8 angstrom resolution. Science 282 (5395):1853–1858. doi:10.1126/science.282.5395.1853

Peters JW, Schut GJ, Boyd ES, Mulder DW, Shepard EM, Broderick JB, King PW, Adams MWW (2015) [FeFe]- and [NiFe]-hydrogenase diversity, mechanism, and maturation. Biochim Biophys Acta Mol Cell Res 1853(6):1350–1369. doi:10.1016/j.bbamcr.2014.11.021

Philipps G, Happe T, Hemschemeier A (2012) Nitrogen deprivation results in photosynthetic hydrogen production in *Chlamydomonas reinhardtii*. Planta 235(4):729–745. doi:10.1007/s00425-011-1537-2

Pinto TS, Malcata FX, Arrabaça JD, Silva JM, Spreitzer RJ, Esquível MG (2013) Rubisco mutants of *Chlamydomonas reinhardtii* enhance photosynthetic hydrogen production. Appl Microbiol Biotechnol 97(12):5635–5643. doi:10.1007/s00253-013-4920-z

Polle JEW, Kanakagiri SD, Melis A (2003) *tla1*, a DNA insertional transformant of the green alga *Chlamydomonas reinhardtii* with a truncated light-harvesting chlorophyll antenna size. Planta 217(1):49–59. doi:10.1007/s00425-002-0968-1

Posewitz MC, King PW, Smolinski SL, Zhang LP, Seibert M, Ghirardi ML (2004) Discovery of two novel radical S-adenosylmethionine proteins required for the assembly of an active Fe hydrogenase. J Biol Chem 279(24):25711–25720. doi:10.1074/jbc.M403206200

Reifschneider-Wegner K, Kanygin A, Redding KE (2014) Expression of the [FeFe] hydrogenase in the chloroplast of *Chlamydomonas reinhardtii*. Int J Hydrog Energy 39(8):3657–3665. doi:10.1016/j.ijhydene.2013.12.157

Robertson D, Boynton JE, Gillham NW (1990) Cotranscription of the wild-type chloroplast *atpE* gene encoding the CF_1/CF_0 epsilon subunit with the 3′ half of the *rps7* gene in *Chlamydomonas reinhardtii* and characterization of frameshift mutations in *atpE*. Mol Gen Genet 221 (2):155–163

Roessler PG, Lien S (1984) Purification of hydrogenase from *Chlamydomonas reinhardtii*. Plant Physiol 75(3):705–709. doi:10.1104/pp.75.3.705

Roseboom W, De Lacey AL, Fernandez VM, Hatchikian EC, Albracht SP (2006) The active site of the [FeFe]-hydrogenase from desulfovibrio desulfuricans. II. Redox properties, light sensitivity and CO-ligand exchange as observed by infrared spectroscopy. J Biol Inorg Chem 11 (1):102–118

Ruehle T, Hemschemeier A, Melis A, Happe T (2008) A novel screening protocol for the isolation of hydrogen producing *Chlamydomonas reinhardtii* strains. BMC Plant Biol 8. doi:10.1186/1471-2229-8-107

Rumpel S, Siebel JF, Fares C, Duan J, Reijerse E, Happe T, Lubitz W, Winkler M (2014) Enhancing hydrogen production of microalgae by redirecting electrons from photosystem I to hydrogenase. Energy Environ Sci 7(10):3296–3301. doi:10.1039/c4ee01444h

Schonfeld C, Wobbe L, Borgstadt R, Kienast A, Nixon PJ, Kruse O (2004) The nucleus-encoded protein MOC1 is essential for mitochondrial light acclimation in *Chlamydomonas reinhardtii*. J Biol Chem 279(48):50366–50374. doi:10.1074/jbc.M408477200

Scoma A, Krawietz D, Faraloni C, Giannelli L, Happe T, Torzillo G (2012) Sustained H_2 production in a *Chlamydomonas reinhardtii* D1 protein mutant. J Biotechnol 157 (4):613–619. doi: 10.1016/j.jbiotec.2011.06.019

Shepard EM, McGlynn SE, Bueling AL, Grady-Smith CS, George SJ, Winslow MA, Cramer SP, Peters JW, Broderick JB (2010) Synthesis of the 2Fe subcluster of the [FeFe]-hydrogenase H cluster on the HydF scaffold. Proc Natl Acad Sci U S A 107(23):10448–10453. doi:10.1073/pnas.1001937107

Simmons TR, Berggren G, Bacchi M, Fontecave M, Artero V (2014) Mimicking hydrogenases: from biomimetics to artificial enzymes. Coord Chem Rev 270:127–150. doi:10.1016/j.ccr.2013.12.018

Steinbeck J, Nikolova D, Weingarten R, Johnson X, Richaud P, Peltier G, Hermann M, Magneschi L, Hippler M (2015) Deletion of proton gradient regulation 5 (PGR5) and PGR5-like 1 (PGRL1) proteins promote sustainable light-driven hydrogen production in *Chlamydomonas reinhardtii* due to increased PSII activity under sulfur deprivation. Front Plant Sci 6:892. doi:10.3389/fpls.2015.00892

Stiebritz MT, Reiher M (2012) Hydrogenases and oxygen. Chem Sci 3(6):1739–1751. doi:10.1039/c2sc01112c

Stripp ST, Goldet G, Brandmayr C, Sanganas O, Vincent KA, Haumann M, Armstrong FA, Happe T (2009) How oxygen attacks [FeFe] hydrogenases from photosynthetic organisms. Proc Natl Acad Sci U S A 106(41):17331–17336. doi:10.1073/pnas.0905343106

Stuart TS, Gaffron H (1972) The mechanism of hydrogen photoproduction by several algae: 2. The contribution of photosystem II. Planta 106(2):101–112. doi:10.1007/bf00383990

Suess DLM, Pham CC, Buerstel I, Swartz JR, Cramer SP, Britt RD (2016) The radical SAM enzyme HydG requires cysteine and a dangler iron for generating an organometallic precursor to the [FeFe]-hydrogenase H-cluster. J Am Chem Soc 138(4):1146–1149. doi:10.1021/jacs.5b12512

Sun YL, Chen M, Yang HM, Zhang J, Kuang TY, Huang F (2013) Enhanced H_2 photoproduction by down-regulation of ferredoxin-$NADP^+$ reductase (FNR) in the green alga *Chlamydomonas reinhardtii*. Int J Hydrog Energy 38(36):16029–16037. doi:10.1016/j.ijhydene.2013.10.011

Surzycki R, Cournac L, Peltiert G, Rochaix J-D (2007) Potential for hydrogen production with inducible chloroplast gene expression in Chlamydomonas. Proc Natl Acad Sci U S A 104(44):17548–17553. doi:10.1073/pnas.0704205104

Swanson KD, Ratzloff MW, Mulder DW, Artz JH, Ghose S, Hoffman A, White S, Zadvornyy OA, Broderick JB, Bothner B, King PW, Peters JW (2015) [FeFe]-hydrogenase oxygen inactivation is initiated at the H cluster 2Fe subcluster. J Am Chem Soc 137(5):1809–1816. doi:10.1021/ja510169s

Takahashi H, Iwai M, Takahashi Y, Minagawa J (2006) Identification of the mobile light-harvesting complex II polypeptides for state transitions in *Chlamydomonas reinhardtii*. Proc Natl Acad Sci U S A 103(2):477–482. doi:10.1073/pnas.0509952103

Terashima M, Specht M, Naumann B, Hippler M (2010) Characterizing the anaerobic response of *Chlamydomonas reinhardtii* by quantitative proteomics. Mol Cell Proteomics 9(7):1514–1532. doi:10.1074/mcp.M900421-MCP200

Tolleter D, Ghysels B, Alric J, Petroutsos D, Tolstygina I, Krawietz D, Happe T, Auroy P, Adriano JM, Beyly A, Cuine S, Plet J, Reiter IM, Genty B, Cournac L, Hippler M, Peltier G (2011) Control of hydrogen photoproduction by the proton gradient generated by cyclic electron flow in *Chlamydomonas reinhardtii*. Plant Cell 23(7):2619–2630. doi:10.1105/tpc.111.086876

Torzillo G, Scoma A, Faraloni C, Ena A, Johanningmeier U (2009) Increased hydrogen photoproduction by means of a sulfur-deprived *Chlamydomonas reinhardtii* D1 protein mutant. Int J Hydrog Energy 34(10):4529–4536. doi:10.1016/j.ijhydene.2008.07.093

Torzillo G, Scoma A, Faraloni C, Giannelli L (2015) Advances in the biotechnology of hydrogen production with the microalga *Chlamydomonas reinhardtii*. Crit Rev Biotechnol 35(4):485–496. doi:10.3109/07388551.2014.900734

van Lis R, Baffert C, Coute Y, Nitschke W, Atteia A (2013) *Chlamydomonas reinhardtii* chloroplasts contain a homodimeric pyruvate: ferredoxin oxidoreductase that functions with FDX1. Plant Physiol 161(1):57–71. doi:10.1104/pp.112.208181

Vignais PM, Billoud B, Meyer J (2001) Classification and phylogeny of hydrogenases. FEMS Microbiol Rev 25(4):455–501. doi:10.1111/j.1574-6976.2001.tb00587.x

Volgusheva A, Styring S, Mamedov F (2013) Increased photosystem II stability promotes H_2 production in sulfur-deprived *Chlamydomonas reinhardtii*. Proc Natl Acad Sci U S A 110 (18):7223–7228. doi:10.1073/pnas.1220645110

Volgusheva A, Kukarskikh G, Krendeleva T, Rubin A, Mamedov F (2015) Hydrogen photoproduction in green algae *Chlamydomonas reinhardtii* under magnesium deprivation. RSC Adv 5(8):5633–5637. doi:10.1039/c4ra12710b

Winkler M, Kawelke S, Happe T (2011) Light driven hydrogen production in protein based semi-artificial systems. Bioresour Technol 102(18):8493–8500. doi:10.1016/j.biortech.2011.05.019

Winkler M, Esselborn J, Happe T (2013) Molecular basis of [FeFe]-hydrogenase function: an insight into the complex interplay between protein and catalytic cofactor. Biochim Biophys Acta. doi:10.1016/j.bbabio.2013.03.004

Wittenberg G, Sheffler W, Darchi D, Baker D, Noy D (2013) Accelerated electron transport from photosystem I to redox partners by covalently linked ferredoxin. Phys Chem Chem Phys 15 (45):19608–19614. doi:10.1039/C3CP53264J

Wu SX, Huang R, Xu LL, Yan GY, Wang QX (2010) Improved hydrogen production with expression of *hemH* and *lba* genes in chloroplast of *Chlamydomonas reinhardtii*. J Biotechnol 146(3):120–125. doi:10.1016/j.jbiotec.2010.01.023

Wu S, Xu L, Huang R, Wang Q (2011) Improved biohydrogen production with an expression of codon-optimized *hemH* and *lba* genes in the chloroplast of *Chlamydomonas reinhardtii*. Bioresour Technol 102(3):2610–2616. doi:10.1016/j.biortech.2010.09.123

Wykoff DD, Davies JP, Melis A, Grossman AR (1998) The regulation of photosynthetic electron transport during nutrient deprivation in *Chlamydomonas reinhardtii*. Plant Physiol 117 (1):129–139. doi:10.1104/pp.117.1.129

Xu F-Q, Ma W-M, Zhu X-G (2011) Introducing pyruvate oxidase into the chloroplast of *Chlamydomonas reinhardtii* increases oxygen consumption and promotes hydrogen production. Int J Hydrog Energy 36(17):10648–10654. doi:10.1016/j.ijhydene.2011.05.130

Yacoby I, Pochekailov S, Toporik H, Ghirardi ML, King PW, Zhang S (2011) Photosynthetic electron partitioning between FeFe-hydrogenase and ferredoxin:NADP(+)-oxidoreductase (FNR) enzymes in vitro. Proc Natl Acad Sci U S A 108(23):9396–9401. doi:10.1073/pnas.1103659108

Zhang LP, Happe T, Melis A (2002) Biochemical and morphological characterization of sulfur-deprived and H_2-producing *Chlamydomonas reinhardtii* (green alga). Planta 214(4):552–561. doi:10.1007/s004250100660

Chlamydomonas reinhardtii: Protein Glycosylation and Production of Biopharmaceuticals

Elodie Mathieu-Rivet, Patrice Lerouge, and Muriel Bardor

Abstract Recently, microalgae species such as *Chlamydomonas reinhardtii* have been investigated as potential biofactories for the production of biopharmaceuticals (Mathieu-Rivet et al., Front Plant Sci 5:359, 2014; Rasala and Mayfield, Photosynth Res 123:227–239, 2015). Biopharmaceuticals are protein-based pharmaceuticals which are produced recombinantly in living cells used as biofactories (Walsh, Nat Biotechnol 28:917–924, 2010; Walsh, Nat Biotechnol 32:992–1000, 2014). The pharmaceutical market encompasses more than 200 biopharmaceutical products (Walsh, Nat Biotechnol 32:992–1000, 2014). Most of these biopharmaceuticals are glycosylated proteins, and it is currently well established that their glycosylation is primordial for their stability, half-life, and biological activity (Walsh, Nat Biotechnol 28:917–924, 2010; Lingg et al., Biotechnol J, 7:1462–1472, 2012). Since enzymes involved in the glycosylation processing are localized in the endoplasmic reticulum and the Golgi apparatus, biopharmaceuticals produced in *C. reinhardtii* must travel through these organelles, which are components of the secretory pathway, to acquire an appropriate glycosylation. In this chapter, the *C. reinhardtii* protein glycosylation pathways as well as its capacity to synthesize and transport nucleotide sugars will be described and discussed.

E. Mathieu-Rivet • P. Lerouge
Laboratoire Glycobiologie et Matrice Extracellulaire végétale, Normandie Univ, UNIROUEN, 76000 Rouen, France

M. Bardor (✉)
Laboratoire Glycobiologie et Matrice Extracellulaire végétale, Normandie Univ, UNIROUEN, 76000 Rouen, France

Institut Universitaire de France (I.U.F.), 1 rue Descartes, 75231 Paris Cedex 05, France

Faculté des sciences et techniques, Laboratoire Glycobiologie et Matrice Extracellulaire végétale (Glyco-MEV) Equipe d'Accueil 4358, Institut de Recherche et d'Innovation Biomédicale, Végétale Agronomie Sol Innovation, Université de Rouen, Normandie Université, 76821 Mont-Saint-Aignan Cedex, France
e-mail: muriel.bardor@univ-rouen.fr

M. Hippler (ed.), *Chlamydomonas: Biotechnology and Biomedicine*, Microbiology Monographs 31, DOI 10.1007/978-3-319-66360-9_3

1 Introduction

Since the mid-twentieth century, microalgae have been used for the production of food and high-value added compounds like carotenoids (Sasso et al. 2012; Spolaore et al. 2006). Recently, microalgae have emerged as an alternative production system for new biotechnological applications. As photosynthetic organisms, microalgae are very efficient in converting sunlight into chemical energy, which feature makes them attractive for the production of carbohydrates, lipids, and hydrogen. Therefore, algal biomass represents a great potential for generating new sources of sustainable biofuels (Beer et al. 2009; Lam and Lee 2012; Merchant et al. 2012). Some microalgae species including *Chlamydomonas reinhardtii* have been also investigated as solar-powered protein biofactories for the production of biopharmaceuticals (Barrera and Mayfield 2013; Hempel and Maier 2016).

Biopharmaceuticals are protein-based pharmaceuticals which are produced recombinantly in living cells used as biofactories. Currently, there are more than 200 products on the biomedical market reaching a total cumulative sales value of $140 billion for 2013 (Walsh 2014). These products include antibodies, vaccines, human blood products, enzymes, hormones, and growth factors. Among the different categories, monoclonal antibodies (mAbs) and their derivatives form the largest group and the most lucrative product class with total sales reaching $63 billion in 2013 (Walsh 2014). MAbs are used to treat a wide range of diseases, with oncology and autoimmunity/inflammation covering more than 80% of the market. In 2010, the combined sale value of 25 actively marketed mAbs in these areas was $43 billion of which 75% were generated solely from the top five mAbs producers including Avastin®, Rituxan®, Humira®, Remicade®, and Herceptin (Elvin et al. 2013).

A substantial portion of the biopharmaceuticals on the market is represented by glycosylated proteins (Walsh 2010). Since it has been well established that glycan moieties attached to recombinant proteins are essential for the protein stability and bioactivity and mediate the efficacy of the glycosylated biopharmaceuticals (Lingg et al. 2012), the development of an expression system allowing an efficient manufacturing of the protein glycosylation is essential. Additionally, over the past decade, at least four nonhuman carbohydrate epitopes have been able to induce an immune response in humans (van Beers and Bardor 2012). Therefore, glycan variants of a biopharmaceutical must be adequately analyzed and controlled to ensure product quality and safety (Lingg et al. 2012; Zhang et al. 2016).

Biopharmaceuticals are currently produced in various heterologous expression systems ranging from bacteria to mammalian cell cultures (Demain and Vaishnav 2009; Huang et al. 2012; Wong 2005). Among those, mammalian cells such as Chinese hamster ovary cells (CHO) represent the industrial workhouse cell lines (Hossler et al. 2009), covering more than 50% of the market. For example, among the 18 recombinant biopharmaceuticals which have been approved between January 2008 and June 2011 by the US Food and Drug Administration (FDA), 12 were produced using mammalian cell expression systems, three were manufactured in *Escherichia coli*, and the remaining three were produced by using baculovirus,

yeast, or transgenic goats (Zhu 2012). Despite the industrial success of mammalian cell lines, a constantly increasing need for large amount of biopharmaceuticals, their high production cost, and potential virus contamination have driven scientists to explore new alternative for biopharmaceuticals production.

In this context, plant molecular farming (PMF), which refers to biotechnological production of plant-based biopharmaceuticals, is gaining more and more attention. The growing interest in PMF research encourages development of active research and projects, which could be identified in more than 120 companies, universities, and research institutes worldwide (Obembe et al. 2011). Meanwhile, PMF field is becoming a lucrative biotechnology industry that attracts an increasing number of specialized startup and biotechnology companies. This rapid development observed in PMF area is certainly due to the successful production of several plant-made biopharmaceuticals (De Muynck et al. 2010). Moreover, an important breakthrough was achieved in 2012 when the first plant molecular farming product was approved by the FDA for use in humans (Maxmen 2012). This successful story concerns taliglucerase alfa, a recombinant form of human glucocerebrosidase, an enzyme developed in carrot cells by Protalix BioTherapeutics for the treatment of the lysosomal storage disorder Gaucher's disease (Shaaltiel et al. 2007). In addition, two clinical trial applications for plant-derived pharmaceuticals were also approved in the European Union (EU), one for insulin produced in safflower and another for an HIV-neutralizing monoclonal antibody produced in transgenic tobacco plants (Ma et al. 2015; Stoger et al. 2014). In both cases, new manufacturing processes based on transgenic plants were developed to ensure compliance with pharmaceutical good manufacturing practice (GMP; Ma et al. 2015).

Since 25 years, there is an increasing interest to use microalgae for biopharmaceutical production (Rasala and Mayfield 2015). Microalgae are cheap and easy to grow, classified in generally recognized as safe (GRAS) organisms, which feature makes them potentially attractive cell factories for the large-scale production of biopharmaceuticals. In addition, microalgae can be cultured in closed bioreactor systems to overcome gene dissemination often encountered with transgenic plant breedings (Hempel and Maier 2016). So far, several microalgae species have been evaluated for their potential to express biopharmaceuticals. Among them, *C. reinhardtii* is currently the most deeply investigated (Mathieu-Rivet et al. 2014; Rasala and Mayfield 2015).

2 Production of Biopharmaceuticals in *Chlamydomonas reinhardtii*

Several studies attempted to demonstrate that *C. reinhardtii* is an efficient cellular factory for the production of recombinant proteins, especially biopharmaceuticals (Barahimipour et al. 2016; Dauvillée et al. 2010; Eichler-Stahlberg et al. 2009; Gregory et al. 2013, 2016; Mayfield and Franklin 2005; Mayfield et al. 2003; Rasala

et al. 2010; Sun et al. 2003; Surzycki et al. 2009; Tran et al. 2009, 2013). Most of the efforts in this microalga have been focused on the chloroplastic expression of a transgene of interest.

Chloroplastic expression of a transgene has been favored over expression in the nucleus since this strategy allows accumulation of relatively higher yields of recombinant proteins within the chloroplast (Mayfield et al. 2007; Surzycki et al. 2009). For example, Manuell and collaborators managed to express a mammalian protein, the bovine mammary-associated serum amyloid (M-SAA), up to 5% of the total soluble proteins (Manuell et al. 2007). In *C. reinhardtii,* the chloroplastic compartment represents more than 40% of the cellular volume providing a favorable environment and preventing proteolysis of a recombinant protein. Thus, about 30 biopharmaceuticals have been produced through chloroplastic expression (for a complete review, refer to Almaraz-Delgado et al. 2014; Pérez Espana et al. 2016). These works include studies on several antibodies such as the large single-chain antibody directed against glycoprotein D protein from Herpes simplex virus (lcs-HSV8) (Mayfield et al. 2003), the single-chain fragment HSV8-scFv (Mayfield and Franklin 2005), the heavy chain of human monoclonal antibody directed against anthrax protective antigen 83 (PA83) (Tran et al. 2009), as well as immunotoxin such as the *sc*Fv (single-chain antibody) directed against a B-cell surface molecule called CD22, fused to domains II and III of exotoxin A (PE40) from *Pseudomonas aeruginosa* (Tran et al. 2013). These examples illustrate the high potential of this strategy for the production of complex proteins, as the chloroplast contains the enzymatic arsenal and chaperones required for disulfide bond formation and proper folding of proteins (Mayfield et al. 2007; Tran et al. 2013). Compared to bacterial expression system, this feature renders *C. reinhardtii* attractive for such production of recombinant proteins. Despite these advantages, the transformation of chloroplast appears not to be the best strategy for the expression of biopharmaceuticals. As it has been already mentioned, the majority of biopharmaceuticals are glycosylated proteins for which chloroplastic expression is not appropriate. In fact the chloroplast organelle lacks the glycosylation machinery which is localized in the endoplasmic reticulum (ER) and Golgi apparatus (Dance 2010). However, two works carried out in rice (Chen et al. 2004) and in Arabidopsis (Villarejo et al. 2005) reported the existence of an alternative route for secreted proteins in the chloroplast, suggesting the possibility for some proteins to be glycosylated in the ER and the Golgi apparatus prior to their import into the chloroplast. Therefore, we can hypothesize that such a pathway may exist in *C. reinhardtii*, which would open the door to new strategies for optimizing the expression of glycosylated proteins within its chloroplast.

Efficient production of glycosylated biopharmaceuticals requires nuclear expression of the transgene encoding for the protein of interest and its targeting to the secretion pathway to acquire either *O*- or/and *N*-glycosylation. In contrast to the numerous recombinant proteins produced in the chloroplast (Almaraz-Delgado et al. 2014;

Table 1 Secreted biopharmaceuticals produced in *C. reinhardtii*

Biopharmaceuticals	Function	Protein titer	Reference
Erythropoietin	Treatment for anemia	100 μg L^{-1} of culture medium	Eichler-Stahlberg et al. (2009)
GBSS-AMA1	Malaria vaccine	0.2–1 μg mg^{-1} of purified starch	Dauvillée et al. (2010)
GBSS-MSP1	Malaria vaccine	0.2–1 μg mg^{-1} of purified starch	Dauvillée et al. (2010)
HIV antigen P24	Putative HIV vaccine	0.25% of total cellular proteins	Barahimipour et al. (2016)

Pérez Espana et al. 2016), only a few examples of nucleus-expressed proteins have been reported in *C. reinhardtii* (Lauersen et al. 2013b; Rasala et al. 2012), and among them, only four are biopharmaceuticals (Table 1; Barahimipour et al. 2016; Dauvillée et al. 2010; Eichler-Stahlberg et al. 2009). Strategies used for the production of these four biopharmaceuticals were very distinct. The recombinant erythropoietin (EPO) was secreted in the medium thanks to the insertion of the secretion signal of the arylsulfatase ARS2 in its *N*-terminal part (Eichler-Stahlberg et al. 2009). The two malaria vaccine antigens AMA1 and PSP1 were fused to a truncated granule-bound starch synthase (GBSS) which allow their accumulation in the chloroplast (Dauvillée et al. 2010). Recently, the HIV antigen P24 was accumulated in the cytosol and was shown to represent up to 0.25% of the total cellular proteins (Barahimipour et al. 2016). Despite these efforts, the yields reached in these attempts were very low (Table 1). So far, nuclear expression appeared to be a trickier strategy which does not allow reaching high protein levels. Molecular mechanisms suspected to cause the low expression of nuclear transgenes in *C. reinhardtii* and strategies used to circumvent this limitation are reviewed in another chapter of this book. However, a number of studies conducted recently reported the development of new tools which improve the yield of nuclear-expressed proteins. Major recent advances concern the selection of strains used for the production (Lauersen et al. 2013a, b; Neupert et al. 2009), vectors, and promotors (Lauersen et al. 2015b; Rasala et al. 2012; Scranton et al. 2016), as well as growth conditions (Lauersen et al. 2015a)**.** As an illustration, the comparison of several cultivation systems showed that cells grown in mixotrophic conditions, using both acetate and carbon dioxide as carbon sources, are able to produce relatively high amounts of recombinant protein (10 mg L^{-1} of culture medium) (Lauersen et al. 2015a). This result demonstrates that *C. reinhardtii* can be a competitive biofactory for the production of therapeutic proteins.

Besides the numerous attempts made in order to increase the yields of recombinant protein, another strategy involves maximizing the economic value of *C. reinhardtii*, in order to reduce the high costs of biopharmaceutical manufacturing processes. A concomitant production of other valuable product or use of industrial waste waters to grow the microalgae expressing the protein of interest could be a way to optimize the production costs (Gong et al. 2011).

3 *N*-Glycosylation Pathway in *Chlamydomonas reinhardtii*

In Eukaryotes, *N*-linked glycosylation of secreted proteins is an extensive and universal posttranslational modification which results in the covalent attachment of an oligosaccharide onto asparagine residues belonging to the consensus sequence Asn-X-Ser/Thr/Cys, in which X represents any amino acid except proline.

3.1 N-*Glycosylation Pathway in Plants and Mammals*

In eukaryotic cells, the process of *N*-linked glycosylation is initiated within the endomembrane system of the ER and is continued within the Golgi apparatus for the latest maturation steps. The *N*-glycosylation is initiated in the ER with the biosynthesis of a lipid-linked oligosaccharide (LLO) precursor. The LLO synthesis starts on the cytosolic face of the ER membrane by the stepwise addition of monosaccharides *N*-acetylglucosamine (GlcNAc) and mannose (Man) on a dolichol pyrophosphate (Dol-P-P) to form a $Man_5GlcNAc_2$-P-P-Dol which is then flipped into the lumen of the ER (Helenius and Aebi 2002; Helenius et al. 2002). Here, the precursor undergoes elongation by the addition of several Man and glucose (Glc) residues to form the oligosaccharide precursor $Glc_3Man_9GlcNAc_2$-P-P-Dol (Aebi 2013). This product is subsequently transferred by the oligosaccharyltransferase (OST) complex onto the asparagine of the *N*-glycosylation consensus sequences of the neo-synthesized polypeptides. The precursor is afterward trimmed by the action of α-glucosidases I and II, ER-mannosidase into a high-mannose type *N*-glycan or oligomannoside ($Man_8GlcNAc_2$). In parallel to these events, the nascent protein is submitted to the calnexin-calreticulin control quality cycle to ensure its proper folding. When the glycoprotein is correctly folded, it can then leave the ER to enter the Golgi apparatus where its *N*-glycans will be further subjected to modifications: α-mannosidase I, *N*-acetylglucosaminyltransferase I (GnT I), α-mannosidase II, and finally *N*-acetylglucosaminyltransferase II give rise to an intermediate $GlcNAc_2Man_3GlcNAc_2$ which is common to mammals and land plants (Lerouge et al. 1998; Strasser 2016). Thereafter, this intermediate undergoes further maturation into complex-type *N*-glycans. Even if the *N*-glycosylation processing is highly conserved, the final processed *N*-glycan structures present a high variability when comparing different species together (Brooks 2011; Bardor et al. 2011). The resulting organism-specific complex-type *N*-glycans reflect the difference in the Golgi enzyme repertoires, for example, mature *N*-glycans from plant bore core β1,2-xylose, core α1,3-fucose (Fig. 1), and to a less extent $Lewis^a$ antennae (Lerouge et al. 1998; Bardor et al. 2011; Brooks 2011). In contrast, major maturated *N*-glycans in humans are bearing core α1,6-fucose and Neu5Ac-sialylated lactosamine antennae (Fig. 2; Brooks 2011). In addition to this interspecies differences, *N*-glycan structures variability can be found even in different cell types of the same species or within one cell (Varki et al. 2009b).

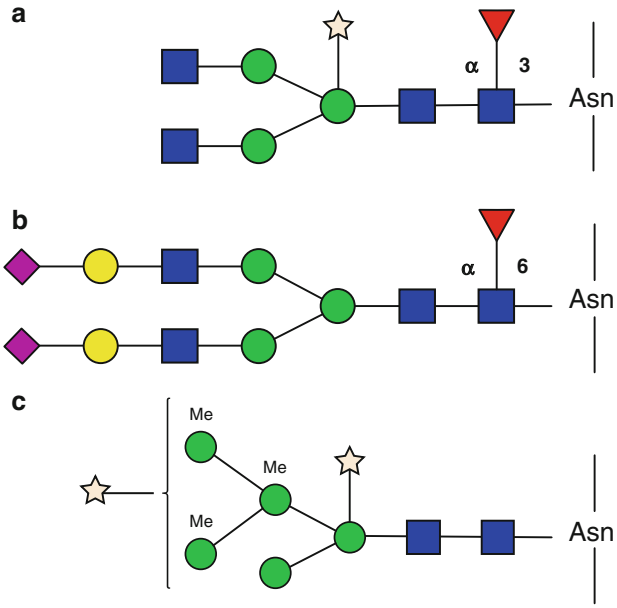

Fig. 1 Major *N*-glycan structures identified in land plants (**a**), in humans (**b**), and in *C. reinhardtii* (**c**). The *symbols* used for representing the *N*-glycan structures are the ones from the Consortium for Functional Glycomics (Varki et al. 2009a). The specific linkage of the core fucose has been indicated to highlight the difference between land plants and mammals. *Me* methyl group, *blue-filled squares* N-acetylglucosamine, *green-filled circles* mannose, *yellow-filled circles* galactose, *filled stars* xylose, *red-filled inverted triangles* fucose, *violet filled diamonds* N-acetylneuraminic acid

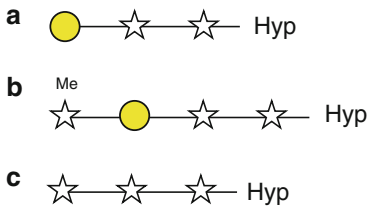

Fig. 2 Linear *O*-glycans structures linked to hydroxyproline residues identified in *C. reinhardtii* (**a**) and (**b**) as compared to those in land plants (**c**). Structures (**a**) and (**b**) have been isolated from *C. reinhardtii* outer cell wall proteins (Ferris et al. 2001; Bollig et al. 2007), and structure (**c**) represents extensins characterized in *A. thaliana* and *N. tabacum* (Bollig et al. 2007). The *symbols* used for representing the *O*-glycan structures are the ones from the Consortium for Functional Glycomics (Varki et al. 2009a). *Me* methyl group, *yellow-filled circles* galactose, *stars* arabinose, *Hyp* hydroxyproline. Both sugars (galactose and arabinose) present a furanose ring

3.2 N-*Glycan Structures in* Chlamydomonas reinhardtii

The mature *N*-glycan structures borne by the endogenous proteins of *C. reinhardtii* were recently identified and showed substantial differences in comparison to those described in plants and humans (Fig. 1; Mathieu-Rivet et al. 2013). In Mathieu-Rivet et al. (2013), the *N*-glycosylation has been studied in three distinct *C. reinhardtii* strains: CC-503 cw92, CC-400 cw15, and CC-1036 pf18. The two first strains are cell wall-deficient strains used as references (Merchant et al. 2007). The latter one possesses a cell wall but is completely impaired in its motility (Witman et al. 1972). The soluble and membrane-bound proteins were extracted from those strains and studied through either glycomic and/or glycoproteomic approaches combined with mass spectrometry analysis. Such studies allowed the identification of two types of *N*-glycans: oligomannosides and maturated *N*-glycans, which account, respectively, for 70% and 30% of the *N*-glycan population. Within the population of oligomannosides, the $Man_5GlcNAc_2$, $Man_4GlcNAc_2$, $Man_3GlcNAc_2$, and $Man_2GlcNAc_2$ were shown to be the main *N*-glycans (Mathieu-Rivet et al. 2013). The complex-type *N*-glycans in *C. reinhardtii* were identified as oligomannosides bearing one or two xylose residues and methyl group substitutions on the C6 on the three outer mannose residues (Mathieu-Rivet et al. 2013; Fig. 1c). The two xylose residues have been determined to be either β(1,2) linked to the core β-mannose as previously demonstrated in land plants (Brooks 2011; Bardor et al. 2011; Strasser 2016) or (1,4) linked on a terminal mannose residue (Fig. 1c; Mathieu-Rivet et al. 2013). Such *N*-glycan structures are unique when compared to plant and mammalian *N*-glycan structures (Fig. 1). The absence of additional GlcNAc residues on these mature *N*-linked glycans also suggested that they may derive from GnT I-independent Golgi events.

3.3 *Synthesis of the Oligosaccharide Precursor Within* Chlamydomonas reinhardtii *Endoplasmic Reticulum*

In silico analysis of the *C. reinhardtii* genome allowed the identification of a number of putative ortholog genes encoding for enzymes potentially involved in the LLO biosynthesis and its transfer onto the nascent glycoprotein (Mathieu-Rivet et al. 2013, 2014). Three monosaccharides serve as building blocks for the synthesis of LLO, namely, GlcNAc, Man, and Glc. They emerge from the cytosolic primary metabolism as nucleotide-activated sugar forms: UDP-GlcNAc, GDP-Man, and UDP-Glc, respectively. These activated forms are then used by the glycoenzymes involved in the synthesis of the LLO precursor. CrALG5 (Cre16.g652850) is a putative dolichol-phosphate glucosyltransferase able to transfer a Glc residue onto dolichol-phosphate. The newly synthesized Glc-P-Dol is then translocated within the ER membrane to

reach the ER lumen where it will be used by glucosyltransferases to end up in the synthesis of the LLO precursor. Similarly, CrDPM1 (Cre03.g150950), a putative dolichol-phosphate mannosyltransferase, gives rise to Man-P-Dol which is then translocated within the ER lumen for further usage. LLO precursor synthesis is initiated on the cytosolic side of the ER membrane and starts with the formation of GlcNAc1-P-P-Dol through the action of an *N*-acetylglucosamine-phosphate transferase encoded by *CrALG7* gene (Cre16g.663100). The addition of a GlcNAc residue is then mediated by the β(1,4)-*N*-acetylglucosaminyltransferases CrALG13 and CrALG14 (Cre13.g585850 and Cre16.g669950, respectively) leading to the formation of a $GlcNAc_2$-P-P-Dol intermediate. To this point, it could be hypothesized that in *C. reinhardtii,* the three proteins CrALG7, CrALG13, and CrALG14 are organized within a protein complex as it has already been described for other organisms (Noffz et al. 2009; Lu et al. 2012). The mannosylation of the LLO starts with a first Man residue added to $GlcNAc_2$-P-P-Dol intermediate by the β(1,4)-mannosyltransferase CrALG1 (Cre12.g516550). The subsequent addition of four branched mannose residues is catalyzed by two putative α(1,3)- and α(1,2)-mannosyltransferases, CrALG2 (Cre11.g474450) and CrALG11 (Cre23.g767350), respectively. All these cytoplasmic steps result finally in the synthesis of a $Man_5GlcNAc_2$-P-P-Dol. Then, the putative CrRFT flippase (Cre22g.765100) is likely responsible for the flip-flop movement of this $Man_5GlcNAc_2$-P-P-Dol intermediate across the membrane bilayer into the ER lumen as previously described in yeast (Helenius and Aebi 2002; Rush et al. 2009). In yeast and mammals, the synthesis of the LLO continues within the ER lumen by the stepwise addition of four mannose residues through the action of ALG3, ALG9, and ALG12 prior to glucosylation of the $Man_9GlcNAc_2$-P-P-Dol by the ALG6, ALG8, and ALG10 glucosyltransferases (Aebi 2013). No ortholog genes for ALG3, ALG9, and ALG12 have been identified within the *C. reinhardtii* genome (Gomord et al. 2010; Levy-Ontman et al. 2014; Mathieu-Rivet et al. 2013) suggesting that the $Man_5GlcNAc_2$-P-P-Dol could be directly submitted to further glucosylation steps. Furthermore, orthologs for two α(1,3)-glucosyltransferases ALG6 (Cre16.g690150) and ALG8 (Cre09.g414250) are predicted in *C. reinhardtii* genome. In contrast, no ALG10 ortholog required for the transfer of the outer α(1,2)-glucose onto the LLO was found (Gomord et al. 2010; Levy-Ontman et al. 2014; Mathieu-Rivet et al. 2013). All together, these results suggest that the LLO precursor from *C. reinhardtii* might be restricted to the $Glc_2Man_5GlcNAc_2$ structure (Gomord et al. 2010). The lack of *ALG* genes (Samuelson et al. 2005) and the ER synthesis of truncated LLO structures have already been described for some parasitic unicellular organisms (Garénaux et al. 2008; Kelleher et al. 2007; Schiller et al. 2012). However, this bioinformatically predicted structure of LLO is in discrepancy with the identified *N*-glycans borne by the endogenous glycoproteins from *C. reinhardtii* (Fig. 1; Mathieu-Rivet et al. 2013). This discrepancy could reflect the existence of uncharacterized enzymes able to add supplementary hexose residues onto the oligosaccharide precursor. Therefore, more work needs to be done to confirm the LLO biosynthetic pathway and its structure within *C. reinhardtii*.

3.4 *Transfer and Maturation of the* N-*Glycans Within* Chlamydomonas reinhardtii *Golgi Apparatus*

After completion, the LLO precursor is then transferred on the nascent protein onto the specific *N*-glycosylation consensus sites. This key reaction giving birth to glycoproteins is catalyzed by an oligosaccharyltransferase (OST; Aebi 2013). The OST has been described to be a hetero-oligomeric protein complex in yeast and mammals (Kelleher and Gilmore 2006). However, the OST from protists such as *Trypanosoma cruzi* and *T. brucei* are composed of a single catalytic subunit (Kelleher et al. 2007). In *C. reinhardtii*, several putative subunits have been identified through sequence homology search in the genome (Mathieu-Rivet et al. 2013). This includes the catalytic subunits CrSTT3A and CrSTT3B, respectively, encoded by the genes Cre02.g121650 and Cre07.g330100, as well as ribophorin orthologs (CrRPN1: Cre12.g523300 and CrRPN2: Cre08.g368450), CRDGL1 (Cre14.g614100), CrDAD1 (Cre02.g108400), and CrOST3 (Cre01.g063500), previously described for other eukaryotes such as yeast and mammals (Pfeffer et al. 2014). After its transfer on the protein, but before leaving the ER, the *N*-glycan is then trimmed through the removal of the glucose residues by the action of putative α-glucosidases (CrGSI: Cre13.g579750; CrGSIIA: Cre03.g190500; CrGSIIB: Cre05.g233250). The resulting oligomannoside structure of the glycoprotein will then be maturated within the Golgi apparatus via the contributions of putative mannosidases (Cre03.g189050 and Cre07.g336600) as well as xylosyltransferases and methyltransferases. Even if two xylose residues have been detected on the *N*-glycan structures, only one candidate gene encoding for the xylosyltransferase activity has been identified (Cre02.g126700). The amino acid sequence deduced from Cre02.g126700 displayed about 16.5% of identity with the β(1,2)-xylosyltransferase from Arabidopsis which catalyzes the transfer of a xylose onto the β-mannose of the core *N*-glycan (Strasser et al. 2000). However, considering the lack of information regarding conserved domains required for β(1,2)-xylosyltransferase activity, the assignment of such a sequence remains highly speculative without further functional evidence. Although two candidate genes encoding for putative fucosyltransferases have been identified in the genome (Cre31.g780450 and Cre18.g749047), only minute amount of a fucosylated glycan was detected by mass spectrometry in the glycan preparations from the strain CC-503 cw92 (Mathieu-Rivet et al. 2013). Therefore, further experiments would be required to functionally characterize these enzymes and demonstrate their capability to fucosylate *N*-glycans in *C. reinhardtii*. Contrary, no *GnT I* ortholog was found in *C. reinhardtii* (Mathieu-Rivet et al. 2013). Both these bioinformatics data and the structure of glycan *N*-linked to secreted proteins suggested that *C. reinhardtii N*-glycosylation pathway is a GnT I-independent processing (Fig. 1; Mathieu-Rivet et al. 2013) in contrast to the one described in land plants and mammals (Lerouge et al. 1998; Strasser 2016).

4 *O*-Glycosylation in *Chlamydomonas reinhardtii*

In additional to *N*-glycosylation, there is a second major type of glycosylation which is based on the attachment through an *O*-linkage of a glycan to the side chain of a serine or threonine residue of a mammalian protein (Corfield 2015) or to the side chain of serine or hydroxyproline residues of a plant protein (Nguema-Ona et al. 2014). In contrast to *N*-glycosylation, no consensus sequence has been identified for the *O*-glycosylation site. Moreover, the *O*-glycan structures are much more complex, highly heterogeneous, and divergent from one organism to another (Nguema-Ona et al. 2014; Solís et al. 2015). So far, less attention has been paid to the *O*-glycosylation of biopharmaceuticals because structural analysis of *O*-glycans is more challenging as compared to *N*-glycans and since there is no need yet for the pharmaceutical industries to provide detailed structural analyses of *O*-glycans to regulatory agencies (Zhang et al. 2013).

O-glycosylation can be found on few examples of biopharmaceuticals dedicated to therapeutic applications in humans. For example, recombinant human EPO, a tumor necrosis factor (TNF) receptor fused to an Fc part, coagulation blood factors IX and VII carry, respectively, *O*-GalNAc, *O*-Fuc, and *O*-Glc modifications (refer to Zhang et al. 2013; Walsh 2010). Functionally, similarly to *N*-glycosylation, *O*-glycosylation was found to impact on biopharmaceutical immunogenicity, secretion, and function (Zhang et al. 2013). Therefore, it is essential to understand the *O*-glycosylation capabilities of the expression system used for the production of biopharmaceuticals.

In this context, it is important to understand the capabilities of *C. reinhardtii* to synthesize *O*-glycans. So far, *O*-glycans have mainly been described in the cell wall of this organism. Indeed, *C. reinhardtii* cell wall does not contain cellulose but is made of crystalline glycoproteins which are essentially *O*-glycosylated proteins (Catt et al. 1978; Goodenough et al. 1986; Roberts et al. 1972). The amino acid sequences of these glycoproteins share a high degree of similarity with extensins, a class of plant hydroxyproline-rich glycoproteins (HRGPs) (Ferris et al. 2001; Woessner and Goodenough 1989). Especially, hydroxyproline residues have been identified as *O*-glycosylation sites in chaotrope-soluble glycoproteins which constitute the vegetative outer cell wall in *C. reinhardtii* (Bollig et al. 2007; Ferris et al. 2001; Miller et al. 1972). Using antibodies recognizing specifically the carbohydrate moiety (Smith et al. 1984) on endosomal fractions enriched either in ER or Golgi apparatus, Zhang and Robinson (1990) showed that glycoproteins could be detected in both compartments. This contrasts with the situation described in plants and mammals, where *O*-glycosylation only occurs in the Golgi apparatus (Gill et al. 2011; Matsuoka et al. 1995). The monosaccharide composition of these chaotrope-soluble glycoproteins highlighted the presence of arabinose and galactose as the most prominent monosaccharides, followed by glucose, xylose, and mannose as minor species (Bollig et al. 2007; Ferris et al. 2001;

Miller et al. 1972). In addition, methylated sugars (i.e., MeHex and MePent which correspond to MeGal and MeAra) have been detected (Bollig et al. 2007; Ferris et al. 2001). Further analysis carried out by mass spectrometry and NMR led to the identification of *O*-glycans bound to hydroxyproline, which in *C. reinhardtii* correspond to linear and branched structures, with the first two L-arabinoses linked to each other in β(1–2) (Fig. 2; Bollig et al. 2007; Ferris et al. 2001). Besides these structural data, information concerning the enzymes involved in this process remains currently scarce. A prolyl-4-hydroxylase has been characterized (Keskiaho et al. 2007). This enzyme expressed in insect cells or in *E. coli* has been shown to efficiently hydroxylate the proline residues of synthetic peptides. Moreover, the downregulation of its transcription in *C. reinhardtii* affects the assembly of a proper cell wall, which is consistent with the role of hydroxyproline residues in the attachment of the oligosaccharide moiety. As far as glycosyltransferases involved in *O*-glycans biosynthesis are concerned, only arabinosyltransferase and galactosyltransferase activities have been detected in vitro using endomembrane preparations from *C. reinhardtii* (Zhang and Robinson 1990; Zhang et al. 1989). To the best of our knowledge, none of these enzymes have been further characterized.

In plant and mammals, *O*-glycosylation is known to occur also on serine residues (Gill et al. 2011; Kieliszewski and Lamport 1994; Velasquez et al. 2011). Although no data on such posttranslational modification has yet been reported in *C. reinhardtii*, a peptidyl-serine α-galactosyltransferase has recently been characterized (Saito et al. 2014). Saito and collaborators (2014) showed that crude cells extracts from the CC-503 cw92 strain could modify synthetic peptides by adding a galactose residue onto serine. Therefore, the enzyme was purified from the endosomal fraction, and its galactosyltransferase activity has been confirmed by an in vitro assay. Altogether, these results suggest that *O*-glycosylation of serine residues can occur in *C. reinhardtii*, even if there is yet no evidence that such *O*-glycoprotein exists in this microalga.

5 Synthesis and Transport of Glycan Building Bocks

Glycans, either *N*- or *O*-linked to proteins, are built by sequential addition of monosaccharides thanks to glycosyltransferases which use activated sugar donors as substrates. These sugar donors are synthesized within the cytosol prior to their transfer into the ER and Golgi compartments. Once they reach the lumen of the organelles, they can be used as substrates for the resident glycosyltransferases.

5.1 Nucleotide Sugar Biosynthesis

Nucleotide sugars result from the conversion of a sugar-1-phosphate in its corresponding nucleotide-diphosphate activated form (Bar-Peled and O'Neill 2011). Sugar-specific kinases and pyrophosphorylases which ensure this conversion are

usually localized within the cytosol. Currently, 10 and 30 different nucleotide sugars have been identified in animals and plants, respectively (Bar-Peled and O'Neill 2011). This large diversity as compared to animals can be explained by the important roles that they play as precursors of the cell wall polysaccharides and glycoproteins. Whereas the biosynthetic pathways of nucleotide sugars are well studied in plants (Bar-Peled and O'Neill 2011), these processes are poorly detailed in microalgae and especially in *C. reinhardtii*. However, based on homologies with Arabidopsis genes encoding for putative enzymes involved in the nucleotide sugar biosynthesis, we report here a bioinformatics analysis of the *C. reinhardtii* genome which suggests that this metabolic process would be conserved in this microalga (Table 2; Fig. 3).

Most of the nucleotide sugars derive from UDP-Glc which is a crossroad in the interconversion pathways. For example, UDP-galactose (UDP-Gal) and UDP-glucuronic acid (UDP-GlcA) derive, respectively, from the epimerization (Barber et al. 2006; Rosti et al. 2007) and the dehydrogenation of UDP-Glc (Klinghammer and Tenhaken 2007; Reboul et al. 2011) (Fig. 3). UDP-Glc results from the activity of an UDP-Glc pyrophosphorylase which uses Glc-1-P as a substrate (Kleczkowski et al. 2004). One sequence encoding for a putative protein sharing 35% identity with the *Arabidopsis thaliana* UTP-Glc-1-phosphate uridylyltransferase is predicted in the *C. reinhardtii* genome (Table 2; Fig. 3). However, its biological function has not yet been demonstrated.

As described previously, the synthesis of *N*-glycan oligosaccharide precursor in eukaryotes starts with the addition of two GlcNAc residues onto the dolichol-phosphate. Since these first steps are conserved in *C. reinhardtii* (Mathieu-Rivet et al. 2013), this suggests that this microalga synthesize UDP-GlcNAc. Four distinct enzymes are required to convert D-fructose-6-phosphate (D-Fru-6-P) into UDP-GlcNAc (Bar-Peled and O'Neill 2011; Fig. 3). First, the amination of Fru-6-P occurs through the enzymatic transfer of the amine group from L-glutamine to the C-2 of this ketose. Secondly, isomerization of fructosamine-6-P into glucosamine-6-P (GlcN-6-P) occurs prior to its *N*-acetylation giving rise to GlcNAc-6-P. Then, the GlcNAc-6-P is converted into GlcNAc-1-P by a phosphomutase. Finally, the GlcNAc-1-P is activated by the UTP: *N*-acetylglucosamine-1-P-uridylyltransferase into UDP-GlcNAc. Candidate genes encoding for these four enzymes are predicted in the genome of *C. reinhardtii* (Table 2; Fig. 3).

The major part of the *N*-glycans identified in *C. reinhardtii* are oligomannosides obtained by the sequential addition of mannose residues by several mannosyltransferases that use GDP-mannose (GDP-Man) as substrate. For the biosynthesis of this nucleotide sugar, Fru-6-P is first converted into mannose-6-phosphate (Man-6-P) through the action of a mannose-6-phosphate isomerase and then into Man-1-P by a phosphomannomutase. Candidate genes (Cre02.g147650 and Cre14.g626900) for both enzymes have been identified in *C. reinhardtii* (Table 2). Then, GDP-Man results from the coupling of Man-1-P and GTP catalyzed by a GDP-Man pyrophosphorylase (GDP-Man PPase) (Conklin et al. 1999; Qin et al. 2008). This reaction is a well-characterized enzymatic step in the Smirnoff-Wheeler pathway (also called the L-galactose pathway) which allows the conversion of D-glucose into L-ascorbic acid in plants. Recently, it has been shown

Table 2 *C. reinhardtii* sequences encoding for putative enzymes involved in the nucleotide sugar biosynthesis

Function	Gene names based on literature	Arabidopsis gene	Putative ortholog in *C. reinhardtii*	% of id/sim
UDP-Glc biosynthesis				
Phosphoglucomutase		At1g23190	Cre06.g278210	53/67
UDP-sugar pyrophosphorylase	AtUSP, SLOPPY	At5g52560	Cre14.g621751	38/48
UTP-Glc-1-phosphate uridylyltransferase		At5g17310	Cre04.g229700	35/52
UDP-Gal*f* biosynthesis				
UDP-galactose 4-epimerase	AtUGE4	At4g10960	Cre04.g214502	56/72
UDP-galactopyranose-mutase	UGM[a]	–	Cre06.g272900[a]	48/60
GDP-Man biosynthesis				
Mannose-6-phosphate isomerase	AtMPI1	At1g67070	Cre02.g147650[b]	36/51
Phosphomannomutase	AtPMM	At2g45790	Cre14.g626900[b]	71/87
GDP-Man pyrophosphorylase	AtVTC1, AtGMPP1	At2g39770	Cre16.g672800[b]	66/82
UDP-GlcA biosynthesis				
UDP-Glc-6-dehydrogenase	UGD	At1g26570	Cre07.g357200	70/82
			Cre06.g278185	70/82
			Cre12.g532450	46/62
UDP-GlcNAc biosynthesis				
GlcN-6-P synthase	–	At3g24090	Cre08.g375500	53/69
GlcN-6-P acetyltransferase	GNA	At5g15770	Cre12g560200	46/63
Phospho-*N*-acetylglucosamine mutase	DRT101	At5g18070	Cre08.g379700	36/50
UTP-*N*-acetyl-glucosamine-1-P-uridylyltransferase	GLCNAC1PUT1	At1g31070	Cr16g6960000	22/37
UDP-Xyl biosynthesis				
UDP-xylose synthase	AtUXS3	At5g59290	Cre03.g169400	61/74
UDP-L-Ara*f* biosynthesis				
UDP-xylose-4-epimerase	AtMUR4	At1g30620	Cre09.g401022[c]	47/63
UDP-arabinopyranose mutase	AtRGP1	At3g02230	Cre13.g565800	78/85

Except for the UDP-Gal mutase[a], all these sequences have been identified by comparison with a TBLASTN using Arabidopsis sequences as keys. For each putative enzyme, the percentages of similarity (sim) and identity (id) have been calculated following a pairwise alignment of the deduced amino acid sequence from the predicted *C. reinhardtii* gene with the Arabidopsis amino acid sequence using the ClustalW program

[a]This sequence has been identified using the characterized enzyme from *C. neoformans* (Accession number AAX09636.1) as a key for the genomic search (Beverley et al. 2005)

[b]Urzica et al. (2012)

[c]Kotani et al. (2013)

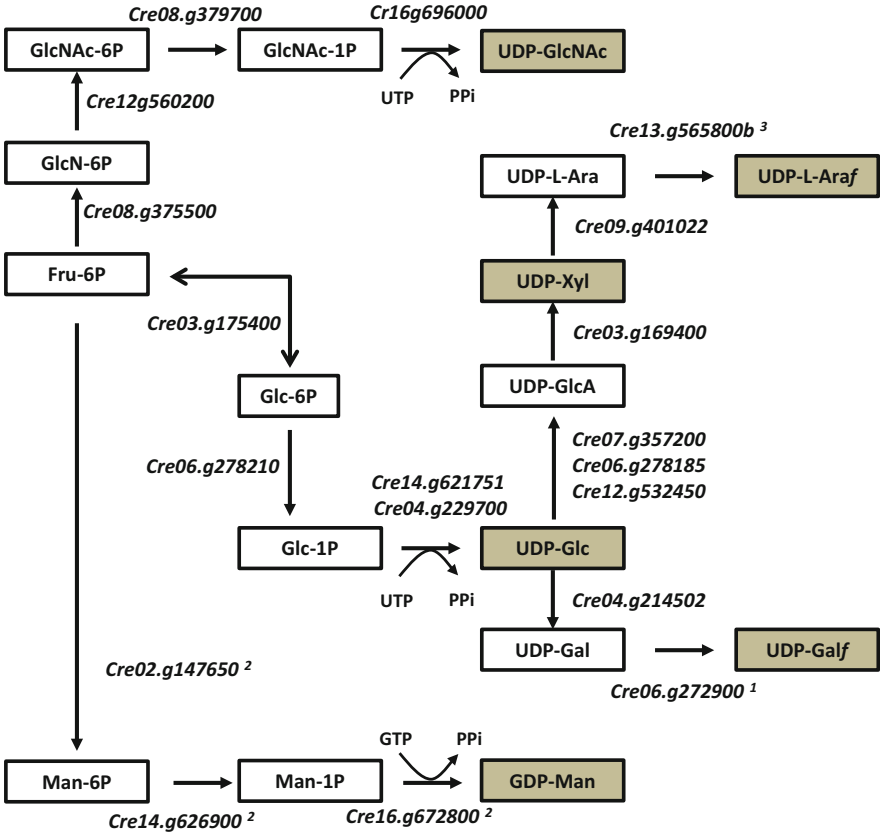

Fig. 3 Schematic representation of putative nucleotide sugar biosynthetic pathways in *C. reinhardtii*. Nucleotide sugars indicated in *gray squares* correspond to substrates used by glycosyltransferases for *N*- and *O*-linked glycans biosynthesis. *C. reinhardtii* genes encoding for putative enzymes involved in the formation of nucleotide sugars have been identified based on their homologies with Arabidopsis sequences as reported in Table 2. Exponent numbers refers to the following papers: (1) Kotani et al. (2013); (2) Urzica et al. (2012); (3) Berverley et al. (2005)

that *C. reinhardtii* genome contains one gene (Cre16.g672800, CrGMP1) encoding an amino acid sequence exhibiting 66% and 82% of identity and similarity, respectively, with the Arabidopsis GDP-Man PPase AtVTC1 (Urzica et al. 2012).

Some mature glycans *N*-linked to *C. reinhardtii* proteins carry one or two xylose residues (Mathieu-Rivet et al. 2013). In plants, UDP-xylose (UDP-Xyl) results from the decarboxylation of UDP-GlcA by a UDP-xylose synthase (UXS). Five genes encoding for UXS have been identified in Arabidopsis (Bar-Peled and O'Neill 2011; Harper and Bar-Peled 2002; Pattathil et al. 2005). Among the five candidates, three encode for soluble enzymes whereas the two others encode for isoforms which are predicted type II membrane proteins with the catalytic domain facing the membrane lumen of the Golgi apparatus. These data suggest that the

decarboxylation of UDP-GlcA occurs in plants both in the cytosol and in the Golgi apparatus (Pattathil et al. 2005). In *C. reinhardtii*, search for a gene encoding for a putative UXS led to the identification of a unique sequence (Cre03.g169400, CrUXS). The deduced amino acid sequence shares 61% of identity with the cytosolic enzyme AtUXS3. Furthermore, this sequence harbors two characteristic motifs required for dehydratase and epimerase activities, the *N*-terminal GxxGxxG motif and the catalytic triad serine, tyrosine, and lysine, reported in AtUXS1, AtUXS2, and AtUXS3 (Harper and Bar-Peled 2002).

The MS analyses of *N*-glycans carried out by soluble and membrane-bound proteins revealed minute amount of *N*-glycan structures containing fucose (Mathieu-Rivet et al. 2013). Although putative fucosyltransferases have been identified in the genome (Cre31.g780450 and Cre18.g749047), search for sequence homology using Arabidopsis genes as references revealed a limited number of candidate genes for enzymes involved in the biosynthesis of GDP-L-fucose. In plants, GDP-L-fucose (GDP-L-Fuc) can be synthesized via two distinct pathways involving either L-Fuc-1-P or GDP-Man. The first one (called the salvage pathway) requires the activity of the bifunctional enzyme L-fucokinase/GDP-L-fucose pyrophosphorylase (AtFKGP) which is responsible for the phosphorylation of L-Fucose and thereafter for the formation of GDP-L-Fuc (Bar-Peled and O'Neill 2011). In addition, GDP-L-fucose can be formed from GDP-Man through the activity of GDP-Man-4,6-dehydratase (GMD) and deoxymannose-3,5-epimerase-4-reductase (GER1). In *C. reinhardtii,* only one sequence (Cre01.g019250) has been shown to display 18% and 37% of identity and similarity with At1g73250 which encodes for GER1 in Arabidopsis.

Others monosaccharides are found in *O*-linked glycans such as galactose and L-arabinose (Bollig et al. 2007). UDP-Gal comes mainly from UDP-Glc via epimerization. Whereas several isoforms of UDP-Gal-4-epimerase (UGE) have been found in most plants, only one single sequence encoding for a putative GME has been identified in *C. reinhardtii* (Cre04.g214502, CrGME; Rosti et al. 2007). Moreover, in this organism, it has been shown that the Gal residues present in *O*-glycans exhibit the unusual furanose conformation (Gal*f*) (Bollig et al. 2007). Bollig and collaborators proposed that UDP-Gal*f* results from the activity of the UDP-galactopyranose-mutase (UGM) which converts the conformation of UDP-galactopyranose (UDP-Gal*p*) into UDP-Gal*f*. UDP-galactopyranose-mutases are found in prokaryotes and a few eukaryotes such as *Cryptococcus neoformans* or *T. cruzi*. A sequence encoding for a putative UGM, sharing 60% of identity with those from *C. neoformans* (Cre06.g272900, CrUGM, Table 2), has been identified in *C. reinhardtii*, although its activity has not be functionally demonstrated (Beverley et al. 2005).

In *C. reinhardtii O*-glycans, as in plant hemicelluloses and proteoglycans, arabinofuranosyl rather than arabinopyranosyl residues were reported (Bollig et al. 2007). UDP-L-arabinopyranose is synthesized from UDP-Xyl and then the conversion to UDP-L-arabinofuranose occurs through the action of a specific mutase (Table 2; Fig. 3). In *C. reinhardtii*, an UDP-arabinopyranose mutase has been recently purified mainly from the cytosol, and a minor activity has been also detected in the microsomal fraction (Kotani et al. 2013). Mass spectrometry

sequencing of the purified enzyme demonstrated that it shares 78% of identity with AtRGP1 that catalyzes the conversion of UDP-L-Ara*p* into UDP-L-Ara*f* in Arabidopsis (Rautengarten et al. 2011).

5.2 Nucleotide Sugar Transporters

Whereas the activation of sugar precursors is occurring in the cytosol, numerous glycosyltransferases involved in the glycan elongation reside inside the ER and Golgi apparatus. As a consequence, a transport of the cytosolic nucleotide sugars across the ER and Golgi membranes is required for the oligosaccharide biosynthesis. This transport is achieved through hydrophobic proteins composed of several transmembrane domains called nucleotide sugar transporters (NSTs) (Reyes and Orellana 2008). These proteins act as antiporters which couple the passage of the sugar nucleotide into the lumen with the exit of a nucleotide monophosphate into the cytosol. For a long time, it was thought that each NST was specialized in the transport of one specific nucleotide sugar (Hirschberg et al. 1998). However, this hypothesis tends to be invalidated with the discovery of numerous examples of NSTs able to transport several distinct activated sugars in eukaryotes. As illustrated, AtUTR1 from *Arabidopsis thaliana* allows the transport into the Golgi apparatus of both UDP-Glc and UDP-Gal (Norambuena et al. 2002; Reyes et al. 2006). However, a simple analysis of amino acid sequences is not sufficient to predict substrate specificity of a NST and further functional analysis is required.

NSTs belong to the drug/metabolite transporter (DMT) superfamily, within which they form a family with the group of triose phosphate translocators (TPT) (Knappe 2003a; Ward 2001). In Arabidopsis, this TPT/NSTs family brings together 51 members, themselves distributed into six distinct subgroups (Rautengarten et al. 2014). In order to identify orthologs encoding for putative TPT/NSTs in the *C. reinhardtii* genome, we used Arabidopsis TPT/NSTs sequences as key entries for bioinformatic searches by TBLASTN. Using this strategy, we found 23 putative genes for which the deduced amino acid sequences harbor the characteristic TPT domain (Pfam 03151). These results are summarized as a phylogenetic tree in Fig. 4. The comparison of this 23 sequences with those from Arabidopsis shows that five of them could be predicted to belong to the group I defined by Rautengarten and collaborators (2014) which gathers NSTs characterized by the presence of the highly conserved lysine/threonine (KT) motif involved in the NST-substrate binding specificity (Knappe 2003a). In Arabidopsis, NSTs-KT proteins are split into four subclades (Rautengarten et al. 2014). According to our phylogenetic analysis, three *C. reinhardtii* sequences are more related to Arabidopsis proteins from the subclades A and B, which have been recently shown to correspond to Golgi bifunctional UDP-rhamnose/UDP-Gal transporters (Rautengarten et al. 2014), and the two others are closely related to proteins from the subclade D for which the function remains unknown. No sequence is predicted for the subclade C which encompasses three Golgi transporters specific for

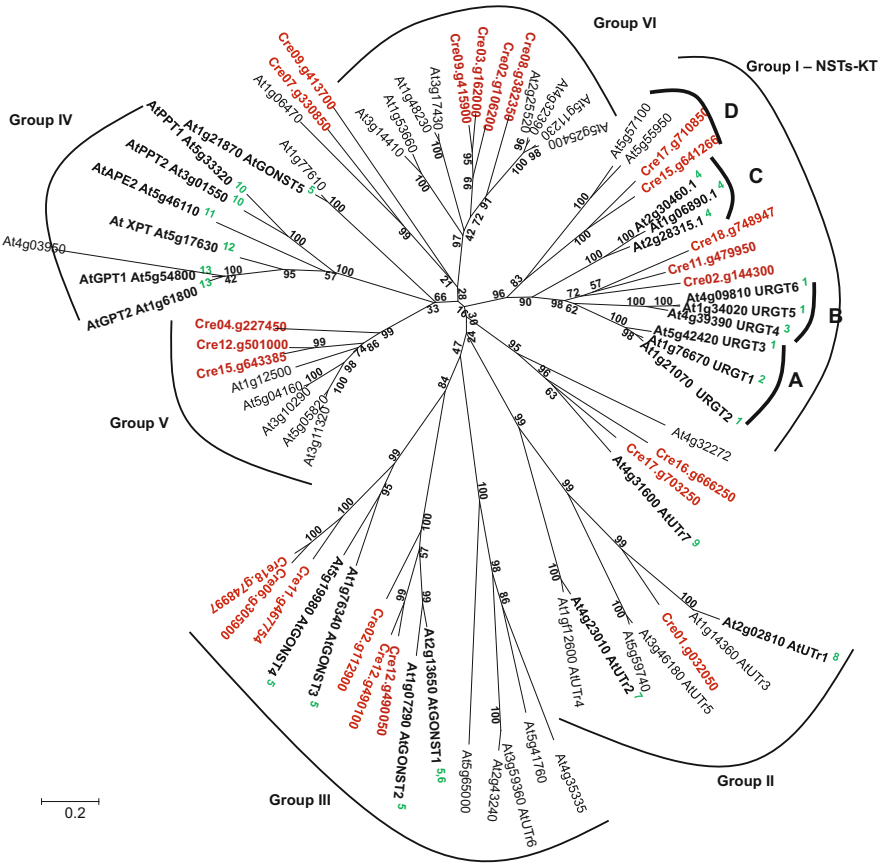

Fig. 4 Phylogenetic relationships between Arabidopsis members of the NST/TPT family and *C. reinhardtii* putative transporters. This phylogenetic tree is constructed based on the full-length amino acid sequences of NSTs/TPT from Arabidopsis (*black font*) and those which have been deduced from predicted genes in *C. reinhardtii* (*red font*). The Arabidopsis proteins in *bold* correspond to transporters functionally characterized. The alignment of the sequences has been made using the ClustalW program. The phylogenetic tree was generated using the neighbor-joining method with the software MEGA5 (Molecular Evolutionary Genetics Analysis). The robustness of branches has been evaluated using 1000 bootstraps. Groups I–VI and subgroups A–D were assigned according to Rautengarten et al. (2014). Exponent numbers refers to the following papers: (1) Rautengarten et al. (2014); (2) Bakker et al. (2005); (3) Rollwitz et al. (2006); (4) Ebert et al. (2015); (5) Handford et al. (2004); (6) Baldwin et al. (2001); (7) Norambuena et al. (2005); (8) Reyes et al. (2006); (9) Handford et al. (2012); (10) Knappe et al. (2003b); (11) Schneider et al. (2002); (12) Eicks et al. (2002); (13) Niewiadomski et al. (2005)

UDP-Xyl (Ebert et al. 2015) although xylosyl residues are found in mature *N*-glycans in *C. reinhardtii* (Mathieu-Rivet et al. 2013). However, as mentioned above, no conclusion can be drawn concerning the substrate specificity of these putative transporters as we cannot exclude that one of the identified sequences

would encode for an UDP-Xyl transporter. In addition, it has been shown in plants, that UDP-Xyl could be synthesized within the Golgi apparatus itself (Harper and Bar-Peled 2002), which would challenge the necessity of such UDP-Xyl transporter.

Six putative TPT-NSTs identified in *C. reinhardtii* fall into the group III, in which are found the Arabidopsis Golgi-localized GDP-Man transporters 1 to 4 (AtGONST1 to 4) (Handford et al. 2004). All these *C. reinhardtii* sequences display in the first transmembrane domain the two conserved amino acids asparagine/lysine (NK) corresponding to a potential substrate-binding site (Handford et al. 2004; Knappe 2003a). Furthermore, two of the six sequences (Cre12.g490100, Cre12.g49050) exhibit the conserved motif GXLNK (where X represents any amino acid) which is required for the specific recognition of GDP-Man (Gao et al. 2001).

Only one putative *C. reinhardtii* TPT-NST is found in the group II that gathers UDP-Glc/UDP-Gal transporters. Whereas some of them like AtUTr2 have been shown to be localized in the Golgi apparatus (Norambuena et al. 2005), others, like AtUTr1 and AtUTr3, are found in the ER (Reyes et al. 2010). The predicted *C. reinhardtii* gene (Cre01.g032050) would encode for a protein which amino acid sequence shares 47% and 49% of identity with AtUTr1 and AtUTr3, respectively. In addition, as it has been shown for AtUTr1 and AtUTr3 (Reyes et al. 2010), the *C*-terminal part of the *C. reinhardtii* predicted protein is characterized by the presence of a KKXX (where X represents any amino acid) retention signal which could be responsible for its retention within the ER. The heterologous expression of AtUTr1 in yeast showed that its affinity is higher for UDP-Glc than for UDP-Gal (Reyes et al. 2010). It has been proposed that this protein in Arabidopsis would be involved in the channeling of the Glc into the ER and thus would be required for the quality control process.

Among the remaining 11 sequences encoding for putative TPT/NSTs found in the *C. reinhardtii* genome, three are related to members of the group V and four fall in the group VI which contain no functionally characterized transporters (Knappe et al. 2003a). No sequence has been found in the group IV which gathers chloroplastic transporters (Eicks et al. 2002; Knappe et al. 2003b; Niewiadomski et al. 2005; Schneider et al. 2002).

6 Concluding Remarks and Future Perspectives

In the last years, *C. reinhardtii* has been evaluated as an emerging new factory for the production of biopharmaceuticals. More than 20 recombinant proteins have been successfully expressed in *C. reinhardtii* either in the chloroplast or in a secreted manner (Mathieu-Rivet et al. 2014; Rasala and Mayfield 2015). Recent findings regarding its *N*- and *O*-glycosylation pathways suggest that many efforts of engineering will have to be done to make it suitable for the production of recombinant secreted glycoproteins. In addition, a careful structural analysis of the

glycans present on such recombinant glycoproteins would be necessary to evaluate which glycan structures have been added onto the protein of interest. Recombinant EPO seems to be an appropriate model for such proof of concept. Indeed, the mature form of the EPO consists of 165 amino acid residues and is decorated with three *N*-linked and one *O*-linked glycans, representing almost 40% of the EPO molecular mass (Jiang et al. 2014). Eichler-Stahlberg and collaborators in 2009 already demonstrated that *C. reinhardtii* is able to produce and secrete successfully a recombinant form of EPO. Unfortunately, in this study, no detailed biochemical characterization of the recombinant protein is reported to gain information regarding its posttranslational modifications.

As far as monoclonal antibodies production in *C. reinhardtii* is concerned, we hypothesize that it would be necessary to engineer the algae *N*-glycosylation pathway in order to humanize the *N*-glycan structures added to the Chlamydomonas-made antibodies. Indeed, it has been well established that complex-type *N*-glycans, especially biantennary *N*-glycans bearing lactosamine antennae such as the one drawn in Fig. 1b, are required for the effector functions of antibodies (Mimura et al. 2001). Therefore, modifications of the *C. reinhardtii N*-glycans would require the complementation of Golgi enzymes repertoire with first the overexpression of heterologous GnT I which is currently missing within the *C. reinhardtii N*-glycosylation pathway. In addition, the complementation with α-mannosidase II, N-acetylglucosaminyltransferase II (GnT II), and β(1,4)-galactosyltransferase (β(1,4)-GalT) which is responsible for the transfer of the galactose onto the terminal GlcNAc residues would be necessary to mature *C. reinhardtii* similarly to the human *N*-glycans (Fig. 5). Additionally, inhibition of the xylosylation and glycan methylation would probably be needful as the overexpression of GnT I and β(1,4)-GalT could not be sufficient for *N*-glycan engineering as exemplified for tobacco plants complemented with the human β(1,4)-GalT (Bakker et al. 2001). Indeed, the presence of the xylose residues and methyl groups might represent a potential risk as they could be recognized as new xenoglycans when injected into humans. This may lead to induce immune responses and allergies as it has already been described for four different glycoepitopes (e.g., plant core β1,2-xylose and core α1,3-fucose; van Beers and Bardor 2012). For other glycoproteins of interest such as EPO, further engineering of the *C. reinhardtii* cells would be required in order to make the algae cells synthesize and transfer sialic acid onto the recombinant proteins as sialic acids are important for the in vivo half-life of blood proteins (Lingg et al. 2012). As described successfully for other expression systems such as plants (Bardor et al. 2011; Dicker and Strasser 2015), bacteria (Berlec and Strukelj 2013; Huang et al. 2012), and yeast (Berlec and Strukelj 2013; Wildt and Gerngross 2005), knock-in and knockout strategies of glycoenzymes would be necessary to engineer the *N*-glycosylation pathway in *C. reinhardtii*.

In the future, the biosimilar market will also attract attention. Indeed, biosimilars will increase and target a multibillion dollar market as quite a number of biopharmaceuticals products have lost or will shortly lose their patent protection (Walsh 2014). In this regards and based on the actual *N*-glycosylation knowledge, *C. reinhardtii* appears already to be an interesting platform for producing recombinant biosimilars carrying high-mannose-type *N*-glycans (Mathieu-Rivet et al. 2014). Its

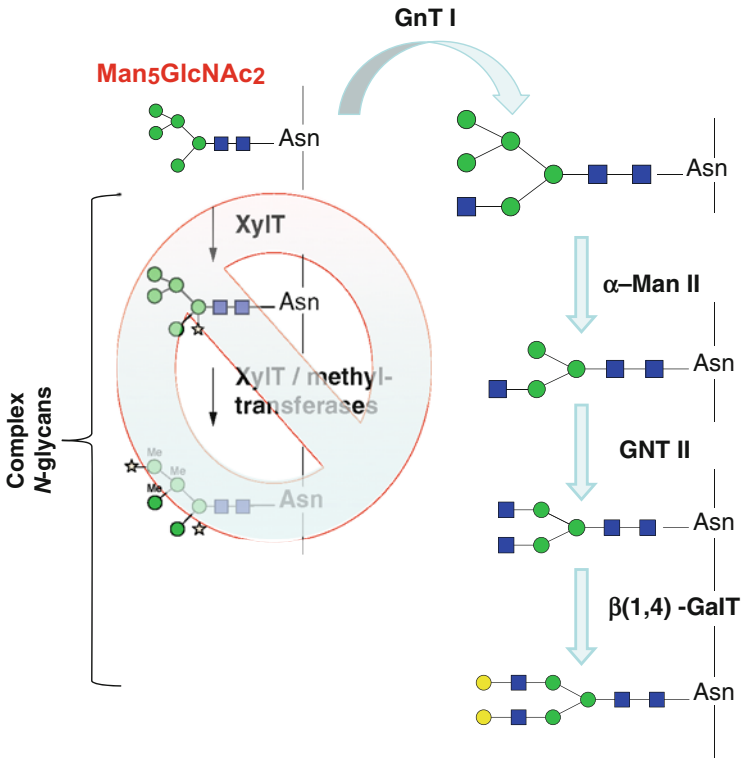

Fig. 5 Engineering of the *N*-glycosylation pathway in *C. reinhardtii* required to humanize the *N*-glycan structures of recombinant proteins such as monoclonal antibodies. The *symbols* used for representing the *N*-glycan structures are the ones from the Consortium for Functional Glycomics (Varki et al. 2009a). $Man_5GlcNAc_2$, oligomannoside bearing five mannose residues; GnT I, *N*-acetylglucosaminyltransferase I; α-Man II, α-mannosidase II; GnT II, *N*-acetylglucosaminyltransferase II; β(1,4)-GalT, β(1,4)-galactosyltransferase; XylT, xylosyltransferase. *Me* methyl group, *blue-filled squares N*-acetylglucosamine (GlcNAc), *green-filled circles* mannose (Man), *yellow-filled circles* galactose

capability to produce and add short mannose terminating *N*-glycans onto its endogenous proteins could represent an advantage for the production of glycosylated biopharmaceuticals which requires effective targeting and internalization into macrophages through the recognition of terminal mannose residues. This is well exemplified in the literature through the glucocerebrosidase which is a lysosomal enzyme administered intravenously into patients suffering from Gaucher's disease (Van Patten et al. 2007). The current preparation of glucocerebrosidase involves its recombinant expression in mammalian cells and in vitro post-purification exoglycosidase digestions to generate trimannose core *N*-glycans ($Man_3GlcNAc_2$). Therefore, alternative expression systems such as *C. reinhardtii* that are capable of producing naturally short mannose terminated *N*-glycans are of interest and should help decrease considerably the production cost.

Acknowledgments The authors are indebted to all coworkers and students at the Glyco-MEV laboratory who are currently contributing to the microalgae research project or did so in the past. They acknowledge Magda Dudek for careful reading of the manuscript. They are also thankful to the University of Rouen, the region Haute-Normandie now called Normandie and the IUF for their financial support.

References

Aebi M (2013) N-linked protein glycosylation in the ER. Biochim Biophys Acta (BBA) Mol Cell Res 1833:2430–2437

Almaraz-Delgado AL, Flores-Uribe J, Pérez-España VH, Salgado-Manjarrez E, Badillo-Corona JA (2014) Production of therapeutic proteins in the chloroplast of *Chlamydomonas reinhardtii*. AMB Express 4:57

Bakker H, Bardor M, Molthoff JW, Gomord V, Elbers I, Stevens LH, Jordi W, Lommen A, Faye L, Lerouge P et al (2001) Galactose-extended glycans of antibodies produced by transgenic plants. Proc Natl Acad Sci 98:2899–2904

Bakker H, Routier F, Oelmann S, Jordi W, Lommen A, Gerardy-Schahn R, Bosch D (2005) Molecular cloning of two *Arabidopsis* UDP-galactose transporters by complementation of a deficient Chinese hamster ovary cell line. Glycobiology 15(2):193–201

Baldwin TC, Handford MG, Yuseff MI, Orellana A, Dupree P (2001) Identification and characterization of GONST1, a golgi-localized GDP-mannose transporter in *Arabidopsis*. Plant Cell 13(10):2283–2295

Barahimipour R, Neupert J, Bock R (2016) Efficient expression of nuclear transgenes in the green alga Chlamydomonas: synthesis of an HIV antigen and development of a new selectable marker. Plant Mol Biol 90:403–418

Barber C, Rösti J, Rawat A, Findlay K, Roberts K, Seifert GJ (2006) Distinct properties of the five UDP-D-glucose/UDP-D-galactose 4-epimerase isoforms of Arabidopsis thaliana. J Biol Chem 281:17276–17285

Bardor M, Burel C, Villarejo A, Cadoret J-P, Carlier A, Lerouge P (2011) Chapter 5: Plant *N*-glycosylation: an engineered pathway for the production of therapeutic plant-derived glycoproteins. In: Brooks S, Rudd P, Apelmelk B (eds) Glycosylation in diverse cell systems – challenges and new frontiers in experimental glycobiology. Essential reviews in experimental biology, vol 4. Society for Experimental Biology, London, pp 93–118

Bar-Peled M, O'Neill MA (2011) Plant nucleotide sugar formation, interconversion, and salvage by sugar recycling. Annu Rev Plant Biol 62:127–155

Barrera DJ, Mayfield SP (2013) High-value recombinant protein production in microalgae. In: Richmond A, Hu Q (eds) Handbook of microalgal culture: applied phycology and biotechnology, 2nd edn. Wiley, Oxford, pp 532–544

Beer LL, Boyd ES, Peters JW, Posewitz MC (2009) Engineering algae for biohydrogen and biofuel production. Curr Opin Biotechnol 20:264–271

Berlec A, Strukelj B (2013) Current state and recent advances in biopharmaceutical production in Escherichia coli, yeasts and mammalian cells. J Ind Microbiol Biotechnol 40(3–4):257–274

Beverley SM, Owens KL, Showalter M, Griffith CL, Doering TL, Jones VC, McNeil MR (2005) Eukaryotic UDP-galactopyranose mutase (GLF gene) in microbial and metazoal pathogens. Eukaryot Cell 4:1147–1154

Bollig K, Lamshöft M, Schweimer K, Marner F-J, Budzikiewicz H, Waffenschmidt S (2007) Structural analysis of linear hydroxyproline-bound O-glycans of *Chlamydomonas reinhardtii*—conservation of the inner core in Chlamydomonas and land plants. Carbohydr Res 342:2557–2566

Brooks S (2011) Chapter 4: Species differences in protein glycosylation and their implication for biotechnology. In: Brooks S, Rudd P, Apelmelk B (eds) Glycosylation in diverse cell

systems – challenges and new frontiers in experimental glycobiology. Essential reviews in experimental biology, vol 4. Society for Experimental Biology, London, pp 93–118
Catt JW, Hills GJ, Roberts K (1978) Cell wall glycoproteins from *Chlamydomonas reinhardii*, and their self-assembly. Planta 138:91–98
Chen M-H, Huang L-F, Li H, Chen Y-R, Yu S-M (2004) Signal peptide-dependent targeting of a rice α-amylase and cargo proteins to plastids and extracellular compartments of plant cells. Plant Physiol 135:1367–1377
Conklin PL, Norris SR, Wheeler GL, Williams EH, Smirnoff N, Last RL (1999) Genetic evidence for the role of GDP-mannose in plant ascorbic acid (vitamin C) biosynthesis. Proc Natl Acad Sci 96:4198–4203
Corfield AP (2015) Mucins: a biologically relevant glycan barrier in mucosal protection. Biochim Biophys Acta (BBA) Gen Subj 1850:236–252
Dance A (2010) From pond scum to pharmacy shelf. Nat Med 16:146–149
Dauvillée D, Delhaye S, Gruyer S, Slomianny C, Moretz SE, d'Hulst C, Long CA, Ball SG, Tomavo S (2010) Engineering the chloroplast targeted malarial vaccine antigens in Chlamydomonas starch granules. PLoS One 5:e15424
De Muynck B, Navarre C, Boutry M (2010) Production of antibodies in plants: status after twenty years. Plant Biotechnol J 8:529–563
Demain AL, Vaishnav P (2009) Production of recombinant proteins by microbes and higher organisms. Biotechnol Adv 27:297–306
Dicker M, Strasser R (2015) Using glyco-engineering to produce therapeutic proteins. Expert Opin Biol Ther 15(10):1501–1516
Ebert B, Rautengarten C, Guo X, Xiong G, Stonebloom S, Smith-Moritz AM, Herter T, Chan LJG, Adams PD, Petzold CJ et al (2015) Identification and characterization of a Golgi-localized UDP-xylose transporter family from Arabidopsis. Plant Cell 27:1218–1227
Eichler-Stahlberg A, Weisheit W, Ruecker O, Heitzer M (2009) Strategies to facilitate transgene expression in *Chlamydomonas reinhardtii*. Planta 229:873–883
Eicks M, Maurino V, Knappe S, Flugge U-I, Fischer K (2002) The plastidic pentose phosphate translocator represents a link between the cytosolic and the plastidic pentose phosphate pathways in plants. Plant Physiol 128:512–522
Elvin JG, Couston RG, van der Walle CF (2013) Therapeutic antibodies: market considerations, disease targets and bioprocessing. Int J Pharm 440:83–98
Ferris PJ, Woessner JP, Waffenschmidt S, Kilz S, Drees J, Goodenough UW (2001) Glycosylated polyproline II rods with kinks as a structural motif in plant hydroxyproline-rich glycoproteins. Biochemistry (Mosc) 40:2978–2987
Gao X-D, Nishikawa A, Dean N (2001) Identification of a conserved motif in the yeast Golgi GDP-mannose transporter required for binding to nucleotide sugar. J Biol Chem 276:4424–4432
Garénaux E, Shams-Eldin H, Chirat F, Bieker U, Schmidt J, Michalski J-C, Cacan R, Guérardel Y, Schwarz RT (2008) The dual origin of *Toxoplasma gondii N*-Glycans. Biochemistry (Mosc) 47:12270–12276
Gill DJ, Clausen H, Bard F (2011) Location, location, location: new insights into O-GalNAc protein glycosylation. Trends Cell Biol 21:149–158
Gomord V, Fitchette A-C, Menu-Bouaouiche L, Saint-Jore-Dupas C, Plasson C, Michaud D, Faye L (2010) Plant-specific glycosylation patterns in the context of therapeutic protein production: PMP-specific glycosylation patterns. Plant Biotechnol J 8:564–587
Gong Y, Hu H, Gao Y, Xu X, Gao H (2011) Microalgae as platforms for production of recombinant proteins and valuable compounds: progress and prospects. J Ind Microbiol Biotechnol 38(12):1879–1890
Goodenough UW, Gebhart B, Mecham RP, Heuser JE (1986) Crystals of the *Chlamydomonas reinhardtii* cell wall: polymerization, depolymerization, and purification of glycoprotein monomers. J Cell Biol 103:405–417
Gregory JA, Topol AB, Doerner DZ, Mayfield S (2013) Alga-produced cholera toxin-Pfs25 fusion proteins as oral vaccines. Appl Environ Microbiol 79:3917–3925

Gregory JA, Shepley-McTaggart A, Umpierrez M, Hurlburt BK, Maleki SJ, Sampson HA, Mayfield SP, Berin MC (2016) Immunotherapy using algal-produced Ara h 1 core domain suppresses peanut allergy in mice. Plant Biotechnol J 14:1541–1550

Handford MG, Sicilia F, Brandizzi F, Chung JH, Dupree P (2004) Arabidopsis thaliana expresses multiple Golgi-localised nucleotide-sugar transporters related to GONST1. Mol Gen Genomics 272:397–410

Handford M, Rodríguez-Furlán C, Marchant L, Segura M, Gómez D, Alvarez-Buylla E, Xiong GY, Pauly M, Orellana A (2012) *Arabidopsis thaliana* AtUTr7 encodes a golgi-localized UDP-glucose/UDP-galactose transporter that affects lateral root emergence. Mol Plant 5(6):1263–1280

Harper AD, Bar-Peled M (2002) Biosynthesis of UDP-xylose. Cloning and characterization of a novel Arabidopsis gene family, UXS, encoding soluble and putative membrane-bound UDP-glucuronic acid decarboxylase isoforms. Plant Physiol 130:2188–2198

Helenius J, Aebi M (2002) Transmembrane movement of dolichol linked carbohydrates during N-glycoprotein biosynthesis in the endoplasmic reticulum. Semin Cell Dev Biol 13 (3):171–178

Helenius J, Ng DTW, Marolda CL, Walter P, Valvano MA, Aebi M (2002) Translocation of lipid-linked oligosaccharides across the ER membrane requires Rft1 protein. Nature 415:447–450

Hempel F, Maier UG (2016) Microalgae as solar-powered protein factories. Adv Exp Med Biol 896:241–262

Hirschberg CB, Robbins PW, Abeijon C (1998) Transporters of nucleotide sugars, ATP, and nucleotide sulfate in the endoplasmic reticulum and Golgi apparatus. Annu Rev Biochem 67:49–69

Hossler P, Khattak SF, Li ZJ (2009) Optimal and consistent protein glycosylation in mammalian cell culture. Glycobiology 19:936–949

Huang C-J, Lin H, Yang X (2012) Industrial production of recombinant therapeutics in Escherichia Coli and its recent advancements. J Ind Microbiol Biotechnol 39:383–399

Jiang J, Tian F, Cai Y, Qian X, Costello CE, Ying W (2014) Site-specific qualitative and quantitative analysis of the N- and O-glycoforms in recombinant human erythropoietin. Anal Bioanal Chem 406:6265–6274

Kelleher DJ, Gilmore R (2006) An evolving view of the eukaryotic oligosaccharyltransferase. Glycobiology 16:47R–62R

Kelleher DJ, Banerjee S, Cura AJ, Samuelson J, Gilmore R (2007) Dolichol-linked oligosaccharide selection by the oligosaccharyltransferase in protist and fungal organisms. J Cell Biol 177:29–37

Keskiaho K, Hieta R, Sormunen R, Myllyharju J (2007) *Chlamydomonas reinhardtii* has multiple prolyl 4-hydroxylases, one of which is essential for proper cell wall assembly. Plant Cell 19:256–269

Kieliszewski MJ, Lamport DTA (1994) Extensin: repetitive motifs, functional sites, post-translational codes, and phylogeny. Plant J 5:157–172

Kleczkowski LA, Geisler M, Ciereszko I, Johansson H (2004) UDP-glucose pyrophosphorylase. An old protein with new tricks. Plant Physiol 134:912–918

Klinghammer M, Tenhaken R (2007) Genome-wide analysis of the UDP-glucose dehydrogenase gene family in Arabidopsis, a key enzyme for matrix polysaccharides in cell walls. J Exp Bot 58:3609–3621

Knappe S, Flügge U-I, Fischer K (2003a) Analysis of the plastidic phosphate translocator gene family in Arabidopsis and identification of new phosphate translocator-homologous transporters, classified by their putative substrate-binding site. Plant Physiol 131:1178–1190

Knappe S, Löttgert T, Schneider A, Voll L, Flügge U-I, Fischer K (2003b) Characterization of two functional phosphoenolpyruvate/phosphate translocator (PPT) genes in Arabidopsis—AtPPT1 may be involved in the provision of signals for correct mesophyll development. Plant J Cell Mol Biol 36:411–420

Kotani A, Tsuji M, Azama Y, Ishii T, Takeda T, Yamashita T, Shimojima M, Konishi T (2013) Purification and characterization of UDP-arabinopyranose mutase from *Chlamydomonas reinhardtii*. Biosci Biotechnol Biochem 77:1874–1878

Lam MK, Lee KT (2012) Microalgae biofuels: a critical review of issues, problems and the way forward. Biotechnol Adv 30:673–690

Lauersen KJ, Vanderveer TL, Berger H, Kaluza I, Mussgnug JH, Walker VK, Kruse O (2013a) Ice recrystallization inhibition mediated by a nuclear-expressed and -secreted recombinant ice-binding protein in the microalga *Chlamydomonas reinhardtii*. Appl Microbiol Biotechnol 97:9763–9772

Lauersen KJ, Berger H, Mussgnug JH, Kruse O (2013b) Efficient recombinant protein production and secretion from nuclear transgenes in *Chlamydomonas reinhardtii*. J Biotechnol 167:101–110

Lauersen KJ, Kruse O, Mussgnug JH (2015a) Targeted expression of nuclear transgenes in *Chlamydomonas reinhardtii* with a versatile, modular vector toolkit. Appl Microbiol Biotechnol 99:3491–3503

Lauersen KJ, Huber I, Wichmann J, Baier T, Leiter A, Gaukel V, Kartushin V, Rattenholl A, Steinweg C, von Riesen L et al (2015b) Investigating the dynamics of recombinant protein secretion from a microalgal host. J Biotechnol 215:62–71

Lerouge P, Cabanes-Macheteau M, Rayon C, Fischette-Lainé AC, Gomord V, Faye L (1998) N-glycoprotein biosynthesis in plants: recent developments and future trends. Plant Mol Biol 38:31–48

Levy-Ontman O, Fisher M, Shotland Y, Weinstein Y, Tekoah Y, Arad S (2014) Genes involved in the endoplasmic reticulum N-glycosylation pathway of the red microalga Porphyridium sp.: a bioinformatic study. Int J Mol Sci 15:2305–2326

Lingg N, Zhang P, Song Z, Bardor M (2012) The sweet tooth of biopharmaceuticals: importance of recombinant protein glycosylation analysis. Biotechnol J 7:1462–1472

Lu J, Takahashi T, Ohoka A, Nakajima K, Hashimoto R, Miura N, Tachikawa H, Gao XD (2012) Alg14 organizes the formation of a multiglycosyltransferase complex involved in initiation of lipid-linked oligosaccharide biosynthesis. Glycobiology 22(4):504–516

Ma JK-C, Drossard J, Lewis D, Altmann F, Boyle J, Christou P, Cole T, Dale P, van Dolleweerd CJ, Isitt V et al (2015) Regulatory approval and a first-in-human phase I clinical trial of a monoclonal antibody produced in transgenic tobacco plants. Plant Biotechnol J 13:1106–1120

Manuell AL, Beligni MV, Elder JH, Siefker DT, Tran M, Weber A, McDonald TL, Mayfield SP (2007) Robust expression of a bioactive mammalian protein in Chlamydomonas chloroplast. Plant Biotechnol J 5:402–412

Mathieu-Rivet E, Scholz M, Arias C, Dardelle F, Schulze S, Le Mauff F, Teo G, Hochmal AK, Blanco-Rivero A, Loutelier-Bourhis C et al (2013) Exploring the N-glycosylation pathway in *Chlamydomonas reinhardtii* unravels novel complex structures. Mol Cell Proteomics 12:3160–3183

Mathieu-Rivet E, Kiefer-Meyer M-C, Vanier G, Ovide C, Burel C, Lerouge P, Bardor M (2014) Protein N-glycosylation in eukaryotic microalgae and its impact on the production of nuclear expressed biopharmaceuticals. Front Plant Sci 5:359

Matsuoka K, Watanabe N, Nakamura K (1995) O-glycosylation of a precursor to a sweet potato vacuolar protein, sporamin, expressed in tobacco cells. Plant J Cell Mol Biol 8:877–889

Maxmen A (2012) Drug-making plant blooms. Nature 485:160

Mayfield SP, Franklin SE (2005) Expression of human antibodies in eukaryotic micro-algae. Vaccine 23:1828–1832

Mayfield SP, Franklin SE, Lerner RA (2003) Expression and assembly of a fully active antibody in algae. Proc Natl Acad Sci 100:438–442

Mayfield SP, Manuell AL, Chen S, Wu J, Tran M, Siefker D, Muto M, Marin-Navarro J (2007) *Chlamydomonas reinhardtii* chloroplasts as protein factories. Curr Opin Biotechnol 18:126–133

Merchant SS, Prochnik SE, Vallon O, Harris EH, Karpowicz SJ, Witman GB, Terry A, Salamov A, Fritz-Laylin LK, Maréchal-Drouard L et al (2007) The Chlamydomonas genome reveals the evolution of key animal and plant functions. Science 318:245–250

Merchant SS, Kropat J, Liu B, Shaw J, Warakanont J (2012) TAG, You're it! Chlamydomonas as a reference organism for understanding algal triacylglycerol accumulation. Curr Opin Biotechnol 23:352–363

Miller DH, Lamport DT, Miller M (1972) Hydroxyproline heterooligosaccharides in Chlamydomonas. Science 176:918–920

Mimura Y, Sondermann P, Ghirlando R, Lund J, Young SP, Goodall M, Jefferis R (2001) Role of oligosaccharide residues of IgG1-Fc in Fc RIIb binding. J Biol Chem 276:45539–45547

Neupert J, Karcher D, Bock R (2009) Generation of *Chlamydomonas* strains that efficiently express nuclear transgenes. Plant J 57:1140–1150

Nguema-Ona E, Vicré-Gibouin M, Gotté M, Plancot B, Lerouge P, Bardor M, Driouich A (2014) Cell wall O-glycoproteins and N-glycoproteins: aspects of biosynthesis and function. Front Plant Sci 5

Niewiadomski P, Knappe S, Geimer S, Fischer K, Schulz B, Unte US, Rosso MG, Ache P, Flügge U-I, Schneider A (2005) The Arabidopsis plastidic glucose 6-phosphate/phosphate translocator GPT1 is essential for pollen maturation and embryo sac development. Plant Cell 17:760–775

Noffz C, Keppler-Ross S, Dean N (2009) Hetero-oligomeric interactions between early glycosyltransferases of the dolichol cycle. Glycobiology 19:472–478

Norambuena L, Marchant L, Berninsone P, Hirschberg CB, Silva H, Orellana A (2002) Transport of UDP-galactose in plants identification and functional characterization of AtUTr1, Arabidopsis Thaliana UDP-Galactose/UDP-glucose transporter. J Biol Chem 277:32923–32929

Norambuena L, Nilo R, Handford M, Reyes F, Marchant L, Meisel L, Orellana A (2005) AtUTr2 is an Arabidopsis thaliana nucleotide sugar transporter located in the Golgi apparatus capable of transporting UDP-galactose. Planta 222:521–529

Obembe OO, Popoola JO, Leelavathi S, Reddy SV (2011) Advances in plant molecular farming. Biotechnol Adv 29:210–222

Pattathil S, Harper AD, Bar-Peled M (2005) Biosynthesis of UDP-xylose: characterization of membrane-bound AtUxs2. Planta 221:538–548

Pérez Espana VH, Lopez Pérez PA, Romero Cortes T, Peralta GM, Duran Figueroa N, Badillo Corona A (2016) Transformation of chloroplasts of Chlamydomonas for the production of therapeutic proteins. In: Liu J, Sun Z, Gerken H (eds) Recent advances in microalgal biotechnology. OMICS, Foster City, pp 219–232

Pfeffer S, Dudek J, Gogala M, Schorr S, Linxweiler J, Lang S, Becker T, Beckmann R, Zimmermann R, Forster F (2014) Structure of the mammalian oligosaccharyltransferase complex in the native ER protein translocon. Nat Commun 5:3072

Qin C, Qian W, Wang W, Wu Y, Yu C, Jiang X, Wang D, Wu P (2008) GDP-mannose pyrophosphorylase is a genetic determinant of ammonium sensitivity in Arabidopsis thaliana. Proc Natl Acad Sci U S A 105:18308–18313

Rasala BA, Mayfield SP (2015) Photosynthetic biomanufacturing in green algae; production of recombinant proteins for industrial, nutritional, and medical uses. Photosynth Res 123:227–239

Rasala BA, Muto M, Lee PA, Jager M, Cardoso RMF, Behnke CA, Kirk P, Hokanson CA, Crea R, Mendez M et al (2010) Production of therapeutic proteins in algae, analysis of expression of seven human proteins in the chloroplast of *Chlamydomonas reinhardtii*. Plant Biotechnol J 8:719–733

Rasala BA, Lee PA, Shen Z, Briggs SP, Mendez M, Mayfield SP (2012) Robust expression and secretion of Xylanase1 in *Chlamydomonas reinhardtii* by fusion to a selection gene and processing with the FMDV 2A peptide. PLoS One 7:e43349

Rautengarten C, Ebert B, Herter T, Petzold CJ, Ishii T, Mukhopadhyay A, Usadel B, Scheller HV (2011) The interconversion of UDP-arabinopyranose and UDP-arabinofuranose is indispensable for plant development in *Arabidopsis*. Plant Cell 23:1373–1390

Rautengarten C, Ebert B, Moreno I, Temple H, Herter T, Link B, Donas-Cofre D, Moreno A, Saez-Aguayo S, Blanco F et al (2014) The Golgi localized bifunctional UDP-rhamnose/UDP-galactose transporter family of Arabidopsis. Proc Natl Acad Sci 111:11563–11568

Reboul R, Geserick C, Pabst M, Frey B, Wittmann D, Lutz-Meindl U, Leonard R, Tenhaken R (2011) Down-regulation of UDP-glucuronic acid biosynthesis leads to swollen plant cell walls and severe developmental defects associated with changes in Pectic polysaccharides. J Biol Chem 286:39982–39992

Reyes F, Orellana A (2008) Golgi transporters: opening the gate to cell wall polysaccharide biosynthesis. Curr Opin Plant Biol 11:244–251

Reyes F, Marchant L, Norambuena L, Nilo R, Silva H, Orellana A (2006) AtUTr1, a UDP-glucose/UDP-galactose transporter from Arabidopsis thaliana, is located in the endoplasmic reticulum and up-regulated by the unfolded protein response. J Biol Chem 281:9145–9151

Reyes F, León G, Donoso M, Brandizzí F, Weber APM, Orellana A (2010) The nucleotide sugar transporters AtUTr1 and AtUTr3 are required for the incorporation of UDP-glucose into the endoplasmic reticulum, are essential for pollen development and are needed for embryo sac progress in *Arabidopsis thaliana*. Plant J 61:423–435

Roberts K, Gurney-Smith M, Hills GJ (1972) Structure, composition and morphogenesis of the cell wall of Chlamydomonas reinhardi. I. Ultrastructure and preliminary chemical analysis. J Ultrastruct Res 40:599–613

Rollwitz I, Santaella M, Hille D, Flügge UI, Fischer K (2006) Characterization of AtNST-KT1, a novel UDPgalactose transporter from *Arabidopsis thaliana*. FEBS Lett 580(17):4246–4251

Rosti J, Barton CJ, Albrecht S, Dupree P, Pauly M, Findlay K, Roberts K, Seifert GJ (2007) UDP-glucose 4-epimerase isoforms UGE2 and UGE4 cooperate in providing UDP-galactose for cell wall biosynthesis and growth of Arabidopsis Thaliana. Plant cell 19:1565–1579

Rush JS, Gao N, Lehrman MA, Matveev S, Waechter CJ (2009) Suppression of Rft1 expression does not impair the transbilayer movement of Man5GlcNAc2-P-P-dolichol in sealed microsomes from yeast. J Biol Chem 284:19835–19842

Saito F, Suyama A, Oka T, Yoko-o T, Matsuoka K, Jigami Y, Shimma Y (2014) Identification of novel peptidyl serine α-galactosyltransferase gene family in plants. J Biol Chem 289:20405–20420

Samuelson J, Banerjee S, Magnelli P, Cui J, Kelleher DJ, Gilmore R, Robbins PW (2005) The diversity of dolichol-linked precursors to Asn-linked glycans likely results from secondary loss of sets of glycosyltransferases. Proc Natl Acad Sci U S A 102:1548–1553

Sasso S, Pohnert G, Lohr M, Mittag M, Hertweck C (2012) Microalgae in the postgenomic era: a blooming reservoir for new natural products. FEMS Microbiol Rev 36:761–785

Schiller B, Hykollari A, Yan S, Paschinger K, Wilson IBH (2012) Complicated N-linked glycans in simple organisms. Biol Chem 393(8):661–673

Schneider A, Häusler R, Kolukisaoglu U, Kunze R et al (2002) An Arabidopsis thaliana knock-out mutant of the chloroplast triose phosphate/phosphate translocator is severely compromised only when starch synthesis, but not starch mobilisation is abolished. Plant J 32:685–699

Scranton MA, Ostrand JT, Georgianna DR, Lofgren SM, Li D, Ellis RC, Carruthers DN, Dräger A, Masica DL, Mayfield SP (2016) Synthetic promoters capable of driving robust nuclear gene expression in the green alga *Chlamydomonas reinhardtii*. Algal Res 15:135–142

Shaaltiel Y, Bartfeld D, Hashmueli S, Baum G, Brill-Almon E, Galili G, Dym O, Boldin-Adamsky SA, Silman I, Sussman JL (2007) Production of glucocerebrosidase with terminal mannose glycans for enzyme replacement therapy of Gaucher's disease using a plant cell system. Plant Biotechnol J 5:579–590

Smith E, Roberts K, Hutchings A, Galfre G (1984) Monoclonal antibodies to the major structural glycoprotein of the Chlamydomonas cell wall. Planta 161:330–338

Solís D, Bovin NV, Davis AP, Jiménez-Barbero J, Romero A, Roy R, Smetana K, Gabius H-J (2015) A guide into glycosciences: how chemistry, biochemistry and biology cooperate to crack the sugar code. Biochim. Biophys. Acta (BBA) Gen. Subj. 1850:186–235

Spolaore P, Joannis-Cassan C, Duran E, Isambert A (2006) Commercial applications of microalgae. J Biosci Bioeng 101:87–96

Stoger E, Fischer R, Moloney M, Ma JK-C (2014) Plant molecular pharming for the treatment of chronic and infectious diseases. Annu Rev Plant Biol 65:743–768

Strasser R (2016) Plant protein glycosylation. Glycobiology 26:926–939

Strasser R, Mucha J, Mach L, Altmann F, Wilson I, Glössl J, Steinkellner H (2000) Molecular cloning and functional expression of beta1, 2-xylosyltransferase cDNA from *Arabidopsis thaliana*. FEBS Lett 472:105–108

Sun M, Qian K, Su N, Chang H, Liu J, Shen G, Chen G (2003) Foot-and-mouth disease virus VP1 protein fused with cholera toxin B subunit expressed in *Chlamydomonas reinhardtii* chloroplast. Biotechnol Lett 25:1087–1092

Surzycki R, Greenham K, Kitayama K, Dibal F, Wagner R, Rochaix J-D, Ajam T, Surzycki S (2009) Factors effecting expression of vaccines in microalgae. Biologicals 37:133–138

Tran M, Zhou B, Pettersson PL, Gonzalez MJ, Mayfield SP (2009) Synthesis and assembly of a full-length human monoclonal antibody in algal chloroplasts. Biotechnol Bioeng 104:663–673

Tran M, Van C, Barrera DJ, Pettersson PL, Peinado CD, Bui J, Mayfield SP (2013) Production of unique immunotoxin cancer therapeutics in algal chloroplasts. Proc Natl Acad Sci 110:E15–E22

Urzica EI, Adler LN, Page MD, Linster CL, Arbing MA, Casero D, Pellegrini M, Merchant SS, Clarke SG (2012) Impact of oxidative stress on ascorbate biosynthesis in *Chlamydomonas* via regulation of the *VTC2* gene encoding a GDP-l-galactose Phosphorylase. J Biol Chem 287:14234–14245

van Beers MMC, Bardor M (2012) Minimizing immunogenicity of biopharmaceuticals by controlling critical quality attributes of proteins. Biotechnol J 7:1473–1484

Van Patten SM, Hughes H, Huff MR, Piepenhagen PA, Waire J, Qiu H, Ganesa C, Reczek D, Ward PV, Kutzko JP et al (2007) Effect of mannose chain length on targeting of glucocerebrosidase for enzyme replacement therapy of Gaucher disease. Glycobiology 17:467–478

Varki A, Cummings RD, Esko JD, Freeze HH, Stanley P, Marth JD, Bertozzi CR, Hart GW, Etzler ME (2009a) Symbol nomenclature for glycan representation. Proteomics 9:5398–5399

Varki A, Freeze HH, Gagneux P (2009b) Chapter 19: Evolution of glycan diversity. In: Varki A, Cummings RD, Esko JD, Freeze HH, Stanley P, Bertozzi CR, Hart GW, Etzler ME (eds) Essentials of glycobiology, 2nd edn. Cold Spring Harbor, New York

Velasquez SM, Ricardi MM, Dorosz JG, Fernandez PV, Nadra AD, Pol-Fachin L, Egelund J, Gille S, Harholt J, Ciancia M et al (2011) O-glycosylated cell wall proteins are essential in root hair growth. Science 332:1401–1403

Villarejo A, Burén S, Larsson S, Déjardin A, Monné M, Rudhe C, Karlsson J, Jansson S, Lerouge P, Rolland N et al (2005) Evidence for a protein transported through the secretory pathway en route to the higher plant chloroplast. Nat Cell Biol 7:1224–1231

Walsh G (2010) Biopharmaceutical benchmarks 2010. Nat Biotechnol 28:917–924

Walsh G (2014) Biopharmaceutical benchmarks 2014. Nat Biotechnol 32:992–1000

Ward JM (2001) Identification of novel families of membrane proteins from the model plant *Arabidopsis thaliana*. Bioinformatics 17:560–563

Wildt S, Gerngross TU (2005) The humanization of N-glycosylation pathways in yeast. Nat Rev Microbiol 3(2):119–128

Witman GB, Carlson K, Berliner J, Rosenbaum JL (1972) Chlamydomonas flagella I. Isolation and electrophoretic analysis of microtubules, matrix, membranes, and mastigonemes. J Cell Biol 54:507–539

Woessner JP, Goodenough UW (1989) Molecular characterization of a zygote wall protein: an extensin-like molecule in *Chlamydomonas reinhardtii*. Plant Cell 1:901–911

Wong C-H (2005) Protein glycosylation: new challenges and opportunities. J Org Chem 70:4219–4225

Zhang Y-H, Robinson DG (1990) Cell-wall synthesis in *Chlamydomonas reinhardtii*: an immunological study on the wild type and wall-less mutants cw2 and cw15. Planta 180:229–236

Zhang Y-H, Lang WC, Robinson DG (1989) In vitro localization of hydroxyproline O-glycosyl transferases in *Chlamydomonas reinhardii*. Plant Cell Physiol 30:617–622

Zhang L, Luo S, Zhang B (2016) Glycan analysis of therapeutic glycoproteins. MAbs *8*:205–215

Zhu J (2012) Mammalian cell protein expression for biopharmaceutical production. Biotechnol Adv 30:1158–1170

Zhang P, Wang T, Bardor M, Song Z (2013) Deciphering the O-glycomics for the development and production of biopharmaceuticals. Pharm Bioprocess 1:89–104

Chlamydomonas: Cilia and Ciliopathies

Dan Meng and Junmin Pan

Abstract Cilia and flagella are evolutionally conserved microtubule-based cellular protrusions that are present from organisms ranging from protozoan and algae to human. In the human body and embryo, motile cilia have been found in embryonic node, ventricles of the brain, respiratory ducts, fallopian tube, and sperm. Cilia motility provides cell movement, movement of fluids surrounding the ciliated cells and fluid-flow-generated signaling. Immotile primary cilia exist in almost every cell in the human body and during embryonic development. The presence of various receptors and ion channels on the ciliary membrane enables the cilia as a signaling center to perceive extracellular inputs. The signals generated will be transduced into the cell to control proper human development and physiology. A well-known example is that hedgehog signaling is indispensable for cilia in mammals. Thus, it is not surprising that defects in ciliary structure, assembly, and signaling have been linked with a cohort of human diseases, called ciliopathies. Chlamydomonas is one of the widely used organisms to study ciliary biology, and the research involving this organism has been playing a leading role in our understanding of ciliary biology and ciliopathies.

1 Introduction

Cilia and eukaryotic flagella are organelles projecting from cell surface of nearly all eukaryotic cells. Traditionally, if they are multiple and short, they are called cilia, e.g., cilia in protozoa such as *Paramecium*, ependymal cilia in the brain ventricles,

D. Meng (✉)
Tianjin Key Laboratory of Food and Biotechnology, School of Biotechnology and Food Science, Tianjin University of Commerce, Tianjin 300134, China
e-mail: mengd@tjcu.edu.cn

J. Pan (✉)
MOE Key Laboratory of Protein Sciences, Tsinghua-Peking Center for Life Sciences, School of Life Sciences, Tsinghua University, Beijing 100084, China

Laboratory for Marine Biology and Biotechnology, Qingdao National Laboratory for Marine Science and Technology, Qingdao, Shandong, China
e-mail: panjunmin@tsinghua.edu.cn

M. Hippler (ed.), *Chlamydomonas: Biotechnology and Biomedicine*, Microbiology Monographs 31, DOI 10.1007/978-3-319-66360-9_4

and cilia in the trachea. Contrarily, they are called flagella if they are a few and long, e.g., sperm and Chlamydomonas flagella. Regardless of the terms used, cilia and eukaryotic flagella are essentially identical organelles, and these two terms are often used interchangeably. A cilium or flagellum is composed of a microtubule-based axoneme surrounded by a ciliary membrane that is continuous with the cytoplasmic membrane. The axoneme in the motile cilium typically contains a ring of nine doublet microtubules that surround a pair of central microtubules to give a 9+2 architecture; whereas that of an immotile cilium usually contains the nine doublet microtubules but lacks the central pair microtubules, a 9+0 architecture. Please note, though the cellular protrusions from bacteria are also called flagella, however, they are distinct structures from cilia as they are assembled from flagellin and do not have the microtubule-based structures.

Cilia are anciently conserved and present from unicellular eukaryotic organisms to human. The last common ancestor of extant eukaryotes is predicted to have cilia or flagella (Mitchell 2004). During evolution, some organisms like fungi and higher plants lose their cilia due to adaption for life on land; animals, however, still keep the ability to assemble cilia (Raven et al. 1999; Silflow and Lefebvre 2001). In mammals, cilia are present in nearly every cell in the body and during embryonic development (Bangs et al. 2015; Wheatley 1995).

Cilia have two major functions; they are motility and signaling. In lower eukaryotes such as protozoan and unicellular algae, their locomotion depends on cilia. Motile cilia are only present a limited number of human tissues. During embryonic development, the nodal cilia drive fluid flow, which determines left-right asymmetry of the mammalian body axis. In the human body, motile cilia in the respiratory system are responsible for removing mucus. The cilia in the fallopian tubes generate fluid flow and may function in propelling eggs into uterus for fertilization. Sperm motility relies on its flagellum. In the brain ventricles, circulation of cerebrospinal fluid is mediated by ependymal cilia. Thus, cilia motility profoundly affects human development and physiology (Zhou and Roy 2015).

In contrast to motile cilia, the primary cilium is immotile with the exception of nodal cilium and present in all almost every cell in the human body as well as embryo. Until the late twentieth century, the primary cilium has been regarded as a vestigial organelle. However, recent advances have shown that primary cilium serves as an antenna to perceive and transduce signals (Pazour and Witman 2003). Various receptors including PDGF receptor, hedgehog receptor, G-protein-coupled receptors, or ion channels are present in the ciliary membrane. The functions of these receptors are critical in controlling development and physiology (Goetz and Anderson 2010; Hilgendorf et al. 2016; Veland et al. 2009). The defects in cilia have been linked with various human diseases, termed ciliopathies (Badano et al. 2006b). Since the first discovery of the association of primary cilia with disease in year 2000 (Pazour et al. 2000), more than 500 review articles have been contributed to cilia-related human diseases. For a recent review, please see Brown and Witman (2014).

Chlamydomonas, a unicellular green alga with two flagella, has played a leading role in the study of ciliary biology and ciliary-related diseases. For additional information about Chlamydomonas and cilia-related disease, please refer to two review articles (Pan 2008; Pazour and Witman 2009). In this chapter, we will briefly introduce the contribution of Chlamydomonas to ciliary research and cilia-related diseases and then provide an overview of various cilia-related disease and development disorders.

2 Advantages of *Chlamydomonas reinhardtii* as a Model Organism for Ciliary Research

Chlamydomonas reinhardtii possesses two motile flagella (Fig. 1). In the axonemal core of the flagellum, it has 9+2 microtubule arrangement. The microtubule-associated structures such as dynein arms, radial spokes, nexin links (nexin-dynein regulatory complex), and central pair microtubules are involved in controlling flagellar movement (Porter and Sale 2000). Upon uneven light stimulation, Chlamydomonas cells shift from random motility to phototactic movement (phototaxis). In addition to provide motility, Chlamydomonas flagella are also involved in flagellar signaling during mating. The adhesion of gametic flagella triggers a signaling cascade leading cell-cell fusion (Pan et al. 2003). Recently, it has been shown that Chlamydomonas flagella can release bioactive vesicles (ciliary ectosomes) into extracellular environment, which provide potential means for ciliary signaling (Wood and Rosenbaum 2015). Chlamydomonas flagella are assembled after completion of cell division and resorbed prior to next cell division

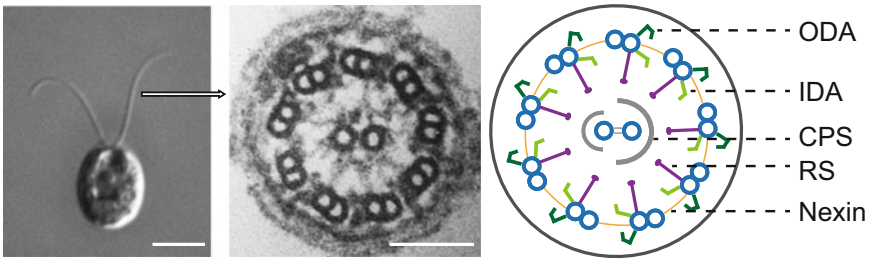

Fig. 1 Flagella of *Chlamydomonas reinhardtii*. *C. reinhardtii* possesses two motile flagella. *On the left* is a DIC image of the cell. *In the middle* is an electron micrograph showing the cross section through the middle of the flagellum. *On the right* is an illustration of the flagellar structure. The flagellum has nine doublet microtubules and one pair of central microtubules (*blue*) surrounded by a ciliary membrane. The doublet microtubules are connected by nexin links (nexin-dynein regulatory complex) (*orange*). The main microtubule-associated structures include outer dynein arms (ODA, *dark green*), inner dynein arms (IDA, *light green*), radial spokes (RS, *purple*), and central pair sheath (CPS, *gray*). Bar, 5 μm in the DIC image, 100 nm in the EM image

(Cavalier-Smith 1974). Thus, Chlamydomonas is suitable for studying various aspect of ciliary biology including ciliary assembly, disassembly, ciliary motility, and cilia-generated signaling.

Chlamydomonas is one of the few model organisms where genetic, genomic, biochemical, and cell biological approaches can be combined to investigate the basic biology of cilia. The database of its genome is available and readily accessible (Blaby et al. 2014; Merchant et al. 2007) (https://phytozome.jgi.doe.gov/pz/portal.html#!search). Chlamydomonas is haploid; it mates and produces meiotic spores amenable to tetrad analysis. In addition, the cells can form temporary dikaryons after mating, which could also allow genetic analysis (Dutcher 2014). Furthermore, the gene function can be explored by various functional genomic tools including mutagenesis especially insertional mutagenesis, RNA interference, and gene transformation (Jinkerson and Jonikas 2015). CRISPR/CAS9 system for targeted gene knockout has recently been worked out in this organism (Baek et al. 2016; Shin et al. 2016). The Chlamydomonas Resource Center keeps all the strains, mutant library, and genome database which are readily available.

In addition, the experimental system has other unique advantages especially in terms of ciliary studies. The cells can be easily cultured and synchronized by a light-dark cycle. All the cells in the light phase possess flagella that are kept at a relatively constant length. The flagella can be amputated simply by lowering pH of the medium (called pH shock) or by mechanical shearing. Amputated flagella can be easily purified in a large quantity by using sucrose sedimentation and centrifugation, which allows identification of flagellar proteins and their posttranslational modification (Boesger et al. 2009; Pan et al. 2011; Pazour et al. 2005). Flagellar amputation does not kill the cells, and the cells can rapidly regenerate full-length flagella within around 2 h. The flagella are assembled in a synchronized manner (Rosenbaum et al. 1969). Thus, flagellar assembly kinetics can be easily scored, and various biochemical activities associated with different stages of flagellar regeneration can be analyzed. Chlamydomonas flagellar mutants can be easily generated and screened. Unlike mouse, Chlamydomonas mutants that lack flagella are not lethal.

There are several systems in this organism for studying flagellar disassembly (Cao et al. 2015). Flagellar disassembly of Chlamydomonas can be induced in a synchronized manner by various chemicals including sodium pyrophosphate, and complete shortening of flagella can be completed within 3 h (Lefebvre et al. 1978). During zygote formation, the flagella of young zygote are gradually resorbed, and the flagellar resorption is synchronized, which provides a physiological context to study the mechanism of flagellar disassembly (Cavalier-Smith 1974; Pan et al. 2004). In addition, similar to mammalian cells, Chlamydomonas flagella also disassemble prior to cell division, which allows this organism being used for studying cell cycle control by ciliary disassembly. It has been shown that ciliary disassembly controls G1 to S phase transition (Liang et al. 2016).

3 Contributions of Chlamydomonas Research to Our Understanding of Ciliopathies and Basic Biology of Cilia

Cilia-related diseases and developmental orders are described as ciliopathies, toward which researches in Chlamydomonas have played a leading role in our understanding. In this section, we will highlight a few examples of Chlamydomonas research that lead to breakthrough contributions to ciliopathies and cilia research. In Sect. 4, we will describe ciliopathies reported thus far and introduce related studies performed in this organism if available.

3.1 Motile Cilia-Related Disease and Developmental Disorders and Flagellar Motility Studies in Chlamydomonas

Defects in motile cilia have been shown to be associated with primary ciliary dyskinesia (PCD), male infertility, situs inversus, and hydrocephalus. PCD is a rare autosomal recessive disease caused by defects in structure or function of motile cilia lining the respiratory tract. The patients are subjected to chronic recurrent respiratory infections including bronchitis, sinusitis, pneumonia, and otitis media. Apparently, it is caused by failure of the PCD patients to clear mucus and bacteria in the airways leading to infections. As motile cilium is also present in sperm, the fallopian tube and the motile cilium in the node of the embryo determine left-right asymmetry (Nonaka et al. 1998; Yoshiba et al. 2012); some patients may also have infertility and situs inversus. PCD is estimated to affect between 1 in 15,000 and 30,000 live births (Barbato et al. 2009). PCD was first described by Kartagener in 1933; patients show a combination of bronchitis, sinusitis, and situs inversus with infertility in male patients (Kartagener 1933). The association of Kartagener syndrome with abnormalities of motile cilia was first reported by Afzelius in 1976 (Afzelius 1976). Because the reported patients' cilia are immotile, so this disease was also named "immotile syndrome." As some patients showed defects in ciliary motility without complete loss of ciliary movement, this disease was renamed primary ciliary dyskinesia (Sleigh 1981).

PCD is a genetically heterogeneous disease. More than 30 genes have been identified to be associated with PCD (Praveen et al. 2015). Most of the patients have mutations in the genes for ciliary axonemal structural components that include outer dynein arms and related proteins like DNAI1, DNAH11, DNAH5, DNAI2, and DNAL1, radial spokes, and central pair proteins like RSPH4A, RSPH9, RSPH1, and HYDIN. Several genes that encode cytoplasmic proteins functioning in dynein arm assembly are also causative for PCD that include CCDC103, DNAAF1–6, DYX1C1, and LRRC6 (Kurkowiak et al. 2015). As hundreds of genes are involved in motile cilia structure and function, the known PCD genes

could only account for about 60% of PCD cases (Knowles et al. 2013; Praveen et al. 2015). Other candidate genes are still to be identified in the future.

The ventricular surface of the brain is covered with motile cilia whose defect in motility is one of the causes of congenital hydrocephalus in mice (Lee 2013). However, the prevalence of hydrocephalus in PCD patients is low. The underlying mechanism is still elusive. Choroid plexus epithelial cells in the brain form nonmotile 9+0 cilia, which, however, acquire transient movement during development and whose defects are also linked with hydrocephalus in mice (Narita and Takeda 2015).

Almost all what we know about ciliary motility comes from the studies in Chlamydomonas. Ciliary motility depends on axonemal structures that include dynein arms, dynein regulatory complex, radial spokes, and central pair microtubules, and these structures are highly coordinated during motility (Porter and Sale 2000). Various mutants defective in these structures are first isolated and characterized in this organism. Most of the genes mutated in human mentioned above are first studied in this organism (Witman 2009). The first gene involved in human PCD has been identified based on the information of flagellar motility mutants in Chlamydomonas (Pennarun et al. 1999). Mutation in *HYDIN* was initially found to cause hydrocephalus in mice (Davy and Robinson 2003). However, the role of HYDIN is not clear. Lechtreck et al. discover that HYDIN is a central pair protein and regulates flagellar motility (Lechtreck and Witman 2007), which reveals the pathology of PCD that is caused by *HYDIN* mutation in human (Olbrich et al. 2012).

3.2 *Polycystic Kidney Disease and Hedgehog Signaling, Discovery of Intraflagellar Transport in Chlamydomonas*

Polycystic kidney disease (PKD) is a genetically inherited disease in human which includes autosomal dominant polycystic kidney disease (ADPKD) and autosomal recessive polycystic kidney disease (ARPKD). ADPKD is the most common life-threatening disease with an incidence of at least 1 in 1000 (Torres et al. 2007). It is diagnosed in adulthood and characterized by bilateral grossly enlarged kidneys resulting from focal cysts in nephrons. ADPKD is caused by mutations in one of the two genes, *PKD1* (in 85% cases) and *PKD2* (in 15% cases), which encode polycystin-1 (PC-1) and polycystin-2 (PC-2), respectively (Geng et al. 1996; Mochizuki et al. 1996). PC-1 and PC-2 localize to primary cilia of the epithelial cells of the nephrons. The finding that PC1 is expressed in the sensory cilia of the nematode *Caenorhabditis elegans* has first revealed possible connection between PKD and cilia (Barr and Sternberg 1999). ARPKD is a rare disease with an incidence of 1 in 20,000, which is characterized by bilateral renal cystic enlargement with radial pattern of fusiform cysts in the dilated collecting ducts (Waters and

Beales 2011). ARPKD patients sometimes also have cysts in the liver. Mutation in polycystic kidney and hepatic disease 1 (*PKHD1*), which encodes a membrane-associated receptor-like protein fibrocystin, is one of the common causes of ARPKD. Fibrocystin is localized to primary cilia and basal bodies and colocalizes with polycystin-2 (Kim et al. 2008).

Ciliary assembly and maintenance require a bidirectional transport of large protein complex within the cilium for delivering ciliary precursors and returning turnover products (termed intraflagellar transport or IFT), which was first discovered in Chlamydomonas (Kozminski et al. 1993). IFT motor kinesin-2 and cytoplasmic dynein 2/1b provide power for the movement. IFT complexes as carriers for ciliary proteins are composed of two protein complexes, IFT-A and IFT-B, which contains 16 and 6 polypeptides, respectively. Genetic disruption of components of IFT-A or IFT-B either block or impairs ciliogenesis depending on the nature of the mutations and the genes involved. Though IFT was first discovered in Chlamydomonas, this machinery has turned out to be involved in ciliogenesis in almost all ciliated organisms including human and has served as the basis for understanding of ciliary assembly (Lechtreck 2015; Rosenbaum and Witman 2002; Scholey 2003; Taschner and Lorentzen 2016). Witman, Pazour, and colleagues found that a Chlamydomonas mutant lacking flagella is caused by mutations in *IFT88*, an orthologous gene of the mouse PKD gene *Tg737*, indicating that the pathology of PKD is related to ciliary defects (Pazour et al. 2000). Subsequent intensive studies have confirmed this hypothesis (Zhang et al. 2004).

Hedgehog signaling pathway in mammals controls many developmental processes including limb formation. Initial studies in mouse have identified two mutants that are defective in hedgehog signaling. Interestingly, the defective genes have turned out to be homologues of Chlamydomonas genes encoding IFT proteins IFT172 and IFT88 (Huangfu et al. 2003). Extensive research afterward has proved that primary cilium is a signaling organizing center of hedgehog signaling (Goetz and Anderson 2010). These findings have triggered a renaissance of interest in ciliary research. Through less than two decades of intensive research, cohort signaling pathways have been found to be linked with cilia. These signaling pathways include calcium signaling (Dell 2015), hedgehog signaling (Goetz and Anderson 2010), receptor tyrosine kinase signaling (Christensen et al. 2012), Wnt signaling (May-Simera and Kelley 2012), Notch signaling (Yabut et al. 2015), and G-protein-coupled signaling (Hilgendorf et al. 2016).

3.3 Bardet-Biedl Syndrome (BBS), Comparative Genomics, and Other Research in Chlamydomonas

The Bardet-Biedl syndrome (BBS) is one of the first diseases discovered to be associated with defects of primary cilia (Zaghloul and Katsanis 2009). It is a complicated disorder characterized by polydactyly, retinal degeneration, cystic

kidneys, hypogonadism, obesity, and learning disabilities (Baker and Beales 2009). Nearly 30% of patients are born with postaxial polydactyly and hypogonadism and at least 40% of patients have renal malformations and abnormal renal function including renal dysplasia, cystic tubular disease, and focal segmental glomerulosclerosis (O'Dea et al. 1996). Secondary features of BBS include speech disorder/delay, brachydactyly/syndactyly, strabismus/cataracts/astigmatism, developmental delay, polyuria/polydipsia, ataxia/poor coordination/imbalance, diabetes mellitus, dentition, cardiovascular anomalies, hepatic involvement, hyposmia/anosmia, nociception/thermosensation, and infections (Baker and Beales 2009; Beales et al. 1999).

BBS is a genetically heterogeneous disorder. Mutations in 19 genes have been found to cause BBS: *BBS1–12*, *MKS1*, *CEP290*, *WDPCP*/*FRITZ*, *SDCCAG8*, *LZTFL1*, *BBIP10*/*BBIP1*, and *IFT27* (Novas et al. 2015). BBS patients may have significant intrafamilial variability characterized by the presence of more than one BBS gene mutations and other modifier loci in some families (Badano et al. 2006a). It is likely that multiple *BBS* gene mutations are necessary to cause BBS though more evidence is needed.

Bardet-Biedl syndrome (BBS) is a genetically heterogeneous syndrome disease affecting multiple organs (see below). The study of *BBS8* reveals that BBS was likely caused by basal body dysfunction (Ansley et al. 2003). Comparative genomics using the genome of Chlamydomonas as anchor has revealed that the human orthologs of almost all known *BBS* genes except for *BBS6* are present in the flagellar apparatus-basal body (FABB) proteome (Li et al. 2004). In addition, this study has identified human disease gene *BBS5*. Therefore, this study further demonstrates that BBS is a ciliopathy and the genes identified may serve as a platform for identifying other disease-causing genes. In a subsequent study in Chlamydomonas, it has been found that BBSome (a complex formed by genes encoding BBS proteins) is a cargo of IFT that is required for export of specific signaling proteins from flagella (Lechtreck et al. 2009).

3.4 Chlamydomonas Research Reveals the Molecular Basis of CEP290, Which Is Involved in Multiple Ciliary Diseases

Mutations in *CEP290* (also known as *NPHP6*) are found in patients with olfactory dysfunction, retinitis pigmentosa, Meckel-Gruber syndrome, Senior-Loken syndrome, and NPHP (see below). The working mechanism of CEP290 has been characterized in Chlamydomonas (Craige et al. 2010). CEP290 is localized to the transition zone and functions in the formation of the Y-link structure. Transition zone, which connects the basal body with the cilia proper, is important to control entry and exit of ciliary proteins (Reiter et al. 2012). Indeed, Chlamydomonas *cep290* mutant exhibits distinct flagellar protein compositions. It is expected that

human *cep290* mutations would disrupt proper signaling of cilia when their protein compositions are compromised, leading to ciliopathies.

3.5 *Possible Connection of Juvenile Epilepsy to Cilia Revealed by Research in Chlamydomonas*

Lesions in a human gene encoding cyclin-dependent kinase-like 5 (CDKL5) cause juvenile epilepsy of unknown etiology (Rademacher et al. 2011). In Chlamydomonas, it was found that LF5 is a homologue of human CDKL5. LF5 localizes to proximal flagella, and *lf5* null mutant causes longer flagella (Tam et al. 2013). In another study, FLS1, another CDKL in Chlamydomonas, has been shown to be involved in flagellar disassembly (Hu et al. 2015). These studies suggest that CDKLs in human may participate in cilia-related functions and juvenile epilepsy may well be another ciliopathy.

3.6 *Other Researches in Chlamydomonas that Contribute to Our Understanding of Basic Biology of Cilia*

A few of other researches in Chlamydomonas also lead the way to our understanding of the basic biology of cilia. IFT was initially found to be required for ciliary assembly and maintenance. Snell and colleagues also found that IFT is involved in cilia-generated signaling by studying Chlamydomonas mating that involves flagellar adhesion of gametes of opposite mating types (Wang et al. 2006). Subsequent studies in mouse have demonstrated that IFT is required for transporting hedgehog signaling components into cilia (Goetz and Anderson 2010).

Ciliary disassembly is required for G1-S transition in ciliated cells (Kim et al. 2011; Li et al. 2011). An aurora-like protein kinase CALK was first found to be required for flagellar disassembly in Chlamydomonas (Pan et al. 2004). In mammalian cells, it was subsequently found that aurora-A is also required for disassembly of primary cilia and aurora-A activation is at the center of various pathways leading to ciliary disassembly (Liang et al. 2016; Pugacheva et al. 2007).

The presence of various receptors and ion channels on the ciliary membranes enables cilium as a signaling center. Recently, Rosenbaum and colleagues found that Chlamydomonas flagella secret bioactive vesicles—ciliary ectosomes (Cao et al. 2015; Wood et al. 2013; Wood and Rosenbaum 2015). In *C. elegans*, extracellular vesicles were subsequently found to be released from ciliary base of neuronal cells (Wang et al. 2014). These vesicles are likely involved in intercellular communications (Wang and Barr 2016).

4 Other Ciliary-Related Diseases or Developmental Disorders

4.1 Nephronophthisis

Nephronophthisis (NPHP) is a chronic autosomal recessive kidney disease that is characterized by cysts in corticomedullary junction and tubulointerstitial fibrosis (Salomon et al. 2009). In contrast to PKD, kidney size in NPHP is normal or diminished. Clinically, NPHP is categorized into three forms depending on the onset age of the end-stage renal disease (ESRD): infantile, juvenile, and adolescent forms (Saunier et al. 2005). Infantile NPHP is rare and progresses to ESRD at mean age of 4 (Gagnadoux et al. 1989). Juvenile NPHP is the most common NPHP with the onset of ESRD at mean age of 13 (Hildebrandt et al. 1997b). The onset of ESRD of adolescent NPHP is at mean age of 19 (Omran et al. 2000).

NPHP1, the first gene implicated in NPHP, was discovered in 1997 (Hildebrandt et al. 1997a). Mutations in 19 other genes (*NPHP1-NPHP18*, *NPHP1L*, *NPHP2L*) have been identified (Wolf 2015). Though a single gene mutation could cause NPHP, more than one gene mutations were found in some NPHP patients (Tory et al. 2007). The proteins encoded by *NPHP* genes are called nephrocystins (Wolf and Hildebrandt 2011). All nephrocystins localize to primary cilia, basal bodies, or centrosomes. Several nephrocystins interact with each other, and some of them also interact with ciliary proteins like BBS proteins (Wolf 2015).

NPHP9 is also known as Nek8, which is a member of NIMA-like protein kinases. Several NIMA-like protein kinases in Chlamydomonas (named CNKs) have been studied and implicated in ciliary functions. FA2 regulates deflagellation (Mahjoub et al. 2002). CNK2 is involved in flagellar length control (Bradley and Quarmby 2005). CNK11 suppresses the flagellar stability associated with the loss of multiple axonemal structures (Lin et al. 2015). Lastly, CNK4 has recently been shown to control axonemal stability as well as flagellar length (Meng and Pan 2016).

NPHP17 is a protein encoded by the IFT gene *IFT172*. IFT172 is an IFT-B component. In Chlamydomonas, it has been shown that IFT172 controls IFT turnaround at the flagellar tip (Pedersen et al. 2005).

4.2 Retinal Degeneration

Defects in the connecting cilium between the outer and inner segments of the mammalian photoreceptor are one of the causes of retinal degeneration or blindness (Horst et al. 1990). All components that are necessary for assembly and maintenance of the outer segment are synthesized in the inner segment and transported through the connecting cilium into the outer segment. The transport is dependent on continuous IFT. Defects in IFT motors and IFT particle proteins affect proper

formation of the connecting cilium and maintain the outer segment, leading to retinal degeneration (Taub and Liu 2016). An *IFT88* mutation in mouse causes abnormal development of outer segment and apoptosis of photoreceptor cells (Pazour and Rosenbaum 2002). Targeted knockout of IFT motor kinesin II in the eye of mouse resulted in abnormal outer segment and retinal degeneration (Marszalek and Goldstein 2000).

Defects in proteins that localize to the connecting cilium are potential causes of blindness. Mutations in retinitis pigmentosa GTPase regulator (RPGR) and CEP290 caused retinitis pigmentosa (den Hollander et al. 2006; Hong et al. 2003; Khanna et al. 2005). Retinal degeneration is also a feature of nephronophthisis (NPHP) (see below) and BBS disorders.

4.3 Hyposmia and Anosmia

The olfactory system is responsible for detecting environmental odors. The odorant receptors, which function in stimuli detection and signal transduction, are compartmentalized on the membrane of the cilia of the olfactory sensory neurons (Jenkins et al. 2009). Defects in olfactory cilia cause loss or reduction in the ability to smell like hyposmia and anosmia (Kulaga et al. 2004; McEwen et al. 2007). In 1975, Douek and colleagues first reported one of the anosmia patients with apparent ciliary defects; cilia were not detected in the olfactory system neurons of the patient (Douek et al. 1975). BBS patients are frequently associated with impaired olfactory function. Mice that lack BBS1 and BBS4 exhibit reduced olfactory ciliated border and accumulation of ciliary proteins in dendrites and cell bodies, which suggests a link between the ciliary dysfunction and anosmia and hyposmia (Iannaccone et al. 2005; Kulaga et al. 2004). The patients with Leber congenital amaurosis (LCA) also have olfactory dysfunction due to ciliary defects. Mice that lack CEP290, a gene mutated in LCA patients, display mislocalization of olfactory ciliary G proteins (McEwen et al. 2007).

4.4 Meckel-Gruber Syndrome

Meckel-Gruber syndrome (MKS) is an autosomal recessive condition that has variable phenotypes and extensive genetic heterogeneity. It leads to prenatal death with incidence of about 1:140,000 living births (Chen 2007). MKS is characterized by cystic kidneys, polydactyly, hepatic fibrosis, and hepatic cysts with the ductal plate malformation and central nervous system (CNS) abnormalities (e.g., enlarged posterior fossa). CNS malformation, cystic kidney, and hepatic fibrotic are important features for MKS diagnosis. Other features like postaxial polydactyly, situs inversus, cleft palate, cardiac abnormalities, and abnormalities of the genitalia

in male fetuses are also reported in MKS patients (Salonen and Norio 1984; Salonen and Paavola 1998).

Although MKS condition was first reported in 1822, the first gene underlying MKS, *MKS1*, was identified in 2006 (Kyttala et al. 2006; Meckel 1822). Twelve genes have been identified as causative genes for MKS including *MKS1*, *TMEM216*, *TMEM67*, *TMEM231*, *CEP290*, *RPGRIP1L*, *CC2D2A*, *NPHP3*, *TCTN2*, *B9D1*, *B9D2*, and *CSPP1* (Szymanska et al. 2014). MKS has extensive genetic heterogeneity and displays allelism with other ciliopathies such as Joubert syndrome (JBTS), oral-facial-digital syndrome (OFD), and BBS. Many MKS proteins are localized to the transition zone and function by forming complex with JBTS proteins (Barker et al. 2014).

4.5 *Joubert Syndrome*

The autosomal recessive Joubert syndrome (JBTS) is a rare disorder which is characterized by hypotonia, ataxia, mental retardation, oculomotor apraxia, and an irregular breathing pattern (Valente et al. 2005). A pathognomonic "molar tooth sign" (MTS), which describes hypoplasia or aplasia of the cerebellar vermis, horizontally oriented and thickened superior cerebellar peduncles, and a deep interpeduncular fossa, is a diagnostic criterion (Maria et al. 1999; Parisi et al. 2007). Many forms of JBTS have been identified and described as JBTS-related disorders (JRSDs). JRSDs have additional clinical features such as retinal dystrophy, renal cysts, polydactyly, hepatic fibrosis, ocular coloboma, and oral frenulae (Parisi et al. 2007).

Mutations in 23 genes have been identified as causative for JBTS (Szymanska et al. 2014). Seven genes including *TMEM216*, *TMEM67*, *TMEM231*, *CEP290*, *RPGRIP1L*, *CC2D2A*, and *CSPP1* are allelic genes with MKS; the other genes include *NPHP1*, *AHI1*, *TNCN1*, *TCTN2*, *TNCN3*, *INPP5E*, *ARL13B*, *OFD1*, *TTC21B*, *KIF7*, *TMEM237*, *CEP41*, *TMEM138*, *C5orf42*, *ZNF423*, and *PDE6D*. A JBTS/MKS complex consisting of nearly 16 proteins was suggested to localize to the transition zone region; it is hypothesized that JBTS/MKS is linked via this complex (Barker et al. 2014).

4.6 *Oral-Facial-Digital Syndrome*

The oral-facial-digital syndrome (OFD) was first described by Mhor (1941). The patient was reported to have oral, facial, and digital phenotypes including highly arched palate, lobate tongue with papilliform outgrowths, a broad nasal root, and hypertelorism. Patient with similar OFD phenotypes was also reported by Papillon-Leage and Psaume (1954). Currently, at least 13 subgroups OFD have been described according to the anomalies of the organs, systems, and inheritance.

Genes mutated in OFD1 have been identified, whereas the affected genes in other groups of OFDS are still unknown.

OFD type 1 (OFD1) is a rare X-linked dominant disorder which is characterized by malformation of the oral cavity, face, and digits as well as CNS abnormalities and cystic kidney disease (Feather et al. 1997). OFD1 has an incidence of about 1:50,000 live births, and it is lethal in males (Baker and Beales 2009; Wahrman et al. 1966). Manifestations in patients include hypertelorism, buccal frenulae, cleft palate, lobulated tongue, alveolar ridge notching, lingual hamartomas, brachydactyly, camptodactyly, syndactyly, rarely polydactyly, the corpus callosum, hydrocephaly, and polycystic kidney disease (Prattichizzo et al. 2008; Thauvin-Robinet et al. 2006). The syndrome is caused by mutation in *OFD1*, which encodes a centrosomal protein localized at the basal body of primary cilium (Ferrante et al. 2001). OFD1could affect ciliogenesis by building distal appendage and recruiting IFT proteins (Ferrante et al. 2006; Singla et al. 2010).

4.7 Alstrom Syndrome

Alstrom syndrome (ALMS) is a rare autosomal recessive disorder with an estimated incidence of less than 1:100,000 (Alstrom et al. 1959; Minton et al. 2006). ALMS was first described by Alstrom et al. in 1959 (Alstrom et al. 1959). It is a multiorgan disorder that is characterized by childhood obesity, sensorineural vision loss and deafness, cardiomyopathy, hypogonadism, the insulin resistance syndrome leading to type 2 diabetes mellitus (T2DM), systemic fibrosis, renal dysfunction, and other multiple organ dysfunctions (Hearn et al. 2005; Marshall et al. 1997, 2005; Ozgul et al. 2007). Cardiac involvement is the major cause of death in young patients, and the renal dysfunction is the major cause of mortality in older patients (Marshall et al. 2005; Minton et al. 2006). Early diagnosis is challenging due to progressive emergence of features and the clinical similarities to the other ciliopathies such as BBS (Marshall et al. 2007).

ALMS1 is the only gene known to cause ALMS (Baker and Beales 2009). *ALMS1* is located on chromosome 2p13 and encodes a protein of 4169 amino acids (Collin et al. 2002; Hearn et al. 2002). ALMS1 is ubiquitously expressed and localized to centrosome and basal body, whereas the exact biological function of ALMS1 is still unknown (Collin et al. 2002; Hearn et al. 2002; Knorz et al. 2010). The fibroblasts from ALMS patient showed normal ciliary structure; however, knockdown of *ALMS1* in renal cell lines could disrupt cilia assembly, indicating that ALMS1 is required for ciliogenesis (Li et al. 2007; Sharma et al. 2008). *ALMS1* knockout mice showed abnormal ciliary structure (Li et al. 2007). The molecular function of ALMS1 still needs to be elucidated.

4.8 Senior-Loken Syndrome

Senior-Loken syndrome (SLS) is an autosomal recessive disorder with overlap phenotypes with other ciliopathies like JTBS, BBS, and NPHP (Hemachandar 2014). It was first described by Senior et al. and Loken et al., in 1961, respectively (Loken et al. 1961; Senior et al. 1961). It is characterized by the combination of juvenile nephronophthisis and tapetoretinal degeneration (Hemachandar 2014).

Mutations in several genes have been shown in SLS patients, and there is an evident genetic overlap between SLS and other ciliopathies such as NPHP, BBS, and JTBS. Actually all mutated genes in SLS have been identified in other ciliopathies. The mutated genes include *NPHP1*, *NPHP2* (also known as *INVS*), *NPHP3*, *NPHP4*, *NPHP5* (also known as IQCB1), *CEP290* (also known as *NPHP6*), and *SDCCAG8* (Davis and Katsanis 2012; Sharma et al. 2008). The proteins encoded by these genes have ciliary localizations (Ronquillo et al. 2012).

4.9 Leber Congenital Amaurosis

Leber congenital amaurosis (LCA) is the most severe and early-onset inherited retinal dystrophy with severe visual impairment causing childhood blindness (Perrault et al. 1999). The incidence of LCA is 1:30,000–1:80,000 of infants (den Hollander et al. 2008). It is characterized with infantile nystagmus, poor pupillary response, hyperopia, keratoconus, non-detectable electroretinogram (ERG), and Franceschetti's oculo-digital sign (Waters and Beales 2011). LCA was first described by Theodor von Leber (1869). In 1954, Franceschetti and Dieterle reported that reduced or extinguished ERG could be used as diagnostic criteria (Franceschetti and Dieterle 1954). The characteristics of LCA sometimes present as manifestations of other syndromes such as Joubert or Senior-Loken syndrome.

LCA is a genetically heterogenous disorder that is autosomal recessive in most cases (Alstrom et al. 1959; Foxman et al. 1985). Twenty-two genes have been identified to be associated with LCA. These genes encode proteins with diverse retinal functions including phototransduction genes (*AIPL1*, *CRX*, *GUCY2D*), vitamin A visual cycle genes (*RPE65*, *LRAT*, *RDH12*) and genes related to ciliary function (*LCA5*, *RPGRIP1*, *CEP290*, *TULP1*) (Chacon-Camacho and Zenteno 2015). These cilia-related genes affect the photoreceptor transport process in the connecting cilia, whose mutations are also found in other ciliopathy syndromes such as Joubert or Senior-Loken syndrome.

4.10 Cranioectodermal Dysplasia

Cranioectodermal dysplasia (CED), also known as Sensenbrenner syndrome, is a rare autosomal recessive disorder (Zaffanello et al. 2006). It is characterized by narrow thorax, developmental delay, hypodontia, sparse hair, joint laxity, dolichocephaly, nephronophthisis, and renal cysts (Hoffer et al. 2013; Li et al. 2015). It was first described by Sensenbrenner et al. in 1975 (Sensenbrenner et al. 1975). The prevalence of CED is very low with less than 50 cases being reported (Alazami et al. 2014).

Mutations in four genes are known to cause CED including *WDR10* (*IFT122*), *WDR35* (*IFT121*), *WDR19* (*IFT144*), and *C14ORF179* (*IFT43*) (Arts et al. 2011; Bredrup et al. 2011; Gilissen et al. 2010; Walczak-Sztulpa et al. 2010). Each gene encodes a functional component of IFT-A. CED genetically and phenotypically overlaps with other disorders such as short-rib polydactyly (SRP) and Jeune syndrome (Li et al. 2015).

4.11 Jeune Syndrome

Jeune syndrome or Jeune asphyxiating thoracic dystrophy (JATD) is a rare autosomal recessive disorder that was first described as familial asphyxiating thoracic dystrophy with severely narrow thoracic cage in 1955 (Jeune et al. 1955). It occurs with an incidence of about 1:100,000–1:130,000 live births in the United States (Saletti et al. 2012). The infantile death often owes to respiratory insufficiency from pulmonary hypoplasia and severely constricted thoracic cage that often results in asphyxiation (Waters and Beales 2011). The syndrome is characterized by short limbs, hypoplastic iliac wings, trident acetabular roofs, and a narrow rigid thoracic cage accompanied with varied abnormalities in thoracic, pancreatic, cardiac, hepatic, renal, and retinal (Jeune et al. 1955; Saletti et al. 2012).

JATD is a genetically heterogeneous disorder. Mutation of one gene in chromosome 15q13 has been identified as causative for JATD (Morgan et al. 2003). Mutations in *IFT80* were found in JATD patients (Beales et al. 2007). IFT80 is a subunit of IFT protein complex. Additional two IFT genes *IFT140* and *IFT172* were also found to be mutated in JATD patients (Halbritter et al. 2013; Perrault et al. 2012; Schmidts 2014; Schmidts et al. 2013). Recently, mutation in *CEP120* has also been found in JATD patient (Shaheen et al. 2015).

4.12 Short-Rib Polydactyly Syndrome

Short-rib polydactyly syndrome (SRP) is a rare autosomal recessive skeletal dysplasia which is characterized by short ribs, micromelia, polydactyly, and multiple

anomalies of major organs (Lavanya and Pratap 1995). SRP is classified into four types including Saldino-Noonan syndrome or SRP type I, Majewski syndrome or SRP type II, Verma-Naumoff syndrome or SRP type III, and Beemer-Langer syndrome or SRP type IV (Eleftheriades et al. 2013). SRP has phenotypic overlaps among the different subtypes of SRP as well as with JATD.

WDR35, *Nek1*, *DYNC2H1*, and *IFT80* have been identified as causal genes for SRP (Dagoneau et al. 2009; Merrill et al. 2009; Mill et al. 2011; Tompson et al. 2007). Proteins encoded by *WDR35*, *DYNC2H1*, and *IFT80* function in IFT, indicating that SRP is one of the ciliopathies.

4.13 Ellis-van Creveld Syndrome

Ellis-van Creveld syndrome (EVC) is very rare autosomal recessive disorder which was described by Ellis and Van Creveld (1940). The prevalence is very low with about 150 cases being reported (Shetty et al. 2015). It is characterized by chondrodysplasia, short stature, polydactyly, cardiac defects, and dysplastic fingernails and teeth (Baujat and Le Merrer 2007). EVC has features overlapped with other syndrome like JATD and SRP.

Mutations in two genes *EvC1* and *EvC2* are causal for EVC. These two genes are located on chromosome 4p16 in a head-to-head configuration (Ruiz-Perez et al. 2003). EVC1 and EVC2 interact with each other and the interaction is necessary for their ciliary localization (Blair et al. 2011). *EvC* proteins have been reported to function in hedgehog signaling pathway in molar development (Nakatomi et al. 2013).

Acknowledgments This work was supported by the National Basic Research Program of China (973 program) (2012CB945003, 2013CB910700), National Natural Science Foundation of China (31330044, 31671387), and Sino-German Center for Research Promotion (GZ990) (to J. P.).

References

Afzelius BA (1976) A human syndrome caused by immotile cilia. Science 193:317–319

Alazami AM, Seidahmed MZ, Alzahrani F, Mohammed AO, Alkuraya FS (2014) Novel IFT122 mutation associated with impaired ciliogenesis and cranioectodermal dysplasia. Mol Genet Genomic Med 2:103–106

Alstrom CH, Hallgren B, Nilsson LB, Asander H (1959) Retinal degeneration combined with obesity, diabetes mellitus and neurogenous deafness: a specific syndrome (not hitherto described) distinct from the Laurence-Moon-Bardet-Biedl syndrome: a clinical, endocrinological and genetic examination based on a large pedigree. Acta Psychiatr Neurol Scand Suppl 129:1–35

Ansley SJ, Badano JL, Blacque OE, Hill J, Hoskins BE, Leitch CC, Kim JC, Ross AJ, Eichers ER, Teslovich TM et al (2003) Basal body dysfunction is a likely cause of pleiotropic Bardet-Biedl syndrome. Nature 425:628–633

Arts HH, Bongers EM, Mans DA, van Beersum SE, Oud MM, Bolat E, Spruijt L, Cornelissen EA, Schuurs-Hoeijmakers JH, de Leeuw N et al (2011) C14ORF179 encoding IFT43 is mutated in Sensenbrenner syndrome. J Med Genet 48:390–395

Badano JL, Leitch CC, Ansley SJ, May-Simera H, Lawson S, Lewis RA, Beales PL, Dietz HC, Fisher S, Katsanis N (2006a) Dissection of epistasis in oligogenic Bardet-Biedl syndrome. Nature 439:326–330

Badano JL, Mitsuma N, Beales PL, Katsanis N (2006b) The ciliopathies: an emerging class of human genetic disorders. Annu Rev Genomics Hum Genet 7:125–148

Baek K, Kim DH, Jeong J, Sim SJ, Melis A, Kim JS, Jin E, Bae S (2016) DNA-free two-gene knockout in Chlamydomonas reinhardtii via CRISPR-Cas9 ribonucleoproteins. Sci Rep 6:30620

Baker K, Beales PL (2009) Making sense of cilia in disease: the human ciliopathies. Am J Med Genet C Semin Med Genet 151C:281–295

Bangs FK, Schrode N, Hadjantonakis AK, Anderson KV (2015) Lineage specificity of primary cilia in the mouse embryo. Nat Cell Biol *17*:113–122

Barbato A, Frischer T, Kuehni CE, Snijders D, Azevedo I, Baktai G, Bartoloni L, Eber E, Escribano A, Haarman E et al (2009) Primary ciliary dyskinesia: a consensus statement on diagnostic and treatment approaches in children. Eur Respir J 34:1264–1276

Barker AR, Thomas R, Dawe HR (2014) Meckel-Gruber syndrome and the role of primary cilia in kidney, skeleton, and central nervous system development. Organogenesis 10:96–107

Barr MM, Sternberg PW (1999) A polycystic kidney-disease gene homologue required for male mating behaviour in C. elegans. Nature 401:386–389

Baujat G, Le Merrer M (2007) Ellis-van Creveld syndrome. Orphanet J Rare Dis 2:27

Beales PL, Elcioglu N, Woolf AS, Parker D, Flinter FA (1999) New criteria for improved diagnosis of Bardet-Biedl syndrome: results of a population survey. J Med Genet 36:437–446

Beales PL, Bland E, Tobin JL, Bacchelli C, Tuysuz B, Hill J, Rix S, Pearson CG, Kai M, Hartley J et al (2007) IFT80, which encodes a conserved intraflagellar transport protein, is mutated in Jeune asphyxiating thoracic dystrophy. Nat Genet 39:727–729

Blaby IK, Blaby-Haas CE, Tourasse N, Hom EF, Lopez D, Aksoy M, Grossman A, Umen J, Dutcher S, Porter M et al (2014) The Chlamydomonas genome project: a decade on. Trends Plant Sci 19:672–680

Blair HJ, Tompson S, Liu YN, Campbell J, MacArthur K, Ponting CP, Ruiz-Perez VL, Goodship JA (2011) Evc2 is a positive modulator of Hedgehog signalling that interacts with Evc at the cilia membrane and is also found in the nucleus. BMC Biol 9:14

Boesger J, Wagner V, Weisheit W, Mittag M (2009) Analysis of flagellar phosphoproteins from Chlamydomonas reinhardtii. Eukaryot Cell 8:922–932

Bradley BA, Quarmby LM (2005) A NIMA-related kinase, Cnk2p, regulates both flagellar length and cell size in Chlamydomonas. J Cell Sci 118:3317–3326

Bredrup C, Saunier S, Oud MM, Fiskerstrand T, Hoischen A, Brackman D, Leh SM, Midtbo M, Filhol E, Bole-Feysot C et al (2011) Ciliopathies with skeletal anomalies and renal insufficiency due to mutations in the IFT-A gene WDR19. Am J Hum Genet 89:634–643

Brown JM, Witman GB (2014) Cilia and diseases. Bioscience 64:1126–1137

Cao M, Ning J, Hernandez-Lara CI, Belzile O, Wang Q, Dutcher SK, Liu Y, Snell WJ (2015) Uni-directional ciliary membrane protein trafficking by a cytoplasmic retrograde IFT motor and ciliary ectosome shedding. Elife 4

Cavalier-Smith T (1974) Basal body and flagellar development during the vegetative cell cycle and the sexual cycle of Chlamydomonas reinhardii. J Cell Sci 16:529–556

Chacon-Camacho OF, Zenteno JC (2015) Review and update on the molecular basis of Leber congenital amaurosis. World J Clin Cases 3:112–124

Chen CP (2007) Meckel syndrome: genetics, perinatal findings, and differential diagnosis. Taiwan J Obstet Gynecol 46:9–14

Christensen ST, Clement CA, Satir P, Pedersen LB (2012) Primary cilia and coordination of receptor tyrosine kinase (RTK) signalling. J Pathol 226:172–184

Collin GB, Marshall JD, Ikeda A, So WV, Russell-Eggitt I, Maffei P, Beck S, Boerkoel CF, Sicolo N, Martin M et al (2002) Mutations in ALMS1 cause obesity, type 2 diabetes and neurosensory degeneration in Alstrom syndrome. Nat Genet 31:74–78

Craige B, Tsao CC, Diener DR, Hou Y, Lechtreck KF, Rosenbaum JL, Witman GB (2010) CEP290 tethers flagellar transition zone microtubules to the membrane and regulates flagellar protein content. J Cell Biol 190:927–940

Dagoneau N, Goulet M, Genevieve D, Sznajer Y, Martinovic J, Smithson S, Huber C, Baujat G, Flori E, Tecco L et al (2009) DYNC2H1 mutations cause asphyxiating thoracic dystrophy and short rib-polydactyly syndrome, type III. Am J Hum Genet 84:706–711

Davis EE, Katsanis N (2012) The ciliopathies: a transitional model into systems biology of human genetic disease. Curr Opin Genet Dev 22:290–303

Davy BE, Robinson ML (2003) Congenital hydrocephalus in hy3 mice is caused by a frameshift mutation in Hydin, a large novel gene. Hum Mol Genet 12:1163–1170

Dell KM (2015) The role of cilia in the pathogenesis of cystic kidney disease. Curr Opin Pediatr 27:212–218

den Hollander AI, Koenekoop RK, Yzer S, Lopez I, Arends ML, Voesenek KE, Zonneveld MN, Strom TM, Meitinger T, Brunner HG et al (2006) Mutations in the CEP290 (NPHP6) gene are a frequent cause of Leber congenital amaurosis. Am J Hum Genet 79:556–561

den Hollander AI, Roepman R, Koenekoop RK, Cremers FP (2008) Leber congenital amaurosis: genes, proteins and disease mechanisms. Prog Retin Eye Res 27:391–419

Douek E, Bannister LH, Dodson HC (1975) Recent advances in the pathology of olfaction. Proc R Soc Med 68:467–470

Dutcher SK (2014) The awesome power of dikaryons for studying flagella and basal bodies in Chlamydomonas reinhardtii. Cytoskeleton (Hoboken) 71:79–94

Eleftheriades M, Iavazzo C, Manolakos E, Hassiakos D, Botsis D, Petersen M, Konstantinidou A (2013) Recurrent short rib polydactyly syndrome. J Obstet Gynaecol 33:14–16

Ellis RW, van Creveld S (1940) A syndrome characterized by ectodermal dysplasia, polydactyly, chondro-dysplasia and congenital morbus cordis: report of three cases. Arch Dis Child 15:65–84

Feather SA, Winyard PJ, Dodd S, Woolf AS (1997) Oral-facial-digital syndrome type 1 is another dominant polycystic kidney disease: clinical, radiological and histopathological features of a new kindred. Nephrol Dial Transplant 12:1354–1361

Ferrante MI, Giorgio G, Feather SA, Bulfone A, Wright V, Ghiani M, Selicorni A, Gammaro L, Scolari F, Woolf AS et al (2001) Identification of the gene for oral-facial-digital type I syndrome. Am J Hum Genet 68:569–576

Ferrante MI, Zullo A, Barra A, Bimonte S, Messaddeq N, Studer M, Dolle P, Franco B (2006) Oral-facial-digital type I protein is required for primary cilia formation and left-right axis specification. Nat Genet 38:112–117

Foxman SG, Heckenlively JR, Bateman JB, Wirtschafter JD (1985) Classification of congenital and early onset retinitis pigmentosa. Arch Ophthalmol 103:1502–1506

Franceschetti A, Dieterle P (1954) Diagnostic and prognostic importance of the electroretinogram in tapetoretinal degeneration with reduction of the visual field and hemeralopia. Confin Neurol 14:184–186

Gagnadoux MF, Bacri JL, Broyer M, Habib R (1989) Infantile chronic tubulo-interstitial nephritis with cortical microcysts: variant of nephronophthisis or new disease entity? Pediatr Nephrol 3:50–55

Geng L, Segal Y, Peissel B, Deng N, Pei Y, Carone F, Rennke HG, Glucksmann-Kuis AM, Schneider MC, Ericsson M et al (1996) Identification and localization of polycystin, the PKD1 gene product. J Clin Invest 98:2674–2682

Gilissen C, Arts HH, Hoischen A, Spruijt L, Mans DA, Arts P, van Lier B, Steehouwer M, van Reeuwijk J, Kant SG et al (2010) Exome sequencing identifies WDR35 variants involved in Sensenbrenner syndrome. Am J Hum Genet 87:418–423

Goetz SC, Anderson KV (2010) The primary cilium: a signalling centre during vertebrate development. Nat Rev Genet 11:331–344

Halbritter J, Bizet AA, Schmidts M, Porath JD, Braun DA, Gee HY, McInerney-Leo AM, Krug P, Filhol E, Davis EE et al (2013) Defects in the IFT-B component IFT172 cause Jeune and Mainzer-Saldino syndromes in humans. Am J Hum Genet 93:915–925

Hearn T, Renforth GL, Spalluto C, Hanley NA, Piper K, Brickwood S, White C, Connolly V, Taylor JF, Russell-Eggitt I et al (2002) Mutation of ALMS1, a large gene with a tandem repeat encoding 47 amino acids, causes Alstrom syndrome. Nat Genet 31:79–83

Hearn T, Spalluto C, Phillips VJ, Renforth GL, Copin N, Hanley NA, Wilson DI (2005) Subcellular localization of ALMS1 supports involvement of centrosome and basal body dysfunction in the pathogenesis of obesity, insulin resistance, and type 2 diabetes. Diabetes 54:1581–1587

Hemachandar R (2014) Senior-loken syndrome – a ciliopathy. J Clin Diagn Res 8:MD04–MD05

Hildebrandt F, Otto E, Rensing C, Nothwang HG, Vollmer M, Adolphs J, Hanusch H, Brandis M (1997a) A novel gene encoding an SH3 domain protein is mutated in nephronophthisis type 1. Nat Genet 17:149–153

Hildebrandt F, Strahm B, Nothwang HG, Gretz N, Schnieders B, Singh-Sawhney I, Kutt R, Vollmer M, Brandis M (1997b) Molecular genetic identification of families with juvenile nephronophthisis type 1: rate of progression to renal failure. APN Study Group. Arbeitsgemeinschaft fur Padiatrische Nephrologie. Kidney Int 51:261–269

Hilgendorf KI, Johnson CT, Jackson PK (2016) The primary cilium as a cellular receiver: organizing ciliary GPCR signaling. Curr Opin Cell Biol 39:84–92

Hoffer JL, Fryssira H, Konstantinidou AE, Ropers HH, Tzschach A (2013) Novel WDR35 mutations in patients with cranioectodermal dysplasia (Sensenbrenner syndrome). Clin Genet 83:92–95

Hong DH, Pawlyk B, Sokolov M, Strissel KJ, Yang J, Tulloch B, Wright AF, Arshavsky VY, Li T (2003) RPGR isoforms in photoreceptor connecting cilia and the transitional zone of motile cilia. Invest Ophthalmol Vis Sci 44:2413–2421

Horst CJ, Johnson LV, Besharse JC (1990) Transmembrane assemblage of the photoreceptor connecting cilium and motile cilium transition zone contain a common immunologic epitope. Cell Motil Cytoskeleton 17:329–344

Hu Z, Liang Y, He W, Pan J (2015) Cilia disassembly with two distinct phases of regulation. Cell Rep 10:1803–1810

Huangfu DW, Liu AM, Rakeman AS, Murcia NS, Niswander L, Anderson KV (2003) Hedgehog signalling in the mouse requires intraflagellar transport proteins. Nature 426:83–87

Iannaccone A, Mykytyn K, Persico AM, Searby CC, Baldi A, Jablonski MM, Sheffield VC (2005) Clinical evidence of decreased olfaction in Bardet-Biedl syndrome caused by a deletion in the BBS4 gene. Am J Med Genet A 132A:343–346

Jenkins PM, McEwen DP, Martens JR (2009) Olfactory cilia: linking sensory cilia function and human disease. Chem Senses 34:451–464

Jeune M, Beraud C, Carron R (1955) Asphyxiating thoracic dystrophy with familial characteristics. Arch Fr Pediatr 12:886–891

Jinkerson RE, Jonikas MC (2015) Molecular techniques to interrogate and edit the Chlamydomonas nuclear genome. Plant J 82:393–412

Kartagener ODM (1933) Zur pathogenese der bronchiektasien. Beitr Klin Tuberk Spezif Tuberkuloseforsch 84:73–85

Khanna H, Hurd TW, Lillo C, Shu X, Parapuram SK, He S, Akimoto M, Wright AF, Margolis B, Williams DS et al (2005) RPGR-ORF15, which is mutated in retinitis pigmentosa, associates with SMC1, SMC3, and microtubule transport proteins. J Biol Chem 280:33580–33587

Kim I, Fu Y, Hui K, Moeckel G, Mai W, Li C, Liang D, Zhao P, Ma J, Chen XZ et al (2008) Fibrocystin/polyductin modulates renal tubular formation by regulating polycystin-2 expression and function. J Am Soc Nephrol 19:455–468

Kim S, Zaghloul NA, Bubenshchikova E, Oh EC, Rankin S, Katsanis N, Obara T, Tsiokas L (2011) Nde1-mediated inhibition of ciliogenesis affects cell cycle re-entry. Nat Cell Biol 13:351–360

Knorz VJ, Spalluto C, Lessard M, Purvis TL, Adigun FF, Collin GB, Hanley NA, Wilson DI, Hearn T (2010) Centriolar association of ALMS1 and likely centrosomal functions of the ALMS motif-containing proteins C10orf90 and KIAA1731. Mol Biol Cell 21:3617–3629

Knowles MR, Daniels LA, Davis SD, Zariwala MA, Leigh MW (2013) Primary ciliary dyskinesia. Recent advances in diagnostics, genetics, and characterization of clinical disease. Am J Respir Crit Care Med 188:913–922

Kozminski KG, Johnson KA, Forscher P, Rosenbaum JL (1993) A motility in the eukaryotic flagellum unrelated to flagellar beating. Proc Natl Acad Sci U S A 90:5519–5523

Kulaga HM, Leitch CC, Eichers ER, Badano JL, Lesemann A, Hoskins BE, Lupski JR, Beales PL, Reed RR, Katsanis N (2004) Loss of BBS proteins causes anosmia in humans and defects in olfactory cilia structure and function in the mouse. Nat Genet 36:994–998

Kurkowiak M, Zietkiewicz E, Witt M (2015) Recent advances in primary ciliary dyskinesia genetics. J Med Genet 52:1–9

Kyttala M, Tallila J, Salonen R, Kopra O, Kohlschmidt N, Paavola-Sakki P, Peltonen L, Kestila M (2006) MKS1, encoding a component of the flagellar apparatus basal body proteome, is mutated in Meckel syndrome. Nat Genet 38:155–157

Lavanya R, Pratap K (1995) Short rib polydactyly syndrome—a rare skeletal dysplasia. Int J Gynaecol Obstet 50:291–292

Leber T (1869) Ueber Retinitis pigmentosa und angeborene Amaurose. Graefes Arch Clin Exp Ophthalmol 15:1–25

Lechtreck KF (2015) IFT-cargo interactions and protein transport in cilia. Trends Biochem Sci 40:765–778

Lechtreck KF, Witman GB (2007) Chlamydomonas reinhardtii hydin is a central pair protein required for flagellar motility. J Cell Biol 176:473–482

Lechtreck KF, Johnson EC, Sakai T, Cochran D, Ballif BA, Rush J, Pazour GJ, Ikebe M, Witman GB (2009) The Chlamydomonas reinhardtii BBSome is an IFT cargo required for export of specific signaling proteins from flagella. J Cell Biol 187:1117–1132

Lee L (2013) Riding the wave of ependymal cilia: genetic susceptibility to hydrocephalus in primary ciliary dyskinesia. J Neurosci Res 91:1117–1132

Lefebvre PA, Nordstrom SA, Moulder JE, Rosenbaum JL (1978) Flagellar elongation and shortening in Chlamydomonas. IV. Effects of flagellar detachment, regeneration, and resorption on the induction of flagellar protein synthesis. J Cell Biol 78:8–27

Li JB, Gerdes JM, Haycraft CJ, Fan Y, Teslovich TM, May-Simera H, Li H, Blacque OE, Li L, Leitch CC et al (2004) Comparative genomics identifies a flagellar and basal body proteome that includes the BBS5 human disease gene. Cell 117:541–552

Li G, Vega R, Nelms K, Gekakis N, Goodnow C, McNamara P, Wu H, Hong NA, Glynne R (2007) A role for Alstrom syndrome protein, alms1, in kidney ciliogenesis and cellular quiescence. PLoS Genet 3:e8

Li A, Saito M, Chuang JZ, Tseng YY, Dedesma C, Tomizawa K, Kaitsuka T, Sung CH (2011) Ciliary transition zone activation of phosphorylated Tctex-1 controls ciliary resorption, S-phase entry and fate of neural progenitors. Nat Cell Biol 13:402–411

Li Y, Garrod AS, Madan-Khetarpal S, Sreedher G, McGuire M, Yagi H, Klena NT, Gabriel GC, Khalifa O, Zahid M et al (2015) Respiratory motile cilia dysfunction in a patient with cranioectodermal dysplasia. Am J Med Genet A 167A:2188–2196

Liang Y, Meng D, Zhu B, Pan J (2016) Mechanism of ciliary disassembly. Cell Mol Life Sci 73:1787–1802

Lin H, Zhang Z, Guo S, Chen F, Kessler JM, Wang YM, Dutcher SK (2015) A NIMA-related kinase suppresses the flagellar instability associated with the loss of multiple axonemal structures. PLoS Genet 11:e1005508

Loken AC, Hanssen O, Halvorsen S, Jolster NJ (1961) Hereditary renal dysplasia and blindness. Acta Paediatr 50:177–184

Mahjoub MR, Montpetit B, Zhao L, Finst RJ, Goh B, Kim AC, Quarmby LM (2002) The FA2 gene of Chlamydomonas encodes a NIMA family kinase with roles in cell cycle progression and microtubule severing during deflagellation. J Cell Sci 115:1759–1768

Maria BL, Quisling RG, Rosainz LC, Yachnis AT, Gitten J, Dede D, Fennell E (1999) Molar tooth sign in Joubert syndrome: clinical, radiologic, and pathologic significance. J Child Neurol 14:368–376

Marshall JD, Ludman MD, Shea SE, Salisbury SR, Willi SM, LaRoche RG, Nishina PM (1997) Genealogy, natural history, and phenotype of Alstrom syndrome in a large Acadian kindred and three additional families. Am J Med Genet 73:150–161

Marshall JD, Bronson RT, Collin GB, Nordstrom AD, Maffei P, Paisey RB, Carey C, Macdermott S, Russell-Eggitt I, Shea SE et al (2005) New Alstrom syndrome phenotypes based on the evaluation of 182 cases. Arch Intern Med 165:675–683

Marshall JD, Beck S, Maffei P, Naggert JK (2007) Alstrom syndrome. Eur J Hum Genet 15:1193–1202

Marszalek JR, Goldstein LS (2000) Understanding the functions of kinesin-II. Biochim Biophys Acta 1496:142–150

May-Simera HL, Kelley MW (2012) Cilia, Wnt signaling, and the cytoskeleton. Cilia 1:7

McEwen DP, Koenekoop RK, Khanna H, Jenkins PM, Lopez I, Swaroop A, Martens JR (2007) Hypomorphic CEP290/NPHP6 mutations result in anosmia caused by the selective loss of G proteins in cilia of olfactory sensory neurons. Proc Natl Acad Sci U S A 104:15917–15922

Meckel JF (1822) Beschreibung zweier, durch sehr ähnliche Bildungsabweichungen entstellter Geschwister. Dtsch Arch Physiol 7:99–172

Meng D, Pan J (2016) A NIMA-related kinase, CNK4, regulates ciliary stability and length. Mol Biol Cell 27:838–847

Merchant SS, Prochnik SE, Vallon O, Harris EH, Karpowicz SJ, Witman GB, Terry A, Salamov A, Fritz-Laylin LK, Marechal-Drouard L et al (2007) The Chlamydomonas genome reveals the evolution of key animal and plant functions. Science 318:245–250

Merrill AE, Merriman B, Farrington-Rock C, Camacho N, Sebald ET, Funari VA, Schibler MJ, Firestein MH, Cohn ZA, Priore MA et al (2009) Ciliary abnormalities due to defects in the retrograde transport protein DYNC2H1 in short-rib polydactyly syndrome. Am J Hum Genet 84:542–549

Mill P, Lockhart PJ, Fitzpatrick E, Mountford HS, Hall EA, Reijns MA, Keighren M, Bahlo M, Bromhead CJ, Budd P et al (2011) Human and mouse mutations in WDR35 cause short-rib polydactyly syndromes due to abnormal ciliogenesis. Am J Hum Genet 88:508–515

Minton JA, Owen KR, Ricketts CJ, Crabtree N, Shaikh G, Ehtisham S, Porter JR, Carey C, Hodge D, Paisey R et al (2006) Syndromic obesity and diabetes: changes in body composition with age and mutation analysis of ALMS1 in 12 United Kingdom kindreds with Alstrom syndrome. J Clin Endocrinol Metab 91:3110–3116

Mitchell DR (2004) Speculations on the evolution of 9+2 organelles and the role of central pair microtubules. Biol Cell 96:691–696

Mochizuki T, Wu G, Hayashi T, Xenophontos SL, Veldhuisen B, Saris JJ, Reynolds DM, Cai Y, Gabow PA, Pierides A et al (1996) PKD2, a gene for polycystic kidney disease that encodes an integral membrane protein. Science 272:1339–1342

Mohr OL (1941) A hereditary sublethal syndrome in man. Nor Vidensk Akad Oslo I Mat Naturv Klasse 14:3–18

Morgan NV, Bacchelli C, Gissen P, Morton J, Ferrero GB, Silengo M, Labrune P, Casteels I, Hall C, Cox P et al (2003) A locus for asphyxiating thoracic dystrophy, ATD, maps to chromosome 15q13. J Med Genet 40:431–435

Nakatomi M, Hovorakova M, Gritli-Linde A, Blair HJ, MacArthur K, Peterka M, Lesot H, Peterkova R, Ruiz-Perez VL, Goodship JA et al (2013) Evc regulates a symmetrical response to Shh signaling in molar development. J Dent Res 92:222–228

Narita K, Takeda S (2015) Cilia in the choroid plexus: their roles in hydrocephalus and beyond. Front Cell Neurosci 9:39

Nonaka S, Tanaka Y, Okada Y, Takeda S, Harada A, Kanai Y, Kido M, Hirokawa N (1998) Randomization of left-right asymmetry due to loss of nodal cilia generating leftward flow of extraembryonic fluid in mice lacking KIF3B motor protein. Cell 95:829–837

Novas R, Cardenas-Rodriguez M, Irigoin F, Badano JL (2015) Bardet-Biedl syndrome: is it only cilia dysfunction? FEBS Lett 589:3479–3491

O'Dea D, Parfrey PS, Harnett JD, Hefferton D, Cramer BC, Green J (1996) The importance of renal impairment in the natural history of Bardet-Biedl syndrome. Am J Kidney Dis 27:776–783

Olbrich H, Schmidts M, Werner C, Onoufriadis A, Loges NT, Raidt J, Banki NF, Shoemark A, Burgoyne T, Al Turki S et al (2012) Recessive HYDIN mutations cause primary ciliary dyskinesia without randomization of left-right body asymmetry. Am J Hum Genet 91:672–684

Omran H, Fernandez C, Jung M, Haffner K, Fargier B, Villaquiran A, Waldherr R, Gretz N, Brandis M, Ruschendorf F et al (2000) Identification of a new gene locus for adolescent nephronophthisis, on chromosome 3q22 in a large Venezuelan pedigree. Am J Hum Genet 66:118–127

Ozgul RK, Satman I, Collin GB, Hinman EG, Marshall JD, Kocaman O, Tutuncu Y, Yilmaz T, Naggert JK (2007) Molecular analysis and long-term clinical evaluation of three siblings with Alstrom syndrome. Clin Genet 72:351–356

Pan J (2008) Cilia and ciliopathies: from Chlamydomonas and beyond. Sci China C Life Sci 51:479–486

Pan JM, Misamore MJ, Wang Q, Snell WJ (2003) Protein transport and signal transduction during fertilization in Chlamydomonas. Traffic 4:452–459

Pan J, Wang Q, Snell WJ (2004) An aurora kinase is essential for flagellar disassembly in Chlamydomonas. Dev Cell 6:445–451

Pan J, Naumann-Busch B, Wang L, Specht M, Scholz M, Trompelt K, Hippler M (2011) Protein phosphorylation is a key event of flagellar disassembly revealed by analysis of flagellar phosphoproteins during flagellar shortening in Chlamydomonas. J Proteome Res 10:3830–3839

Papillon L, Psaume J (1954) Hereditary abnormality of the buccal mucosa: abnormal bands and frenula. Revue Stomatol 55:209–227

Parisi MA, Doherty D, Chance PF, Glass IA (2007) Joubert syndrome (and related disorders) (OMIM 213300). Eur J Hum Genet 15:511–521

Pazour GJ, Rosenbaum JL (2002) Intraflagellar transport and cilia-dependent diseases. Trends Cell Biol 12:551–555

Pazour GJ, Witman GB (2003) The vertebrate primary cilium is a sensory organelle. Curr Opin Cell Biol 15:105–110

Pazour G, Witman GB (2009) The Chlamydomonas flagellum as a model for human ciliary disease. In: Witman GB (ed) The Chlamydomonas sourcebook. Oxford, Elsevier, pp 445–478

Pazour GJ, Dickert BL, Vucica Y, Seeley ES, Rosenbaum JL, Witman GB, Cole DG (2000) Chlamydomonas IFT88 and its mouse homologue, polycystic kidney disease gene tg737, are required for assembly of cilia and flagella. J Cell Biol 151:709–718

Pazour GJ, Agrin N, Leszyk J, Witman GB (2005) Proteomic analysis of a eukaryotic cilium. J Cell Biol 170:103–113

Pedersen LB, Miller MS, Geimer S, Leitch JM, Rosenbaum JL, Cole DG (2005) Chlamydomonas IFT172 is encoded by FLA11, interacts with CrEB1, and regulates IFT at the flagellar tip. Curr Biol 15:262–266

Pennarun G, Escudier E, Chapelin C, Bridoux AM, Cacheux V, Roger G, Clement A, Goossens M, Amselem S, Duriez B (1999) Loss-of-function mutations in a human gene related to Chlamydomonas reinhardtii dynein IC78 result in primary ciliary dyskinesia. Am J Hum Genet 65:1508–1519

Perrault I, Rozet JM, Gerber S, Ghazi I, Leowski C, Ducroq D, Souied E, Dufier JL, Munnich A, Kaplan J (1999) Leber congenital amaurosis. Mol Genet Metab 68:200–208
Perrault I, Saunier S, Hanein S, Filhol E, Bizet AA, Collins F, Salih MA, Gerber S, Delphin N, Bigot K et al (2012) Mainzer-Saldino syndrome is a ciliopathy caused by IFT140 mutations. Am J Hum Genet 90:864–870
Porter ME, Sale WS (2000) The 9 + 2 axoneme anchors multiple inner arm dyneins and a network of kinases and phosphatases that control motility. J Cell Biol 151:F37–F42
Prattichizzo C, Macca M, Novelli V, Giorgio G, Barra A, Franco B, Oral-Facial-Digital Type ICG (2008) Mutational spectrum of the oral-facial-digital type I syndrome: a study on a large collection of patients. Hum Mutat 29:1237–1246
Praveen K, Davis EE, Katsanis N (2015) Unique among ciliopathies: primary ciliary dyskinesia, a motile cilia disorder. F1000Prime Rep 7:36
Pugacheva EN, Jablonski SA, Hartman TR, Henske EP, Golemis EA (2007) HEF1-dependent Aurora A activation induces disassembly of the primary cilium. Cell 129:1351–1363
Rademacher N, Hambrock M, Fischer U, Moser B, Ceulemans B, Lieb W, Boor R, Stefanova I, Gillessen-Kaesbach G, Runge C et al (2011) Identification of a novel CDKL5 exon and pathogenic mutations in patients with severe mental retardation, early-onset seizures and Rett-like features. Neurogenetics 12:165–167
Raven P, Evert R, Eichhorn S (1999) Biology of plants, 6th edn. Freeman/Worth, New York
Reiter JF, Blacque OE, Leroux MR (2012) The base of the cilium: roles for transition fibres and the transition zone in ciliary formation, maintenance and compartmentalization. EMBO Rep 13:608–618
Ronquillo CC, Bernstein PS, Baehr W (2012) Senior-Loken syndrome: a syndromic form of retinal dystrophy associated with nephronophthisis. Vis Res 75:88–97
Rosenbaum JL, Witman GB (2002) Intraflagellar transport. Nat Rev Mol Cell Biol 3:813–825
Rosenbaum JL, Moulder JE, Ringo DL (1969) Flagellar elongation and shortening in Chlamydomonas. The use of cycloheximide and colchicine to study the synthesis and assembly of flagellar proteins. J Cell Biol 41:600–619
Ruiz-Perez VL, Tompson SW, Blair HJ, Espinoza-Valdez C, Lapunzina P, Silva EO, Hamel B, Gibbs JL, Young ID, Wright MJ et al (2003) Mutations in two nonhomologous genes in a head-to-head configuration cause Ellis-van Creveld syndrome. Am J Hum Genet 72:728–732
Saletti D, Grigio TR, Tonelli D, Ribeiro OD, Marini F (2012) Case report: anesthesia in patients with asphyxiating thoracic dystrophy: Jeune syndrome. Rev Bras Anestesiol 62:424–431
Salomon R, Saunier S, Niaudet P (2009) Nephronophthisis. Pediatr Nephrol 24:2333–2344
Salonen R, Norio R (1984) The Meckel syndrome in Finland: epidemiologic and genetic aspects. Am J Med Genet 18:691–698
Salonen R, Paavola P (1998) Meckel syndrome. J Med Genet 35:497–501
Saunier S, Salomon R, Antignac C (2005) Nephronophthisis. Curr Opin Genet Dev 15:324–331
Schmidts M (2014) Clinical genetics and pathobiology of ciliary chondrodysplasias. J Pediatr Genet 3:46–94
Schmidts M, Frank V, Eisenberger T, Al Turki S, Bizet AA, Antony D, Rix S, Decker C, Bachmann N, Bald M et al (2013) Combined NGS approaches identify mutations in the intraflagellar transport gene IFT140 in skeletal ciliopathies with early progressive kidney disease. Hum Mutat 34:714–724
Scholey JM (2003) Intraflagellar transport. Annu Rev Cell Dev Biol 19:423–443
Senior B, Friedmann AI, Braudo JL (1961) Juvenile familial nephropathy with tapetoretinal degeneration. A new oculorenal dystrophy. Am J Ophthalmol 52:625–633
Sensenbrenner JA, Dorst JP, Owens RP (1975) New syndrome of skeletal, dental and hair anomalies. Birth Defects Orig Artic Ser 11:372–379
Shaheen R, Schmidts M, Faqeih E, Hashem A, Lausch E, Holder I, Superti-Furga A, Consortium UK, Mitchison HM, Almoisheer A et al (2015) A founder CEP120 mutation in Jeune asphyxiating thoracic dystrophy expands the role of centriolar proteins in skeletal ciliopathies. Hum Mol Genet 24:1410–1419

Sharma N, Berbari NF, Yoder BK (2008) Ciliary dysfunction in developmental abnormalities and diseases. Curr Top Dev Biol 85:371–427

Shetty P, Shetty D, Priyadarshana PS, Bhat S (2015) A rare case report of Ellis Van Creveld syndrome in an Indian patient and literature review. J Oral Biol Craniofac Res 5:98–101

Shin SE, Lim JM, Koh HG, Kim EK, Kang NK, Jeon S, Kwon S, Shin WS, Lee B, Hwangbo K et al (2016) CRISPR/Cas9-induced knockout and knock-in mutations in Chlamydomonas reinhardtii. Sci Rep 6:27810

Silflow CD, Lefebvre PA (2001) Assembly and motility of eukaryotic cilia and flagella. Lessons from Chlamydomonas reinhardtii. Plant Physiol 127:1500–1507

Singla V, Romaguera-Ros M, Garcia-Verdugo JM, Reiter JF (2010) Ofd1, a human disease gene, regulates the length and distal structure of centrioles. Dev Cell 18:410–424

Sleigh MA (1981) Primary ciliary dyskinesia. Lancet 2:476

Szymanska K, Hartill VL, Johnson CA (2014) Unraveling the genetics of Joubert and Meckel-Gruber syndromes. J Pediatr Genet 3:65–78

Tam LW, Ranum PT, Lefebvre PA (2013) CDKL5 regulates flagellar length and localizes to the base of the flagella in Chlamydomonas. Mol Biol Cell 24:588–600

Taschner M, Lorentzen E (2016) The intraflagellar transport machinery. Cold Spring Harb Perspect Biol 8

Taub DG, Liu Q (2016) The role of intraflagellar transport in the photoreceptor sensory cilium. Adv Exp Med Biol 854:627–633

Thauvin-Robinet C, Cossee M, Cormier-Daire V, Van Maldergem L, Toutain A, Alembik Y, Bieth E, Layet V, Parent P, David A et al (2006) Clinical, molecular, and genotype-phenotype correlation studies from 25 cases of oral-facial-digital syndrome type 1: a French and Belgian collaborative study. J Med Genet 43:54–61

Tompson SW, Ruiz-Perez VL, Blair HJ, Barton S, Navarro V, Robson JL, Wright MJ, Goodship JA (2007) Sequencing EVC and EVC2 identifies mutations in two-thirds of Ellis-van Creveld syndrome patients. Hum Genet 120:663–670

Torres VE, Rossetti S, Harris PC (2007) Update on autosomal dominant polycystic kidney disease. Minerva Med 98:669–691

Tory K, Lacoste T, Burglen L, Moriniere V, Boddaert N, Macher MA, Llanas B, Nivet H, Bensman A, Niaudet P et al (2007) High NPHP1 and NPHP6 mutation rate in patients with Joubert syndrome and nephronophthisis: potential epistatic effect of NPHP6 and AHI1 mutations in patients with NPHP1 mutations. J Am Soc Nephrol 18:1566–1575

Valente EM, Marsh SE, Castori M, Dixon-Salazar T, Bertini E, Al-Gazali L, Messer J, Barbot C, Woods CG, Boltshauser E et al (2005) Distinguishing the four genetic causes of Jouberts syndrome-related disorders. Ann Neurol 57:513–519

Veland IR, Awan A, Pedersen LB, Yoder BK, Christensen ST (2009) Primary cilia and signaling pathways in mammalian development, health and disease. Nephron Physiol 111:39–53

Wahrman J, Berant M, Jacobs J, Aviad I, Ben-Hur N (1966) The oral-facial-digital syndrome: a male-lethal condition in a boy with 47/xxy chromosomes. Pediatrics 37:812–821

Walczak-Sztulpa J, Eggenschwiler J, Osborn D, Brown DA, Emma F, Klingenberg C, Hennekam RC, Torre G, Garshasbi M, Tzschach A et al (2010) Cranioectodermal Dysplasia, Sensenbrenner syndrome, is a ciliopathy caused by mutations in the IFT122 gene. Am J Hum Genet 86:949–956

Wang J, Barr MM (2016) Ciliary extracellular vesicles: txt msg organelles. Cell Mol Neurobiol 36:449–457

Wang Q, Pan J, Snell WJ (2006) Intraflagellar transport particles participate directly in cilium-generated signaling in Chlamydomonas. Cell 125:549–562

Wang J, Silva M, Haas LA, Morsci NS, Nguyen KC, Hall DH, Barr MM (2014) C. elegans ciliated sensory neurons release extracellular vesicles that function in animal communication. Curr Biol 24:519–525

Waters AM, Beales PL (2011) Ciliopathies: an expanding disease spectrum. Pediatr Nephrol 26:1039–1056

Wheatley DN (1995) Primary cilia in normal and pathological tissues. Pathobiology 63:222–238
Witman GB (2009) Cell motilty and behavior. Academic Press, Oxford
Wolf MT (2015) Nephronophthisis and related syndromes. Curr Opin Pediatr 27:201–211
Wolf MT, Hildebrandt F (2011) Nephronophthisis. Pediatr Nephrol 26:181–194
Wood CR, Rosenbaum JL (2015) Ciliary ectosomes: transmissions from the cell's antenna. Trends Cell Biol 25:276–285
Wood CR, Huang K, Diener DR, Rosenbaum JL (2013) The cilium secretes bioactive ectosomes. Curr Biol 23:906–911
Yabut O, Pleasure SJ, Yoon K (2015) A notch above sonic hedgehog. Dev Cell 33:371–372
Yoshiba S, Shiratori H, Kuo IY, Kawasumi A, Shinohara K, Nonaka S, Asai Y, Sasaki G, Belo JA, Sasaki H et al (2012) Cilia at the node of mouse embryos sense fluid flow for left-right determination via Pkd2. Science 338:226–231
Zaffanello M, Diomedi-Camassei F, Melzi ML, Torre G, Callea F, Emma F (2006) Sensenbrenner syndrome: a new member of the hepatorenal fibrocystic family. Am J Med Genet A 140:2336–2340
Zaghloul NA, Katsanis N (2009) Mechanistic insights into Bardet-Biedl syndrome, a model ciliopathy. J Clin Invest 119:428–437
Zhang QH, Taulman PD, Yoder BK (2004) Cystic kidney diseases: all roads lead to the cilium. Physiology 19:225–230
Zhou F, Roy S (2015) SnapShot: motile cilia. Cell 162:224.e221

Chlamydomonas: Intraflagellar Transport

Gai Liu and Kaiyao Huang

Abstract Cilia/flagella are microtubule-based organelles emanating from the surface of most eukaryotic cells and accomplish motile and sensory functions. Malfunction of cilia results in a variety of ciliopathies such as polycystic kidney disease, retinal degeneration, and male infertility. The assembly of nearly all cilia/flagella depends on a conserved transport machinery–intraflagellar transport (IFT), which has 22 subunits and is composed of IFT-A and IFT-B complex. IFT moves bidirectionally in flagella and is driven by the anterograde motor kinesin-2 and the retrograde motor dynein 1b/2. Co-expression and crystal structure analysis of IFT complex demonstrated that IFT-B can be divided into IFT-B1 and IFT-B2 subcomplex, and each subcomplex has a tubulin-binding module, suggesting that tubulin is a primary cargo of IFT. Other cargoes include axonemal components from outer dynein arms (ODA), inner dynein arms (IDA), radial spoke proteins (RSP) and dynein regulatory complexes (DRC), and membrane proteins. The IFT and cargoes form long trains and short trains in flagella under the electron microscopy. By transporting the flagellar precursors, turnover products, or signal molecules, IFT plays a critical role in flagellar assembly, disassembly, and signal transduction in Chlamydomonas. In addition to moving in flagella, IFT proteins also locate at the basal body and tip of flagella, where the regulation of IFT occurs. Future studies need to illustrate the interaction mechanism between the IFT and cargoes, relationship between IFT and the flagellar membrane trafficking, and the complexity and flexibility of the structure of IFT in vivo and to reconstitute the IFT machinery in vitro.

1 Introduction

The flagella/cilia are microtubule-based organelles projecting from the surface of most eukaryotic cells and can be divided into motile cilia and immotile cilia (primary cilia). Both types of cilia are composed of basal body (centriole), axoneme, and ciliary membrane. The outer dynein, inner dynein, radial spoke, and center pair

G. Liu • K. Huang (✉)
Key Laboratory of Algal Biology, Institute of Hydrobiology, Chinese Academy of Sciences, Wuhan 430072, China
e-mail: gailiu@ihb.ac.cn; huangky@ihb.ac.cn

M. Hippler (ed.), *Chlamydomonas: Biotechnology and Biomedicine*, Microbiology Monographs 31, DOI 10.1007/978-3-319-66360-9_5

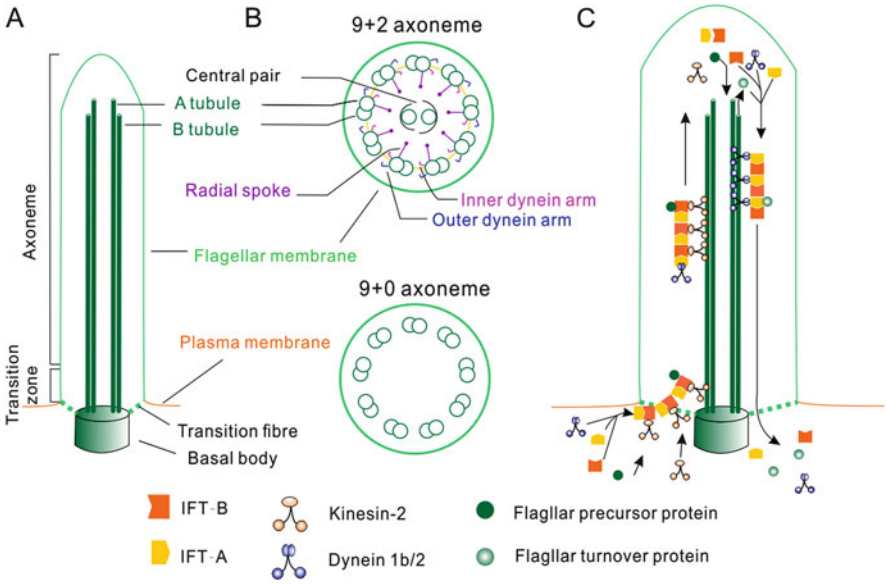

Fig. 1 Schematic structure of flagella/cilia and machinery of IFT. (**a**) Flagellum consisted of four main structures: flagellar membrane, axoneme, transition zone, and basal body. (**b**) Cross-sectional diagrams of motile flagella with a central pair microtubule doublets (9+2) and a non-motile primary cilium without the central pair microtubule doublets (9+0). The 9+2 axoneme is composed of 9 outer microtubule doublets. Each microtubule doublet consists of A and B tubules. The A tubules display three kinds of projections, outer dynein arms (ODAs), inner dynein arms (IDAs), and radial spokes. (**c**) The working model of IFT. IFT trains are assembled from IFT-A and IFT-B complexes near the basal body and the transition fibers; the retrograde motor (dynein 1b/2) and flagellar precursor proteins bind to the IFT trains as cargoes; the anterograde motors (kinesin-2) drive IFT trains cross the transition fibers and move along the B tubules toward the flagellar tip; the IFT trains are remodeled at the tip, while cargoes are unloaded and turnover products are loaded to the retrograde IFT trains; the retrograde motor (dynein 1b/2) drive retrograde IFT trains and turnover products back to the cell body along the A tubules

are specially associated with the axonemes of motile cilia (Fig. 1a, b). The unicellular green alga Chlamydomonas is the classic model to study flagella/cilia, which are dispensable for survival in this organism but provide driving force for Chlamydomonas cells moving toward light (positive phototaxis) or away from light (negative phototaxis). In addition to this regulated and rhythmical beating, non-beating motilities were also observed in the flagellum, such as the gliding of cells across the solid surface aided by a pair of flagella, the mobilization of membrane proteins along the length of the flagella, and the bidirectional movement of microspheres attached to the flagellar surface (Bloodgood 1992).

In the early 1990s, Keith Kozminski, a graduate student in Dr. Rosenbaum's lab at Yale University, took advantage of the video-enhanced high-resolution differential interference contrast (DIC) microscopy to investigate non-beating motility in flagella; unexpectedly, he observed particles moving bidirectionally under the flagellar membrane. The movements are continuous, the rate of anterograde

transport (from the base to the tip) is ~2 μm/s, and the rate of retrograde transport (from the tip to the base) is ~3.5 μm/s (Kozminski et al. 1993). Since this type of movement is faster than the cell gliding and the movement of microspheres, clearly, it is a novel movement in flagella. Back to the early 1960s, Ringo et al. also observed some raft-like electron-dense structures laid between the axoneme and membrane under transmission electron microscopy (TEM) (Ringo 1967). The relationship between moving particles and the electron-dense rafts were studied by using correlative light microscopy with TEM, in which Chlamydomonas cells were flat embedded and fixed between two Teflon-coated coverslips. The membrane bulges in DIC were well matched with the electron-dense rafts in TEM, and both of them disappeared in flagella of *fla10-1* at restrictive temperature (Kozminski et al. 1995). So these granule-like particles movement were named intraflagellar transport (IFT), and the raft-like electron-dense structures between the flagellar membrane and axoneme were named IFT particles.

During the last 20 years, tremendous progress has been achieved in identifying the components of IFT particles, in uncovering the crystal structure of IFT complexes and dissecting the assembly process of IFT. More importantly, mutations of IFT genes in human result in human diseases and the non-cilia-related functions of IFT have also been demonstrated. IFT is widely studied in the model organisms such as *C. elegans*, zebrafish, and mouse. In this chapter, I will focus on the research progress of IFT in Chlamydomonas and explain how these works deepen our understanding of the function of IFT in ciliary assembly, ciliary disassembly, and ciliary signal transduction.

2 Components of IFT Particles

Based on the biochemical and genetic studies, and searching homologue of putative IFT protein first identified in *C. elegans* and zebrafish, we now know that there are 22 IFT proteins in Chlamydomonas. Anterograde IFT is driven by kinesin-2, and retrograde IFT is driven by cytoplasmic dynein complex dynein 1b/2.

2.1 Anterograde IFT Motor

The anterograde motor for IFT is a heterotrimeric complex of kinesin-2, which was purified from flagella of Chlamydomonas, and consisted of motor subunits FLA10, FLA8, and non-motor subunit KAP (Cole et al. 1998; Miller et al. 2005; Mueller et al. 2005). The first identified mutant of kinesin-2 is *fla10-1* generated in 1970s. It has full length flagella at the permissive temperature (20 °C) but fails to maintain flagella at the restrictive temperature (32 °C) (Huang et al. 1977). *fla10-1* cells were unable to regenerate flagella if they were deflagellated shortly after shifting to 32 °C, indicating FLA10 is required for the flagella assembly (Huang et al. 1977;

Kozminski et al. 1995). And this requirement was also confirmed by the FLA10 null mutant obtained lately (Matsuura et al. 2002). *Fla10-1* allele possesses a C to A missense mutation, which alters the neutral asparagine residue at 329 to basic lysine residue in the kinesin motor domain (Vashishtha et al. 1996).

The *fla10-1* mutant was used by Kozminski et al. to determine whether FLA10 is the motor-driving IFT particles. The amount of FLA10 reduced remarkably in flagella of *fla10-1* after 90 min incubation at 32 °C. Concomitantly, almost no IFT movement could be observed in *fla10-1* flagella under the DIC microscopy when the flagella had shortened to 80% of the full length. Meanwhile, the number of the electron-dense IFT rafts between the axoneme and membrane reduced to one third of original state. These evidences demonstrated that lack of kinesin-2 motor FLA10 resulted in termination of IFT in flagella (Kozminski et al. 1995). FLA10 is primarily located between the outer doublet microtubules and flagellar membrane (Kozminski et al. 1995), and it exists as puncta along the axoneme undergoing flagellar regeneration by immunostaining (Vashishtha et al. 1996), similar to the distribution of the IFT rafts. In addition, kinesin-2 is a plus-end-directed microtubule motor, so FLA10 was defined as the subunit of the anterograde transport motor for IFT.

The second subunit of kinesin-2 motor FLA8 was first identified by sequencing of the purified kinesin-2 complex using mass spectrometry. FLA8 shows 89% homologous to the FLA10. The two alleles *fla1* and *fla8* are temperature-sensitive mutants, and both possess single amino acid substitution linked to motor domain (Miller et al. 2005). FLA8 phosphorylation regulates the interaction between kinesin-2 and IFT-B complex (Liang et al. 2014).

The non-motor subunit of kinesin-2 in Chlamydomonas is named KAP/FLA3, which was identified by searching the homologue of sea urchin KAP in Chlamydomonas. The *fla3-1* allele possesses a residue substitution in a conserved C-terminal domain. In *fla3-1* mutants, kinesin-2 is not efficiently retained in the basal body or targeted to the flagella at permissive temperature, and localization to the basal body is disrupted at restrictive temperature indicating KAP is required for the localization of kinesin-2 at the basal body. The frequency of anterograde IFT particles is reduced, and the anterograde IFT particles appear larger and pause frequently for a while in flagella of *fla3-1*, suggesting dissociation of IFT from kinesin-2 complex occurs in flagella (Mueller et al. 2005).

2.2 Retrograde IFT Motor

The motor-driving IFT particles back to the base of flagella from the tip (retrograde IFT) is cytoplasmic dynein 1b/2 complex, composed of heavy chain (DHC1b) (Pazour et al. 1999), light intermediate chain (D1bLIC) (Reck et al. 2016; Hou et al. 2004), intermediate chain (D1bIC2/FAP133 and D1bIC1/FAP163) (Patel-King et al. 2013), and light chain (LC8/FLA14, Tctex1, Tctex2b, and LC7b) (Pazour et al. 1998; Schmidts et al. 2015). Cytoplasmic dynein 1b/2 exists as a

homodimer in Chlamydomonas and is transported to the tip of flagella by anterograde motor kinesin-2 (Pedersen et al. 2006).

The first evidence that linked dynein with retrograde IFT came from the studies of the dynein light chain LC8/FLA14, which was initially identified as a light chain of outer arm dynein in Chlamydomonas (Piperno and Luck 1979). The null mutant of LC8 was *fla14*, characterized with short, paralyzed flagella and lack of axonemal structures such as radial spokes, inner and outer dynein arms, and beak-like projections of the B tubules of the outer doublet microtubules. The anterograde IFT was normal, but retrograde IFT was absent in *fla14* mutant, resulted in accumulation of IFT particles between the doublet microtubules and the flagellar membrane, suggesting that LC8 was a component of the retrograde IFT motor (Pazour et al. 1998). Later, Tctex1, Tctex2b, and LC7b were also identified as dynein 1b/2 light chains. For example, retrograde IFT was dramatically reduced in the null mutant of *tctex2b*, and flagella assembled more slowly than wild-type cells (Schmidts et al. 2015).

The heavy chain of cytoplasmic dynein 1b/2 complex is DHC1b. The cells of the *dhc1b* null mutant grow normally but have stumpy flagella, swollen with IFT particles, aberrant microtubules, and other amorphous material (Porter et al. 1999; Pazour et al. 1999). DHC1b was localized primarily at the basal body region and, in flagella with puncta, a pattern similar to IFT particles and kinesin-2. Most of DHC1b were found in the membrane/matrix fraction of flagella, and the ATP facilitates it releasing from axonemes, which was almost consistent with the distribution of FLA10 and IFT139 in flagella (Pazour et al. 1999). Recently, three temperature sensitive *dhc1b* mutants were also identified and showed more subtle phenotype (Engel et al. 2012; Iomini et al. 2001; Lin et al. 2013). The *dhc1b-2* (Engel et al. 2012) mutant possesses half-length flagella, while *dhc1b-3* (Engel et al. 2012) and *fla24* (Lin et al. 2013) both have normal-length flagella at permissive temperature. The amount of retrograde IFT in flagella of *dhc1b-3* was obviously reduced, but the flagellar length could be maintained over 24 h at restrictive temperature, and the flagella of *dhc1b-2* and *fla24* were shortened much faster and were even lost at restrictive temperature (Engel et al. 2012; Lin et al. 2013). These studies demonstrated that different domain of DHC1b may play different roles in cargo loading and the interaction with the axoneme.

D1bLIC is the only light-intermediate chain identified so far in cytoplasmic dynein 1b/2 complex of Chlamydomonas. D1bLIC was first characterized as the homologue of mammalian light intermediate chain D2LIC. D1bLIC is in the same complex as the dynein heavy chain DHC1b and co-localize with DHC1b at the basal body region and along the axoneme of flagella (Perrone et al. 2003). GFP-fused D1bLIC displayed robust anterograde and retrograde movement identical to the IFT particles (Reck et al. 2016). The null mutant of Chlamydomonas d1blic has variable length of flagella and accumulated IFT particles in the flagella (Hou et al. 2004). In *d1blic* knockdown mutants, the velocity and frequency of retrograde IFT are severely reduced but detectable, suggesting that retrograde motor is still active. The flagellar protein composition in *d1blic* knockdown mutants was investigated by quantitative proteomics. Different to IFT and BBSome

(Bardet–Biedl syndrome) proteins, kinesin-2 subunits are reduced in the *d1blic* knockdown mutant, suggesting that kinesin-2 can dissociate from the accumulated IFT particles and return to the cell dispensable of D1bLIC (Reck et al. 2016). This hypothesis is consistent with other studies that no accumulation of kinesin-2 could be observed in *dhc1b-3* temperature sensitive (Engel et al. 2012) and *d1blic* null mutants (Pedersen et al. 2006).

Two intermediate chains, D1bIC2/FAP133 (Rompolas et al. 2007) and D1bIC1/FAP163 (Patel-King et al. 2013), were identified as components of dynein 1b/2. Chlamydomonas FAP133 is localized at the basal body region and along the flagella with puncta, co-purified with other dynein 1b/2 subunits and forms a macromolecular complex above 2 MDa with FLA10 and IFT components. In the absence of DHC1b or D1bLIC, FAP133 fails to localize at the basal body region but is concentrated in a region of the cytoplasm near the cell center (Rompolas et al. 2007). The second dynein intermediate chain D1bIC1/FAP163 is a homologue of FAP133, forms a complex with D1bIC2 and LC8, and is actively transported by IFT in Chlamydomonas. When the D1bIC1 homologue was knocked down in planaria, typical ciliary defects of dynein 1b/2 mutation were observed (Patel-King et al. 2013).

2.3 IFT Complex

After the discovery of IFT, scientists were curious about the protein composition of IFT particles. Using sucrose gradient centrifugation and ^{35}S-labeling method, Piperno et al. reported a novel 17S complex consisted of at least 13 polypeptides present in the flagellar matrix fraction of *fla10-1* at permissive but absent at restrictive temperature (Piperno and Mead 1997). At the same time in Dr. Rosenbaum's laboratory, Dr. Cole identified a group of more than 15 proteins co-sedimenting at 16S which disappeared from flagella of *fla10-1* at restrictive temperature (Cole et al. 1998). Subsequent studies demonstrated that the 16S complex is the same as the novel 17S complex reported by Piperno et al. (Piperno et al. 1998; Piperno and Mead 1997). In addition, Cole et al. observed that 16S proteins also disappeared in flagella of *fla1*/*fla8-2*, which was a temperature sensitive mutant of another subunit of anterograde motor of kinesin-2 (Cole et al. 1998). These data confirmed that the IFT complex is in 16S fraction.

The 16S fraction was further enriched, separated on two-dimensional gel, and then sequenced by mass spectrometry (MS) (Cole et al. 1998). The gel filtration and ionic strength alternation experiments indicated that the 16S complex could be further divided into two complexes, IFT-A and IFT-B. IFT-A is composed of IFT144, IFT140, IFT139, and IFT122, which sedimented at 16.1–16.4 S; and IFT-B is composed of 10 subunits, including IFT172/FLA11, IFT88, IFT81, IFT80, IFT74/72, IFT57/55, IFT52, IFT46, IFT27, and IFT20, which sedimented at 16S (Cole et al. 1998). IFT43, the smallest IFT-A subunit, was identified subsequently in the 17S complex mentioned above (Piperno et al. 1998). Additional IFT proteins, such as the sixth IFT-A subunit IFT121, and two small IFT-B subunits, IFT25/FAP232 and

IFT22/FAP9, were identified in 16S fraction with an improved purification method (Wang et al. 2009) or by analyzing flagellar associated proteins (FAP) from flagellar proteomics (Lechtreck et al. 2009b). Other IFT subunits, such as IFT70 (CrDYF-1, Fleer, or FAP259) (Fan et al. 2010), IFT56 (CrDYF-13 or TTC26) (Ishikawa et al. 2014), IFT54 (CrDYF-11, Elipsa, or FAP116), and IFT38 (CrDYF-3, Qilin or FAP22) (Taschner et al. 2016), were first identified from cilium defect mutants in *C. elegans* or zebrafish, then their homologs in Chlamydomonas were identified. To date, 22 IFT proteins have been identified in Chlamydomonas.

3 Assembly of IFT

Co-sedimentation of numerous IFT proteins at 16S in sucrose gradient and enrichment of various protein interaction motifs suggests that IFT proteins might interact with each other to assemble the raft-like particles. Combination of in vivo and in vitro approaches sheds new lights on the detailed assembly process of IFT complex. Lucker et al. showed that IFT-B could be further separated into a 500 kDa IFT-B core complex (also named IFT-B1 recently) and other peripheral subunits which were released when 300 mM NaCl was added to the sucrose gradient. The initial 500-kDa IFT-B core complex contains IFT88, IFT81, IFT74/72, IFT52, IFT46, and IFT27 (Lucker et al. 2005). Subsequently, newly identified IFT25 (Lechtreck et al. 2009b; Wang et al. 2009), IFT22 (Silva et al. 2012; Wang et al. 2009), and IFT56 (Ishikawa et al. 2014) were also suggested as the member of IFT-B1 complex using recombinant co-expression and pull-down assay (Taschner et al. 2011, 2014; Swiderski et al. 2014). Other peripheral IFT-B subunits, including IFT172, IFT80, IFT57, IFT54, IFT38, and IFT20 could be overexpressed in insect cells or *E.coli* system and form a stable complex named as IFT-B2 (Taschner et al. 2016; Katoh et al. 2016). Using similar approach, Behal et al. revealed that IFT-A is consisted of a 12S core complex (IFT144, IFT140 and IFT122) and peripheral components (IFT139, IFT121, IFT43) (Behal et al. 2012).

In addition, numerous interactions were characterized between individual IFT subunits using traditional in vitro assays such as yeast two/three hybrid, protein co-expression in *E. coli,* or insect system and pull-down assay (Lucker et al. 2005, 2010; Bhogaraju et al. 2011; Taschner et al. 2014, 2016). Most of the interactions were mapped to the specific domains of the IFT proteins. In IFT-B1 complex, the middle part of IFT52 binds to TPR domain of IFT88 and IFT70, while the C-terminal fraction binds to the C-terminal part of IFT46 (Taschner et al. 2011). IFT81 interacts with IFT74 through N-terminal coiled coil domain (Lucker et al. 2010). In IFT-B2 complex, the N-terminal CH domain of IFT38 bind to IFT80, and its coiled coil domain binds to the coiled coil domain of IFT57 (Taschner et al. 2016). In IFT-A complex, the C-terminal of IFT43 and IFT121 interact directly (Behal et al. 2012). At the base of animal cilia, an module named CPLANE (ciliogenesis and planar polarity effector) recruits peripheral IFT-A proteins to the basal body and mediates the assembling of IFT-A core and peripheral components (Toriyama et al. 2016). The

detailed interaction map and the corresponding methods applied to demonstrate the interaction were summarized in Fig. 2. However, all these interactions between individual IFT subunits or subcomplexes need to be confirmed in vivo.

4 Movement of IFT

The movement of IFT can be recorded by video-enhanced DIC microscopy and time-lapse fluorescence microscopy (Allen et al. 1981). Kozminski et al. first used video-enhanced DIC to capture the movement of IFT in the flagella (Kozminski et al. 1993; Orozco et al. 1999). Subsequently, video-enhanced DIC was used to characterize the anterograde IFT or retrograde IFT in kinesin-2 mutant *fla10-1* and *fla3-1* and dynein 1b/2 mutant *fla14* (Pazour et al. 1998; Kozminski et al. 1995).

Piperno et al. first used the kymography to analyze velocity and frequency of IFT particles and demonstrated that the velocity of retrograde IFT particles and frequency of bidirectional transport were decreased in retrograde IFT mutants *fla15 (ift144)*, *fla16 (ift139)*, and *fla17* (*ift139*) at permissive temperature (Piperno et al. 1998). In another study, the IFT movement of wild type and 13 mutants were analyzed in detail. Iomini et al. demonstrated that retrograde particles are more numerous than anterograde IFT particles in flagella of wild-type cells, and IFT consists of at least four phases: phases II and IV, in which particles undergo anterograde and retrograde transport, and phases I and III, in which particles are remodeled/exchanged at the proximal and distal end of the flagella (Iomini et al. 2001). In addition, IFT movement was examined in steady-state, growing, and disassembling flagella. The rate of IFT is nearly constant and independent of flagellar length, except in very short flagella; IFT particle entry into flagella is periodic, but gaps or pauses in particle entry were observed (Dentler 2005).

The application of time-lapse fluorescence microscopy to visualize the movement of GFP-tagged IFT motor in cilia was first carried out in *C. elegans* (Orozco et al. 1999). Due to the low expression and low fluorescence of original GFP expressed in Chlamydomonas, until 6 years later, KAP became the first protein labeled with GFP in flagella of Chlamydomonas (Mueller et al. 2005). IFT27 is the first IFT protein tagged with GFP and the rate of IFT27::GFP movement is nearly the same as the velocity of IFT particles determined by DIC (Qin et al. 2007). Subsequently, co-expression of IFT20::mCherry and BBS4::GFP in the same cells was obtained and demonstrated that BBS4 is a cargo of IFT (Lechtreck et al. 2009a). To overcome the problem of low florescence of GFP signal in flagella and high autofluorescence of chloroplast in cell body, Mueller et al. used the confocal fluorescence microscopy to visualize the KAP::GFP (Mueller et al. 2005). Qin et al. modified the standard epifluorescence microscopy by adding an illumination system that guaranteed only the flagellum was excited with a 488 laser (Huang et al. 2007; Qin et al. 2007). Engel et al. first employed the spinning disk confocal microscopy and total internal reflection fluorescence (TIRF) microscopy to record the movement of IFT27::GFP and KAP::GFP (Engel et al. 2009). Because

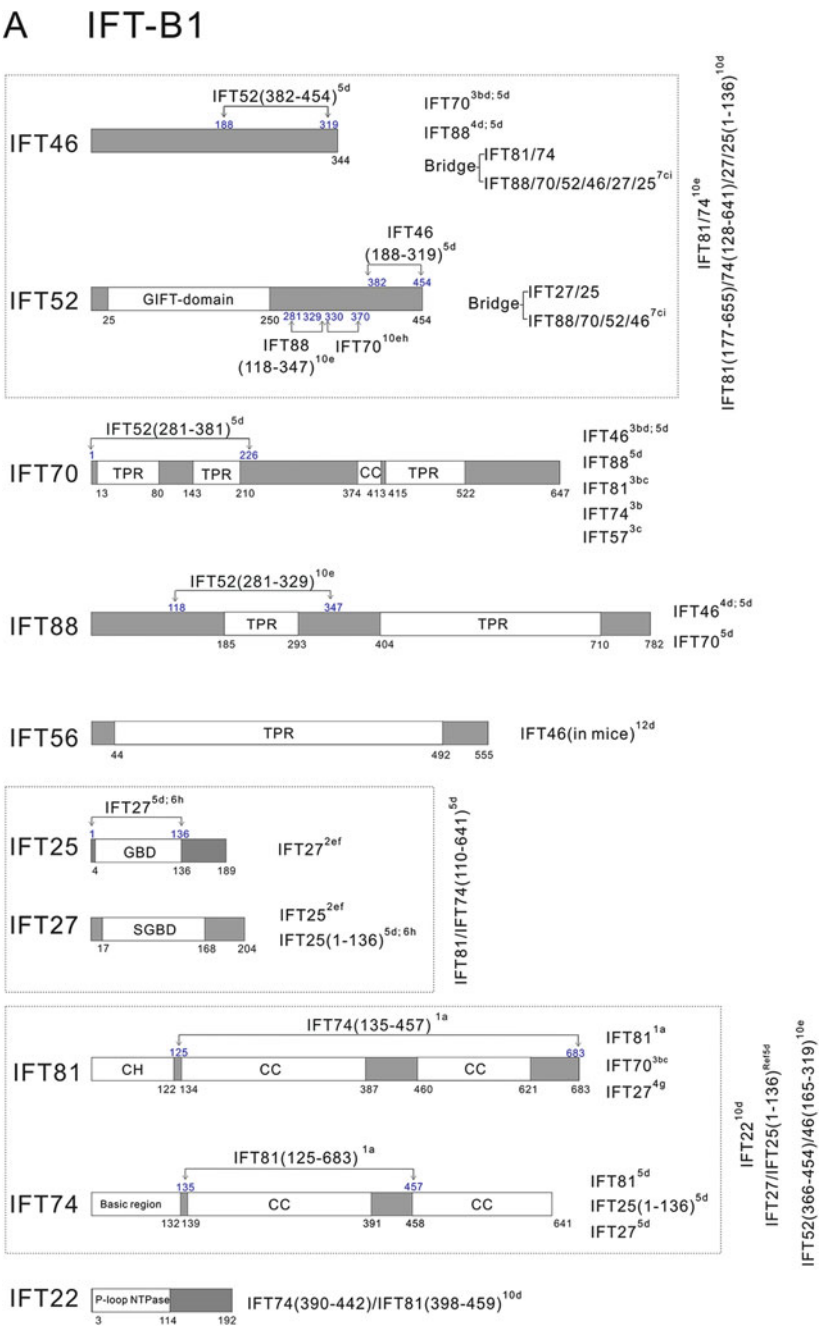

Fig. 2 The interactions between individual IFT subunits or IFT subcomplexes. (**a**) IFT-B1 complex; (**b**) IFT-B2 complex; (**c**) IFT-A complex. The minimal fragments required for interactions are labeled on the protein domain graphs; otherwise, the interacting partners are

only about 30–300 nm of specimen closed to the cover slip can be excited and signal-to-noise ratio is extremely high, the TIRF or two-color TIRF are widely used to visualize the IFT and cargo movement in flagella of Chlamydomonas (Lechtreck 2016). However, only several IFT or motor proteins have been targeted with GFP or mCherry so far; brighter fluorescence proteins and new strategy to increase the expression of the fusion proteins in Chlamydomonas are needed.

5 The Localization and Structure of IFT

The localization of IFT and motors has been determined by epifluorescence microscopy, confocal fluorescence microscopy, high-resolution fluorescence microscopy, and electron microscopy (EM). The structure of IFT has been studied by a correlative light and EM (CLEM) approach and by analyzing the crystal structure of IFT complex expressed in vitro.

5.1 Immunofluorescence Microscopy

Because there are about 22 proteins in IFT complex, it is always a curious question how this complex was organized in vivo. Kozminski first showed that IFT is a granule-like particle, localized between the flagellar membrane and the outer doublet microtubules, and appears as linear rafts of lollipop-shaped electron-dense projections (Kozminski et al. 1993). Immunofluorescence microscopy revealed that the IFT172, IFT139, and IFT81 proteins, and kinesin motor FLA10 are found as dots along the flagella. Interestingly, all of these proteins are also concentrated at basal body region. IFT-B complex protein such as IFT172 and IFT81 appears as semicircular trilobed arc, whereas the IFT-A complex protein such as IFT139 appears as semicircular bilobed arc; the localization of anterograde motor FLA10 are very similar as IFT172 (Cole et al. 1998).

Fig. 2 (continued) listed *on the right side* of IFT proteins. Heterodimers are marked using *dotted box*. All the interactions were summarized from references listed and experimental assays listed. Each reference and experimental assay has a code (number or letter) and is marked as superscript on interacting partners. The protein domain graphs are generated based on the predictions using InterPro (URL: www.ebi.ac.uk/interpro) and Simple Modular Architecture Research Tool (SMART, URL: smart.embl-heidelberg.de). *GIFT* GldG/IFT, *TPR* tetratricopeptide repeat-containing domain, *GBD* galactose-binding like domain, *SGBD* small GTP-binding protein domain, *CH* calponin-homology domain, *CC* coiled coil domain

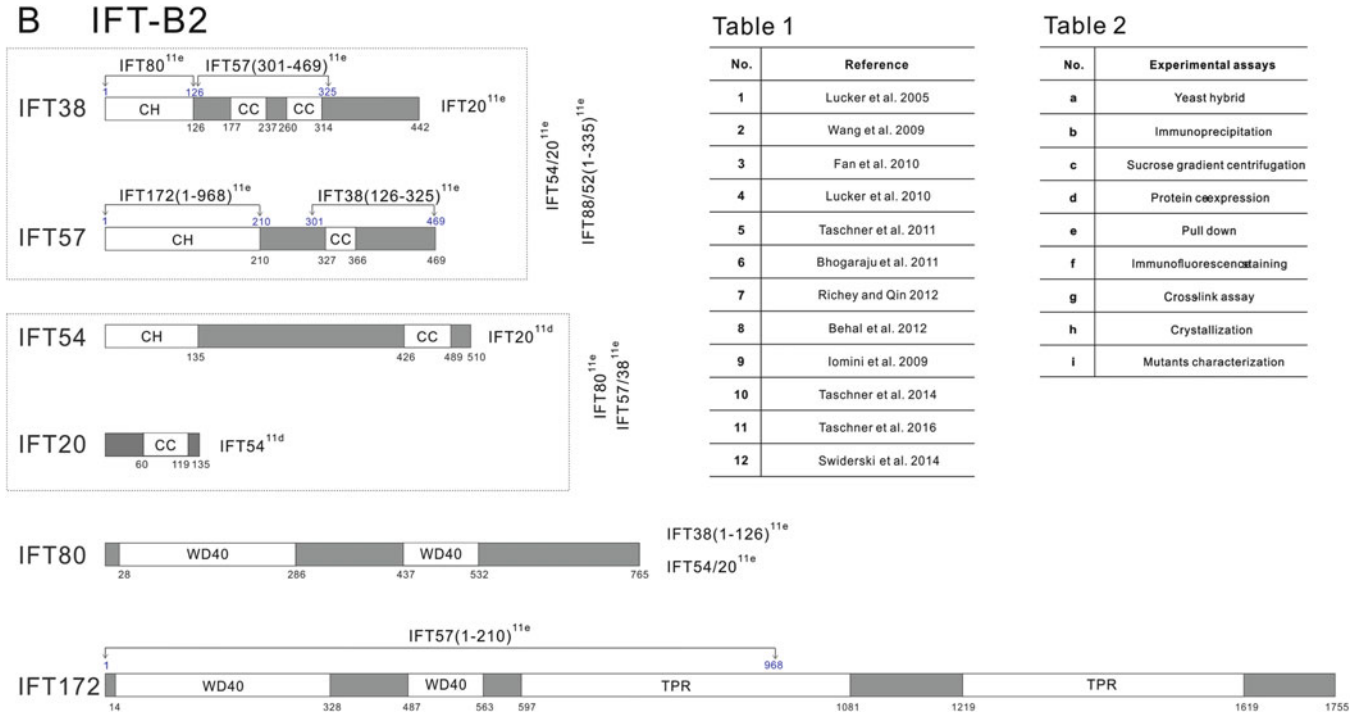

Table 1

No.	Reference
1	Lucker et al. 2005
2	Wang et al. 2009
3	Fan et al. 2010
4	Lucker et al. 2010
5	Taschner et al. 2011
6	Bhogaraju et al. 2011
7	Richey and Qin 2012
8	Behal et al. 2012
9	Iomini et al. 2009
10	Taschner et al. 2014
11	Taschner et al. 2016
12	Swiderski et al. 2014

Table 2

No.	Experimental assays
a	Yeast hybrid
b	Immunoprecipitation
c	Sucrose gradient centrifugation
d	Protein coexpression
e	Pull down
f	Immunofluorescence staining
g	Crosslink assay
h	Crystallization
i	Mutants characterization

Fig. 2 (continued)

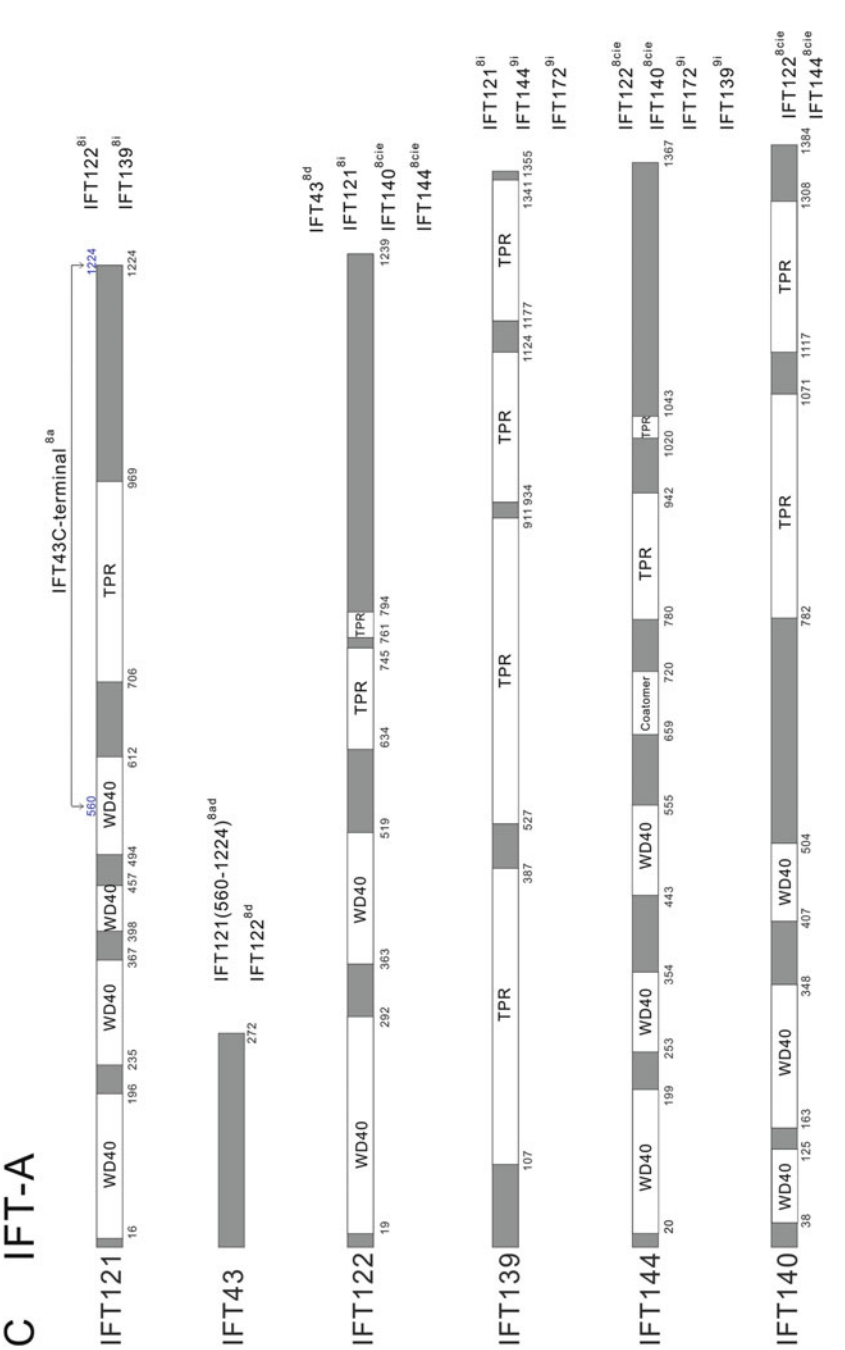

Fig. 2 (continued)

Another IFT-B protein IFT52 also appears on flagella as small punctate spots and accumulated at the basal body of interphase cells, it looks like a band beneath each flagellum at side view and as horseshoes-shaped rings when viewed from the anterior of the cell, and the IFT52 is associated with transitional fibers (Deane et al. 2001). IFT74 is localized at two big dots in basal body and at several small dots in flagella (Pedersen et al. 2005; Qin et al. 2007). IFT27 co-localized with FLA10 at two dots in the basal body region in addition to punctate localization in flagella (Qin et al. 2007). IFT46 and its cargo-specific adaptor outer row dynein ODA16 are concentrated at the basal body and co-localize with FLA10 in both flagella and basal body region (Ahmed et al. 2008). IFT25 co-localized with IFT46 at the basal body, but only about 50% dots are co-localized in flagella (Wang et al. 2009; Lechtreck et al. 2009b). IFT70/CrDYF-1 is punctate dot in flagella as other IFT proteins, and concentrated at basal body, appearing as three lobes (Fan et al. 2010).

Combination of the confocal and structured illumination microscopy (SIM), Brown et al. showed that the IFT-B (IFT46) and IFT-A (IFT139) co-localized with two anterior pools (dots) but IFT-B also localized at a more posterior semi-circular pool (dot). In *ift74* mutant, IFT-A pool was more dispersed and co-localized less extensively with IFT-B, especially along with the inner surface of the plasma membrane. The IFT-B (IFT46) was reducing in the posterior pool. Suggesting IFT74 is required for recruitment of IFT-A to IFT-B and injection of IFT enter to flagella (Brown et al. 2015).

Anterograde IFT motor protein KAP is concentrated at the basal body region, and as punctuate dot along the flagella, it looks like a pancake or a dot, not like a FLA10 as three small dots. The localization of FLA10 is dependent on the KAP, but the IFT139 localization as normal when KAP disappear, suggesting the localization of retrograde IFT is not dependent on the kinesin motor (Mueller et al. 2005).

Retrograde IFT motor proteins such as cDHC1b and D1bLIC predominantly localized to the basal body region and in punctate spots along the length of the two flagella (Pazour et al. 1999; Perrone et al. 2003; Hou et al. 2004). Another subunit of retrograde IFT motor D1bIC2 primarily located at the basal body region and sparsely distributed along the flagella, the signal at the basal body looks like a dot (Rompolas et al. 2007).

Because of the specificity of the antibodies and the limitation of two-dimensional immunofluorescence pictures, the localization data of IFT and motors was not always the same even used the same antibody and strain. However, we still can make two general conclusions. The IFT proteins and motors are localized in flagella as dots, and most of the time they are co-localized, suggesting they moved as a complex. Nearly all of IFT and motor proteins are concentrated at the basal body, the IFT-B proteins and anterograde motor appear as semicircular trilobed arc, and the IFT-A proteins and retrograde motor appear as semicircular dilobed arc. The two anterior lobes (pool) are co-localized. In the future, high-resolution microscopy such as stimulated emission depletion (STED) microscopy, stochastic optical reconstruction microscopy (STORM) and photoactivated localization microscopy (PALM) needs to be employed to confirm these conclusions.

5.2 Electron Microscopy

Silver-enhanced immunogold labeling demonstrated that IFT52 encircles the basal body and is associated with the transitional fibers (Deane et al. 2001). Analysis of longitudinal thin sections of flagella from flat-embedded cells with immunogold EM showed that several IFT46 particles predominantly located between the flagellar membrane and the outer doublet B MT subfibers, and also near the plus end of A MT subfibers, where IFT tip turnaround may occur (Pedersen et al. 2006).

In addition, high-resolution ultrastructure of IFT particles was analyzed by using electron-tomographic analysis of sections from flat-embedded Chlamydomonas cells. In retrograde IFT motor mutant *fla14*, long and narrow trains were identified and were thought to be responsible for anterograde transport since there is no retrograde IFT movement in this mutant. In longitudinal sections, the long trains displayed a periodic structure pattern between the flagellar membrane and the microtubules. Each unit of long anterograde trains is made of two similar particles laterally, so the trains appear to be made of a doublet string of particles longitudinally. The individual IFT particles are highly complex and varied longitudinally through the trains of particles. The pairs of particles (unit) connected to each other by obliquely bridge domain, has a repeat of ~40 nm. The average length of long trains is about 700 nm, suggesting there are about 17 units in each long train. Each unit has four putative sites connected to the outer doublet microtubule and four putative sites linked to flagellar membrane. In the cross section of the flagella of wild-type and *pf28* cells, another shorter and more compact IFT trains was identified, and it displayed a repeat of 16 nm, and the length of short trains is 251 nm, which is thought to be responsible for retrograde IFT (Pigino et al. 2009).

Subsequent study from the same group (Vannuccini et al. 2016) demonstrated that during the flagellar regeneration, the number of short trains increase, but the number of long trains decrease, suggesting that the short trains are bidirectional, comprising both anterograde and retrograde moving component. Based on the organization and a lateral extension, the short trains were divided into two subtypes: narrow short trains and wide short trains. The narrow short trains shared a more compact organization and the lateral extension slightly wider than the underlying microtubule. The wide short trains were characterized by a looser organization and a lateral extension over the doublet about twofold. In addition, the narrow short trains possess a thin end projection, pointing toward to the tip of the axoneme and have three major domains, a, b, and c. The central major domain linked the flagellar membrane and the surface of β-tubule, which is flanked by two lobes, b and c. The b lobe is compact and is tightly linked to the central domain. The c lobe is separated from a domain by a cleft. The lobe b appeared to be almost continuous, and the lobe c exhibited a definite 16 nm periodicity, resulting in a globular subdomain, a thinner stem, and a basal subdomain, which is a reminiscent of lollipop-like particle showed by TEM (Kozminski et al. 1995).

Recently, Stephanek et al. developed a correlative light and EM (CLEM) approach, in which the anterograde IFT and retrograde IFT can be identified by

cross-reference to the movement direction of the particles just before the fixation (Stepanek and Pigino 2016). They found that the length (size) of the anterograde IFT and retrograde IFT are very similar. Anterograde IFT is about 233 nm, and the retrograde IFT is about 209 nm. Both may correspond to the short strains identified in the previous study (Pigino et al. 2009). The anterograde IFT is compact with clear boundaries and like a plate and their repeating units are 8–16 nm; however, the retrograde IFT is less condense and less regular compared to the anterograde IFT. The anterograde is on the track of the B-microtubule, and the retrograde IFT is on the track of A-microtubule, so that these two trains will not collide in cilia. In addition, a standing IFT about 650 nm in length was also identified in this study, which may be the long trains identified in *fla14* mutant, but the author did not determine which track this kind of IFT is associated with (Pigino et al. 2009).

5.3 Crystal Structure

The crystal structure of a complex composed of IFT25 and IFT27 was first revealed in 2011 (Bhogaraju et al. 2011). A truncated version of IFT25 (1–135 residues) was co-expressed with CrIFT27. Crystal structure of this complex showed that CrIFT25ΔC and IFT27 form a heterodimer in vitro. IFT25 displayed a jelly roll fold with nine β-stands and arranged into two antiparallel sheets. It may bind the calcium with residues D50 and T35 and by several main chain carbonyls. IFT27 is structurally similar to Rab8 and Rab11 but misses the prenylation site which can attach the membrane. The crystal structure CrIFT25ΔC/27 displayed an elongated shape with 80Ā × Ā40 × 25Ā. Nine residues of IFT25 in two loops regions (residues 36–42 and 117–125) mediated the binding to IFT27. The residues from β-strand β3 (F72), the C-terminal α-helex α5 (F186, E191, V194, F197 and Y95), and the loop connecting α2 and β4 (Y89 and Y95) of IFT 27 contribute the complex interaction. IFT27 binds GTP/GDP with micromolar affinity and show low intrinsic GTPase activity (Bhogaraju et al. 2011).

Later, crystal structure analysis demonstrated that IFT74 and IFT81 can form a heterodimer in vitro and the N-terminal domain of IFT74 (IFT74N) was highly basic with the isoelectric point (pI) $>$ 12. The N-terminal domain of IFT81 (IFT81N) is highly conserved and adopts the fold of a calponin homology (CH) domain which can bind the globular domain of tubulin to determine the specificity, and IFT74N recognizes the β-tubulin tail to increase the binding affinity (Bhogaraju et al. 2013). In the crystal structure of IFT70/52(330–381), the IFT70 formed a superhelical structure with 15 tetratricopeptide repeat (TPR), the residues 330–363 of IFT52 adopt an extended conformation, and the residues 364–369 fold into a short helix. The residues 330–370 of IFT52 bind the IFT70 largely through hydrophobic interaction. Two proteins are antiparallel, and IFT52 peptide is largely buried in the interior of IFT70 superhelix; in addition, IFT52(330–370) peptide became a part of the hydrophobic core of IFT70 (Taschner et al. 2014).

The crystal structure of TtIFT52(540–603)/TtIFT46(236–347) reveals that the IFT52C consists of three helices binding to the four helix of IFT46C via mainly hydrophobic interaction (Taschner et al. 2014). IFT52N possesses an extended central beta-sheet flanked by several helices and beta-hairpins. The conserved patch on the surface of IFT52N is required to mediating the interaction between IFT-B1 and IFT-B2 subcomplex (Taschner et al. 2016). The overall structure of the IFT54 CH domain is very similar to that of the IFT81 CH domain; although the IFT54 CH domain does not contain the basic residues, it does display a different Arg/Lys-rich basic patch which may be responsible for tubulin binding of IFT54 (Taschner et al. 2016).

6 The Function of IFT

IFT has been identified in nearly all cilia/flagella and plays a critical role in ciliary assembly, disassembly, and signal transduction. It may also be important for other flagellar motility such as gilding.

6.1 Function of IFT in Flagella Assembly

In IFT null mutants such as *fla10-2*, *fla8-3*, *dhc1b-1*, *ift122*, *bld1*, and *ift88-1*, no flagella or only very short flagella could be generated (Matsuura et al. 2002; Dutcher et al. 2012; Pazour et al. 1999, 2000; Behal et al. 2012). In temperature sensitive mutants of IFT and motors, including *fla10-1*, *fla3-1*, *fla17*, and *fla15*, the full length flagella would shorten gradually when cells were shifted to restrictive temperature (Kozminski et al. 1995; Mueller et al. 2005; Iomini et al. 2009; Piperno et al. 1998). All these data demonstrated that IFT is indispensable for assembly and maintenance of flagella.

The bidirectional moving IFT was suggested as the cargo transporters for flagella assembly. Piperno et al. showed that active transport of IDA4 but not ODA6 required the activity of FLA10 (Piperno et al. 1996). In the matrix of flagella, the IDA4 protein was partly associated with the 17S IFT complex (Piperno and Mead 1997). These data suggested IDA4 maybe an IFT cargo. The *ift46-1* null mutants possess very short flagella. Both inner and outer dynein arms were absent in *ift46-1* flagella, but only outer dynein arms disappeared in a partially suppressed mutant $Sup_{ift46}1$ which have full length flagella (Hou et al. 2007). Interaction between ODA16 and IFT46 was confirmed by pull-down assays in vitro (Ahmed et al. 2008). So IFT46 is required for transport of outer dynein arms into the flagella. The *ift56* null mutant cells have almost full length flagella and normal IFT movements but display motility defects. Biochemical and proteomic analyses indicated that a group of IDAs and IDA regulatory proteins were reduced in *ift56* flagella, which might bind to IFT56 via IDA chaperone (Ishikawa et al. 2014).

Two forms of radial spoke complex 12S and 20S exist in flagella and cell body (Qin et al. 2004). In regenerating flagella, only 12S complex is increased in the matrix fraction, which suggested that the 12S is preassembled in cell body and transported to the flagella tip as anterograde cargo. Incubation of *fla10-1* mutant at restrictive temperature only induces the reduction of 12S complex, indicating that 12S complex is transported by IFT.

Tubulin, the most abundant component of flagella, was demonstrated as an IFT cargo. Two-color imaging combined with photobleaching showed that GFP-labeled α-tubulin is primarily transported by IFT (Craft et al. 2015). Pull-down and microtubule sedimentation assays revealed that tubulin binds to the module formed by the N-terminal calponin homology (CH) domain of IFT81 and the highly basic N-terminal domain of IFT74 (Bhogaraju et al. 2013). The null mutant of *ift74-2* rescued with a truncated IFT74 lacking the 130 N-terminal residues could generate 80% full-length flagella, but displayed severely reduction in the initial rate of flagellar regeneration (Brown et al. 2015). A similar phenotype was observed in IFT81 CH domain mutants (Kubo et al. 2016). A double mutant of IFT81N and IFT74N could only generate very short flagella, which indicated that combination of IFT81N and IFT74N functions as the main but not only module for IFT of tubulin (Kubo et al. 2016). Recent study showed that the CH domain of IFT54 within the IFT-B2 complex could serve as the second tubulin binding site (Taschner et al. 2016).

Several ciliary proteins are dispensable for cilia assembly but required for phototaxis and motility, such as BBSome proteins and nexin-dynein regulatory complex (N-DRC). Two-color imaging demonstrated that the BBSome subunit BBS4 and the component of N-DRC DRC4 might be cargoes of IFT. However, these cargoes are not always associated with IFT. Instead, they could unload from IFT and diffuse for a while (Lechtreck et al. 2009a; Wren et al. 2013). Considering hundreds of proteins were required for flagella assembly, there are still many IFT cargoes to be identified.

6.2 Function of IFT in Flagella Disassembly

Flagella are dynamic structures. At steady state, the axonemal blocks undergo continuous turnover at the distal tip (Marshall and Rosenbaum 2001). In response to osmotic stress, during zygote formation or incubation of low concentration of sodium pyrophosphate (NaPPi), flagella gradually resorb to null (also called shortening or disassembly), accompanied with breakdown products increasing (Pan et al. 2004; Pan and Snell 2005).

Several evidences indicated that removing of the turnover and breakdown products is dependent on IFT. The 20S radial spoke complexes, existed in both cell body and flagella as mentioned in Sect. 6.1, are not detectable in the cell body of non-flagella mutant, such as *bld1*, *bld2*, and *ift88*. Unexpectedly, it is also absent in the cell body of retrograde motor mutant *dhc1b* and *fla14* but present in the short flagella of *fla14*. The distribution difference of 20S complexes suggested that this

complex is a turnover product released from axoneme, since it is generated in flagella only. Furthermore, retrograde IFT is required to transport the 20S radial spoke complexes out of flagella (Qin et al. 2004).

In another study, by comparing the amount of 12S and 20S radial spoke complexes in flagella of wild type and shortening flagella induced, NaPPi. Pan et al. showed that much more 20S complexes were generated as breakdown products during flagella resorption, but the anterograde cargo 12S complex remained the same. The amount of IFT components including IFT and motor were all unexpectedly increased. Since no accumulation of IFT rafts were observed, it was suggested that IFT particles were entering the shortening flagella without cargo and carried the increasing breakdown products back to cell body (Pan and Snell 2005).

During flagellar resorption, various posttranslational modifications, such as deacetylation, phosphorylation, and methylation, are detected in flagella (L'Hernault and Rosenbaum 1983, 1985; Pan et al. 2004; Sloboda and Howard 2009). Huang et al. revealed that ubiquitin conjugation system functions in flagella and ubiquitinated proteins, such as α-tubulin and PKD2, increase in flagella during flagellar resorption. Since no proteasome machinery seems present in the flagella, the ubiquitinated flagellar proteins need to degrade or reuse in cell body. Indeed, the amount of ubiquitinated proteins in flagella of retrograde IFT mutants, such as *fla16*, *d1blic*, and *dhc1b-2*, were more than tenfold of that in shortening flagella of wild type with functional IFT. These data suggested that removing of the ubiquitinated proteins also depend on retrograde IFT (Huang et al. 2009).

Proteomics analysis of temperature-sensitive mutant *dhc1b-3* flagella revealed that various axonemal cargoes were significantly accumulated in flagella at restrictive temperature, while almost no retrograde transport was detected. This study further confirmed that IFT plays a role in removing cargo out of flagella (Engel et al. 2012). Nevertheless, since flagella could still resorb to null without IFT in temperature-sensitive mutants *fla10-1*, other mechanism such as ectosome released from flagella membrane may also involve in removing turnover cargoes (Long et al. 2016).

6.3 Function of IFT in Signal Transduction

Besides driving motility, flagella also function as sensory antenna (Ishikawa and Marshall 2011; Pan et al. 2005). The mating process of Chlamydomonas serves as a great model to study the role of IFT in signal transduction (Wang and Snell 2003). Agglutinins, SAG1 and SAD1, were distributed on the flagellar surface of mating-type plus and *minus* gametes, respectively (Ferris et al. 2005). Interactions between SAG1 and SAD1 induce the adhesion of flagella between plus and minus gametes (Pan and Snell 2000; Wang and Snell 2003). The C-terminal of SAG1 (SAG1-C65) is normally distributed on plasma membrane surface but redistributed to the base of flagella and subsequently into the flagella, when plus and minus gametes are mixed. However, this signaling-induced trafficking was blocked in response to cytoplasmic

dynein inhibitor ciliobrevin D or in the temperature-sensitive mutant *fla24* (mutant of *DHC1b*), which suggested that retrograde IFT motor is required for SAG1-C65 redistribution (Cao et al. 2015).

The agglutinin-induced adhesion event will activate a serial of signal transduction cascades. One of the responses is the activation of a protein tyrosine kinase (PTK), which subsequently phosphorylates a cGMP-dependent protein kinase (PKG). However, when IFT was blocked in plus and minus *fla10-1* cells at restrictive temperature, flagella adhesion failed to activate the PTK, and flagellar PKG level was also reduced, which indicated that IFT is essential to adhesion-induced signaling pathway (Wang et al. 2006; Wang and Snell 2003).

Mating signaling also involves PKD2, which functions in flagella to convert flagellar adhesion of gametes into a calcium influx. Photobleaching indicated that a fraction (<10%) of PKD2-GFP moved similar to IFT in wild type but ceased after IFT termination, and the recovery of PKD2-GFP in flagella was also attenuated after IFT termination. So at least partial of PKD2 movement is dependent on IFT (Huang et al. 2007). Other signaling proteins in association with IFT include phospholipase D (PLD), but PLD only require IFT to exit from flagella (Lechtreck et al. 2013).

6.4 IFT and Other Flagella Motility

The direct relationship between the IFT and flagellar beating has not been investigated in detail, but indirect effect may occur since the IFT is important for transport the precursors of inner dynein, outer dynein complex to flagella. Kozminski compared the bead movement, gilding with IFT in different strains, during the assembly and disassembly and different stress conditions. The bead movement and gilding are stopped in gilding mutant *gf1* and during flagellar resorption and EGTA treatment, but IFT works normally. When cells were treated with 100 mM NaCI and 6% sucrose, all the three movements stop (Kozminski et al. 1993). Following this work, Shih et al. show that flagellar major glycoproteins co-localize with IFT trains, which are transported by at least four motors (only one was activated at a time), the retrograde IFT motor dynein-1b provided the force for the gilding, so the IFT plays a critical role in flagella gilding (Shih et al. 2013).

7 The Regulation of IFT

The velocity and frequency of IFT movement along the axoneme are constant with the exception of very short flagella under the DIC (Dentler 2005), but the entry of IFT to the flagella and the remodel of IFT at the tip are highly regulated, and posttranslational modification may play an important role. Liang et al. demonstrated that phosphorylated one of kinesin-2 motor subunit FLA8 by a calcium-dependent kinase

resulted in inactivation of kinesin-2, and abolished the interaction with the IFT-B complex, subsequently inhibited the entry of IFT into the cilia at basal body. Moreover, phosphorylated FLA8 is required for IFT-B uploading from the kinesin-2 at the tip of flagella (Liang et al. 2014). Taking into account that IFT46 and IFT25 are phosphorylated proteins, the phosphorylation and calcium are important in the regulation of IFT.

During the flagellar regeneration, more tubulin needs to be transported into the flagella, but the velocity and frequency of anterograde IFT did not increased, so each IFT particle carries more tubulin cargoes (Craft et al. 2015), and this data suggested that extent of occupancy of IFT trains by tubulin cargoes are highly regulated in cells. This data is consistent with previous observation that an anterograde IFT train in short flagella carries more kinesin-associated protein and IFT27 protein than trains in long flagella (Engel et al. 2009).

Flagellar tip normally only has single doublet and elongated in flagella of gametes. Pedersen first showed that microtubule (MT) plus end-tracking protein EB1 localizes at the tip of flagella. In the temperature-sensitive mutant of *fla11*(IFT172), the tip localization of CrEB1 disappeared, and other IFT proteins such as IFT140 are accumulated near the flagellar tip, and these data suggested that IFT172 may work together with CrEB1 at the flagellar tip in IFT remodeling (Pedersen et al. 2003, 2005). Recent in vivo imaging indicated that fluorescent protein-tagged CrEB1 moves along the flagella only by diffusion and may accumulate at the tip by capture (Harris et al. 2016). Recently, another tip protein FAP256 (CEP104) was identified by comparing the quantity of flagellar proteins in half-length flagella versus full length flagella. In Chlamydomonas, FAP256 localized at the tip during the assembly and disassembly, but in mammalian cells, the CEP104 localizes on the distal ends of both centrioles of non-dividing cells and moved to the tip of the elongating cilium. Knockout of FAP256 in Chlamydomonas and knockdown of CEP104 in retinal pigment epithelial cells attenuated the formation of cilia; these data suggested that tip proteins may play an important role in regulating the remodeling of IFT at the tip (Satish Tammana et al. 2013).

8 Conclusion Remarks and Future Perspectives

During the last 20 years, tremendous progress has been made in characterization of each subunit of IFT complex; analyzing the movement of IFT proteins in flagella; dissecting the function of the IFT in flagellar assembly, flagellar disassembly, and flagellar signal transduction; and studying the structure of the IFT complex using EM and crystallography. These achievements obtained from Chlamydomonas as a model have become the basis and resource for cilia research in other model organisms such as *C. elegans* (Ou et al. 2005; Orozco et al. 1999), zebrafish (Li and Sun 2011; Malicki et al. 2011), fly (Vieillard et al. 2015; Sanchez et al. 2016), and mammals (Badano et al. 2006). On the other hand, the work in other systems complements and motivates the flagella research in Chlamydomonas. For example, IFT-B protein such as IFT38/

Qilin was first identified in zebrafish (Sun et al. 2004) and IFT70/DYF-1 was first characterized in *C. elegans* (Ou et al. 2005). Especially, mutation of IFT88 and IFT27 induce human diseases highlights the importance of studying the IFT in human health (Pazour et al. 2000; Eguether et al. 2014). However, several important questions need to be addressed in the future: First is the interaction mechanism between the IFT and cargoes. We now know that the tubulin may be transported by IFT81/74 (Bhogaraju et al. 2013) and IFT54 (Taschner et al. 2016), respectively, and outer dynein arm complex are transported by the IFT46 (Hou et al. 2007). It looks like one IFT protein or a protein complex needs to transport more cargoes because there are more than 600 proteins in flagella (Pazour et al. 2005). Analyzing the interaction map between these proteins and IFT proteins needs tools such as quantitative proteomics and fluorescence resonance energy transfer (FRET). Second is understanding the relationship between IFT and the flagellar membrane trafficking. Several evidences pinpointed the importance of the IFT in the dynamics of flagellar membrane: IFT particles are firmly associated with the flagellar membrane under EM (Pigino et al. 2009; Vannuccini et al. 2016); isolated flagellar membrane and cytoplasmic vesicles during the flagellar regeneration all contain a bunch of IFT proteins (Long et al. 2016). But how the IFT is associated with flagella membrane is unknown since there is no motif in IFT proteins that can bind the membrane. Third is understanding the complexity of the structure of IFT in vivo. We have a good overview of how each individual IFT protein form IFT-A complex and IFT-B complex and the crystal structure of IFT-B complex (Taschner and Lorentzen 2016), but we still miss the crystal structure of IFT-A complex, super-complex of IFT-B-anterograde motor, and super-complex of IFT-A-retrograde motor, and we still do not know how these complexes assemble to short trains and long trains identified at EM. In addition, most data of the protein interaction are obtained from in vitro experiment and need to be confirmed in vivo. Fourth is how the functions of the IFT are regulated, for example, how the IFT loads cargoes and gets association with anterograde motor at the basal body and how cargoes are uploaded and the retrograde motor are activated at the flagellar tip. A recent study demonstrated that posttranslational modifications may play a critical role: FLA8 was phosphorylated by a calcium kinase and inactivated at the tip (Liang et al. 2014), but we still do not know how the kinase became active at the tip. It looks like the flagella or cilia are not uniform as we thought, and local signal such as calcium or GTP gradient may play a critical role. Fifth is reconstitution of IFT machinery in vitro. This is one of the best ways to understanding the working mechanism and regulation of IFT. For this purpose, Chlamydomonas will be an excellent system since the IFT complexes and motor complexes can be isolated using pure flagella. IFT machinery is simple because there is only one anterograde motor compared two anterograde motors in *C. elegans*. Now, it is the right time to undertake such a work since a lot of knowledge of IFT core complex and motor has been accumulated. To answer the above questions, we need to combine the methods of biochemical, genetics, cell biology, and proteomics, and especially take advantage of the knowledge obtained from other cilia research models.

Acknowledgments This project was supported by the National Natural Science Foundation of China (31371354 to Dr. Kaiyao Huang and 31400654 to Dr. Gai Liu).

References

Ahmed NT, Gao C, Lucker BF, Cole DG, Mitchell DR (2008) ODA16 aids axonemal outer row dynein assembly through an interaction with the intraflagellar transport machinery. J Cell Biol 183(2):313–322. doi:10.1083/jcb.200802025

Allen RD, Allen NS, Travis JL (1981) Video-enhanced contrast, differential interference contrast (AVEC-DIC) microscopy: a new method capable of analyzing microtubule-related motility in the reticulopodial network of *Allogromia laticollaris*. Cell Motil 1(3):291–302

Badano JL, Mitsuma N, Beales PL, Katsanis N (2006) The ciliopathies: an emerging class of human genetic disorders. Annu Rev Genomics Hum Genet 7:125–148. doi:10.1146/annurev.genom.7.080505.115610

Behal RH, Miller MS, Qin H, Lucker BF, Jones A, Cole DG (2012) Subunit interactions and organization of the *Chlamydomonas reinhardtii* intraflagellar transport complex a proteins. J Biol Chem 287(15):11689–11703. doi:10.1074/jbc.M111.287102

Bhogaraju S, Taschner M, Morawetz M, Basquin C, Lorentzen E (2011) Crystal structure of the intraflagellar transport complex 25/27. EMBO J 30(10):1907–1918. doi:10.1038/emboj.2011.110

Bhogaraju S, Cajanek L, Fort C, Blisnick T, Weber K, Taschner M, Mizuno N, Lamla S, Bastin P, Nigg EA, Lorentzen E (2013) Molecular basis of tubulin transport within the cilium by IFT74 and IFT81. Science 341(6149):1009–1012. doi:10.1126/science.1240985

Bloodgood RA (1992) Directed movements of ciliary and flagellar membrane components: a review. Biol Cell 76(3):291–301

Brown JM, Cochran DA, Craige B, Kubo T, Witman GB (2015) Assembly of IFT trains at the ciliary base depends on IFT74. Curr Biol 25(12):1583–1593. doi:10.1016/j.cub.2015.04.060

Cao M, Ning J, Hernandez-Lara CI, Belzile O, Wang Q, Dutcher SK, Liu Y, Snell WJ (2015) Uni-directional ciliary membrane protein trafficking by a cytoplasmic retrograde IFT motor and ciliary ectosome shedding. Elife 4. doi:10.7554/eLife.05242

Cole DG, Diener DR, Himelblau AL, Beech PL, Fuster JC, Rosenbaum JL (1998) Chlamydomonas kinesin-II-dependent intraflagellar transport (IFT): IFT particles contain proteins required for ciliary assembly in *Caenorhabditis elegans* sensory neurons. J Cell Biol 141(4):993–1008

Craft JM, Harris JA, Hyman S, Kner P, Lechtreck KF (2015) Tubulin transport by IFT is upregulated during ciliary growth by a cilium-autonomous mechanism. J Cell Biol 208 (2):223–237. doi:10.1083/jcb.201409036

Deane JA, Cole DG, Seeley ES, Diener DR, Rosenbaum JL (2001) Localization of intraflagellar transport protein IFT52 identifies basal body transitional fibers as the docking site for IFT particles. Curr Biol 11(20):1586–1590

Dentler W (2005) Intraflagellar transport (IFT) during assembly and disassembly of *Chlamydomonas* flagella. J Cell Biol 170(4):649–659. doi:10.1083/jcb.200412021

Dutcher SK, Li L, Lin H, Meyer L, Giddings TH Jr, Kwan AL, Lewis BL (2012) Whole-genome sequencing to identify mutants and polymorphisms in *Chlamydomonas reinhardtii*. G3 (Bethesda) 2(1):15–22. doi:10.1534/g3.111.000919

Eguether T, San Agustin JT, Keady BT, Jonassen JA, Liang Y, Francis R, Tobita K, Johnson CA, Abdelhamed ZA, Lo CW, Pazour GJ (2014) IFT27 links the BBSome to IFT for maintenance of the ciliary signaling compartment. Dev Cell 31(3):279–290. doi:10.1016/j.devcel.2014.09.011

Engel BD, Ludington WB, Marshall WF (2009) Intraflagellar transport particle size scales inversely with flagellar length: revisiting the balance-point length control model. J Cell Biol 187(1):81–89. doi:10.1083/jcb.200812084

Engel BD, Ishikawa H, Wemmer KA, Geimer S, K-i W, Hirono M, Craige B, Pazour GJ, Witman GB, Kamiya R, Marshall WF (2012) The role of retrograde intraflagellar transport in flagellar assembly, maintenance, and function. J Cell Biol 199(1):151–167. doi:10.1083/jcb.201206068

Fan ZC, Behal RH, Geimer S, Wang Z, Williamson SM, Zhang H, Cole DG, Qin H (2010) *Chlamydomonas* IFT70/CrDYF-1 is a core component of IFT particle complex B and is required for flagellar assembly. Mol Biol Cell 21(15):2696–2706

Ferris PJ, Waffenschmidt S, Umen JG, Lin H, Lee JH, Ishida K, Kubo T, Lau J, Goodenough UW (2005) Plus and minus sexual agglutinins from *Chlamydomonas reinhardtii*. Plant Cell 17 (2):597–615. doi:10.1105/tpc.104.028035

Harris JA, Liu Y, Yang P, Kner P, Lechtreck KF (2016) Single-particle imaging reveals intraflagellar transport-independent transport and accumulation of EB1 in *Chlamydomonas* flagella. Mol Biol Cell 27(2):295–307. doi:10.1091/mbc.E15-08-0608

Hou Y, Pazour GJ, Witman GB (2004) A dynein light intermediate chain, D1bLIC, is required for retrograde intraflagellar transport. Mol Biol Cell 15(10):4382–4394. doi:10.1091/mbc.E04-05-0377

Hou Y, Qin H, Follit JA, Pazour GJ, Rosenbaum JL, Witman GB (2007) Functional analysis of an individual IFT protein: IFT46 is required for transport of outer dynein arms into flagella. J Cell Biol 176(5):653–665

Huang B, Rifkin MR, Luck DJ (1977) Temperature-sensitive mutations affecting flagellar assembly and function in *Chlamydomonas reinhardtii*. J Cell Biol 72(1):67–85

Huang K, Diener DR, Mitchell A, Pazour GJ, Witman GB, Rosenbaum JL (2007) Function and dynamics of PKD2 in *Chlamydomonas reinhardtii* flagella. J Cell Biol 179(3):501–514. doi:10.1083/jcb.200704069

Huang K, Diener DR, Rosenbaum JL (2009) The ubiquitin conjugation system is involved in the disassembly of cilia and flagella. J Cell Biol 186(4):601–613. doi:10.1083/jcb.200903066

Iomini C, Babaev-Khaimov V, Sassaroli M, Piperno G (2001) Protein particles in Chlamydomonas flagella undergo a transport cycle consisting of four phases. J Cell Biol 153(1):13–24

Iomini C, Li L, Esparza JM, Dutcher SK (2009) Retrograde intraflagellar transport mutants identify complex A proteins with multiple genetic interactions in *Chlamydomonas reinhardtii*. Genetics 183(3):885–896. doi:10.1534/genetics.109.101915

Ishikawa H, Marshall WF (2011) Ciliogenesis: building the cell's antenna. Nat Rev Mol Cell Biol 12(4):222–234. doi:10.1038/nrm3085

Ishikawa H, Ide T, Yagi T, Jiang X, Hirono M, Sasaki H, Yanagisawa H, Wemmer KA, Stainier DYR, Qin H, Kamiya R, Marshall WF (2014) TTC26/DYF13 is an intraflagellar transport protein required for transport of motility-related proteins into flagella. Elife 3. doi:10.7554/eLife.01566

Katoh Y, Terada M, Nishijima Y, Takei R, Nozaki S, Hamada H, Nakayama K (2016) Overall architecture of the intraflagellar transport (IFT)-B complex containing Cluap1/IFT38 as an essential component of the IFT-B peripheral subcomplex. J Biol Chem 291(21):10962–10975. doi:10.1074/jbc.M116.713883

Kozminski KG, Johnson KA, Forscher P, Rosenbaum JL (1993) A motility in the eukaryotic flagellum unrelated to flagellar beating. Proc Natl Acad Sci U S A 90(12):5519–5523

Kozminski KG, Beech PL, Rosenbaum JL (1995) The *Chlamydomonas* kinesin-like protein FLA10 is involved in motility associated with the flagellar membrane. J Cell Biol 131(6 Pt 1):1517–1527

Kubo T, Brown JM, Bellve K, Craige B, Craft JM, Fogarty K, Lechtreck KF, Witman GB (2016) Together, the IFT81 and IFT74 N-termini form the main module for intraflagellar transport of tubulin. J Cell Sci 129(10):2106–2119. doi:10.1242/jcs.187120

Lechtreck KF (2016) Methods for studying movement of molecules within cilia. In: Satir P, Christensen ST (eds) Cilia: methods and protocols. Springer, New York, pp 83–96. doi:10.1007/978-1-4939-3789-9_6

Lechtreck K-F, Johnson EC, Sakai T, Cochran D, Ballif BA, Rush J, Pazour GJ, Ikebe M, Witman GB (2009a) The *Chlamydomonas reinhardtii* BBSome is an IFT cargo required for export of specific signaling proteins from flagella. J Cell Biol 187(7):1117–1132. doi:10.1083/jcb.200909183

Lechtreck KF, Luro S, Awata J, Witman GB (2009b) HA-tagging of putative flagellar proteins in *Chlamydomonas* reinhardtii identifies a novel protein of intraflagellar transport complex B. Cell Motil Cytoskeleton 66(8):469–482. doi:10.1002/cm.20369

Lechtreck KF, Brown JM, Sampaio JL, Craft JM, Shevchenko A, Evans JE, Witman GB (2013) Cycling of the signaling protein phospholipase D through cilia requires the BBSome only for the export phase. J Cell Biol 201(2):249–261. doi:10.1083/jcb.201207139

L'Hernault SW, Rosenbaum JL (1983) *Chlamydomonas* alpha-tubulin is posttranslationally modified in the flagella during flagellar assembly. J Cell Biol 97(1):258–263

L'Hernault SW, Rosenbaum JL (1985) *Chlamydomonas* alpha-tubulin is posttranslationally modified by acetylation on the epsilon-amino group of a lysine. Biochemistry 24(2):473–478

Li J, Sun Z (2011) Qilin is essential for cilia assembly and normal kidney development in zebrafish. PLoS One 6(11):e27365

Liang Y, Pang Y, Wu Q, Hu Z, Han X, Xu Y, Deng H, Pan J (2014) FLA8/KIF3B phosphorylation regulates kinesin-II interaction with IFT-B to control IFT entry and turnaround. Dev Cell 30 (5):585–597. doi:10.1016/j.devcel.2014.07.019

Lin H, Nauman NP, Albee AJ, Hsu S, Dutcher SK (2013) New mutations in flagellar motors identified by whole genome sequencing in *Chlamydomonas*. Cilia 2(1):14. doi:10.1186/2046-2530-2-14

Long H, Zhang F, Xu N, Liu G, Diener DR, Rosenbaum JL, Huang K (2016) Comparative analysis of ciliary membranes and ectosomes. Curr Biol 26:3327–3335

Lucker BF, Behal RH, Qin H, Siron LC, Taggart WD, Rosenbaum JL, Cole DG (2005) Characterization of the intraflagellar transport complex B core: direct interaction of the IFT81 and IFT74/72 subunits. J Biol Chem 280(30):27688–27696

Lucker BF, Miller MS, Dziedzic SA, Blackmarr PT, Cole DG (2010) Direct interactions of intraflagellar transport complex B proteins IFT88, IFT52, and IFT46. J Biol Chem 285 (28):21508–21518

Malicki J, Avanesov A, Li J, Yuan S, Sun Z (2011) Analysis of cilia structure and function in zebrafish. Methods Cell Biol 101:39–74. doi:10.1016/B978-0-12-387036-0.00003-7

Marshall WF, Rosenbaum JL (2001) Intraflagellar transport balances continuous turnover of outer doublet microtubules: implications for flagellar length control. J Cell Biol 155(3):405–414. doi:10.1083/jcb.200106141

Matsuura K, Lefebvre PA, Kamiya R, Hirono M (2002) Kinesin-II is not essential for mitosis and cell growth in Chlamydomonas. Cell Motil Cytoskeleton 52(4):195–201. doi:10.1002/cm.10051

Miller MS, Esparza JM, Lippa AM, Lux FG 3rd, Cole DG, Dutcher SK (2005) Mutant kinesin-2 motor subunits increase chromosome loss. Mol Biol Cell 16(8):3810–3820. doi:10.1091/mbc.E05-05-0404

Mueller J, Perrone CA, Bower R, Cole DG, Porter ME (2005) The FLA3 KAP subunit is required for localization of kinesin-2 to the site of flagellar assembly and processive anterograde intraflagellar transport. Mol Biol Cell 16(3):1341–1354. doi:10.1091/mbc.E04-10-0931

Orozco JT, Wedaman KP, Signor D, Brown H, Rose L, Scholey JM (1999) Movement of motor and cargo along cilia. Nature 398(6729):674

Ou G, Blacque OE, Snow JJ, Leroux MR, Scholey JM (2005) Functional coordination of intraflagellar transport motors. Nature 436(7050):583–587. doi:10.1038/nature03818

Pan JM, Snell WJ (2000) Regulated targeting of a protein kinase into an intact flagellum – an aurora/Ipl1p-like protein kinase translocates from the cell body into the flagella during gamete activation in *Chlamydomonas*. J Biol Chem 275(31):24106–24114. doi:10.1074/jbc.M002686200

Pan JM, Snell WJ (2005) *Chlamydomonas* shortens its flagella by activating axonemal disassembly, stimulating IFT particle trafficking, and blocking anterograde cargo loading. Dev Cell 9 (3):431–438. doi:10.1016/j.devcel.2005.07.010

Pan J, Wang Q, Snell WJ (2004) An aurora kinase is essential for flagellar disassembly in *Chlamydomonas*. Dev Cell 6(3):445–451

Pan JM, Wang Q, Snell WJ (2005) Cilium-generated signaling and cilia-related disorders. Lab Investig 85(4):452–463. doi:10.1038/labinvest.3700253

Patel-King RS, Gilberti RM, Hom EF, King SM (2013) WD60/FAP163 is a dynein intermediate chain required for retrograde intraflagellar transport in cilia. Mol Biol Cell 24(17):2668–2677. doi:10.1091/mbc.E13-05-0266

Pazour GJ, Wilkerson CG, Witman GB (1998) A dynein light chain is essential for the retrograde particle movement of intraflagellar transport (IFT). J Cell Biol 141(4):979–992

Pazour GJ, Dickert BL, Witman GB (1999) The DHC1b (DHC2) isoform of cytoplasmic dynein is required for flagellar assembly. J Cell Biol 144(3):473–481

Pazour GJ, Dickert BL, Vucica Y, Seeley ES, Rosenbaum JL, Witman GB, Cole DG (2000) *Chlamydomonas* IFT88 and its mouse homologue, polycystic kidney disease gene tg737, are required for assembly of cilia and flagella. J Cell Biol 151(3):709–718

Pazour GJ, Agrin N, Leszyk J, Witman GB (2005) Proteomic analysis of a eukaryotic cilium. J Cell Biol 170(1):103–113

Pedersen LB, Geimer S, Sloboda RD, Rosenbaum JL (2003) The microtubule plus end-tracking protein EB1 is localized to the flagellar tip and basal bodies in *Chlamydomonas reinhardtii*. Curr Biol 13(22):1969–1974

Pedersen LB, Miller MS, Geimer S, Leitch JM, Rosenbaum JL, Cole DG (2005) *Chlamydomonas* IFT172 is encoded by FLA11, interacts with CrEB1, and regulates IFT at the flagellar tip. Curr Biol 15(3):262–266. doi:10.1016/j.cub.2005.01.037

Pedersen LB, Gelmer S, Rosenbaum JL (2006) Dissecting the molecular mechanisms of intraflagellar transport in *Chlamydomonas*. Curr Biol 16(5):450–459. doi:10.1016/j.cub.2006.02.020

Perrone CA, Tritschler D, Taulman P, Bower R, Yoder BK, Porter ME (2003) A novel dynein light intermediate chain colocalizes with the retrograde motor for intraflagellar transport at sites of axoneme assembly in *chlamydomonas* and mammalian cells. Mol Biol Cell 14(5):2041–2056. doi:10.1091/mbc.E02-10-0682

Pigino G, Geimer S, Lanzavecchia S, Paccagnini E, Cantele F, Diener DR, Rosenbaum JL, Lupetti P (2009) Electron-tomographic analysis of intraflagellar transport particle trains in situ. J Cell Biol 187(1):135–148

Piperno G, Luck DJ (1979) Axonemal adenosine triphosphatases from flagella of *Chlamydomonas reinhardtii*. Purification of two dyneins. J Biol Chem 254(8):3084–3090

Piperno G, Mead K (1997) Transport of a novel complex in the cytoplasmic matrix of *Chlamydomonas* flagella. Proc Natl Acad Sci U S A 94(9):4457–4462. doi:10.1073/pnas.94.9.4457

Piperno G, Mead K, Henderson S (1996) Inner dynein arms but not outer dynein arms require the activity of kinesin homologue protein KHp1(FLA10) to reach the distal part of flagella in *Chlamydomonas*. J Cell Biol 133(2):371–379. doi:10.1083/jcb.133.2.371

Piperno G, Siuda E, Henderson S, Segil M, Vaananen H, Sassaroli M (1998) Distinct mutants of retrograde intraflagellar transport (IFT) share similar morphological and molecular defects. J Cell Biol 143(6):1591–1601. doi:10.1083/jcb.143.6.1591

Porter ME, Bower R, Knott JA, Byrd P, Dentler W (1999) Cytoplasmic dynein heavy chain 1b is required for flagellar assembly in *Chlamydomonas*. Mol Biol Cell 10(3):693–712

Qin HM, Diener DR, Geimer S, Cole DG, Rosenbaum JL (2004) Intraflagellar transport (IFT) cargo: IFT transports flagellar precursors to the tip and turnover products to the cell body. J Cell Biol 164 (2):255–266. doi:10.1083/jcb.200308132

Qin H, Wang Z, Diener D, Rosenbaum J (2007) Intraflagellar transport protein 27 is a small G protein involved in cell-cycle control. Curr Biol 17(3):193–202. doi:10.1016/j.cub.2006.12.040

Reck J, Schauer AM, VanderWaal Mills K, Bower R, Tritschler D, Perrone CA, Porter ME (2016) The role of the dynein light intermediate chain in retrograde IFT and flagellar function in *Chlamydomonas*. Mol Biol Cell. doi:10.1091/mbc.E16-03-0191

Richey EA, Qin H (2012) Dissecting the sequential assembly and localization of intraflagellar transport particle complex B in *Chlamydomonas*. PLoS One 7(8):e43118

Ringo DL (1967) Flagellar motion and fine structure of the flagellar apparatus in *Chlamydomonas*. J Cell Biol 33(3):543–571

Rompolas P, Pedersen LB, Patel-King RS, King SM (2007) *Chlamydomonas* FAP133 is a dynein intermediate chain associated with the retrograde intraflagellar transport motor. J Cell Sci 120 (Pt 20):3653–3665. doi:10.1242/jcs.012773

Sanchez GM, Alkhori L, Hatano E, Schultz SW, Kuzhandaivel A, Jafari S, Granseth B, Alenius M (2016) Hedgehog signaling regulates the ciliary transport of odorant receptors in drosophila. Cell Rep 14(3):464–470. doi:10.1016/j.celrep.2015.12.059

Satish Tammana TV, Tammana D, Diener DR, Rosenbaum J (2013) Centrosomal protein CEP104 (*Chlamydomonas* FAP256) moves to the ciliary tip during ciliary assembly. J Cell Sci 126 (Pt 21):5018–5029. doi:10.1242/jcs.133439

Schmidts M, Hou Y, Cortes CR, Mans DA, Huber C, Boldt K, Patel M, van Reeuwijk J, Plaza JM, van Beersum SE, Yap ZM, Letteboer SJ, Taylor SP, Herridge W, Johnson CA, Scambler PJ, Ueffing M, Kayserili H, Krakow D, King SM, Beales PL, Al-Gazali L, Wicking C, Cormier-Daire V, Roepman R, Mitchison HM, Witman GB (2015) TCTEX1D2 mutations underlie Jeune asphyxiating thoracic dystrophy with impaired retrograde intraflagellar transport. Nat Commun 6:7074. doi:10.1038/ncomms8074

Shih SM, Engel BD, Kocabas F, Bilyard T, Gennerich A, Marshall WF, Yildiz A (2013) Intraflagellar transport drives flagellar surface motility. Elife 2:e00744. doi:10.7554/eLife.00744

Silva DA, Huang X, Behal RH, Cole DG, Qin H (2012) The RABL5 homolog IFT22 regulates the cellular pool size and the amount of IFT particles partitioned to the flagellar compartment in *Chlamydomonas reinhardtii*. Cytoskeleton 69(1):33–48. doi:10.1002/cm.20546

Sloboda RD, Howard L (2009) Protein methylation in full length *Chlamydomonas* flagella. Cell Motil Cytoskeleton 66(8):650–660. doi:10.1002/cm.20387

Stepanek L, Pigino G (2016) Microtubule doublets are double-track railways for intraflagellar transport trains. Science 352(6286):721–724. doi:10.1126/science.aaf4594

Sun Z, Amsterdam A, Pazour GJ, Cole DG, Miller MS, Hopkins N (2004) A genetic screen in zebrafish identifies cilia genes as a principal cause of cystic kidney. Development 131 (16):4085–4093. doi:10.1242/dev.01240

Swiderski RE, Nakano Y, Mullins RF, Seo S, Banfi B (2014) A mutation in the mouse ttc26 gene leads to impaired hedgehog signaling. PLoS Genet 10(10):e1004689. doi:10.1371/journal.pgen.1004689

Taschner M, Lorentzen E (2016) The intraflagellar transport machinery. Cold Spring Harb Perspect Biol 8(10). doi:10.1101/cshperspect.a028092

Taschner M, Bhogaraju S, Vetter M, Morawetz M, Lorentzen E (2011) Biochemical mapping of interactions within the intraflagellar transport (IFT) B core complex: IFT52 binds directly to four other IFT-B subunits. J Biol Chem 286(30):26344–26352

Taschner M, Kotsis F, Braeuer P, Kuehn EW, Lorentzen E (2014) Crystal structures of IFT70/52 and IFT52/46 provide insight into intraflagellar transport B core complex assembly. J Cell Biol 207(2):269–282. doi:10.1083/jcb.201408002

Taschner M, Weber K, Mourao A, Vetter M, Awasthi M, Stiegler M, Bhogaraju S, Lorentzen E (2016) Intraflagellar transport proteins 172, 80, 57, 54, 38, and 20 form a stable tubulin-binding IFT-B2 complex. EMBO J 35(7):773–790. doi:10.15252/embj.201593164

Toriyama M, Lee C, Taylor SP, Duran I, Cohn DH, Bruel AL, Tabler JM, Drew K, Kelly MR, Kim S, Park TJ, Braun DA, Pierquin G, Biver A, Wagner K, Malfroot A, Panigrahi I, Franco B, Al-Lami HA, Yeung Y, Choi YJ, Duffourd Y, Faivre L, Riviere JB, Chen J, Liu KJ, Marcotte EM, Hildebrandt F, Thauvin-Robinet C, Krakow D, Jackson PK, Wallingford JB (2016) The ciliopathy-associated CPLANE proteins direct basal body recruitment of intraflagellar transport machinery. Nat Genet 48(6):648–656. doi:10.1038/ng.3558

Vannuccini E, Paccagnini E, Cantele F, Gentile M, Dini D, Fino F, Diener D, Mencarelli C, Lupetti P (2016) Two classes of short intraflagellar transport train with different 3D structures are present in *Chlamydomonas* flagella. J Cell Sci 129(10):2064–2074. doi:10.1242/jcs.183244

Vashishtha M, Walther Z, Hall JL (1996) The kinesin-homologous protein encoded by the *Chlamydomonas* FLA10 gene is associated with basal bodies and centrioles. J Cell Sci 109:541–549

Vieillard J, Duteyrat JL, Cortier E, Durand B (2015) Imaging cilia in *Drosophila melanogaster*. Methods Cell Biol 127:279–302. doi:10.1016/bs.mcb.2014.12.009

Wang Q, Snell WJ (2003) Flagellar adhesion between mating type plus and mating type minus gametes activates a flagellar protein-tyrosine kinase during fertilization in *Chlamydomonas*. J Biol Chem 278(35):32936–32942. doi:10.1074/jbc.M303261200

Wang Q, Pan J, Snell WJ (2006) Intraflagellar transport particles participate directly in cilium-generated signaling in *Chlamydomonas*. Cell 125(3):549–562. doi:10.1016/j.cell.2006.02.044

Wang Z, Fan ZC, Williamson SM, Qin H (2009) Intraflagellar transport (IFT) protein IFT25 is a phosphoprotein component of IFT complex B and physically interacts with IFT27 in *Chlamydomonas*. PLoS One 4(5):e5384. doi:10.1371/journal.pone.0005384

Wren KN, Craft JM, Tritschler D, Schauer A, Patel DK, Smith EF, Porter ME, Kner P, Lechtreck KF (2013) A differential cargo-loading model of ciliary length regulation by IFT. Curr Biol 23 (24):2463–2471. doi:10.1016/j.cub.2013.10.044

The Sexual Developmental Program of *Chlamydomonas reinhardtii*

Yoshiki Nishimura

Abstract Sexual reproduction in the green alga *Chlamydomonas reinhardtii* is regulated by environmental conditions and by cell-cell interactions. After gametogenesis, flagellar adhesion between gametes triggers a signal transduction cascade that leads to gamete activation, cell fusion, and zygote formation. During zygote development, photosynthesis is downregulated, and a thick cell wall is assembled to form a zygospore, which is the dormant stage to survive severe environmental conditions, such as nutrient depletion and desiccation. With environmental improvement, zygospores initiate the germination process, including meiosis, tetrad formation, and release of four vegetative cells. Sexual reproduction of *C. reinhardtii* is a microcosm of various biological processes including cellular responses to nitrogen depletion, complicated signal transductions mediated by cAMP, intercellular communication based on flagella, intra-flagellar transport, cell-cell adhesion, and inheritance of mitochondria/chloroplast DNA. Comprehensive understanding of sexual reproduction of *C. reinhardtii* could illuminate the molecular mechanisms and evolution of eukaryotic sex.

1 Gametogenesis/Sexual Differentiation

In sexually reproducing eukaryotes, fertilization involves a set of orchestrated cellular and molecular events. The initial events of fertilization involve adhesive interactions between gametes of opposite mating types, cell-cell fusion, and signal transduction (Goodenough et al. 2007; Harris 2009; Goodenough and Heitman 2014). *Chlamydomonas reinhardtii* has served as a model system to dissect the complex nature of sexual reproduction in eukaryotes. This unicellular alga consists of two mating types: plus (*mt*+) and minus (*mt*−). Morphologically, *mt*+ and *mt*− vegetative cells have almost no distinct differences. By gametic differentiation, *C. reinhardtii* vegetative cells are transformed into mating-competent and sexually differentiated cells—gametes. The sexual life cycle of *C. reinhardtii* includes four significant events:

Y. Nishimura (✉)
Laboratory of Plant Molecular Genetics, Department of Botany, Kyoto University, Oiwake-cho, Kita-Shirakawa, Sakyo-ku, Kyoto 606-8502, Japan
e-mail: yoshiki@pmg.bot.kyoto-u.ac.jp

M. Hippler (ed.), *Chlamydomonas: Biotechnology and Biomedicine*, Microbiology Monographs 31, DOI 10.1007/978-3-319-66360-9_6

(1) gametogenesis (sexual differentiation), (2) mating/zygote formation, (3) zygote maturation (zygospore formation), and (4) germination (meiosis/tetrad formation) (Fig. 1). Zygospores are a dormant stage, protected by a thick cell wall, and can survive adverse environmental conditions such as desiccation, cold temperatures, and nutrient deficiencies (Beck and Haring 1996; Harris 2009).

1.1 The Initiation of Gametogenesis

In most sexual microorganisms, gametogenesis is triggered by environmental stresses such as depletion of essential nutrients. Gametogenesis in *C. reinhardtii* is initiated by two environmental cues. One is the loss of a nitrogen source, and the other is irradiation with high light (Sager and Granick 1954; Treier et al. 1989).

Upon removal of nitrogen (N), vegetative cells undergo two distinct programs (Goodenough et al. 2007). First, the cells acclimate to N starvation through a variety of metabolic changes, including upregulation of proteins required for transport and reduction of nitrate (Fernandez and Galvan 2007; Sanz-Luque et al. 2015), extracellular nitrogen-scavenging enzymes (Vallon et al. 1993), reduction and compositional change of cytoplasmic and chloroplast ribosomes (Siersma and Chiang 1971; Martin 1976; Picard-Bennoun and Bennoun 1985), and a downregulation of photosynthetic apparatus through selective destabilization of the b_6/f complex (Bulte and Wollman 1992). Second, the cells express a gamete differentiation program, which includes the formation of sex-specific agglutinin proteins responsible for flagellar adhesion to find a mating partner (Adair et al. 1982; Goodenough 1993; Ferris et al. 2005), the activation of sex-specific mating structures responsible for cell-cell fusion between gametes (Detmers et al. 1983; Ferris et al. 1996), expression of mating type-specific homeodomain genes (Kurvari et al. 1998; Lee et al. 2008), the synthesis of gametic autolysin that facilitates the shedding of the cell wall (Jaenicke et al. 1987; Kinoshita et al. 1992), and preferential methylation of *mt+* cpDNA (Burton et al. 1979; Lopez et al. 2015a; Umen and Goodenough 2001; Feng and Chiang 1984; Bolen et al. 1982).

1.1.1 Nitrogen and Gametogenesis

Nitrogen (N) is a key nutrient that is required for the synthesis of the building blocks of proteins and nucleic acids. Its supply is limited in soil and in the ocean; therefore N-use efficiency is of compelling interest in agriculture and aquaculture. *Chlamydomonas reinhardtii* has been used as a model system to dissect the N starvation responses of plants and algae, which includes modulation of photosynthesis and activation of sexual reproduction (gametogenesis) (Fernandez and Galvan 2007; Sanz-Luque et al. 2015). Recently, green algae have also captured the attention of researchers owing to their potential in production of biofuels (triacylglycerol (TAG), H_2, or ethanol) (Wang et al. 2009; Merchant et al. 2012;

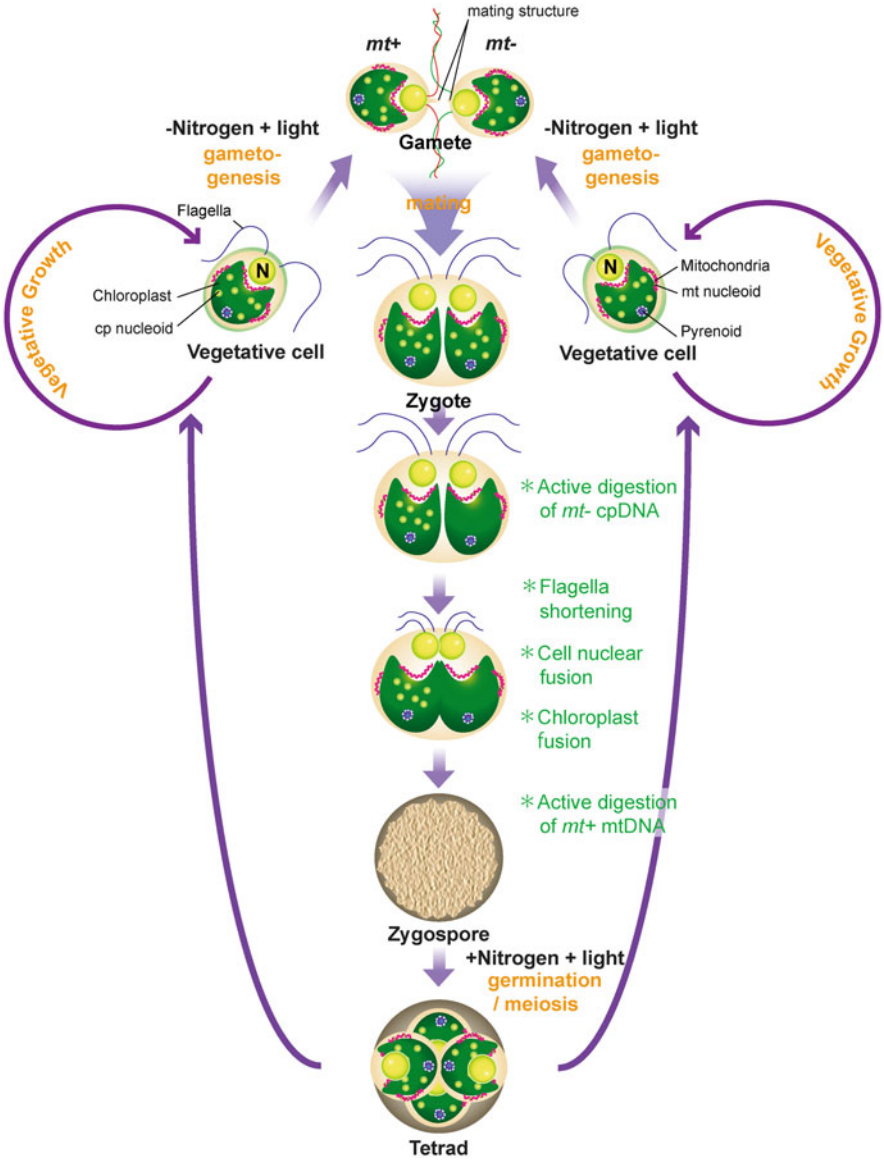

Fig. 1 The sexual life cycle of *Chlamydomonas reinhardtii*. Vegetative cells of two mating types (*mt*+ and *mt*−) divide mitotically. When exogenous nitrogen becomes limiting, they differentiate into gametes, expressing mating type-specific gametic traits including mating type-specific flagella modification (represented as *red* or *green* flagella) and formation of mating structures. When gametes are mixed, two gametes of opposite mating types form a pair and fuse to become binucleate quadriflagellated cells (QFC: zygotes). During zygote maturation, two cell nuclei (N) fuse, flagella lose stickiness and shorten, and two chloroplasts fuse. *Mt*− chloroplast (cp) nucleoids (DNA-protein complex) and *mt*+ mitochondrial nucleoids are degraded to achieve uniparental inheritance of cp and mtDNA exclusively from the *mt*+ and *mt*− parent, respectively. Finally, a thick cell wall is assembled around the zygotes to become zygospores, which is a dormant stage for *C. reinhardtii*. When zygospores are returned to light in nitrogen-containing

Schmollinger et al. 2014) and high-value chemicals in cosmeceuticals and functional foods, such as β-carotene, astaxanthin, docosahexaenoic acid, and phycobilin pigments (Borowitzka 2013). N depletion is indubitably one of the most critical triggers for TAG accumulation.

Chlamydomonas reinhardtii can utilize a number of different N sources, both inorganic (nitrate, nitrite, and ammonium) and organic (purines, urea, urate, and amino acids); among them ammonium is the preferred N source. Genome sequence analyses have found eight ammonium transporters of the AMT family, six of which are probably bound to the plasma membrane, and two are predicted to localize in the chloroplast envelope to facilitate assimilation of ammonium into Gln and Glu via the Gln synthetase (GS)/Glu oxoglutarate amidotransferase (GOGAT) cycle (Fernandez and Galvan 2007, 2008; Sanz-Luque et al. 2015).

When ammonium is depleted, genes responsible for the uptake of other nitrogen sources are upregulated. Nitrate and nitrite are taken up via transporters encoded by members of the *NRT1*, *NRT2*, and *NAR1* families. Nitrate is then reduced to the level of ammonium through the action of enzymes including cytoplasmic and chloroplastic nitrate reductases encoded by *NIA1/NIT1* and *NII1*, respectively (Quesada and Fernández 1994; Fernandez et al. 1998). Amino acids also serve as a nitrogen source, and Arg is directly transported into cells (Kirk and Kirk 1978). To incorporate His, enzymes such as histidase and urocanase that degrade His are upregulated (Hellio et al. 2004). Other amino acids are assimilated by the action of an L-amino acid oxidase that is drastically induced under N deficiency (Vallon et al. 1993).

RNA-seq, microarray, and classic differential display analyses revealed that N deficiency has further impact on gene expression in *C. reinhardtii* (Merchán et al. 2001; Abe et al. 2004, 2005; Boyle et al. 2012; Schmollinger et al. 2014). Respiratory metabolism is prioritized; photosynthesis-related proteins are repressed (Bulte and Wollman 1992); there is activation of a nitrogen-sparing mechanism including turnover of cytoplasmic and chloroplastic ribosomes (Siersma and Chiang 1971), reduction of proteins with a high N content (Schmollinger et al. 2014), and, finally, the activation of a gametogenesis program (Abe et al. 2004, 2005; Zones et al. 2015). Many of the genes involved in nitrate/nitrite uptake and assimilation are positively regulated by a transcription factor with an RWP/RK domain (*NIT2*), which is structurally related to the Nin (for nodule inception) proteins from plants (Schnell and Lefebvre 1993; Camargo et al. 2007). It is interesting that a key transcription factor for *mt−* gametogenesis (*MID* (minus dominance)) also possess the RWP/RK domain (Ferris and Goodenough 1997).

A specific molecular mechanism to measure the absolute abundance of intracellular N remains unclear. However, generally, N metabolism is tightly connected with carbon (C) metabolism (Zheng 2009; Nunes-Nesi et al. 2010). Therefore, N

Fig. 1 (continued) media, they undergo meiosis to release four haploid meiotic products that resume vegetative growth. Occasionally, zygotes forego the meiotic pathway and instead resume vegetative growth as vegetative diploids

level can be measured through the C/N ratio. A proteomic study showed that when *C. reinhardtii* cells were exposed to a high CO_2 (3%) condition (without reduction of nitrogen), a multiple number of gametogenesis-related proteins and hydroxyproline-rich glycoproteins were upregulated, indicating that N deficiency might be sensed as an increase of C/N ratio (Baba et al. 2011). By contrast, the exposure to high CO_2 did not produce fully mating-competent gametes, consistent with the former observations that nitrogen is not the sole trigger for gametogenesis (Goodenough et al. 2007; Harris 2009).

1.1.2 Light and Gametogenesis

The importance of light in initiating gametogenesis was noticed by Sager and Granick (1954). A simple explanation would be that high light irradiation accelerates photosynthesis and/or N assimilation, thereby further depleting the available nitrogen source in the environment. In line with this, some key enzymes for nitrogen assimilation in the GS/GOGAT cycle are under the control of light. GS that catalyzes the formation of Gln from ammonium and Glu in an ATP-dependent reaction is inactivated in the dark and reactivated by the light (Cullimore and Sims 1981), and the reversible regulation may be dependent on thioredoxins and the redox status of cells (Florencio et al. 1993). The activity of GOGAT that catalyzes the transfer of the amide group from Gln to 2-oxoglutarate is also regulated by redox status via ferredoxin (Martinez-Rivas et al. 1991).

Subsequent research revealed that light irradiation facilitates the conversion of mating-incompetent pre-gametes into gametes (Treier et al. 1989; Beck and Acker 1992). Based on the action spectrum analysis, Weissig and Beck showed the importance of blue/UVA light in gametogenesis (Weissig and Beck 1991), which later leads to the identification of a flagella-plasma membrane-associated phototropin as the blue/UVA light receptor responsible for gametogenesis (Huang and Beck 2003; Huang et al. 2004).

To study the molecular mechanism underlying initiation of gametogenesis, a series of mutants defective in the early process of gametogenesis was screened, including *lrg* (*light regulation of gametogenesis*) and *dif* (*differentiation*). The *lrg2* mutant is partially defective in blue light-induced gametogenesis, showing a delay in pre-gamete to gamete conversion. By contrast, the *lrg1* and *lrg4* mutants do not require light irradiation for gametogenesis (Buerkle et al. 1993; Gloeckner and Beck 1995) and do not respond chemotactically to ammonium (Ermilova et al. 2003). *lrg6* also differentiates gametes in a light-independent manner. The corresponding genes for *lrg1*, *3*, and *4* have not been identified to date owing to the lack of easily identifiable markers. *lrg6* was isolated by insertional mutagenesis, and therefore Dame et al. (2002) identified the corresponding gene by the plasmid rescue technique, which turned out to be a putative transporter. Matsuda and his group have reported *dif* mutants. *dif1* and *2* are conditional mutants that remain mating incompetent at the restrictive temperature (35 °C) under conditions of nitrogen starvation (Saito and Matsuda 1991). *dif3* is an unconditional mutant

defective in gametogenesis (Abe et al. 2005). These mutants have served as important tools to dissect the complex hierarchy of gamete-specific genes.

The conversion of vegetative cells to gametes requires de novo protein synthesis of gamete-specific proteins (von Gromoff and Beck 1993), accompanied by a drastic alteration in gene expression patterns. Since the late 1980s, genes involved in gametogenesis have been analyzed extensively. Numbers of gamete-specific genes have been documented. Among these are the *GLE* gene, which encodes a Gamete Lytic Enzyme (Kinoshita et al. 1992), and the *GAS* (*Gamete specific*) genes (von Gromoff and Beck 1993). The expression of *GAS28* and *GAS29* is restricted to gametes in WT, whereas they are expressed even in the dark in *lrg* mutants. These genes encode hydroxyproline-rich proteins (HGRPs) that exhibit typical features of volvocalean cell wall constituents (Rodriguez et al. 1999).

A pioneer transcriptomic analysis of gametogenesis was reported in 2004 using the EST (Expressed Sequence Tag) database and the microarray technique (Abe et al. 2004, 2005). Abe et al. analyzed the expression profiles of several previously identified genes and 18 newly identified genes by EST database analysis (*NSG Nitrogen Starved Gametogenesis*) in synchronized cells. They classified these genes based on the gene expression profiles after the removal of nitrogen (Abe et al. 2004). Early genes mainly included genes related to nitrogen metabolism, such as nitrate reductase (*NIA1*) and nitrate transporters (*NRT2*). They also analyzed the expression profile of *NSG* and other marker genes in *dif2* and *dif3* mutants. Based on this analysis, they classified the gamete-specific gene expressions into two programs, (1) −N adaptation program and (2) mating program, and proposed that the corresponding gene for *dif2* would be the master regulator for both programs (Abe et al. 2005). Recently, more comprehensive analyses employing next-generation sequencing have revealed approximately 361 gametic genes with expression patterns specific to mating type (Lopez et al. 2015).

While many gamete-specific gene expressions have been studied, protein phosphorylation could be another important step in finalizing gametogenesis. Upon incubation in the dark, gametes lost their mating ability, resulting in dark-inactivated pre-gametes. Reillumination rapidly restored mating competence, independently of de novo protein synthesis. Possible involvement of posttranslational processes such as phosphorylation of proteins has been suggested for this final step of gametogenesis (Pan et al. 1996, 1997).

1.2 Sexual Differentiation

1.2.1 *MID*: A Master Regulator of Gametogenesis

Mating type is controlled by a region called the *MT* locus, which includes key regulatory genes for gametogenesis and genes with mating type-/zygote-specific expression patterns. The *MT* locus on linkage group (LG) VI is characterized by sequence rearrangements and suppressed recombination (Ebersold 1967; Ferris

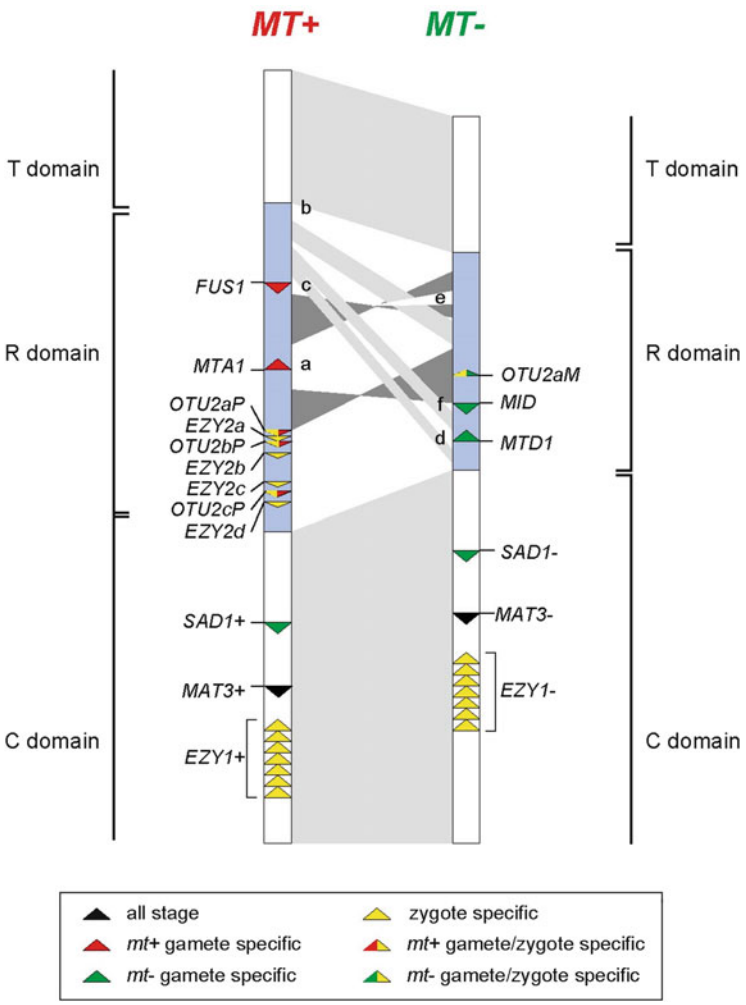

Fig. 2 Schematic drawing of the MT+/MT− mating locus that is located in the left arm of linkage group VI. The T (telomere-proximal), R (rearranged), and C (centromere-proximal) domains are indicted. *Letters* (a–f) indicate regions within the R domain that are unique to *MT*− or *MT*+. The orientation and position of the genes are represented by *arrowheads*, and the *color* indicates the expression profiles as summarized in the *lower box*

et al. 2002; Goodenough et al. 2007; De Hoff et al. 2013) (Fig. 2). The *MT* locus carries six unique regions (*a–f*) that are found within the rearranged (R) domain, three (a–c) specific to MT^+ and three (d–f) specific to *MT*−. The R domain is located between the telomere proximal (T) and centromere-proximal (C) domains. Several key genes for sexual differentiation are encoded in the *MT* locus, and two of the most important genes are *MID* and *FUS1*, unique to region f of the MT^- locus and region c of the MT^+ locus, respectively. Indeed, *mt*− cells lacking *MID* can be

transformed into cells that behave like *mt+* gametes on mating by ectopically expressing the *FUS1* gene (Ferris et al. 1996). Recently, the detailed structure and expression profiles of the genes at the *MT* locus were analyzed using next-generation sequencing, which revealed the complex nature of the region. Some genes are specifically encoded for mating type; some genes are encoded at both MT^+ and MT^- loci but show various mating type-/gamete-/zygote-specific expressions patterns, whereas other genes are shared and constitutively expressed (De Hoff et al. 2013). The mechanism of recombination was postulated to be a sequence arrangement of the R domain between MT^+ and MT^-. However, de Hoff et al. reported that recombination was suppressed even in an artificial *mt−* X *mt−* cross, while normal recombination rates were observed for an *mt+* X *mt+* cross, indicating the presence of an unknown mechanism to suppress recombination at the *MT* locus (De Hoff et al. 2013).

When an *mt+*/*mt−* heterozygous vegetative diploid is nitrogen starved, the diploid mates as an *mt−*, which demonstrates the dominance of *mt−* over *mt+* (Ebersold 1967). *MID* was originally identified as the gene responsible for this minus dominance (Ferris and Goodenough 1997). *MID* encodes an *mt−*-specific transcription factor that belongs to the RWP-RK family. The expression of *MID* is upregulated in response to N depletion and cells expressing the *MID* gene differentiate as *mt−*. In contrast, a loss of function mutation or a deletion of *MID* prevents the cells from differentiating as *mt−* gametes and instead results in a "pseudo-plus" phenotype, indicating that *MID* encodes a transcription factor that both turns on an *mt−*-specific differentiation program and turns off *mt+*-specific genes (Ferris and Goodenough 1997). For efficient gametogenesis, an additional upregulation of *MID* expression in the late stage of gametogenesis is required, which is supported by a unique gene, *MTD1*, that is also encoded in region *d* of the *MT* locus (region *d*) (Lin and Goodenough 2007). *MID* orthologs have been identified specifically in males or *mt−* cells of the oogamous *Volvocaceae* (Nozaki et al. 2006) and the isogamous (Hamaji et al. 2008), indicating the significance of the *MID* gene in the evolutionary process of sex determination. Geng et al. showed that the ectopic expression of male *MID* homologs in female *Volvox carteri* (*VcMID*) produced functional sperm packets. Further, RNA interference (RNAi)-mediated knockdown of *VcMID* in male cells produced functional eggs. These results indicate that *MID* homologs act as master regulators for male gametogenesis in species other than *C. reinhardtii* (Geng et al. 2014).

1.2.2 Activation of Gametes: Agglutinins and Mating Structure

During gametogenesis, the flagella get coated with mating type-specific glycoprotein agglutinins. The agglutinins are fibrous hydroxyproline-rich (HRGP) glycoproteins that are responsible for flagellar adhesion between *mt+* and *mt−* gametes to find mating partners. The *mt+* and *mt−* agglutinins are encoded by the autosomal genes, *Sexual AGglutination* (*SAG*) (Goodenough et al. 1976, 1978) and *Sexual ADhesion* (*SAD*), encoded just outside of R domain of the *MT* locus

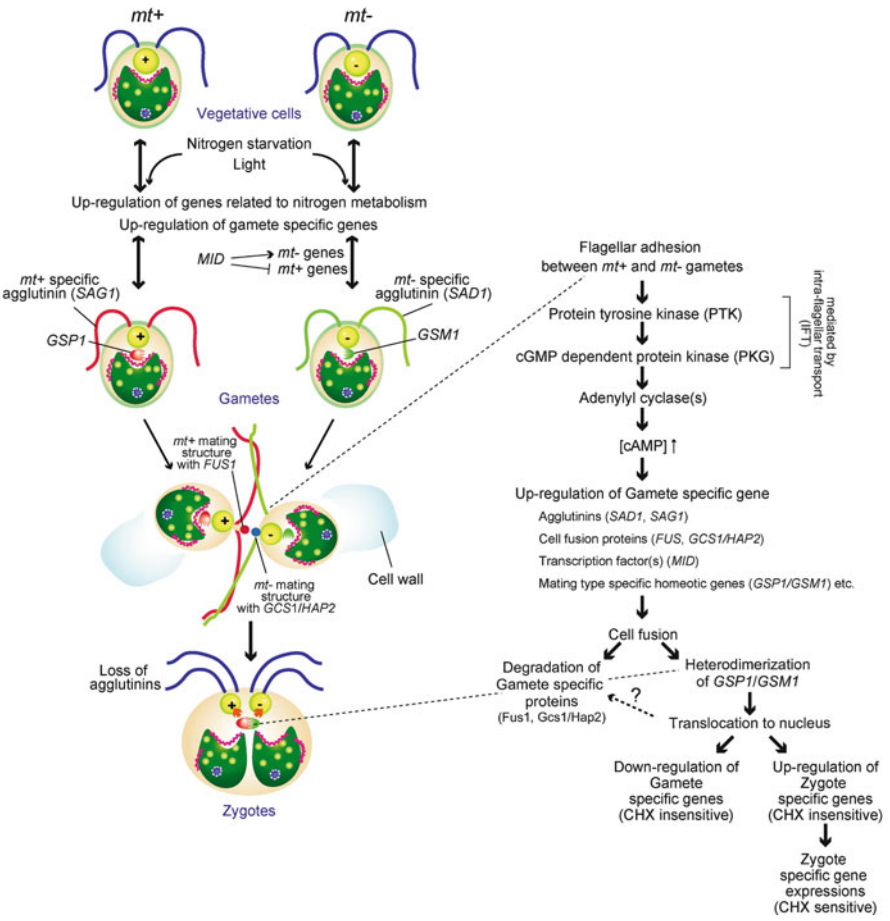

Fig. 3 Genetic control and signal transduction for gametogenesis, mating, and zygote maturation in *C. reinhardtii*. Nitrogen starvation and light signals induce vegetative cells to differentiate into *mt*+ and *mt*− gametes, controlled by two mating loci (*MT*+ and *MT*−). Upon mixing, agglutinins mediate flagellar adhesion. A rapid increase in cAMP triggers cell wall loss and activation of mating structures. Activated mating structures fuse to form zygotes, allowing the formation of the Gsp1/Gsm1 heterodimer, which subsequently translocates into nuclei and switches on the zygote program

(Cooper et al. 1983), respectively. *SAG1* is likely repressed by the *MID* gene, because *SAG1* is not expressed in *mt*− gametes despite the presence of a functional copy (Ferris et al. 2005) (Fig. 3). In contrast, *SAD1* expression is upregulated by *MID*. When *mt*+ and *mt*− gametes encounter one another, they interact by their flagella, forming large clumps of rapidly twitching cells. Initial adhesion can occur anywhere along the length of the flagella. Once flagellar adhesion occurs, the site of adhesion migrates to the tips of the interacting flagella (Goodenough 1993; Hoffman and Goodenough 1980).

Another critical event during gametogenesis is the preparation of a mating-specific structure that triggers cell-cell fusion upon mating. Formation of mating structures occurs in both mating types. The process of mating-specific structures has been carefully studied by electron microscopy. The first step is the formation of a ringlike structure (doublet zone) that associates with the plasma membrane (membrane zone) in *mt*+ cells (Goodenough and Weiss 1975; Weiss et al. 1977). The corresponding zone of *mt*− cells also differentiates during gametogenesis, although the membrane zone is broader, and no doublet zone is observed (Weiss et al. 1977).

2 Mating

2.1 Cell-Cell Fusion

The agglutinins bring gametes of opposite mating types together, resulting in formation of the fertilization tubule connecting mating gametes (Friedmann et al. 1968). The fertilization tube immediately expands, and the two cells coalesce into a quadriflagellated zygote (Fig. 4).

The initial interaction of flagella and agglutination induces a cascade of signaling pathways, which includes a protein tyrosine kinase (Wang and Snell 2003), cyclic GMP (cGMP)-dependent kinase (Wang et al. 2006), and adenylyl cyclase (s) (Saito et al. 1993), and results in a tenfold increase in intracellular cAMP that triggers dramatic alterations in the cells, most of which can be mimicked by incubation of gametes of a single mating type in the cell-permeable analog of cAMP, dibutyryl cAMP (Pijst et al. 1984; Pasquale and Goodenough 1987). For upregulation of cAMP, intraflagellar transport (IFT) is critical because *fla10-1* gametes, which have a mutation in the kinesin-II gene that is required for IFT, exhibit wild-type levels of flagellar adhesion but fail to undergo gamete activation (Pan and Snell 2002). IFT is a ubiquitous process first discovered in Chlamydomonas (Kozminski et al. 1993), which is responsible for constitutive transport of proteins into and out of cilia and flagella (reviewed in Rosenbaum and Witman 2002) (Fig. 3).

In response to the cAMP signal, both gametes shed their cell wall, which is a thick, multilayered, glycoprotein-containing extracellular matrix, through the activation of an extracellularly stored pro-metalloprotease (Buchanan et al. 1989; Kinoshita et al. 1992; Kubo et al. 2001, 2002) (Fig. 4). The mating structures located on the apical cell membranes between the two flagella of both gametes are then activated (Detmers et al. 1983). The activation of the *mt*+ mating structure is initiated by the formation of a bud, with separation of the membrane from the underlying doublet zone, which is followed by the nucleation of actin microfilaments. As fusion progresses, the doublet zone detaches from the plasma membrane, and the actin microfilaments form tubular projections extending from the surface of

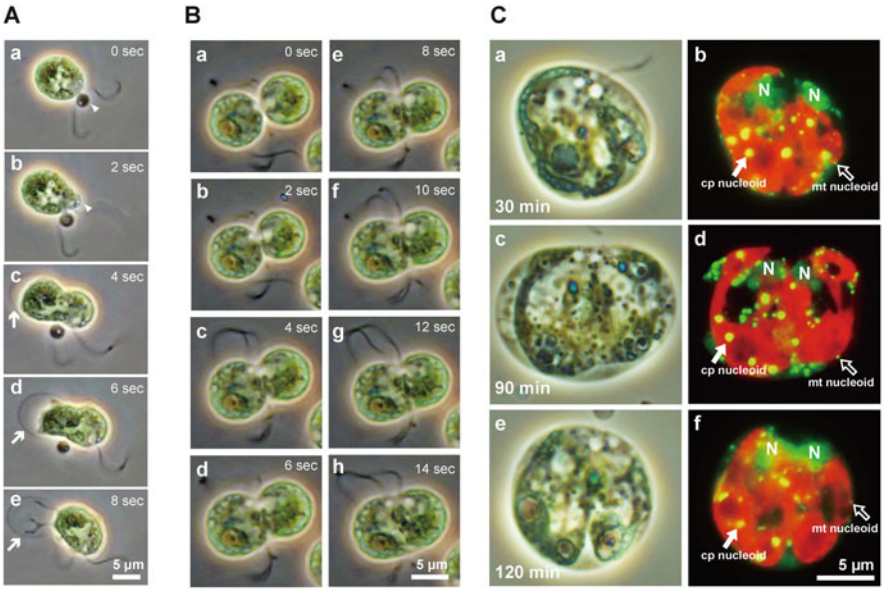

Fig. 4 (**A**) A gamete shedding its cell wall. From the area between the two flagella (a–b, *white triangle*), the gametes escape from the cell wall (c–d, *white arrow*) to prepare for cell fusion. (**B**) The process of cell fusion to form zygotes. Cell fusion is very rapid and completed within 15 s from initiation. (**C**) Active digestion of *mt*− cp nucleoids in young zygotes. Phase contrast (a, c, e) and fluorescent images (b, d, f) of SYBR Green I-stained young zygotes 30 min (a, b), 90 min (c, d), and 120 min (e, f) after mating. Red signal (b, d, f) is autofluorescence from the chloroplasts, and DNAs are visualized as green signals. Cp nucleoids appear as *yellow spots* due to overlapping with the red chlorophyll autofluorescence. Mt nucleoids appear as *smaller green spots* outside red chlorophyll autofluorescence. Thirty minutes after mating, both *mt*+ (*left*) and *mt*− chloroplasts possess cp nucleoids (b, *white arrows*). However, 90 min after mating, *mt*− cp nucleoids are completely degraded, which is the basis for uniparental inheritance of cpDNA. After degradation of *mt*− cp nucleoids, two cell nuclei (N) fuse, and chloroplasts also fuse to each other (e, f)

the fertilization tubule. The *mt*− structure also changes upon activation. The initial small bud enlarges and becomes dome-shaped (Goodenough et al. 1982). Actin-mediated protrusion of the cell membrane can be found in other cell-cell interaction events such as fertilization in yeast, cell-cell fusion between sperm and egg (Wilson and Snell 1998), and invasive cell migration of cancer cells that result in malignant tumor progression (Nürnberg et al. 2011).

Continued flagellar adhesion brings the activated mating structures close to each other. The *mt*+ gamete-specific protein Fus1 present on the plasma membrane of the *mt*+ mating structure is essential for fusion of the *mt*+ and *mt*− mating structures (Misamore et al. 2003). Complete cell fusion requires an additional factor, *GCS1* (generative cell specific)/*HAP2*, on the *mt*− mating type structure, which is conserved ubiquitously in higher plants, algae, and *Plasmodium* that causes acute malaria (Mori et al. 2006; Liu et al. 2008). Treatment with antibodies against the male gamete protein *HAP2* has been shown to inhibit fertilization in

P. berghei, and therefore *HAP2* is considered a potential transmission-blocking target for malaria (Blagborough and Sinden 2009) (Fig. 3).

2.2 Zygote Maturation

2.2.1 Gsp1/Gsm1 as the Master Regulator to Initiate Zygote Development

Upon zygote formation, two homeodomain proteins, *Gamete-Specific Plus* (*GSP1*) (Kurvari et al. 1998) and *Gamete-Specific Minus* (*GSM1*) (Lee et al. 2008), contributed by the *mt*+ and *mt*− gametes, respectively, physically interact and translocate from the cytosol to the nucleus, thereby initiating the zygote development program. When *GSP1* is expressed ectopically in unmated *mt*− gametes, zygote-specific genes are expressed (Zhao et al. 2001). Similarly, *mt*+ cells transformed with *GSM1* driven by a constitutive promoter also express zygote-specific genes (Lee et al. 2008). Furthermore, in a mutant lacking *GSP1*, downregulation of gamete-specific genes and upregulation of zygote-specific genes were missing, and the phenotype was not rescued by db-cAMP treatment (Nishimura et al. 2012). These reports indicate the critical importance of the Gsp1/Gsm1 system as the final step in the transition from gametic to the zygotic developmental program. The signal transduction system downstream of Gsp1/Gsm1 remains largely unknown, but recently a cis-element for zygotic gene transcription (ZYRE) has been detected, which is a good candidate for Gsp1/Gsm1 binding sites (Hamaji et al. 2016).

Similar heterodimerization between two classes of homeodomain proteins has been shown to play a critical role in sexual development in various fungi (Casselton and Olesnicky 1998), such as the ascomycete *Saccharomyces cerevisiae* (**a**1/α2) (Johnson 1995), the basidiomycetes *Ustilago maydis* (HD1/HD2) (Schulz et al. 1990), *Coprinopsis cinerea* (Spit et al. 1998), and *Cryptococcus neoformans* (Sxi2**a**/Sxi1α) (Hull et al. 2005). In these organisms, heterodimerization serves to bring two homeodomains together to influence DNA target site selection and to regulate their nuclear/cytosolic localization (Casselton and Olesnicky 1998). Furthermore, Gsp1/Gsm1 dyads are similar and functionally related to the *KNOX/BELL* dyads that regulate meristem specification in land plants. This prompted Lee et al. to propose that complex developmental programs for the diploid phase of land plants might have evolved through the elaboration of a KNOX-BELL-regulated developmental program that emerged in the sexual cycle of green algae (Goodenough et al. 2007; Lee et al. 2008; Goodenough and Heitman 2014).

2.2.2 Elimination of Gamete-Specific Transcripts/Proteins

Gametes are specialized for cell fusion, but the newly formed zygotes become incapable of further agglutination and membrane fusion reactions, probably to

avoid fusion of multiple gametes which could be deleterious for zygote development processes. After zygote formation, their flagella lose adhesiveness (Hunnicutt and Snell 1991), and proteins required for cell-cell fusion (Fus1/Hap2) are rapidly degraded (Liu et al. 2010). RT-qPCR analysis revealed that the mRNA level of *SAG1*, *SAD1*, and *FUS1* decreased rapidly after zygote formation. The rapid reduction of these mRNAs was not observed in a mutant lacking *GSP1*, indicating that the rapid suppression of gamete-specific genes is under the control of Gsp1/Gsm1 (Nishimura et al. 2012). Then flagella are gradually shortened and absorbed into the cell body, which is mediated by aurora protein kinase CALK (Pan et al. 2004) and IFT machineries (Pan and Snell 2005) (Fig. 3).

2.2.3 Uniparental Inheritance of Chloroplast/Mitochondrial DNA

One notable event during the sexual life cycle is uniparental inheritance of chloroplast (cp) and mitochondrial (mt) DNA. In *C. reinhardtii*, although the *mt*+ and *mt*− gametes contribute an equal amount of organelles and organellar DNA molecules to the zygote, only the cpDNA from the *mt*+ parent is retained (Sager 1954) owing to the active degradation of *mt*− cpDNA within 60 min after mating (Sager and Lane 1972; Kuroiwa et al. 1982; Nishimura et al. 1999, 2002) (Fig. 4). Conversely, the *mt*+ mtDNA is eliminated, although this elimination occurs more than 6 h after mating (Nakamura et al. 2003; Aoyama et al. 2006). As a result of the selective destruction of the organellar genomes, *C. reinhardtii* shows the uniparental inheritance of the cpDNA and the mtDNA from the *mt*+ and *mt*− parents, respectively (Boynton et al. 1987). Active degradation of paternal mtDNA was found in other organisms such as medaka fish (Nishimura et al. 2006), mouse (Kaneda et al. 1995; Shitara et al. 2000), and slime mold (Moriyama and Kawano 2003), and it would be one of the common mechanisms to achieve uniparental inheritance of cp/mtDNA.

To date, considerable efforts have been made to isolate and characterize mutants with defective uniparental inheritance (Sager and Ramanis 1974; Sager et al. 1981). Gillham et al. isolated three mutations, *mat-3-1*, *mat-3-2*, and *mat-3-3*, all showing increased transmission of the *mt*− cpDNA (Gillham et al. 1987). However, the *mat-3* cells are usually small and contain significantly reduced amounts of cpDNA, suggesting that the increased biparental transmission of cpDNA might be a side effect of the reduced amount of *mt*+ cpDNA (Armbrust et al. 1995).

Based on insertional mutagenesis, a mutant that shows drastically increased biparental inheritance of cpDNA and mtDNA (*biparental* (*bp*) *31*) was isolated. *bp31* did not show any disturbance in cell size, mating efficiency, and zygote formation, but the development of zygotes is completely blocked. The gene responsible for the phenotype of *bp31* turned out to be *GSP1*, indicating that the uniparental inheritance of both cp and mtDNAs is governed by the Gsp1/Gsm1 system (Nishimura et al. 2012). In comparison, the uniparental inheritance of mtDNA is regulated by homeobox proteins Sxi1α/Sxi2a in the basidiomycete fungus *Cryptococcus neoformans* (Yan et al. 2004).

The simplest model for the uniparental inheritance of cpDNA would be that the process consists of two distinct events that are likely to occur at different stages of the life cycle: a "protection" of *mt*+ cpDNA, perhaps during gametogenesis, and a "destroyer" of unprotected *mt*− cpDNA during early zygote development. However, the actual mechanisms remain unknown.

Sager and Lane proposed that *mt*− cpDNA was digested by the action of restriction enzymes, whereas the *mt*+ cpDNA was protected by methylation—a model analogous to the bacterial restriction-methylation system (Sager and Lane 1972). Evidence to support this hypothesis includes an increase in the methylation level of *mt*+ cpDNA (Burton et al. 1979; Royer and Sager 1979; Sano et al. 1980) and the presence of *mt*+ gamete-specific methyltransferase (Sano et al. 1981; Sano and Sager 1980). The gene for the chloroplast-resident DNA methyltransferase was identified (Nishiyama et al. 2002), and its ectopic expression in *mt*− gametes resulted in the subtle increase of leaky transmission of *mt*− cpDNA (Nishiyama et al. 2004). By contrast, a series of reports from independent groups has argued that methylation of *mt*+ cpDNA could not explain protection unambiguously. Bolen et al. isolated a mutant *me1* in which cpDNA was hypermethylated. Normal uniparental inheritance was observed in the cross using the mutant *me1*, indicating that methylation level cannot be the direct explanation for the protection of *mt*+ cpDNA (Bolen et al. 1982). Feng and Chiang reported that normal uniparental inheritance of cpDNA was observed in cells with hypomethylated cpDNA treated with the methylation inhibitors, L-ethionine and 5-azacytidine (Feng and Chiang 1984). Umen and Goodenough also assessed the impact of 5-azacytidine treatment on *mt*+ cpDNA protection and proposed that methylation of cpDNA is not responsible for the protection of *mt*+ cpDNA; instead it would be responsible for the preferential replication of *mt*+ cpDNA upon germination of zygospores (Umen and Goodenough 2001). Preferential replication of a specific group of cpDNA genomes was found to cause a bias in the inheritance of cpDNA, indicating the importance of the preferential replication of *mt*+ cp DNA upon the zygote germination process to achieve strict uniparental inheritance (Nishimura and Stern 2010).

In the related species *Chlamydomonas monoica*, a homothallic or "self-mating" strain of Chlamydomonas, two mutants have been obtained that alter uniparental inheritance. The *mtl-1* mutant fails to protect *mt*+-derived cpDNA in zygotes and has a mating type-specific zygotic lethal effect (Van Winkle-Swift and Salinger 1988). The *sup-1* mutant is defective for cpDNA degradation, suppressing the lethal effect of *mtl-1*, and leads to biparental inheritance of cpDNA in zygotes (van den Ende and Van Winkle-Swift 1994). These reports suggest that the regulatory system for "protection" and "destroyer" would be rather simple, mediated by a limited number of genes.

One of the candidate genes that could be involved in uniparental inheritance is *EZY1* (Armbrust et al. 1993), which is repeated tandemly seven to eight times at both the *MT*+ and *MT*− mating loci, and the repeats are transcribed immediately upon zygote formation under the regulation of Gsp1/Gsm1 (Zhao et al. 2001; Lee et al. 2008; Nishimura et al. 2012). The *EZY1* protein localizes specifically to both mt+ and mt− cp nucleoids. Brief irradiation of mt+ gametes prior to mating, which

is known to disturb uniparental inheritance (Sager and Ramanis 1967), inhibited the transcription of *EZY1*. Polypeptide 4 was originally identified by Nakamura et al. as a zygote polypeptide whose expression is UV sensitive and likely corresponds to EZY1 (Nakamura et al. 1988). *EZY2* is encoded in tandem with *OTU2* at the MT^+ locus, expressed specifically in young zygotes, and possesses a chloroplast-targeting signal. Therefore, it could also be a good candidate as the regulatory gene for the uniparental inheritance of cpDNA (Ferris et al. 2002).

2.2.4 Zygospore Formation/Germination

During zygote maturation, chloroplasts appear to disintegrate, chlorophylls are degraded, and lipid-storage granules are accumulated. The zygotes proceed to develop thick cell walls that are denser and thicker than those of vegetative cells and that are insoluble in chaotropes or detergents. Then, the zygotes become adhesive, and if they are maintained in liquid medium, they adhere in flat sheets, forming a structure called a "pellicle." After ~5–7 days' incubation in the dark, zygotes develop into zygospores, which is a dormant stage for Chlamydomonas. When the environment is improved, zygospores undergo meiosis and germination to produce four haploid progeny (Harris 2009).

Young zygotes of Chlamydomonas express HRGPs, which are the major component of the cell wall. The zygote-specific genes that are involved in this process are *ZSP1* (Woessner et al. 1986) and *ZSP2* (Suzuki et al. 2000). Other HRGPs (*GAS28*, *30*) and glycoproteins (*GAS31*) are expressed in the late phase of gametogenesis and are further upregulated in zygotes (Hoffmann and Beck 2005). Kubo et al. identified candidate zygotic genes that may be related to cell wall synthesis through sugar metabolism (*EZY4* UDP-glucose 4-epimerase-like protein; *EZY11* UDP-glucose protein, protein transglycosylase; *EZY12* UDP-glucose 6-dehydrogenase; *EZY16* cell wall protein pherophorin-C15). Since *EZY11*, *12*, and *16* were upregulated without cell fusion, the authors proposed that these genes may be involved in cell wall synthesis of both vegetative/gamete cells and zygotes (Kubo et al. 2008). Recently, genome-wide analysis of transcriptome in early zygotes and transcriptome/methylome in vegetative cells, gametes, and zygotes was conducted, which identified 361 gametic genes with mating-type specificity and 627 zygote-specific genes (Lopez et al. 2015). Furthermore, comparative transcriptome analysis using *bp31* (*gsp1* null mutant) revealed that most of the zygote-specific genes were under the regulation of *GSP1-GSM1*. The zygote specific genes encoded proteins with various functions; cell wall modifying enzymes, proteins involved in nucleotide-sugar metabolism, vesicle transportation, and several chloroplast nucleoid proteins, indicating that *GSP1-GSM1* is a master regulator that orchestrate the multifaceted system to achieve the haploid-diploid transition (Sunjoo et al. 2017).The database would be a treasure trove for further understanding of the sexual lifecycle in Chlamydomonas.

The activation of the zygotic program leads to zygospore formation. Zygospores are thought to be dormant and protected by thick cell walls to survive severe

environmental conditions, such as desiccation, cold temperatures, or nutrient deficiencies (Beck and Haring 1996; Harris 2009). When the environment becomes favorable, zygospores germinate. The presence of thick cell walls makes zygospore analysis highly difficult. Aoyama et al. (2014) managed to analyze transcriptome of germinating zygospores, revealing upregulation of various biological pathways, including photosynthesis, methionine biosynthesis, polyketides, and small heat-shock proteins. Haploid vegetative cells are produced through meiosis and tetrad formation, completing the sexual developmental program of *Chlamydomonas reinhardtii*.

Acknowledgments This author would like to acknowledge the kind help and comments from Dr. Patrick Ferris about the MT locus. This work was supported by the Ministry of Education, Culture, Sports, Science, and Technology of Japan grants to T.S. and Y.N., the Funding Program for Next Generation World-Leading Researchers (NEXT Program: GS015), a Grant-in-Aid for Challenging Exploratory Research (26650111, 16K14768), Grant-in-Aid for Scientific Research on Innovative Areas (17H05840), a Grant for Basic Research Projects from the Sumitomo Foundation, Core stage back-up program from Kyoto University and Strategic Research Foundation Grant-Aided Project for Private Universities awarded to Y.N., and a Grant-in-Aid for JSPS Fellows (grant 26·786 to Y.K.).

References

Abe J et al (2004) The transcriptional program of synchronous gametogenesis in Chlamydomonas reinhardtii. Curr Genet 46(5):304–315

Abe J et al (2005) The regulatory networks of gene expression during the sexual differentiation of Chlamydomonas reinhardtii, as analyzed by mutants for gametogenesis. Plant Cell Physiol 46 (2):312–316

Adair WS et al (1982) Sexual agglutinins from the Chlamydomonas flagellar membrane. Partial purification and characterization. J Biol Chem 257(8):4593–4602

Aoyama H et al (2006) Complete elimination of maternal mitochondrial DNA during meiosis resulting in the paternal inheritance of the mitochondrial genome in Chlamydomonas species. Protoplasma 228(4):231–242

Aoyama H et al (2014) Comparative analysis of zygospore transcripts during early germination in Chlamydomonas reinhardtii. J Plant Physiol 171(18):1685–1692

Armbrust EV, Ferris PJ, Goodenough UW (1993) A mating type-linked gene cluster expressed in Chlamydomonas zygotes participates in the uniparental inheritance of the chloroplast genome. Cell 74(5):801–811

Armbrust EV, Ibrahim A, Goodenough UW (1995) A mating type-linked mutation that disrupts the uniparental inheritance of chloroplast DNA also disrupts cell-size control in Chlamydomonas. Mol Biol Cell 6(12):1807–1818

Baba M, Suzuki I, Shiraiwa Y (2011) Proteomic analysis of high-CO_2-inducible extracellular proteins in the unicellular green alga, Chlamydomonas reinhardtii. Plant Cell Physiol 52 (8):1302–1314

Beck CF, Acker A (1992) Gametic differentiation of Chlamydomonas reinhardtii: control by nitrogen and light. Plant Physiol 98(3):822–826

Beck CF, Haring MA (1996) Gametic differentiation of Chlamydomonas. Int Rev Cytol 168:259–302

Blagborough AM, Sinden RE (2009) Plasmodium berghei HAP2 induces strong malaria transmission-blocking immunity in vivo and in vitro. Vaccine 27(38):5187–5194

Bolen PL et al (1982) Extensive methylation of chloroplast DNA by a nuclear gene mutation does not affect chloroplast gene transmission in chlamydomonas. Cell 28(2):335–343

Borowitzka MA (2013) High-value products from microalgae-their development and commercialisation. J Appl Phycol 25(3):743–756

Boyle NR et al (2012) Three acyltransferases and nitrogen-responsive regulator are implicated in nitrogen starvation-induced triacylglycerol accumulation in Chlamydomonas. J Biol Chem 287 (19):15811–15825

Boynton JE et al (1987) Transmission of mitochondrial and chloroplast genomes in crosses of Chlamydomonas. Proc Natl Acad Sci U S A 84(8):2391–2395

Buchanan MJ et al (1989) Activation of the cell wall degrading protease, lysin, during sexual signalling in Chlamydomonas: the enzyme is stored as an inactive, higher relative molecular mass precursor in the periplasm. J Cell Biol 108:199–207

Buerkle S, Gloeckner G, Beck CF (1993) Chlamydomonas mutants affected in the light-dependent step of sexual differentiation. Proc Natl Acad Sci U S A 90(15):6981–6985

Bulte L, Wollman FA (1992) Evidence for a selective destabilization of an integral membrane protein, the cytochrome b6/f complex, during gametogenesis in Chlamydomonas reinhardtii. Eur J Biochem 204(1):327–336

Burton WG, Grabowy CT, Sager R (1979) Role of methylation in the modification and restriction of chloroplast DNA in Chlamydomonas. Proc Natl Acad Sci U S A 76(3):1390–1394

Camargo A et al (2007) Nitrate signaling by the regulatory gene NIT2 in Chlamydomonas. Plant Cell 19(11):3491–3503

Casselton LA, Olesnicky NS (1998) Molecular genetics of mating recognition in basidiomycete fungi. Microbiol Mol Biol Rev 62(1):55–70

Cooper JB et al (1983) Chlamydomonas agglutinin is a hydroxyproline-rich glycoprotein. Proc Natl Acad Sci U S A 80(19):5898–5901

Cullimore JV, Sims AP (1981) Pathway of ammonia assimilation in illuminated and darkened Chlamydomonas reinhardii. Phytochemistry 20(5):933–940

De Hoff PL et al (2013) Species and population level molecular profiling reveals cryptic recombination and emergent asymmetry in the dimorphic mating locus of C. reinhardtii. PLoS Genet 9(8):e1003724

Detmers PA, Goodenough UW, Condeelis J (1983) Elongation of the fertilization tubule in Chlamydomonas: new observations on the core microfilaments and the effect of transient intracellular signals on their structural integrity. J Cell Biol 97(2):522–532

Ebersold WT (1967) Chlamydomonas reinhardi: heterozygous diploid strains. Science 157 (3787):447–449

Ermilova EV et al (2003) Chemotactic behavior of Chlamydomonas reinhardtii is altered during gametogenesis. Curr Microbiol 46(4):261–264

Feng TY, Chiang KS (1984) The persistence of maternal inheritance in Chlamydomonas despite hypomethylation of chloroplast DNA induced by inhibitors. Proc Natl Acad Sci U S A 81 (11):3438–3442

Fernandez E, Galvan A (2007) Inorganic nitrogen assimilation in Chlamydomonas. J Exp Bot 58 (9):2279–2287

Fernandez E, Galvan A (2008) Nitrate assimilation in Chlamydomonas. Eukaryot Cell 7 (4):555–559

Fernandez E, Galvan A, Quesada A (1998) Nitogen assimilation and its regulation. In: Rochaix JD, Goldschmidt-Clermont M, Merchant SS (eds) The molecular biology of chloroplast and mitochondria in Chlamydomonas. Kluwer Academic, Dordrecht, pp 637–659

Ferris PJ, Goodenough UW (1997) Mating type in Chlamydomonas is specified by mid, the minus-dominance gene. Genetics 146(3):859–869

Ferris PJ, Woessner JP, Goodenough UW (1996) A sex recognition glycoprotein is encoded by the plus mating-type gene fus1 of Chlamydomonas reinhardtii. Mol Biol Cell 7(8):1235–1248

Ferris PJ, Armbrust EV, Goodenough UW (2002) Genetic structure of the mating-type locus of Chlamydomonas reinhardtii. Genetics 160(1):181–200
Ferris PJ et al (2005) Plus and minus sexual agglutinins from Chlamydomonas reinhardtii. Plant Cell 17(2):597–615
Florencio F, Gadal P, Buchanan B (1993) Thioredoxin-linked activation of the chloroplast and cytosolic forms of Chlamydomonas reinhardtii glutamine synthetase. Plant Physiol Biochem 31:649–655
Friedmann I, Colwin A, Colwin L (1968) Fine structural aspects of fertilization in Chlamydomonas reinhardtii. J Cell Sci 3:115–128
Geng S, De Hoff P, Umen JG (2014) Evolution of sexes from an ancestral mating-type specification pathway. PLoS Biol 12(7):e1001904
Gillham NW et al (1987) Mating type linked mutations which disrupt the uniparental transmission of chloroplast genes in chlamydomonas. Genetics 115(4):677–684
Gregory Dame, Gernot Gloeckner, Christoph F. Beck, (2002) Knock-out of a putative transporter results in altered blue-light signalling in Chlamydomonas. The Plant Journal 31(5):577–587
Gloeckner G, Beck C (1995) Genes involved in light control of sexual differentiation in Chlamydomonas reinhardtii. Genetics 141(November):937–943
Goodenough UW (1993) Tipping of flagellar agglutinins by gametes of Chlamydomonas reinhardtii. Cell Motil Cytoskeleton 25(2):179–189
Goodenough U, Heitman J (2014) Origins of eukaryotic sexual reproduction. Cold Spring Harb Perspect Biol 6(3):1–22
Goodenough U, Weiss R (1975) Gametic differentiation in Chlamydomonas reinhardtii. III. Cell wall lysis and microfilament-associated mating structure activation in wild-type and mutant strains. J Cell Biol 67:623–637
Goodenough UW, Hwang C, Martin H (1976) Isolation and genetic analysis of mutant strains of Chlamydomonas reinhardtii defective in gametic differentiation. Genetics 82:169–186
Goodenough UW, Hwang C, Warren AJ (1978) Sex-limited expression of gene loci controlling flagellar membrane agglutination in the Chlamydomonas mating reaction. Genetics 89:235–243
Goodenough UW, Detmers PA, Hwang C (1982) Activation for cell fusion in Chlamydomonas: analysis of wild-type gametes and nonfusing mutants. J Cell Biol 92(2):378–386
Goodenough U, Lin H, Lee JH (2007) Sex determination in Chlamydomonas. Semin Cell Dev Biol 18(3):350–361
Hamaji T et al (2008) Identification of the minus-dominance gene ortholog in the mating-type locus of Gonium pectorale. Genetics 178(1):283–294
Hamaji T et al (2016) Identification and characterization of a cis-regulatory element for zygotic gene expression in Chlamydomonas reinhardtii. *G3* 6(6):1541–1548
Harris EH (2009) The chlamydomonas sourcebook, 2nd edn. Elsevier, Amsterdam
Hellio C, Veron B, Le Gal Y (2004) Amino acid utilization by Chlamydomonas reinhardtii: specific study of histidine. Plant Physiol Biochem 42(3):257–264
Hoffman JL, Goodenough UW (1980) Experimental dissection of flagellar surface motility in chlamydomonas. J Cell Biol 86(2):656–665
Hoffmann XK, Beck CF (2005) Mating-induced shedding of cell walls, removal of walls from vegetative cells, and osmotic stress induce presumed cell wall genes in Chlamydomonas. Plant Physiol 139(2):999–1014
Huang K, Beck CF (2003) Phototropin is the blue-light receptor that controls multiple steps in the sexual life cycle of the green alga Chlamydomonas reinhardtii. Proc Natl Acad Sci U S A 100 (10):6269–6274
Huang K, Kunkel T, Beck CF (2004) Localization of the blue-light receptor phototropin to the flagella of the green alga Chlamydomonas reinhardtii. Mol Biol Cell 15(8):3605–3614
Hull CM, Boily M, Heitman J (2005) Sex-specific homeodomain proteins Sxi 1 α and Sxi2 a coordinately regulate sexual development in *Cryptococcus neoformans*. Eukaryot Cell 4 (3):526–535

Hunnicutt GR, Snell WJ (1991) Rapid and slow mechanisms for loss of cell adhesiveness during fertilization in Chlamydomonas. Dev Biol 147(1):216–224
Jaenicke L et al (1987) Cell-wall lytic enzymes (autolysins) of Chlamydomonas reinhardtii are (hydroxy)proline-specific proteases. Eur J Biochem 170:485–491
Johnson AD (1995) Molecular mechanisms of cell-type determination in budding yeast. Curr Opin Genet Dev 5:552–558
Kaneda H et al (1995) Elimination of paternal mitochondrial DNA in intraspecific crosses during early mouse embryogenesis. Proc Natl Acad Sci U S A 92(10):4542–4546
Kinoshita T et al (1992) Primary structure and expression of a gamete lytic enzyme in Chlamydomonas reinhardtii: similarity of functional domains to matrix metalloproteases. Proc Natl Acad Sci 89(10):4693–4697
Kirk DL, Kirk MM (1978) Carrier-mediated uptake of arginine and urea by Chlamydomonas reinhardtii. Plant Physiol 61(4):556–560
Kozminski KG et al (1993) A motility in the eukaryotic flagellum unrelated to flagellar beating. Proc Natl Acad Sci U S A 90(12):5519–5523
Kubo T et al (2001) Two tandemly-located matrix metalloprotease genes with different expression patterns in the chlamydomonas sexual cell cycle. Curr Genet 40(2):136–143
Kubo T et al (2002) Genealogical relationships among laboratory strains of Chlamydomonas reinhardtii as inferred from matrix metalloprotease genes. Curr Genet 41(2):115–122
Kubo T et al (2008) Characterization of novel genes induced by sexual adhesion and gamete fusion and of their transcriptional regulation in Chlamydomonas reinhardtii. Plant Cell Physiol 49 (6):981–993
Kuroiwa T et al (1982) Epifluorescent microscopic evidence for maternal inheritance of chloroplast DNA. Nature 298(5873):481–483
Kurvari V, Grishin NV, Snell WJ (1998) A gamete-specific, sex-limited homeodomain protein in Chlamydomonas. J Cell Biol 143(7):1971–1980
Lee JH et al (2008) Early sexual origins of homeoprotein heterodimerization and evolution of the plant KNOX/BELL family. Cell 133(5):829–840
Lin H, Goodenough UW (2007) Gametogenesis in the Chlamydomonas reinhardtii minus mating type is controlled by two genes, MID and MTD1. Genetics 176(2):913–925
Liu Y et al (2008) The conserved plant sterility gene HAP2 functions after attachment of fusogenic membranes in Chlamydomonas and Plasmodium gametes. Genes Dev 22(8):1051–1068
Liu Y, Misamore MJ, Snell WJ (2010) Membrane fusion triggers rapid degradation of two gamete-specific, fusion-essential proteins in a membrane block to polygamy in Chlamydomonas. Development 137(9):1473–1481
Lopez DA et al (2015) Dynamic changes in the transcriptome and methylome of Chlamydomonas reinhardtii throughout its life cycle. Plant Physiol 169(4):2730–2743
Martin NC (1976) Turnover of chloroplast and cytoplasmic ribosomes during gametogenesis in Chlamydomonas. Dev Biol 51:190–201
Martinez-Rivas JM, Vega JM, Márquez AJ (1991) Differential regulation of the nitrate-reducing and ammonium-assimilatory systems in synchronous cultures of Chlamydomonas reinhardtii. FEMS Microbiol Lett 78:85–88
Merchán F et al (2001) Low-expression genes induced by nitrogen starvation and subsequent sexual differentiation in Chlamydomonas reinhardtii, isolated by the differential display technique. Planta 213(2):309–317
Merchant SS et al (2012) TAG, You're it! Chlamydomonas as a reference organism for understanding algal triacylglycerol accumulation. Curr Opin Biotechnol 23(3):352–363
Misamore MJ, Gupta S, Snell WJ (2003) The Chlamydomonas Fus 1 protein is present on the mating type plus fusion organelle and required for a critical membrane adhesion event during fusion with minus gametes. Mol Biol Cell 14(6):2530–2542
Mori T et al (2006) GENERATIVE CELL SPECIFIC 1 is essential for angiosperm fertilization. Nat Cell Biol 8(1):64–71

Moriyama Y, Kawano S (2003) Rapid, selective digestion of mitochondrial DNA in accordance with the mat A hierarchy of multiallelic mating types in the mitochondrial inheritance of Physarum polycephalum. Genetics 164(3):963–975
Nakamura S, Sato C, Kuroiwa T (1988) Polypeptides related to preferential digestion of male chloroplast nucleoids in Chlamydomonas. Plant Sci 56:129–136
Nakamura S, Aoyama H, van Woesik R (2003) Strict paternal transmission of mitochondrial DNA of Chlamydomonas species is explained by selection against maternal nucleoids. Protoplasma 221(3-4):205–210
Nishimura Y, Stern DB (2010) Differential replication of two chloroplast genome forms in heteroplasmic Chlamydomonas reinhardtii gametes contributes to alternate inheritance patterns. *Genetics*
Nishimura Y et al (1999) The active digestion of uniparental chloroplast DNA in a single zygote of Chlamydomonas reinhardtii is revealed by using the optical tweezer. Proc Natl Acad Sci U S A 96(22):12577–12582
Nishimura Y et al (2002) An mt(+) gamete-specific nuclease that targets mt(−) chloroplasts during sexual reproduction in C. reinhardtii. Genes Dev 16(9):1116–1128
Nishimura Y et al (2006) Active digestion of sperm mitochondrial DNA in single living sperm revealed by optical tweezers. Proc Natl Acad Sci U S A 103(5):1382–1387
Nishimura Y et al (2012) Gsp1 triggers the sexual developmental program including inheritance of chloroplast DNA and mitochondrial DNA in Chlamydomonas reinhardtii. Plant Cell 24 (6):2401–2414
Nishiyama R et al (2002) A chloroplast-resident DNA methyltransferase is responsible for hypermethylation of chloroplast genes in Chlamydomonas maternal gametes. Proc Natl Acad Sci U S A 99(9):5925–5930
Nishiyama R et al (2004) Role of a nonselective de novo DNA methyltransferase in maternal inheritance of chloroplast genes in the green alga, Chlamydomonas reinhardtii. Genetics 168 (2):809–816
Nozaki H et al (2006) Males evolved from the dominant isogametic mating type. Curr Biol 16(24): R1018–R1020
Nunes-Nesi A, Fernie AR, Stitt M (2010) Metabolic and signaling aspects underpinning the regulation of plant carbon nitrogen interactions. Mol Plant 3(6):973–996
Nürnberg A, Kitzing T, Grosse R (2011) Nucleating actin for invasion. Nat Rev Cancer 11 (3):177–187
Pan J, Snell WJ (2002) Kinesin-II is required for flagellar sensory transduction during fertilization in Chlamydomonas. Mol Biol Cell 13:1417–1426
Pan J, Snell WJ (2005) Chlamydomonas shortens its flagella by activating axonemal disassembly, stimulating IFT particle trafficking, and blocking anterograde cargo loading. Dev Cell 9 (3):431–438
Pan JM, Haring MA, Beck CF (1996) Dissection of the blue-light-dependent signal-transduction pathway involved in gametic differentiation of Chlamydomonas reinhardtii. Plant Physiol 112 (1):303–309
Pan JM, Haring MA, Beck CF (1997) Characterization of blue light signal transduction chains that control development and maintenance of sexual competence in Chlamydomonas reinhardtii. Plant Physiol 115(3):1241–1249
Pan J, Wang Q, Snell WJ (2004) An aurora kinase is essential for flagellar disassembly in Chlamydomonas. Dev Cell 6(3):445–451
Pasquale SM, Goodenough UW (1987) Cyclic AMP functions as a primary sexual signal in gametes of Chlamydomonas reinhardtii. J Cell Biol 105:2279–2292
Picard-Bennoun M, Bennoun P (1985) Change in cytoplasmic ribosome properties during gametogenesis in the alga Chlamydomonas reinhardtii. Curr Genet 9:239–243
Pijst HLA et al (1984) Cyclic AMP is involved in sexual reproduction of Chlamydomonas eugametos. FEBS Lett 174(1):132–136

Quesada A, Fernández E (1994) Expression of nitrate assimilation related genes in Chlamydomonas reinhardtii. Plant Mol Biol 24(1):185–194
Rodriguez H, Haring MA, Beck CF (1999) Molecular characterization of two light-induced, gamete-specific genes from Chlamydomonas reinhardtii that encode hydroxyproline-rich proteins. Mol Gen Genet 261(2):267–274
Rosenbaum JL, Witman GB (2002) Intraflagellar transport. Nat Rev Mol Cell Biol 3(11):813–825
Royer HD, Sager R (1979) Methylation of chloroplast DNAs in the life cycle of Chlamydomonas. Proc Natl Acad Sci U S A 76(11):5794–5798
Sager R (1954) Mendelian and non-Mendelian inheritance of streptomycin resistance in Chlamydomonas reinhardi. Proc Natl Acad Sci U S A 40(5):356–363
Sager R, Granick S (1954) Nutritional control of sexuality in Chlamydomonas reinhardi. J Gen Physiol 37(6):729–742
Sager R, Lane D (1972) Molecular basis of maternal inheritance. Proc Natl Acad Sci U S A 69 (9):2410–2413
Sager R, Ramanis Z (1967) Biparental inheritance of nonchromosomal genes induced by ultraviolet irradiation. Proc Natl Acad Sci U S A 58(3):931–937
Sager R, Ramanis Z (1974) Mutations that alter the transmission of chloroplast genes in Chlamydomonas. Proc Natl Acad Sci U S A 71(12):4698–4702
Sager R, Grabowy C, Sano H (1981) The mat-1 gene in Chlamydomonas regulates DNA methylation during gametogenesis. Cell 24(1):41–47
Saito T, Matsuda Y (1991) Isolation and charactreization of Chlamydomonas temperature-sensistive mutants affecting gametic differentiation under nitrogen-starved conditions. Curr Genet 19:65–71
Saito T, Small L, Goodenough UW (1993) Activation of adenylyl cyclase in Chlamydomonas reinhardtii by adhesion and by heat. J Cell Biol 122(1):137–147
Sano H, Sager R (1980) Deoxyribonucleic acid methyltransferase from the eukaryote, Chlamydomonas reinhardi. Eur J Biochem 105(3):471–480
Sano H, Royer HD, Sager R (1980) Identification of 5-methylcytosine in DNA fragments immobilized on nitrocellulose paper. Proc Natl Acad Sci U S A 77(6):3581–3585
Sano H, Grabowy C, Sager R (1981) Differential activity of DNA methyltransferase in the life cycle of Chlamydomonas reinhardi. Proc Natl Acad Sci U S A 78(5):3118–3122
Sanz-Luque E et al (2015) Understanding nitrate assimilation and its regulation in microalgae. Front Plant Sci 6(Oct)
Schmollinger S et al (2014) Nitrogen-sparing mechanisms in Chlamydomonas affect the transcriptome, the proteome, and photosynthetic metabolism. Plant Cell 26(4):1410–1435
Schnell RA, Lefebvre PA (1993) Isolation of the Chlamydomonas regulatory gene. Genetics 134 (3):737–747
Schulz B et al (1990) The b alleles of U. maydis, whose combinations program pathogenic development, code for polypeptides containing a homeodomain-related motif. Cell 60 (2):295–306
Shitara H et al (2000) Selective and continuous elimination of mitochondria microinjected into mouse eggs from spermatids, but not from liver cells, occurs throughout embryogenesis. Genetics 156(3):1277–1284
Siersma PW, Chiang K-S (1971) Conservation and degradation of cytoplasmic and chloroplast ribosomes in Chlamydomonas reinhardtii. J Mol Biol 58(1):167–185
Spit A et al (1998) A role for heterodimerization in nuclear localization of a homeodomain protein. Proc Natl Acad Sci U S A 95(11):6228–6233
Suzuki L et al (2000) A zygote-specific protein with hydroxyproline-rich glycoprotein domains and lectin-like domains involved in the assembly of the cell wall of Chlamydomonas reinhardtii (chlorophyta). J Phycol 36:571–583
Treier U et al (1989) Gametic differentiation in Chlamydomonas reinhardtii: light dependence and gene expression patterns. Arch Microbiol 152(6):572–577

Umen JG, Goodenough UW (2001) Chloroplast DNA methylation and inheritance in Chlamydomonas. Genes Dev 15(19):2585–2597
Vallon O et al (1993) Extensive accumulation of an extracellular L-amino-acid oxidase during gametogenesis of Chlamydomonas reinhardtii. Eur J Biochem 215(2):351–360
van den Ende H, Van Winkle-Swift KP (1994) Mating-type differentiation and mate selection in the homothallic Chlamydomonas monoica. Curr Genet 25(3):209–216
Van Winkle-Swift KP, Salinger AP (1988) Loss of mt+-derived zygotic chloroplast DNA is associated with a lethal allele in Chlamydomonas monoica. Curr Genet 13:331–337
von Gromoff ED, Beck CF (1993) Genes expressed during sexual differentiation of Chlamydomonas reinhardtii. Mol Gen Genet 241(3–4):415–421
Wang Q, Snell WJ (2003) Flagellar adhesion between mating type plus and mating type minus gametes activates a flagellar protein-tyrosine kinase during fertilization in Chlamydomonas. J Biol Chem 278(35):32936–32942
Wang Q, Pan J, Snell WJ (2006) Intraflagellar transport particles participate directly in cilium-generated signaling in Chlamydomonas. Cell 125(3):549–562
Wang ZT et al (2009) Algal lipid bodies: stress induction, purification, and biochemical characterization in wild-type and starchless Chlamydomonas reinhardtii. Eukaryot Cell 8 (12):1856–1868
Weiss RL, Goodenough DA, Goodenough UW (1977) Membrane differentiations at sites specialized for cell fusion. J Cell Biol 72:144–160
Weissig H, Beck CF (1991) Action spectrum for the light-dependent step in gametic differentiation of Chlamydomonas reinhardtii. Plant Physiol 97(1):118–121
Wilson NF, Snell WJ (1998) Microvilli and cell-cell fusion during fertilization. Trends Cell Biol 8 (3):93–96
Woessner JP, Gillham NW, Boynton JE (1986) The sequence of the chloroplast atpB gene and its flanking regions in Chlamydomonas reinhardtii. Gene 44(1):17–28
Sunjoo Joo, Yoshiki Nishimura, Evan Cronmiller, Ran Ha Hong, Thamali Kariyawasam, Ming Hsiu Wang, Nai Chun Shao, Saif-El-Din El Akkad, Takamasa Suzuki, Tetsuya Higashiyama, EonSeon Jin, Jae-Hyeok Lee, Gene regulatory networks for the haploid-to-diploid transition of Chlamydomonas reinhardtii. Plant Physiology:pp.00731.2017
Yan Z et al (2004) SXI1alpha controls uniparental mitochondrial inheritance in Cryptococcus neoformans. Curr Biol 14(18):R743–R744
Zhao H et al (2001) Ectopic expression of a Chlamydomonas mt+-specific homeodomain protein in mt− gametes initiates zygote development without gamete fusion. Genes Dev 15 (20):2767–2777
Zheng Z-L (2009) Carbon and nitrogen nutrient balance signaling in plants. Plant Signal Behav 4 (7):584–591
Zones JM et al (2015) High-resolution profiling of a synchronized diurnal transcriptome from Chlamydomonas reinhardtii reveals continuous cell and metabolic differentiation. Plant Cell 27(10):2743–2769

Thylakoid Ultrastructure: Visualizing the Photosynthetic Machinery

Janina Steinbeck, Megan L. O'Mara, Ian L. Ross, Henning Stahlberg, and Ben Hankamer

Abstract The surface of our planet receives ~3020 ZJ per year of solar energy annually, which is >5000 times the energy required to power our entire global economy (~0.6 ZJ per year). Of this energy, ~43% is photosynthetic active light radiation (PAR) that can be used to drive microalgal biotechnologies for the production of food, fuels, high value products, carbon sequestration, and bioremediation. The first step of all light-driven microalgal processes is light capture. A diverse array of highly efficient, self-assembling, light-responsive "solar interfaces," the thylakoid membranes, have evolved to tap into this abundant, but constantly changing, energy resource to power the biosphere. The photosynthetic machinery within the thylakoids is intricately arranged in a complex 3D architecture and designed to adapt dynamically (i.e., 4D: representing changes in 3D structures over time) to constantly changing environmental conditions, to maximize solar to chemical energy conversion. The ATP and NADPH generated are used to produce the complex set of biomolecules that collectively form biomass. Here, we review the structural organization of these amazing photosynthetic interfaces in the model organism *Chlamydomonas reinhardtii* and summarize recent advances in structural biology, which underpin the development of next-generation atomic resolution dynamic simulations of these systems. Revealing such a 4D atlas of 3D structures in atomic resolution detail is of fundamental importance to enable structure-guided design of natural photosynthetic systems for biotechnological application and to provide a blueprint for the design of nanoscale components, which are the building blocks for the development of next-generation artificial solar fuel systems.

J. Steinbeck
Institute for Molecular Bioscience, The University of Queensland, St Lucia, QLD, Australia

Westfälische Wilhelms-Universität Münster, Münster, Germany

M.L. O'Mara
Research School of Chemistry, The Australian National University, Canberra, ACT, Australia

I.L. Ross • B. Hankamer (✉)
Institute for Molecular Bioscience, The University of Queensland, St Lucia, QLD, Australia
e-mail: b.hankamer@uq.edu.au

H. Stahlberg
Center for Cellular Imaging and NanoAnalytics, Biozentrum, University of Basel, Mattenstr. 26, 4058 Basel, Switzerland

M. Hippler (ed.), *Chlamydomonas: Biotechnology and Biomedicine*, Microbiology Monographs 31, DOI 10.1007/978-3-319-66360-9_7

1 Introduction

1.1 Global Algal Biotechnology Challenges

The global economy is valued at approximately $119 trillion (Tn) per year (C.I.A. 2017) and is powered by the $6 Tn per year energy sector. By 2050, expansion of the human population to ~9.6 billion people (UN 2015) and continued global economic growth, is forecasted to require 50% more fuel (IEA 2010), 70% more food (FAO, UN 2009), 50% more freshwater (OECD 2012), as well as CO_2 emission cutoff of 80% (IPCC 2014) to maintain political, social, fuel, and climate security. Microalgae sit at the nexus of these challenges as they tap into the huge energy resource of the sun (i.e., 3020 ZJ per year of solar energy received by the Earth surface of which 43% is photosynthetic active light radiation compared to ~0.6 ZJ per year global energy demand; 1 ZJ = 1×10^{-21} J[10], British Petroleum 2015; Ringsmuth et al. 2016), to capture CO_2 and H_2O and drive the production of the food, fuel, and atmospheric oxygen that supports life on the Earth. Consequently, microalgae provide a basis for the development of solar-driven biotechnologies for the production of high value products (e.g., omega-3 fatty acids and antioxidants), recombinant proteins (Gregory et al. 2013; Tran et al. 2013), foods and food supplements (e.g., proteins), feedstocks (e.g., animal and aquaculture feeds), and renewable fuels (crude oil, biodiesel, ethanol, methane, and H_2).

1.2 Solar Interfaces: Toward Structural Designs Inspired by Nature

Over ~3 billion years of natural selection, microalgae have evolved a diverse array of highly efficient, self-assembling, light-responsive "solar interfaces." Intriguingly, although these thylakoid structures adapt to light, the cross section of grana and pseudo-grana (~400 nm × ~1000 nm) (Fig. 1, Mustárdy and Garab 2003; Shimoni et al. 2005; Brumfeld et al. 2008; Nevo et al. 2012; Ford and Holzenburg 2014; Mullineaux 2014; Pribil et al. 2014) is of the same order of magnitude as the wavelength of the incoming light (PAR at 400–700 nm), with fascinating implications for energy delocalization and the operation of quantum processes at ambient temperatures (Engel et al. 2007). Via these thylakoid membranes, microalgae tap into the abundant, but constantly changing, solar energy resource. The photosynthetic machinery is not only intricately arranged in a complex 3D structure of membranes and compartments within our cells but also designed to adapt dynamically in 4D (i.e., 3D + time) to these constantly changing light conditions to maximize chemical energy storage in the form of ATP and NADPH. These two molecules are produced by the light-driven reactions of photosynthesis and are subsequently used by other cellular processes to synthesize the complex set of biomolecules that collectively form biomass. Revealing the dynamic 3D structures

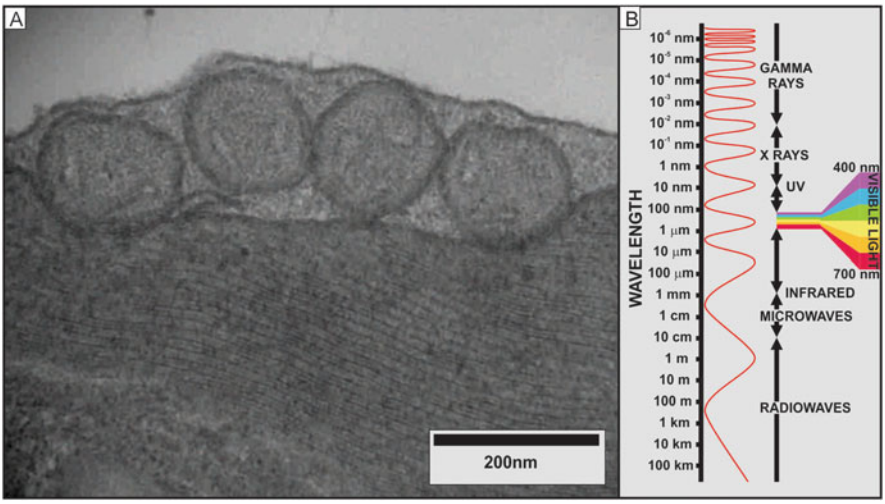

Fig. 1 Nature's "diffraction grating." Microalgae of 10–100 μm in diameters contain interconnected stacked membrane structure called "thylakoid membranes," *shown in A* for the algae of *Chlamydomonas reinhardtii* (image shows *stm3* mutant (Mussgnug et al. 2005) taken by Alastair Mc Dowall). These membrane stacks are typically ~400 nm in diameter and ~1000 nm long, which have dimensions that are similar to the wavelength of the incoming light rays of the photosynthetically active radiation (400–700 nm, *shown in B*). These dimensions may allow the photosynthetic membranes to exploit quantum processes and phenomena called "energy delocalization" to more efficiently store and process incoming light energy

of the *Chlamydomonas reinhardtii* thylakoid membranes at the atomic level, and how they restructure during adaptive processes, is of fundamental importance for our understanding of the detailed mechanisms controlling photosynthetic operation and to enable structure-guided design of natural photosynthetic systems for biotechnological application.

In recent years, major technological advances have been made in structural biology, which now enable the visualization of real-time movements of individual proteins within live cells, molecular resolution cellular cryo-electron tomography, and atomic resolution structure determination of individual membrane proteins using single-particle analysis. A multitude of studies at different resolutions have provided individual pieces of the complex structural 3D (and indeed 4D) puzzle of the solar interfaces (Fig. 2d). We now know that the photosynthetic membranes contain a range of membrane protein complexes that conduct photosynthesis. Photosystem I (PSI) and Photosystem II (PSII) capture photons and use the derived energy to pump electrons to higher energy levels. These are in turn used by neighboring cytochrome b_6f (Cyt b_6f) complexes, which transfer protons across the biological membrane into the thylakoid lumen. The increased concentration of protons yields a proton gradient across the thylakoid membrane. This gradient is used by ATP synthases (ATPase) to synthesize ATP, which is the central energy currency of the cell used to drive cellular processes. These membrane proteins are

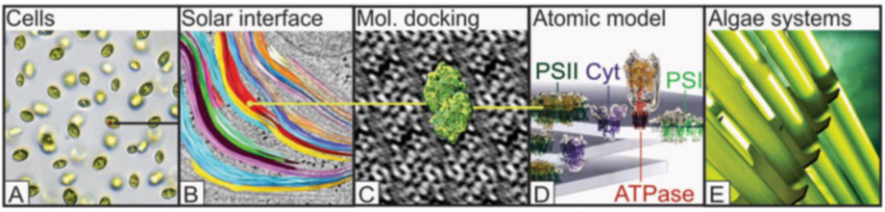

Fig. 2 Resolving the solar interfaces to enable structure-guided design. (**a**) Microalgae cells as seen by a light microscope (courtesy Gisela Jakob). (**b**) The thylakoid membranes (solar interfaces) visualized by electron microscopy. (**c**) PSII membrane proteins can be arranged in regular patterns (pseudo-2D crystals) in these membranes, here shown in a computer reconstruction from electron microscopy images, with an atomic model of PSII (*green*) superimposed. (**d**) The membrane proteins involved in the photosynthetic machinery PSII, cyt b_6f, PSI, and ATPase, are shown as cartoon in a hypothetical arrangement in membranes. (Models generated, using the UCSF Chimera software, version 1.9). (**e**) Such models can facilitate structure-guided design of next-generation high-efficiency microalgae systems with increased photon conversion efficiency and assist bioinspired design of artificial solar fuel systems

specifically arranged within the thylakoid membranes to optimize the efficiency of the functional photosynthetic units.

Based on recent technological advances in structural biology, we are now tantalizingly close to being able to resolve at molecular resolution the 3D arrangement of the photosynthetic machinery of algae (Fig. 2a) and solar interfaces within them (Fig. 2b). Atomic structures of the involved protein complexes can now technically be docked into the 3D tomograms of algae (Fig. 2c) to yield 3D atomic models of the thylakoid membranes (Fig. 2d), containing the above photosynthetic complexes. Such models provide the basis for extension into 4D, using dynamic simulations to analyze how these systems respond to light. These 3D and 4D atlases are of fundamental importance for our understanding of these systems, as they reveal critical principles for the design of self-assembling, low-cost, and highly efficient solar interfaces that can be developed to generate competitive microalgal biotechnologies (Fig. 2e) and bioinspired artificial solar fuel technologies (e.g., H_2 from water and C-based fuels from CO_2).

2 Zooming into the Cell: A Brief Historical Perspective

2.1 *Ultrastructural Studies of* Chlamydomonas reinhardtii *from 1950 to 1970*

Over the past 60 years, microscopy has increased in spatial resolution by three orders of magnitude from 200 nm resolution to 0.2 nm resolution or 2 Å (Staehelin 2003). Advances in transmission electron microscopy (TEM) in the 1950s exceeded the 2D resolution of light microscopes (200 nm), allowing details as small as 10 nm

to be resolved, leading to the discovery of thylakoid membranes and the first characterization of their 3D architecture. A 2D atlas of wild-type Chlamydomonas cells was determined using electron microscopy, with a particular focus on the chloroplast ultrastructure (Sager and Palade 1954, 1957). This was followed by the first 3D model reconstruction of a *C. reinhardtii* cell in 1972, which was obtained by imaging serial section electron microscopy (Schötz 1972). Estimations of chloroplast and mitochondria volumes were in good agreement with a study performed by Boynton et al. (1972) and it was concluded that the chloroplast occupies ∼40% of the total cell volume, whereas mitochondria occupy only 1–3%. However, cell preparations for EM generally involved chemical fixation at room temperature or 0 °C with fixatives such as glutaraldehyde and osmium tetroxide, dehydration, and subsequent resin embedding. Resin-embedded samples were cut into thin sections of 200–500 Å thickness and stained with uranyl acetate (Sager and Palade 1957; Johnson and Porter 1968; Schötz 1972). Such chemical fixation and dehydration protocols typically introduce artifacts and the thick sections used, in turn, further limited resolution. As a result, in recent years most structural studies have been conducted at ultralow temperature in vitreous ice (see "cryo" conditions, Sect. 3).

Further analysis of the *C. reinhardtii* chloroplast showed it to have a cup-shaped structure and to surround the nucleus. In the chloroplast, distinctive structures were identified including an asymmetrically positioned, light-sensitive eyespot (enabling phototropic cell movement) and the pyrenoid with surrounding starch deposits (Fig. 3a). The pyrenoid is the site of the so-called dark reactions of photosynthesis (i.e., light independent) and carbon concentrating mechanisms (Badger et al. 1998; Meyer and Griffiths 2013 for review). The thylakoid membranes, which are the site of the "light reactions" of photosynthesis, appear in electron micrographs as flat discs (Figs. 1 and 3b). Stromal regions free of thylakoids contain soluble proteins. The thylakoid membranes of green algae are reportedly less organized (pseudo-grana) than the highly packed multidisc grana and connecting stromal lamellae of higher plants (e.g., Austin and Staehelin 2011). Nevertheless, as Figs. 1 and 3b show, thylakoids of *C. reinhardtii* can exhibit a high level of organization with pseudo-grana frequently arrayed in stacks of two to ten discs, which merge and bifurcate along the length of the thylakoids (Goodenough and Levine 1969). In comparison, grana stacks of higher plants can reportedly contain 10–100 thylakoid discs (Staehelin 2003). A range of factors may influence the size of the granal stacks including environmental and sample preparation conditions, LHCII levels (Mussgnug et al. 2005, 2007), thylakoid lipid composition, photoautotrophic or mixotrophic growth conditions, and the cell cycle state: stacks of larger size ($n > 5$) are reported to form in photoautotrophic compared to mixotrophic growth conditions. Cells in the stationary phase are also reported to form larger stacks as well as DCMU-treated cells (Goodenough and Levine 1969), whereas low ionic strength can prevent membrane stacking (Goodenough and Levine 1969; see also Barber and Chow 1979 for mechanism in higher plants). Mutants impaired in the synthesis of active components of photosynthetic complexes show alterations in membrane ultrastructure, indicating that the photosynthetic complexes themselves influence

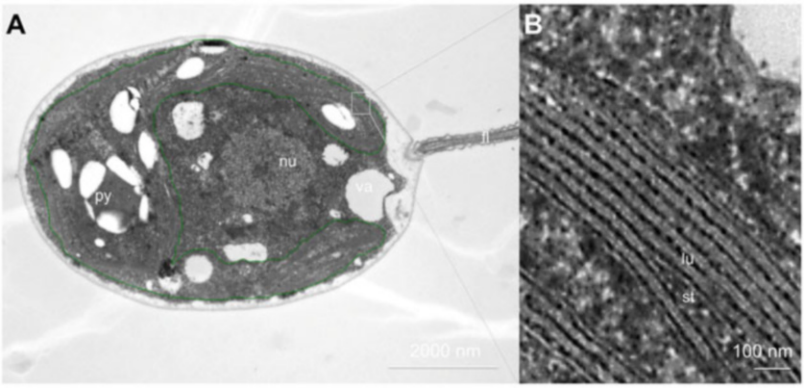

Fig. 3 *Chlamydomonas reinhardtii* wild-type cell grown under mixotrophic conditions fixed with glutaraldehyde and osmium tetroxide and stained with uranyl acetate. Resin-embedded cells were cut into 50-nm-thin sections and screened with a transmission electron microscope (JEOL JEM1010, Veleta Olympus SoftImaging digital camera) by Richard Webb. (**a**) Cross section of wild-type cell with cup-shaped chloroplast marked in *green*. *py* pyrenoid with surrounding starch pellets, *nu* nucleus, *va* contractile vacuole, *fl* flagella. (**b**) Close-up of thylakoid membrane stack of eight bilayer pairs. *lu* dark regions mark the thylakoid lumen, *st* the stromal side merges into two single bilayers

the thylakoid structure in which they are embedded: two PSI mutants without active P700 were found to have hyper-stacked thylakoids ($n > 6$), whereas thylakoids from PSII mutants with inactive cyt_{559} as well as a plastocyanin mutant formed more single discs with the tendency to unstack (Goodenough and Levine 1969).

2.2 *Freeze-Fracture (-Etch) and Immunogold Labeling Studies from 1970 to 1990: 3D Protein Distribution in Membranes*

Evidence for structural segregation of protein complexes in different compartments of thylakoids was first described by freeze-fracture studies. The freeze-fracturing of frozen biological specimen at −100 °C can split membranes along the central hydrophobic plane of their bilayer to produce two complementary fracture faces. The structural details are preserved and enhanced by shadowing to generate platinum–carbon replicas under vacuum (Moor and Mühlethaler 1963). Goodenough and Staehelin found that *C. reinhardtii* membrane surfaces of stacked membranes differed from those of unstacked thylakoids in that they carried dense populations of regularly spaced large particles (Goodenough and Staehelin 1971). These large particles (13–20 nm diameter) were identified as PSII–LHCII particles, as they were absent in PSII mutants (Fig. 4b, Wollman et al. 1980; Olive and Vallon 1991). Freeze-fracture investigations of a range of

mutants were supplemented with immunogold labeling of antibody-tagged protein complexes and collectively led to the following conclusions (reviewed in Olive and Vallon 1991; Staehelin 2003): approximately 80% of PSII particles were exclusively found in thylakoid grana stacks (Fig. 4c), while over 90% of PSI–LHCI complexes (10–16 nm in diameter) were associated with the stroma lamellae (Fig. 4d, Olive and Vallon 1991). ATP synthase complexes (~8 nm in diameter) were found predominantly in the stromal lamellae (density in spinach, 700 per μm^2, Miller and Staehelin 1976), while cytochrome b_6f was reported to be equally distributed between stacked and stromal thylakoids. The cyt b_6f monomer is reported to have a complex size of ~8.5 nm. A cyt b_6f-deficient mutant lacked not only these 8.5 nm particles but also a range of differently sized complexes suggesting that it forms a diverse set of supercomplexes by multiple interactions with many proteins (Olive and Vallon 1991). LHCII trimers were reported to be present as individual particles (~8 nm) in the grana as well as stromal lamellae and in PSII–LHCII supercomplexes in stacked grana (Olive et al. 1981). Experiments with purified LHCII proteins in reconstituted lipid vesicles showed that these complexes concentrated in the central adhesion zone of two vesicles and that an increase in the ionic strength induced the formation of membrane stacks (McDonnel and Staehelin 1980). This led to the conclusion that LHCII supports electrostatic attraction between thylakoid membranes and is

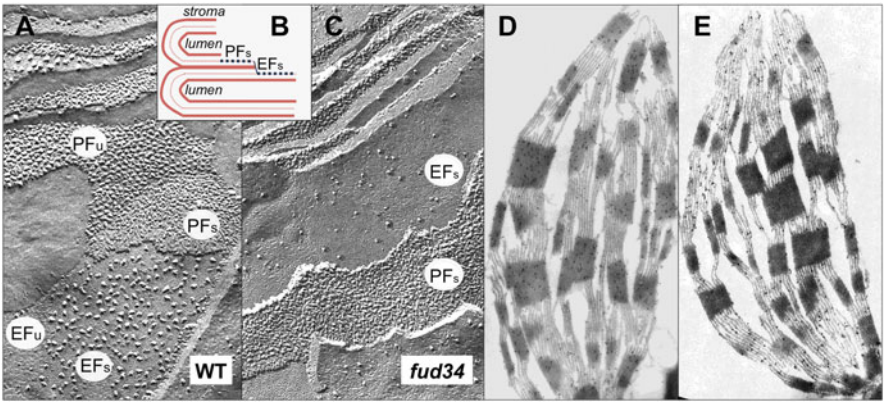

Fig. 4 Freeze-fracture of *Chlamydomonas reinhardtii* (**a**, **b**, **c**) and immunogold images of spinach thylakoid membranes (**d**, **e**) elucidating the distribution of PSII and PSI. (**a**, **b**, **c**) Fracture faces of thylakoid membranes EFs and PFs belong to stacked regions, EFu and PFu, to unstacked regions (*PF* protoplasmic fracture face of the membrane, *EF* exoplasmic fracture face). The large particles present in the stacked EFs regions of the wild type (**a**, ~1300 EF particles per μm^2) are absent in the PSII-deficient mutant *fud34* (**b**, ~300 EF particles per μm^2). (**d**, **e**) localization of PSI and PSII centers in thin sections of isolated spinach thylakoids labeled with antibodies to (**c**) the D2 polypeptide of PSII and (**d**) PSI-A1 and A2. PSI centers are located in stroma thylakoids and end membranes of grana, while PSII centers are mostly located in stacked regions of the membrane. x35,000. Images are a kind courtesy of Olivier Vallon, Jacqueline Olive, Michel Recouvreur, and Francis-André Wollman

therefore important for the stacking process. This is consistent with the higher plant studies of Barber and Chow (1979) and Standfuss et al. (2005).

In response to different environmental conditions including varying light intensities, different amounts of stacking have been observed spectroscopically, biochemically, and structurally. When PSII receives excessive excitation energy, LHCII complexes become phosphorylated and at least some reversibly translocate to the stromal lamellae, where they eventually attach to PSI, resulting in the thylakoids becoming less stacked (Delosme et al. 1996; Finazzi 2005; Chuartzman et al. 2008; Iwai et al. 2008). This so-called state transition from state 1 to state 2 helps to balance the excitation energy between the two photosystems (Allen et al. 1981). Other protein complexes that redistribute during state transitions to regulate the electron transport chain include the cytochrome b_6f complex and plastocyanin (Staehelin 2003). Up to 20% of cyt b_6f complexes translocate from thylakoid stacks to the stroma lamellae when cells shift to state 2 (Vallon et al. 1991). In dark-adapted spinach leaves, plastocyanin was twofold more concentrated in stromal thylakoids, but migrated to thylakoid stacks in the light (Haehnel et al. 1989), indicating a switch from cyclic electron flow around PSI to linear electron flow from PSII to PSI upon dark-to-light transition in accordance with spectroscopic data (Alric et al. 2010; Alric 2014).

Freeze-fracture and immunogold labeling techniques with a resolution of about 50 Å still provide some of the best images of lateral distribution of photosynthetic complexes with unique information regarding the localization, heterogeneity, dimensions, and shapes of specific photosynthetic complexes embedded within the thylakoid membranes. However, they provide only a few pieces of the puzzle and static snapshots of particular time points and lack atomic resolution detail.

2.3 Structures of the Photosynthetic Complexes at Atomic Resolution Revealed by Crystallography since 1990

A common feature of the photosynthetic electron transfer chain components is that they were first identified as photoinduced absorption changes and characterized on a spectral basis. Over time, these components were biochemically identified in terms of subunits, cofactors, and protein complexes (see chapter "Chlamydomonas: Bioenergetic Pathways in the Chloroplast Photosynthetic Electron Transfer" for a more functional description of the photosynthetic subunits). Ultimately, atomic resolution structures were obtained. High-resolution crystal structures relate structure to function and are critical to elucidate the mechanism of energy transfer within them. These high-resolution structures can be mapped into the lower-resolution 3D organization of the thylakoid membrane to yield pseudo-atomic resolution atlases. The following paragraphs briefly summarize the structures of the main photosynthetic complexes of *C. reinhardtii* and of related organisms of photosynthetic lineage where high-resolution structures are not yet available for *C. reinhardtii*—for a detailed

description of the molecular structures of the complexes, the reader is encouraged to read further literature provided in the text.

2.3.1 Crystallographic Techniques Leading to Atomic Resolution

X-ray diffraction (XRD), nuclear magnetic resonance (NMR), and electron crystallography (cryo-EM) of two-dimensional (2D) crystals have been used in the determination of membrane protein structures. With over 80% of the total entries in the Protein Data Bank (PDB), X-ray crystallography has been used to determine the majority of protein structures to date. Among the vast numbers of protein structures deposited in the PDB, membrane proteins represent less than 2% of the entries (Carpenter et al. 2008; White 2016), although they are estimated to contribute to 20–30% of the proteome of organisms (Krogh et al. 2001). This discrepancy highlights the challenge of solving membrane protein structures including those involved in photosynthesis. Proteins extracted from biological membranes are by their nature insoluble in aqueous systems and are therefore solubilized in detergents to prevent aggregation. Additionally, they are often flexible and unstable once extracted. Collectively, these properties lead to technical challenges including difficulties in expression, solubilization, purification, crystallization or cryopreservation, data collection, and structure determination, thereby increasing the number of variable parameters and making the study of such proteins both time-consuming and expensive. Despite these difficulties, structural biology of membrane proteins has enjoyed rapid progress since the 1990s. The first atomic resolution crystal structure of an integral membrane protein published was that of the photosynthetic reaction center of the purple bacteria *Rhodopseudomonas viridis* at 3 Å resolution (Deisenhofer et al. 1985), which was celebrated with the award of a Nobel Prize. X-ray crystallography had amassed a large community of users and method developers who setup high-throughput protocols for crystallization and automated data processing, to enable structure determination. This technique, however, requires intermolecular attraction and accurate biochemical alignment of the membrane proteins to form a 3D crystal, which is challenging in itself and can restrict or alter the conformational state of the protein. Electron microscopy applied to membrane-reconstituted 2D crystals of membrane proteins has the advantage that it requires less protein and provides images of membrane proteins embedded in a near-native lipid bilayer environment (Renault et al. 2006). Since the recent invention of direct electron detector cameras for electron microscopy in 2013 (see Sect. 3.4), the method of "single-particle cryo-electron microscopy" (see Sect. 3.6) now allows for the direct determination of the atomic structure of detergent-solubilized membrane proteins by electron microscopy imaging and image processing. This fast and efficient method has provided an amazing opportunity to study the atomic structure of membrane proteins from small quantities of samples and in very short times.

2.3.2 Photosystem II and Light-Harvesting Complexes II

High-resolution crystal structures of the PSII core complex have been solved by X-ray crystallography for two cyanobacterial species, *Thermosynechococcus vulcanus* and *Synechococcus elongatus* (Zouni et al. 2001; Kamiya and Shen 2003; Biesiadka et al. 2004; Ferreira et al. 2004; Loll et al. 2005; Guskov et al. 2009; Umena et al. 2011; Suga et al. 2014) and the red alga *Cyanidium caldarium* (Ago et al. 2016). This PSII core complex includes the heterodimeric D1/D2 reaction center and cytochrome b_{559} (Cyt b_{559}) which coordinates the key electron transfer components, the flanking intrinsic light-harvesting proteins CP43 and CP47, as well as PsbO of the oxygen-evolving complex (which stabilize the water-splitting Mn cluster) and the low molecular weight subunits PsbH, I, J, K, L, M, T, U, X, Z (Fig. 5a, e). The cyanobacterial PSII structure has been extended to analyze the different S states of the water oxidation cycle using time-resolved X-ray free electron laser analyses (Kern et al. 2013, 2014), to provide important insights for atomic resolution 4D modeling. Such crystal structures from cyanobacteria have served as models for chloroplast PSII complexes of higher plants. Although the cyanobacterial and higher plant PSII complexes have many fundamental similarities, there are also substantial differences between them including the composition of the extrinsic subunits of the water-oxidizing complex and some of the small (10–15 kDa) structural membrane protein subunits. A near-atomic resolution structure of spinach photosystem II–LHCII supercomplex at 3.2 Å was very recently solved by cryo-electron microscopy (Wei et al. 2016). Differences may reflect an adaptation to the very different antenna systems (extrinsic cyanobacterial phycobilisomes vs. intrinsic plant and algal chlorophyll a/b light- harvesting complex proteins) (Büchel and Kühlbrandt 2005). Indeed, these structural differences can affect specific crystal contacts, and presumably this and their lower thermal stability provide two explanations of why higher plant PSII complexes and those of microalgae have not yet been solved to atomic resolution.

Associated with PSII are the light-harvesting complexes (LHCII), which are reported to be the most abundant membrane proteins on earth, accounting for up to 50% of total chlorophyll in algal and plant thylakoid membranes. Two minor LHCIIs, CP26 and CP29, mediate energy transfer from the peripheral major trimeric LHCIIs to CP43/CP47 or D1/D2 in *C. reinhardtii*. The structure of these complexes are highly conserved between plants and algae, with the difference that the minor LHC CP24 is missing in algae, and the group of major trimeric LHCII genes divides into four instead of three types (see Minagawa 2009 for detailed review). The first atomic resolution structure of major LHCII was revealed by cryo-electron microscopy of 2D-arrayed crystals of detergent-solubilized pea LHCIIs at 3.4 Å (Kühlbrandt et al. 1994). Ten years later, X-ray crystallography of three-dimensional crystals solved the structures from spinach at 2.7 Å and from pea at 2.5 Å (Liu et al. 2004; Standfuss et al. 2005). The crystal structure of the minor LHCII CP29 from spinach was solved in 2011 (Pan et al. 2011), but the structure of CP26 has not been reported. One difference between CP29 and CP26 is that CP29

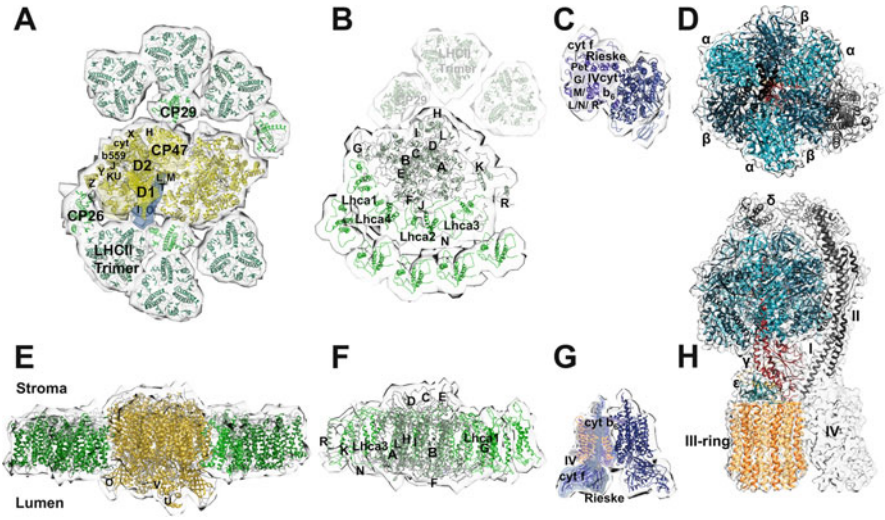

Fig. 5 The molecular players involved in photosynthesis. Photosynthetic membrane proteins are shown as top view (stromal side, **a**, **b**, **c**, **d**) and side view (**e**, **f**, **g**, **h**) projections, as they group together to form presumed supercomplexes in the membrane plane modeled with the software UCSF Chimera (version 1.9). Electron densities at 30 Å resolution indicated as gray shadows around the crystal structures were calculated using the software EMAN2. (**a**, **e**) The photosystem II supercomplex in the $C_2S_2M_2L_2$ state with six LHCII trimers (*dark green*) and four LHCII monomers (*light green*) attached to the PSII core dimer (*yellow*). The subunits of one PSII core are labeled (A) with the oxygen-evolving complex at the luminal side (E). Crystal structure models used: 3arc for PSII core and 3wu2 for the oxygen-evolving complex (Umena et al. 2011), 3bhw for LHCII trimer (Standfuss et al. 2005) and 3pl9 for CP29 (Pan et al. 2011). (**b**, **f**) The photosystem I (core in *gray*, LHCI subunits in *green*) with the crystal structure from pea (3lw5, Amunts et al. 2010) as a model, and one additional LHCI-ring to the four LHCI present in higher plants modeled to the core according to Drop et al. (2014b). Locations of PSI subunits are indicated within the crystal structure. Additionally, the location of the LHCII trimers and CP29 attached to PSI in state 2 is indicated in more *transparent colors* in (**b**). (**c**, **g**) The Chlamydomonas cytochrome b_6f crystal structure (1p90, Stroebel et al. 2003). Subunits are labeled at one side of the cyt b_6f dimer. (**d**, **h**) The CF_0–CF_1–ATP synthase with the stromal CF_1 subunit (with $(\alpha,\beta)_3$, γ, δ, ε) and the CF_0 subunit (with I, II, III, and IV in the probable stoichiometry of 1:1:13:1 for *C. reinhardtii*). The whole CF_0–CF_1 complex functions as a rotary proton-driven motor, in which the rotary subunits are III, γ, and ε, and the stationary subunits are I, II, IV, δ, α, and β. This overall structure is a mosaic of high-resolution molecular structures of the CF_0 14(III)-ring from spinach (2w5j, Vollmar et al. 2009), the CF_1 subunits plus the stator (2wss, Rees et al. 2009), and more subunits of the stator (2cly, Dickson et al. 2006)

lacks a "trimeric motif" suggesting a specific role of this monomeric protein, while trimerization of CP26 was observed in an Arabidopsis mutant deficient in one of the major LHCII polypeptides (Hobe et al. 1995; Minagawa et al. 2001).

The three-dimensional structure of the Chlamydomonas PSII–LHCII supercomplex has been determined to a resolution of 13–30 Å by averaging negatively stained single-particle images (Nield et al. 2000), and similar structures have been inferred from 2D projection maps by Tokutsu et al. (2012) and Drop et al.

(2014a). In 2000, a supercomplex consisting of two LHCII trimers and four LHCII monomers per PSII core dimer, similar to the C_2S_2-type PSII supercomplex of plants was described with the dimensions of 35 nm × 17.5 nm × 13.5 nm (Nield et al. 2000). It was long thought that the CP24 monomer of plants missing in algae is required for the binding of additional LHCII trimers to form larger $C_2S_2M_2$–PSII supercomplexes. However, 2D supercomplexes even larger than the $C_2S_2M_2$–PSII from plants with six LHCII trimers attached per PSII core dimer have been reported in *C. reinhardtii* (Tokutsu et al. 2012; Drop et al. 2014a). Depending on the state of the cell, several subtypes of PSII complexes appear to be present in the thylakoid membrane. PSII megacomplexes are predominant in state 1 (e.g., low-light conditions or artificially induced by DCMU incubation in the dark, see Fig. 5a), while in state 2 (e.g., anaerobic or high-light conditions or artificially induced by the proton uncoupler CCCP) the core PSII core complex is predominant, with LHCII dissociation from it being triggered by phosphorylation during state transition (Iwai et al. 2008; see also Sect. 2.2.3 for state transition).

2.3.3 Photosystem I, Light-Harvesting Complexes I, Its Electron Donor Plastocyanin, and Electron Acceptor Ferredoxin

Eukaryotic PSI cores characterized to date are generally monomers (Ben-Shem et al. 2003; Amunts et al. 2007, 2010; Mazor et al. 2015; Qin et al. 2015, structures available to date are from pea), while those of cyanobacteria are commonly trimeric (Boekema et al. 1987; Bibby et al. 2001; Jordan et al. 2001). The Chlamydomonas PSI is very similar to that of higher plants, consisting of the highly conserved PsaA/PsaB core heterodimer and subunits (PsaC–PsaO) surrounding it. The main difference between the higher plant and Chlamydomonas reinhardtii PSI is that the light-harvesting apparatus bound to the core can be larger in Chlamydomonas. While the crystal structure of the pea PSI–LHCI supercomplex shows only four LHCIs attached to the core (2.8 Å resolution, Mazor et al. 2015; Qin et al. 2015), single-particle images of the PSI–LHCI supercomplex from *C. reinhardtii* suggest 14 (Germano et al. 2002), 11 (Kargul et al. 2003), 6 (Kargul et al. 2005), or 9 LHCI polypeptides (Drop et al. 2011) that are attached to the core in an asymmetric manner (i.e., on the PsaG/F/K side). This semicircle shaped "LHCI belt" is formed from the PsaG end in the order Lhca1, Lhca4, Lhca2, and Lhca3 in higher plants. In Chlamydomonas, which encodes nine LHCI genes, it is suggested that the "LHCI belt" contains a second row of light-harvesting complexes (see Fig. 5b, f, Kargul et al. 2003; Drop et al. 2011). Another difference between *C. reinhardtii* and higher plants is that the chlorophyll fluorescence of the *C. reinhardtii* PSI–LHCI complex with a far-red peak at 715–717 nm is of shorter wavelength than that of higher plants (Bassi et al. 1992; Knoetzel et al. 1992). The structural differences accounting for this fluorescence shift are still under debate, and a higher resolution structure of Chlamydomonas PSI would assist with answering these questions.

Under state 2 conditions, LHCII proteins detach from PSII and are reported to associate with PSI, though not necessarily stoichiometrically (see Sects. 2.2 and

2.3.2). An enlarged PSI supercomplex associated with the minor LHCII protein CP29 (Kargul et al. 2005) and one to two LHCII trimers at 20 Å resolution was isolated from *C. reinhardtii* (Drop et al. 2014b). These LHCII subunits are located at the PsaH/L site of PSI, opposite to the "LHCI belt." PsaH (which is not present in cyanobacteria) is also thought to prevent trimerization of PSI in eukaryotes (Scheller et al. 2001). The largest complex observed has an antenna size of 340 chls/P_{700}. The phosphorylation pattern of the LHCII subunits is not trivial: while LHCII types I, II, and IV are phosphorylated when associated with PSI, LHCII type III and CP29 were found to be phosphorylated when associated with PSII, but not when bound to PSI (Drop et al. 2014b). Also LhcSR3, a protein involved in the dissipation of excess light energy at PSII, is found to partially associate with PSI under high-light conditions (Bergner et al. 2015).

The structures of both the electron donor and acceptor of PSI have been determined at high resolution, yielding a more complete picture of the charge transfer mechanism of PSI: the crystal structure of Chlamydomonas plastocyanin was published at 1.5 Å resolution (Redinbo et al. 1993) and that of the alternative electron donor cytochrome c_6 (Cyt c_6) at 1.9 Å (Kerfeld et al. 1995). The binding site of plastocyanin to PSI is reported to be PsaF (Hippler et al. 1989; Meimberg et al. 1999). While several high-resolution structures exist for different ferredoxin isoforms, e.g., the [2Fe-2S] ferredoxin from *S. platensis* (Fukuyama et al. 1980), from spinach at 1.7 Å (Binda et al. 1998), or the green alga *Chlorella fusca* at 1.4 Å (Bes et al. 1999), only a homology predicted model based on the structure of *C. fusca* is available for *C. reinhardtii* (Garcia-Sanchez et al. 2000). The docking site of ferredoxin to PSI is thought to be at PsaD and E (reviewed in Sétif 2001; Sétif et al. 2002). Moreover, the structure of the complex that is formed by ferredoxin and ferredoxin–NADP reductase (FNR), which is known to bind to PSI, is also solved to 2.2 Å for spinach (Karplus et al. 1991) and 2.6 Å for maize (Kurisu et al. 2001).

The last major photosynthetic complex structure to be elucidated is that of the PSI–cytochrome b_6f supercomplex, which is able to facilitate cyclic electron transport (CET) around PSI. The formation of this complex has long been proposed to enable the promotion of CET in favor of linear electron flow under conditions where the demand for ATP is enhanced. A complex consisting of all important subunits to perform CET was reported in 2010 and was shown to have functional CET activity in vitro (Iwai et al. 2010). However, full structural evidence for the existence of this elusive complex is still missing. In higher plants, the structure of an alternative CET complex of two PSI complexes associated with the NAD(P)H dehydrogenase (NDH), which is able to accept electrons from PSI as an alternative route to the major CET, has been determined to a resolution of 20 Å (Kouril et al. 2014). This NDH complex is absent in *C. reinhardtii*, but an Nda2 complex homologue fulfilling the same function is present (Jans et al. 2008).

2.3.4 The Cytochrome b_6f Complex

The crystal structure of Chlamydomonas cytochrome b_6f complex was solved at 3.1 Å in 2003 (Stroebel et al. 2003, Fig. 5c, g). In the same year, another crystal structure of the cytochrome b_6f complex from the cyanobacterium *Mastigocladus laminosus* was published (Kurisu et al. 2003). Both structures exhibited similarities to the mitochondrial cytochrome bc_1 complex, suggesting that they evolved from a common ancestor, in which cytochrome *b* and the Rieske iron–sulfur protein (ISP) were central. The chloroplast and mitochondrial complexes can exist as dimers in the membrane and are thought to operate via the Q-cycle, in which they couple the electron transfer from plastoquinol (or ubiquinol) to plastocyanin (or cytochrome *c*) to transfer protons across the membrane, thereby generating a proton motif force (pmf, for a more detailed description, see chapter "Chlamydomonas: Bioenergetic Pathways in the Chloroplast Photosynthetic Electron Transfer"). While the transmembrane helices of the main subunits cytochrome b_6, cytochrome *f*, Rieske ISP, and subunit IV are almost identical, the transmembrane region occupied by the small subunits PetG/L/M/N of b_6f appears partially filled with a specific lipid in bc_1. At the extrinsic surfaces, two important differences become obvious: although cyt *f* and c_1 are functional homologs, they are not related in sequence. Therefore, the c-haem iron binds at different positions. Both cyt *f* and the Rieske ISP are shifted in their luminal position in comparison to their bc_1 counterparts. Moreover, two additional cofactors in the form of chlorophyll *a* and β-carotene are present in b_6f. Beside two highly conserved b-haems at the stromal side, a third additional b-haem is covalently bound to cyt b_6 located between the b_H-haem and the Q_i site. The identification of this extra haem at a position that is accessible from the stroma gave rise to the idea that electrons might be directly recycled from the acceptor side of PSI to an oxidized quinone at Q_i as part of the cyclic electron transfer around PSI (reviewed in Baniulis et al. 2008; Johnson 2011).

2.3.5 The ATP Synthase (F-type ATPase)

The ATP synthase enzyme is a molecular motor that uses a transmembrane pmf generated by the photosynthetic electron transport chain to catalyze ATP synthesis. This multi-subunit complex divides into the transmembrane CF_0 subunit (with subunits I, II, III, and IV in the probable stoichiometry of 1:1:13:1 for *C. reinhardtii*) and the stromal CF_1 subunit (with subunits $(\alpha,\beta)_3$, γ, δ, ε, Fig. 5d, h). Proton movement through CF_0 is coupled to ATP synthesis/hydrolysis at sites in the β-subunits of CF_1. The whole CF_0–CF_1 complex functions as a rotary proton-driven motor, in which the stationary subunits are I, II, IV, δ, α, and β and the rotary subunits are III, γ, and ε.

A complete crystal structure of the entire CF_0CF_1-ATPase is not available to date. However, single- particle cryo-EM has recently been used to study related ATPase complexes from other organisms at lower resolution. Schep et al. (2016)

studied the *Thermus thermophilus* V/A-ATPase at 6.4 Å resolution, and Allegretti et al. (2015) analyzed the dimeric F-type ATPase from bovine mitochondria at 6.2 Å resolution. These studies revealed the overall arrangement of the different subunits including the proton channel-forming A-subunit in the transmembrane region. The first high-resolution asymmetric structure of the mitochondrial CF_1-ATPase from bovine heart was solved at 2.8 Å resolution in 1994 (Abrahams et al. 1994; later refined to 1.9 Å, Bowler et al. 2007). Among several crystal structures of bovine CF_1, only two differ from the ground-state structure, in which one β-site is empty and the other two are filled with nucleotides: in the intermediate states of ATP hydrolysis, all three sites contain nucleotides (Menz et al. 2001; Rees et al. 2009). Besides the CF_1 crystal structures of thermophilic *Bacillus* at 3.1 Å (Stocker et al. 2005), from yeast at 3.6 Å (Kabaleeswaran et al. 2006) and from *E. coli* at 3.3 Å (Cingolani and Duncan 2011), the chloroplast CF_1 structure from spinach has also been solved at 3.2 Å (Groth and Pohl 2001). These structures revealed that a conformational binding change mechanism in the catalytic β-subunits for ATP synthesis is induced by the rotation of the central stalk (γ and ε, high-resolution structure at 2.4 Å from Gibbons et al. 2000). This central stalk is in close contact with the ring formed by the III-subunits of CF_0.

Chloroplast and mitochondrial and bacterial F-ATPases are highly conserved in structure and mechanism, but have significant unique features: the number of rotary subunits III (called c-subunits in mitochondria) seems to be specific for each organism. This was a surprise, as it was long anticipated that the number of III-subunits would be a fixed integer dividable by three (probably 12), as there are three ATP binding sites per complex and a full cycle of the rotor yields three ATP molecules (see Boyer 1997 for review). Although a high-resolution structure of the entire CF_0 complex is still lacking, the structure of the III-ring is well resolved. The best available structure of all CF_0 subunits today is the cryo-EM structure from the bacterium *Ilyobacter tartaricus* at 7 Å (Hakulinen et al. 2012). The first high-resolution structure of the III-ring from yeast mitochondria showed that it consisted of ten subunits (Stock et al. 1999), similar to *E. coli* and thermophilic *Bacillus* (Jiang et al. 2001; Mitome et al. 2004). Bovine mitochondrial III-ring numbers 8 copies (Watt et al. 2010), other bacterial III-rings consist of 11 (*Ilyobacter tartaricus*, Stahlberg et al. 2001: Atomic force and cryo-electron microscopy; Meier et al. 2005: crystal structure) or 13 subunits (*Bacillus pseudofirmus*, Preiss et al. 2013). The cyanobacterium *Spirulina platensis* has a 15-III-ring (Pogoryelov et al. 2005), while the chloroplast III-ring of spinach was determined to comprise 14 subunits (Seelert et al. 2000: atomic force microscopy; Vollmar et al. 2009: crystal structure). Biochemical analysis of the *C. reinhardtii* III-ring suggests that it consists of 13 III-subunits (Meyer Zu Tittingdorf et al. 2004). Since it is believed that one full rotation cycle is required for the catalysis of ATP formation at CF_1, the stoichiometry of the III-monomers determines the H^+/ATP ratio and thus the conversion efficiency of the ATPase to produce ATP: the more subunits, the higher is the H^+/ATP ratio and the torque and the easier it is to produce ATP at the cost of lower efficiency. This can be beneficial for organisms exposed to low electrochemical potential (such as alkaliphilic bacteria) or variable

pmf—as present in chloroplasts due to varying photosynthesis efficiency at fluctuating light conditions and day–night cycles.

The discovery of the number of III-monomers might also affect the long-standing debate concerning the importance of cyclic electron transport in providing extra ATP for the Calvin–Benson–Bassham (CBB) cycle in addition to the final products of linear electron transfer, ATP, and NADPH. Carbon dioxide assimilation by the CBB cycle requires an ATP/NADPH ratio of 3:2. Linear electron flow was formerly calculated to extract 4 electrons from water to produce 2 NADPH molecules and to pump 12 protons across the membrane. Since in *C. reinhardtii*, 13 protons are needed to produce the required 3 ATP molecules, alternative pathways without net electron transfer must supply the extra protons needed. The demand for higher amounts of ATP can even increase under stress conditions. One important mechanism that contributes to meet this demand is cyclic electron transport around PSI.

Other differences between chloroplast and mitochondrial F-ATPases are that chloroplast CF_1 can hydrolyze ATP when detached from CF_0 (but no synthesis of ATP is possible) and that in contrast to mitochondria, neither CF_1 nor CF_0 can accumulate in the absence of the other (Lemaire et al. 1988). Moreover, chloroplast ATPase must be light activated by a thioredoxin-mediated reduction of a disulfide bond of γ-CF_1 (the γ-structure is not well resolved in the chloroplast CF_1 structure), probably to prevent ATP hydrolysis in the dark.

3 Advances in 3D and 4D Imaging

Building on these advances in our understanding of the structures of individual complexes, the discipline is now approaching the feasibility of visualizing complexes within the thylakoid structures at near-atomic resolution and analyzing dynamic molecular assemblies that form functional modules essential to enable the cell to adapt to constantly changing light levels. In this section, we review how these techniques can assist algae specialists to visualize the cell at ever- increasing levels of resolution and ultimately enable 4D molecular level simulations.

3.1 Optical Microscopy

At the lowest resolution considered here, >250 nm, optical microscopy is commonly used to visualize whole populations of algae and individual cells which typically have a diameter of $\sim$10–30 μm. This provides a real-time overview of the biophysical structure of entire cells and large organelles such as the chloroplast. Optical microscopes can also be coupled to time-resolved spectroscopy equipment to monitor localized laser-induced photo-bleaching (Mullineaux and Kirchhoff

2007), which in the case of algae can be used to measure membrane fluidity and photosystem dynamics.

3.2 Wide-Field and Confocal Microscopy

These techniques are commonly used to improve in vivo organellar and molecular imaging (e.g., using fluorescent tags) (Stephens and Allan 2003; Murphy and Davidson 2012). Early wide-field and confocal microscopy techniques illuminated the entire thickness of the specimen. This however resulted in high background noise and often photo-bleaching and phototoxicity, a particular problem in photosynthetic organisms. As the highest resolution, information is obtained from a single focal plane; *light sheet microscopy* (Huisken et al. 2004; Huisken and Stainier 2009) was developed to improve spatial and temporal resolution as well as signal-to-noise ratio, yielding higher quality 4D images and reduced photobleaching and phototoxicity due to reduced light exposure. *"Lattice light sheet"* microscopy advanced this technique further by replacing the usual Gaussian light source, which has a beam that is too broad for high-resolution subcellular imaging, with a "non-diffracting Bessel beam," which sweeps across the focal plane at submicron thicknesses. In super-resolution mode, this technology has now advanced to the point that intricate cellular ultrastructure can be imaged at low illumination and in real time ($\sim$0.02 s^{-1}) at the level of organelles, tubules, and membranes and to localize fluorescently tagged proteins in the $\sim$10–100-nm-diameter range (Chen et al. 2014). This technique is thus applicable to most of the rapidly growing algae cells commonly used for biotechnological applications (thickness $\sim$10–20 μm). The technique can reportedly be extended into a "fifth dimension," color, to monitor the real-time orchestrated movement of multiple tagged proteins (see Sect. 3.7) in cells and how their dynamic rearrangements impact upon cellular response. In terms of understanding photosystem dynamics, this opens up fascinating opportunities to investigate the migration of tagged PSII, specific LHCIIs, and PSI to investigate state transitions or potentially the interaction of photosynthetic units during cyclic electron transport. In addition, it enables the possibility of investigating how changes in illumination conditions alter the stacking and unstacking of the thylakoid grana or pseudo-grana.

3.3 Correlative Light and Electron Microscopy (CLEM)

CLEM (Betzig et al. 2006; Watanabe et al. 2011; de Boer et al. 2015) and variants thereof connect the live cell imaging capability of optical and fluorescence microscopy (Sects. 3.1 and 3.2), which typically localize tagged proteins to several hundred nanometers, to electron microscopy (Sects. 3.4 to 3.6), which offers significantly higher resolution but of much smaller regions and for fewer samples

(Cortese et al. 2013). Using CLEM, light microscopy is first conducted to identify regions of interest within live cells, before the cells are flash frozen, sectioned, and transferred for electron microscopy. This is of considerable utility for algal biotechnologists interested in the structural biology of cellular (e.g., photosynthetic) processes and recombinant protein production (e.g., localization and export of GFP-tagged proteins).

Photo-activated localization microscopy (PALM, Betzig et al. 2006) and stochastic optical reconstruction microscopy (STORM, Rust et al. 2006) also connect into this analytical space. Both PALM and STORM are wide-field techniques distinct from the laser scanning confocal microscopy, which is based on point scanning. Both techniques are typically used to locate fluorescently labeled proteins. PALM tends to use endogenously expressed tagged proteins (e.g., GFP tagged). STORM is based on immunolabeling and uses paired dyes consisting of an *activator* and *reporter* molecule. Light-induced excitation of the activator results in the excitation of the closely located reporter molecules. These techniques have been extended into super-resolution and 3D and live cell imaging (Shroff et al. 2007; Shtengel et al. 2009). It is also of note that PALM and Storm could potentially be supported by atomic force microscopy (AFM) to localize tagged photosynthetic complexes (Kirchhoff et al. 2008) in their native membrane environment and to monitor their molecular dynamics (Preiner et al. 2015).

3.4 Atomic Force Microscopy (AFM)

AFM can be used as a surface imaging technique in which the forces between the tip and the sample are used to create a simulated three-dimensional topography map based on the height of each point of the surface. Since AFM is not dependent on lenses or beam irradiation, it is not limited by special resolution due to diffraction limit and aberration. Recently, an affinity-mapping atomic force microscopy (AFM) technique (Vasilev et al. 2014) was developed to uniquely identify and locate proteins within a membrane surface. By selective binding of the electron transfer protein plastocyanin (Pc) to the lumenal membrane surface of the cyt b_6f complex using a Pc-functionalized atomic force microscope (AFM) probe, the position of cyt b_6f complexes and its proximity to PSII in grana thylakoid membranes from spinach was identified (Johnson et al. 2014). Thus, the membrane surface topography could be directly correlated with Pc-cytb_6f interactions, allowing the construction of a map of the grana thylakoid membrane with nanodomains of co-localized PSII and cytb_6f complexes. This technique has the potential to identify interaction partners (e.g., reduced Pc and photosystem I), to obtain a more detailed picture of the thylakoid membrane topography.

3.5 *Transmission Electron Microscopy (TEM)*

Transmission electron microscopes can visualize atoms in part due to the fact that electrons have much shorter wavelengths (few pico-meters) instead of hundreds of nanometers for light microscopes. However, the ability to resolve biological structures to such resolutions is limited by the sensitivity of the biological specimens to the bombardment with electrons in an electron microscope.

Painstaking work over decades has culminated in significant advances, which have in recent times collectively facilitated a "resolution revolution" in electron microscopy (Kühlbrandt 2014), most notably demonstrated recently by several atomic resolution structures of membrane proteins solved by cryo-EM as using single-particle analysis (e.g., Liao et al. 2013; Amunts et al. 2014; see also Sects. 2.3 and 3.6). Key improvements include *electron sources* with increased coherence and brightness, which are important both for image resolution and contrast, the capability to correct for the spherical aberrations of the lens systems of the TEM with so-called *Cs aberration correctors* that contribute to improved contrast transfer function (CTF) characteristics of the TEM, though at the cost of contrast. For biological samples, imaging is often conducted without Cs correction and at high defocus to boost contrast. *Phase plates* have also been developed for electron microscopes, which offset the phase of the scattered electrons in the microscope, thereby producing a strongly increased contrast upon formation of a phase contrast image further down in the electron microscope (Danev et al. 2014; Asano et al. 2015; Danev and Baumeister 2016). Moving down through the TEM, we come to the sample itself and the support and stage that it is mounted on. Cryo-EM requires specific *cryo-preparation techniques*, which have been developed both for tomography and single-particle analysis to allow cell sections, isolated membrane proteins, and macromolecular assemblies to be embedded in thin vitreous ice sheets. Rapid vitrification techniques, designed to convert liquid water to a noncrystalline and non-diffraction vitreous (glass-like) ice, are achieved by plunge-freezing thin aqueous layers of sample into liquid ethane at liquid nitrogen temperature, which allows quick-freezing to maintain the sample in a thin-film vitreous ice in a near-native state (McDowall et al. 1983; Adrian et al. 1984; Dubochet et al. 1988). As this plunge-freezing technique is limited to thin samples (<10 μm), high-pressure freezing approaches were also developed to preserve thicker samples (<200 μm). To improve the resolution and contrast obtainable by cryo-tomography, samples in vitreous ice can now be milled down into thin sheets using a *cryo-FIB* (*focused ion beam*), which represent the gold standard of TEM tomography in terms of high resolution on unperturbed cellular structures. Engel et al. (2015) recently presented the architecture of the Chlamydomonas cell in its native state at close to molecular resolution by demonstrating this technique at its state of the art. Specifically, they used cryo-FIB milling to trim away unwanted sample sections from one or both sides of the section of interest, thereby significantly reducing the background noise and enhancing the signal-to-noise ratio (SNR) of the recovered image. *New cartridge holders* for the EM grids provide improved stability and operability and

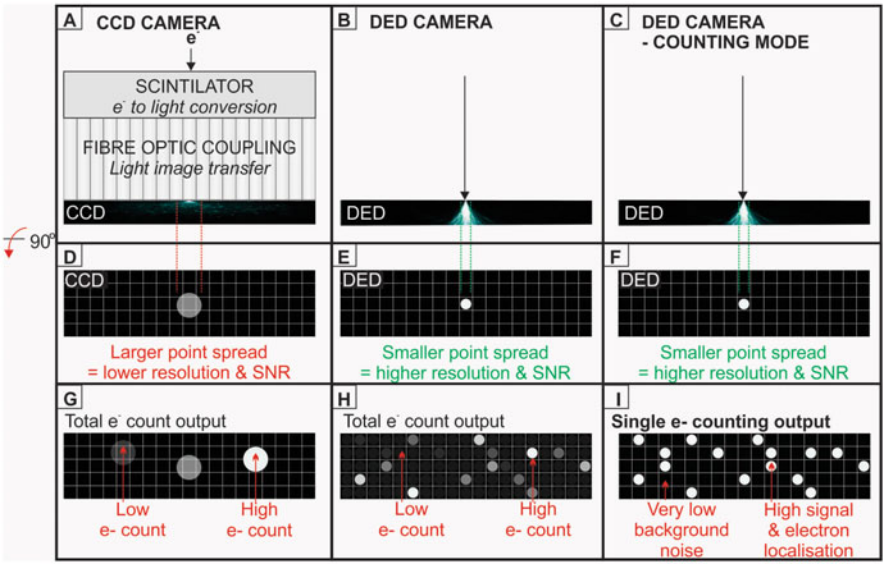

Fig. 6 Comparison of CCD (**a**) and DED (**b**, **c**) camera systems. (**a**) In a charge-coupled device (CCD) camera, each photon is transferred via a fiber optic coupling to the CCD detector. Signal and resolution are lost at each step of this process (i.e., electron capture by the upper scintillator, transfer of light through the fiber optic coupling, and reconversion at the detector plate). (**d**) Top view of the CCD detector; individual pixels are shown as *squares* and a photon interacting with it as a *circle*. The point spread function of the photon (signal) is indicated by the large diameter of the circle. The larger the circle, the lower the achievable resolution. The loss in signal-to-noise ratio is indicated by the *gray scale of the circle* (i.e., *white*, high signal intensity; *black*, background). (**b**, **c**) Since DED cameras detect electrons directly at their surface, they eliminate the need for the scintillator and fiber optic couplings. (**e**, **f**) The *small circle* in comparison to (**d**) illustrates the smaller point spread functions of DED and improved signal-to-noise ratio. (**g**) Low (*dark gray*), medium (*mid-gray*), and high (*white*) total number of electron counts acquired using a CCD camera ("analog" mode). (**h**, **i**) The DED counting mode (**i**), compared to the integrating mode (**h**), operates at very low electron doses and high readout rates, which together allow each individual electron event to be detected

allow high sample tilt and automation of handling. *Improved grid supports* with a reported 40-fold reduction in beam-induced motion and the use of conducting graphene supports are reported to reduce drift and charging artifacts (Pantelic et al. 2012; Russo and Passmore 2014).

Despite these many advances, perhaps the most dramatic was enabled by the introduction of *direct electron detectors* (DED, Liao et al. 2013; Amunts et al. 2014; Kühlbrandt 2014), which have enabled atomic resolution single-particle analysis. As their name suggests, direct electron detectors (Fig. 6b, c) detect electrons directly at their surface, thereby improving the signal-to-noise ratio and yielding a smaller point spread function (compare Fig. 6g, h). Current Gatan and FEI Falcon DED detectors operate using this principle. The ability of the DED to

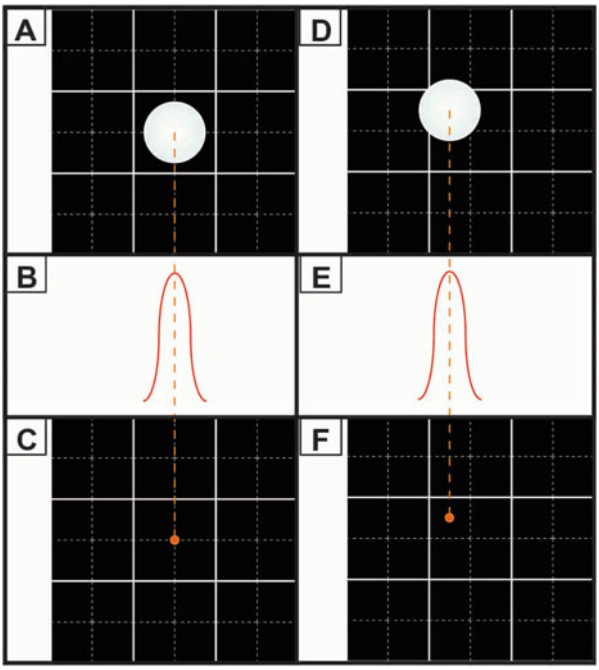

Fig. 7 Super-resolution electron detection of DED cameras. (**a**, **d**) Each electron event (*top*) on a DED camera has a spread signal distribution, represented in a top view as a *white circle*. (**b**, **e**) This is approximated by the *orange* Gaussian distribution. As a result, the center of each location of the electron impact can be determined with sub-pixel accuracy (in these examples at the center of the pixel (**c**) or to the *top left-hand quadrant* (**f**), enabling so-called super-resolution electron detection. The superior detective quantum efficiency (DQE), a measure of the signal-to-noise ratio across the frequency range (Ruskin et al. 2013), is enhanced for the Gatan K2 Summit DED camera, as its "super-resolution" counting mode allows a physical 4k × 4k camera to readout an effective 8k × 8k image, thus providing access to information beyond the physical Nyquist limit of the 4k camera chip resolution. The Nyquist limit corresponds to 2x the pixel resolution (i.e., if the pixel size is 2 Å, the Nyquist limit is 4 Å)

count single electrons (Fig. 6i) essentially makes it possible to eliminate background noise, further enhancing the signal-to-noise ratio and thus resolution.

In contrast to the "analog" mode where electron counts accumulate within each pixel, the sub-pixel accuracy (Fig. 7) of "counting mode" allows a physical 4k × 4k camera to readout an effective 8k × 8k image. This "super resolution" mode available in the Gatan K2 Summit DED camera further increases resolution and data collection area for electron microscopy (Ruskin et al. 2013). This is the only DED camera so far offering high-speed single electron counting and therefore reaches the highest detective quantum efficiency (DQE) performance of the available large area detectors. The fast readout speed of DED cameras and their extremely low background noise allow for dose-fractionated collection of image series: instead of accumulating an image of a longer exposure time or exposure

dose, DEDs can be operated in a so-called movie mode, whereby the camera saves up to 100 frames in series onto the hard drive as an image stack. These recorded subframes of a dose-fractionated exposure can be aligned to a common origin to thereby largely eliminate the effects of sample drift that can originate from physical movement of the electron microscopes or by the electron beam exposure itself. Online drift correction for recorded image series, followed by averaging of aligned image stacks, greatly improves image quality and also the success rate of data collection, since with such a setup, any sample drift can usually be recognized and computationally corrected after data collection. This massively reduces the required quantity of data to yield a comparable structure (or alternatively, delivers superior structural information from comparably sized datasets). Collectively, these advances have enabled improved high-resolution electron tomography (Sect. 3.5) and facilitated atomic resolution single-particle cryo-EM analysis (Sect. 3.6). The state-of-the-art systems offer the opportunity to solve the structures of photosynthetic complexes for *C. reinhardtii* in their native state at atomic resolution.

3.6 Electron Tomography

Advanced EM systems incorporating various combinations of the features above (Sect. 3.4) as well as energy filters (e.g., Gatan Image Filter, GIF) to remove inelastically scattered electrons, which contribute to image noise, now allow electron tomography to produce 3D reconstructions of cell and membrane architecture at resolutions down to few nanometers. Sub-volume analysis of small 3D volumes cropped from large 3D reconstructions of entire organelles enable the 3D alignment, classification, and averaging of repeated molecules in the structure, such as specific large membrane protein complexes in photosynthetic thylakoid membranes. Sub-volume averaging applied to electron tomography datasets produce 3D reconstructions up to 1 nm in resolution (e.g., Kudryashev et al. 2016) and offer the prospect of further improvement in the near future. While 3VIEW serial blockface scanning EM allows 3D imaging of large volumes up to hundreds of micrometers in diameter of resin-embedded cells at ~20 nm resolution (Dohnalkova et al. 2010), TEM electron tomography typically reaches much better resolution of ~1–4 nm and can even detect individual photosynthetic membranes and membrane protein complexes to provide a molecular resolution framework for docking atomic structures of assemblies and membrane proteins solved by single-particle analysis or crystallography. A notable example of state-of-the-art electron tomography of microalgal cells was provided by Engel et al. (2015). Three-dimensional images and videos of the Chlamydomonas chloroplast in close-to-living conditions at near-atomic resolution reveal the detailed structures of the microtubules that connect the thylakoids to the pyrenoid, which could explain how the two stages of photosynthesis (light-harvesting and carbon fixation) can be coordinated even though they occur in different locations within the chloroplast.

Tomogram Segmentation Accurate, high-throughput cell segmentation at molecular resolution is an essential link between the 1 and 4 nm resolution 3D cell reconstructions obtained by electron tomography and the ability to dock into them, the atomic structures of large macromolecular assemblies and membrane protein complexes (Davies et al. 2011: ATPases in mitochondria; Kouřil et al. 2011: PSII complexes in spinach grana) solved by single-particle analysis or crystallography (see Sects. 2.3 and 3.6). Early seminal tomographic analyses such as those of Marsh et al. (2001) required many months of painstaking manual segmentation of cellular organelles and large macromolecular assemblies such as ribosomes. However, as the volume of data sets continues to increase in parallel with the attainable resolution, automated tomogram segmentation is becoming increasingly important. A large number of segmentation algorithms are already in use and under continued development. These involve Kernel (e.g., Gaussian, mean, and median filters) (Nagayoshi et al. 2005; Catarious et al. 2006; Pantelic et al. 2006), wavelet transform (Stoschek and Hegerl 1997), Nonlinear anisotropic diffusion (NAD) (Frangakis and Hegerl 2001; Heymann and Belnap 2007; Alber et al. 2008; Lučić et al. 2013), iterative median (van der Heide et al. 2007), bilateral and gradient-based edge detectors (Pantelic et al. 2007; Ali et al. 2012), Canny edge detectors (Canny 1986), active contour snake algorithms (Kass et al. 1988), and watershed transforms (Volkmann 2002). Regardless of the choice, ideally automated segmentation algorithms must be robust, accurate (able to contour macromolecules ~10 nm in diameter), simple to use (e.g., not requiring frequent manual parameter adjustment), fast (computationally efficient), generally applicable (able to segment all detected sub-volumes simultaneously), and selective (capable of segmenting single target structures, e.g., only ribosomes). In addition, to assign metadata (e.g., annotate individual macromolecules in 3D cell reconstructions) and to automate the extraction of sub-volumes for sub-volume averaging/single-particle tomography (Nicastro et al. 2006; Cope et al. 2011; Castaño-Díez et al. 2012; Hrabe et al. 2012; Galaz-Montoya et al. 2015), additional information that enable "structural finger printing" and object center identification will likely be required. Sub-volume averaging of repeated in situ structures such as ribosomes can increase the structural information gained from them for subsequent molecular docking of atomic structures solved by single-particle analysis and crystallography.

3.7 Single-Particle Analysis (SPA)

SPA has emerged as a powerful technique for atomic resolution protein structure determination, particularly for large multi-protein macromolecular assemblies and membrane protein complexes, which are of fundamental biological importance, but often fragile and difficult to isolate, in particular in the quantities required for crystallography (see also Sect. 2.3.1). SPA makes use of high-resolution particle images captured by electron cryo-transmission electron microscopy (cryo-TEM). For high-resolution studies, typically ~10^4–10^6 randomly oriented *single-particle*

images are computationally aligned and classified according to their molecular orientation. Particles which are similarly oriented are then averaged to yield *class sums* with improved signal-to-noise ratios. Ideally, these represent defined single-particle views (2D projections) of the target molecule. By computing the angles relating these views, the complex can be reconstructed in 3D, yielding a *3D structure* that is then iteratively refined to high resolution. In recent years, with the advance of direct electron detectors and their ability to reduce charging and drift related artifacts, single-particle analysis can now routinely yield atomic resolution reconstructions from stable, homogeneous, and monodispersed protein preparations. The ultimate possibilities for resolving large and dynamic macromolecular complexes with this technique are, for example, demonstrated for the 70S ribosome from *E. coli* (Fischer et al. 2015). Notable advances in the optimization of protein preparations include the ProteoPlex screen (Chari et al. 2015), which is a generic sparse matrix method to optimize the stability, homogeneity, and solubility of macromolecular complexes based on the thermal unfolding of the target complex in the presence of various buffers and small molecules. Based on such analysis, glycerol gradient/crosslinking/free detergent removal approaches (e.g., GraFix: Kastner et al. 2008; GraDeR: Hauer et al. 2015) can be used to prepare stable, homogeneous preparations for single-particle analysis. This has been successfully demonstrated for a CF_0CF_1-ATPase (Hauer et al. 2015).

3.8 EM Tagging and Staining Techniques to Visualize Proteins in Membranes

The advances described above have enabled visualization of biomembranes both in 3D within the cell (Lučić et al. 2013) and as structural models of the proteins that reside in those membranes. A significant gap that still exists is the visualization of how these protein complexes are actually distributed within the set of membranes within a cell or within a membrane subdomain. Access to this viewpoint is crucial to understand how these molecular machines interact, dynamically rearrange, and function in concert. The functions of biological membranes are highly dependent upon the restricted 2D distribution of the protein complexes within them, as well as the directionality of those complexes with respect to the membrane surfaces. The relationship between adjacent membranes (e.g., in chloroplast grana stacks) can also be critical and also requires the identification of intrinsic protein complexes.

The electron density of lipid membranes and the proteins embedded within them are quite similar, so that the intrinsic contrast between proteins and lipids is low, making the transmembrane domains difficult to resolve. Furthermore, although surface techniques such as freeze-fracture methods (see Sect. 2.2) and atomic force microscopy have been used to obtain images of proteins embedded in membranes (Johnson et al. 2014; Phuthong et al. 2015), the technique provides a surface contour and not the full 3D structure. Finally, it is difficult to

unambiguously determine what proteins are present in a specific assembly visualized by TEM, a problem which has been largely solved for light microscopy through the use to a plethora of fluorescent tags. Similarly, electron microscopy techniques are needed to: (1) *Identify* specific proteins in electron micrographs. CLEM (Sect. 3.3) has been useful in that it directs TEM imaging toward regions that possess fluorescent labels, thereby greatly reducing the search space. However, fluorescent labels often lack the resolution needed for specific identification of a protein target in EM. (2) *Orientate* membrane complexes, especially smaller complexes, since key biological questions are not solely concerned with the distribution and identification of the very largest complexes but also with small subcomponents.

A variety of solutions have been proposed and tested for solving these problems but to date no ideal experimental approach exists. Physical approaches as described above (Sects. 3.4 and 3.5) improve imaging overall and not just this specific problem. Others such as stains and physical disruption by freeze-fracture methods not only introduce artifacts and are unsuitable for cryo-EM but also lack the ability to direct stains to target regions or proteins. Chemical and biological approaches generally rely upon specific tags, which recognize target biomolecules (or biological processes).

3.8.1 Clonable Tags

Most recent progress in stain technology involves the use of clonable tags. The appeal of a clonable tag is readily apparent. Assuming no artifacts are introduced by the tag (e.g., altered function or localization of the protein), the tag colocates precisely with the protein. The generation of an electron-dense region to display the location of the tag usually relies upon one of two approaches, either the attachment of a heavy metal to the tag (e.g., gold) or the generation of an electron-dense polymer in the region of the tag, typically due to an enzymatic activity possessed by the tag. Such tags may also include fluorescent proteins or tags (e.g., ReASH) to facilitate correlated microscopy. Electron-dense tags include metallothionein, a small (62aa) Cys-rich protein which can bind gold atoms forming a ~1-nm-diameter gold cluster. Such clusters are very small but when present in sufficient number are readily apparent in TEM, while including fluorescent protein tags allows for CLEM (de Castro et al. 2014; Morphew et al. 2015). His-tags, already incorporated into many proteins of interest, can be detected in TEM by the addition of gold nano-clusters attached to tris-NTA, which forms stable complexes with His6 or His10 tags (Lata et al. 2005; Zhao et al. 2010; Anthony et al. 2014). Other clonable tags typically employ peroxidases to catalyze the oxidation of an organic substrate (e.g., diaminobenzene) with subsequent deposition of an osmiophilic polymer, which is rendered electron-dense with stain. These include miniSOG (Shu et al. 2011), FlASH, ReASH (Gaietta et al. 2002, 2006; Hoffmann et al. 2010), and an engineered ascorbate peroxidase (APEX; Martell et al. 2012). The resulting polymer is not tightly localized to the target protein but is

distributed in its vicinity. This is a disadvantage if high spatial resolution is required for the target protein but is quite helpful if what is desired is a high contrast image of the region around the target protein. Quantum dots (QDs) have become widespread in light microscopy owing to their excellent stability and resistance to photobleaching, and they can be readily coupled to antibodies (as well as clonable tags). Generally though, quantum dots are too large (20–30 nm) for EM and are typically coupled to samples via antibodies (Vu et al. 2015). The ongoing development of small, electron-dense, highly fluorescent QDs able to be coupled to a variety of tags and targets should eventually make QDs useful as specific detection systems for a variety of clonable tags such as those described above. Finally, Halo tags, SNAP tags, and CLIP tags are all short peptides that can be specifically derivatized with organic adducts including tetramethylrhodamine (TMR) which is both fluorescent and capable of oxidizing DAB in the presence of light (Liss et al. 2015). No clonable tag exists which is free from additional sample manipulation and staining, unlike fluorescent protein in light microscopy, which can be imaged in situ in living cells and require no manipulation of the tag for visualization in sections. This reduces the intrinsic advantage conferred by clonability. Modern tagging techniques could however potentially be used with freeze-fracture methods, to obtain novel identification methods for proteins in lipid bilayers. Of all approaches, the electron-dense metals (e.g., metallothionein, gold-NTA) are most suited for cryo-EM, since there is a reasonable chance that the sample can be stained in solution without significant disruption.

3.8.2 Non-clonable Tags

Clearly antibodies are the best developed tags for specific target proteins, as they are widely available, and can be coupled to a range of electron-dense or fluorescent groups including gold particles and a huge tunable array of chromophores. However, antibodies are large proteins (unless antibody fragments are used) and must be introduced into the cellular compartments, typically by permeabilization of the membranes. This often results in significant background and artifactual staining, and the spatial resolution is very low by TEM standards. In theory, any detection system applicable to a cloned tag should also be applicable to an uncloned protein as long as a way can be found to specifically detect the target protein. Gold et al. (2014) recently described the use of a 4 nm QD core specifically linked to a target membrane protein. This system required purification and biotin labeling of the target protein and incorporation in mitochondrial membranes, followed by attachment of QDs via a streptavidin linker. As such, this strategy is not generally applicable to any target protein. Nonetheless, the general strategy is feasible and could be applied with some thought to a variety of protein targets when some intrinsic property of the protein can be exploited for specific labeling (e.g., proteases can be labeled with specific high affinity inhibitors, kinases with specific peptide substrates). Similarly, peroxidases and metallothioneins could be applied to TEM sections or even included in aqueous samples containing biomembranes prior

to sample processing for cryo-EM. The main task is to identify a highly specific property of the target protein to direct the tag appropriately.

3.9 3D Atlas Construction

The recent improvements in electron microscopy techniques enable the construction of an atomic resolution 3D atlas of biomembranes and cells by combining multiscale datasets (e.g., from optical microscopy, electron tomography, single-particle analysis, crystallography, and NMR). The process will incorporate cellular as well as protein structures and the information gained from the biophysical modeling of membranes. This work will initially be based on existing software but is likely to require further software development at many levels including that of noisy data, the automation of docking processes, and the incorporation of molecular dynamics. By combining cryo-ET with atomic resolution protein structures available from crystallography and now high-resolution single-particle analysis, the development of an atomic resolution map of the chloroplast seems to be at hand.

4 Toward a 4D Atlas: Modeling Membrane and Protein Dynamics

4.1 Dynamic Simulations

Enormous strides have also been made in our ability to experimentally resolve and characterize individual proteins and molecules in the thylakoid membrane. Despite this progress, experimental techniques are limited by their temporal or spatial resolution. At present, molecular dynamics (MD) simulation is the only method that can provide atomic-level detail of the structural dynamics of membrane–protein interactions on a nanosecond to microsecond timescale. MD simulations utilize classical Newtonian mechanics, in conjunction with semiempirical chemical force fields, to calculate the time evolution of a system. This information allows structural, dynamic, and thermodynamic properties of membrane-embedded proteins and the surrounding phospholipid membrane to be determined. Crucially, the reliability of MD simulations can be validated by their ability to reproduce key experimental data.

Recent advances in computational capabilities have extended both the size and timescales accessible in molecular dynamics simulation techniques. The first published MD simulation of a protein was a 10 ps simulation of bovine pancreatic trypsin inhibitor (BSTI, 58 amino acids in length) (McCammon et al. 1977). In comparison, by 2009 atomistic simulations of BSTI in explicit water of 1031 μs duration were performed on custom-built computing facilities (Shaw et al. 2010). Algorithm and computational parallelization have enabled long-timescale

simulations of extremely large biomolecular systems, such as atomistic simulations of the solvated virus capsids. While these simulations are still computational expensive, one such simulation system characterized the dynamics and water flux through a poliovirus capsid containing 6,480,236 atoms over a simulation timescale of 200 ns (Andoh et al. 2014). While this is an extreme case, multiple simulations involving 500,000 atoms, on timescales of hundreds of nanoseconds have become the current scientific standard. The reconfiguration of GPUs for scientific programming in 2008 prompted the overhaul of many molecular dynamics simulation packages to allow GPU-acceleration of MD simulations. Biomolecular simulation packages such as AMBER, GROMACS, CHARMM, and NAMD have reported up to eightfold increases in simulation speeds using GPU-accelerated MD simulations (http://www.nvidia.com/object/computational_chemistry.html), greatly enhancing the achievable simulation timescales.

4.2 Atomistic Molecular Dynamics Simulations of Membrane Proteins

The explosion of structural data from X-ray crystallography and related techniques (e.g., XFELS) in recent years has provided a wealth of avenues to investigate the proteins comprising the machinery of the thylakoid membrane. Molecular dynamics simulations utilize an underlying force field which describes the functional form and a set of parameters used to calculate the potential energy of the system. In atomistic simulations, every atom in the system is explicitly accounted for in the force field, while united-atom force fields group the hydrogens and carbons in terminal methyl groups or methylene bridges together as a single particle. By iteratively calculating Newton's equation of motion, the protein and surrounding environment move toward a minimum potential energy conformation. While simulations of proteins rely on knowledge of the protein structure itself, simulation of the thylakoid membrane requires prior knowledge of the lipid composition of the phospholipid membrane and accurate lipid parameters that reproduce the biophysical properties of lipid membranes. Although parameter sets for major phospholipid species, such as phosphatidylcholines and phosphatidylethanolamines have been widely available since the 1990s (e.g., Huang et al. 1994; Berger et al. 1997), these parameters have been continually refined and improved, and so MD simulations of phospholipid bilayers have also expanded in their complexity. Despite this progress, a significant hurdle is the high proportion of galactolipids in the thylakoid membrane, particularly in association with PSII. Due to their specialized function, parameter sets for galactolipids were not reported until 2012 (Kapla et al. 2012), posing an under-explored problem in MD simulations. One recent MD study uses phosphatidylglycerol in conjunction with five different galactolipids as a model for the cyanobacteria thylakoid membrane (Van Eerden et al. 2015) and attempted to characterize the domain organization in the thylakoid membrane. Further

simulations have examined the dynamics of water permeation through photosystem II (PSII) embedded in a model thylakoid membrane containing the same fatty acids and lipid class distribution as the native thylakoid membrane of *T. vulcanus* (Ogata et al. 2013). Intriguingly, these simulations suggest that the transfer of water, oxygen, and protons involves different pathways through the protein, which may have implications for the functional mechanism of the oxygen-evolving complex (OEC). Vassiliev et al. (2012) calculated the energetics of water permeation to the OEC of PSII to identify the most likely transport paths and the dynamic range of motions observed in the crystallographic water channels through PSII. Other atomistic MD simulations examined the proton-coupled quinol/quinone redox reactions of cytochrome b_6f which generates a proton gradient across the thylakoid membrane: the role of chlorophyll in substrate uptake and gating (Hasan and Cramer 2014) and the presence of quinone-dependent proton pathways through cytochrome b_6f were identified via changes in substrate-dependent water wires within the protein (Hasan et al. 2013). Earlier studies examined the structural dynamics of the thylakoid F-type ATPase in an effort to characterize the rotary motor mechanism (Ito and Ikeguchi 2010; Lin et al. 2010). Collectively, these simulations have made significant contributions to our understanding of the molecular interactions linking membrane and protein structure to their respective functions within the thylakoid membrane. Although these atomistic molecular dynamics simulations provide a wealth of detailed information, they are still limited by the physical size of the system and timescales that can be practically simulated using current supercomputing resources.

4.3 Coarse-Grained Molecular Dynamics Simulations

Coarse-grain approaches for membrane systems are highly appealing for simulations of combined membrane and protein dynamics. Simulations are computationally more tractable because reductions in the degrees of freedom enable simulations on greater timescales and length scales than are feasible with traditional atomistic models. Since its release in 2007, the MARTINI coarse-grained force field has gained widespread popularity in the MD community (Marrink et al. 2007). It utilizes a mapping scheme for proteins and lipids in which every four non-hydrogen atoms (and their bound hydrogens) are mapped to one coarse-grained interaction sites. As is the case with atomistic force fields, each interaction site is assigned to a particular parameter set, based on its chemical composition, calibrated to reproduce the partitioning free energies of biomolecules (Marrink et al. 2007). These coarse-grained systems have facilitated characterization of phospholipid self-assembly around integral membrane proteins (Scott et al. 2008) and provided insights into lipid structure, organization, and phase transitions. In thylakoid membranes with their unique lipid composition, of predominantly galactolipids (~40% monogalactosyldiacylglycerol (MGDG), ~32% digalactosyldiacylglycerol (DGDG), ~15% sulfoquinovosyldiacylglycerol (SQDG)), and ~15% phosphatidylglycerol (PG) (Sakurai et al. 2006), recent coarse-grained

simulations have shown that MGDG promotes phase transitions to inverted hexagonal phases between stacked laminar thylakoid bilayers, which are believed to be important for the violaxanthin cycle (Van Eerden et al. 2015). While these simulations represent a landmark in detailing the dynamics of the thylakoid membrane, we are still limited by the scale that these systems can be analyzed at. Furthermore, these large-scale simulations do not yet include the thylakoid proteins themselves.

4.4 Concerted Architecture on a Grand Scale

Quantum mechanical calculations and atomistic and coarse-grained MD simulations all have a particular set of problems to which they are most applicable. The discipline is now poised to simulate the time-resolved details of the structural and dynamic changes of thylakoid membrane in response to its environment, providing a 4D atlas of the thylakoid membranes. This requires multi-scale approaches and mapping schemes and drilling down on the area of interest at the required level of detail. Such multi-scale mapping schemes have been implemented and extensively utilized on a smaller scale in coarse-grained to atomistic mapping schemes for MD simulations of both lipids and proteins (e.g., Marrink et al. 2007; Van Eerden et al. 2015), while hybrid QM–MM (quantum mechanics/molecular modeling) simulations attempt to use the molecular modeling approaches underpinning MD simulations to derive the most favorable structural conformations for QM calculations, as was used in a recent QM–MM study of photosystem II (Bovi et al. 2014). Although QM–MM approaches were first described in the 1970s (Warshel and Levitt 1976), implementation of these approaches is still problematic, requiring a high degree of user experience and intervention.

5 Conclusion

The last 60 years represents an era of rapid progress in structure elucidation and imaging techniques. These include advances in instrumentation, structural biology, and computational techniques that together have provided the details of cellular structure that would not have been conceivable two decades ago. These techniques provide the structural detail covering the full volume of the cell at the nanometer resolution and can focus to increase the level of detail, allowing individual membrane proteins and macromolecular assemblies to be resolved in atomic detail. Thus, most of the technologies are now in place to begin the task of attempting pseudo-atomic resolution modeling of the photosynthetic solar interfaces of *Chlamydomonas reinhardtii* and other green alga.

3D reconstructions of this type can be used to initiate simulation techniques that will provide the time resolution of the atomic interactions governing protein function. Reconstruction of the overall architecture of the thylakoid membrane

structure and the dynamic, time-resolved responses of each part of the photosynthetic machinery to constantly changing light levels would provide the basis for 4D modeling. Furthermore, such models enable structure-guided design of specialized fit-for-purpose cell lines for high-density biotechnological applications. For example, microalgae can also be used for the production of specific building blocks for the production of artificial bioinspired solar fuel systems of the future and to test these components in vivo. These applications could be facilitated by incorporation of cutting-edge genome editing technologies (e.g., CRISPR/CAS, TALENs, ZFN) for targeted engineering.

Practical realization of these goals is tantalizingly close: electron tomography is already beginning to reveal the intricate cellular structures thought to be involved in connecting the light-driven reactions and the ATP and NADPH that they produce to CO_2 fixation via the Calvin-Benson-Bassham cycle, providing a new level of insight into these light-driven cell factories. The advance of XFELS and its ability to time-resolved structural information at the femtosecond level allow the capture of key steps in the dynamic process of photosynthesis. These advances provide critical experimental data to drive the formation of a repository of a time-resolved 3D atlas of the *Chlamydomonas reinhardtii* photosynthetic machinery, in which simulations can be used to provide the temporal information linking each piece of structural data. Such a 4D atlas would provide the information to hone in from nm length scales toward atomic resolution detail, or eventually, the electronic detail, of the photosynthetic machinery as it responds to dynamic changes in the environment, such as diurnal light cycles. The integration of this information in a 4D atlas could provide a powerful basis to design "fit-for-purpose" algae-based as well as artificial solar fuel systems to meet the changing global energy requirements of the twenty-first century and beyond. In particular, such advances are likely critical to fast track urgently needed CO_2 neutral solar fuel systems to reduce CO_2 emissions from fossil-based fuels which still provide 80% of global energy demand. This is because globally we may exceed CO_2 limits which will lock us into 1.5 °C and 2 °C global warming by 2020 and 2030, respectively, at which point global greenhouse gas emissions must be reduced by 50% of current emissions levels to protect against further warming, as this is the reported level of CO_2 absorption by the biosphere (see Ringsmuth et al. 2016 and references therein).

Acknowledgments The authors thank Olivier Vallon, Jacqueline Olive, Michel Recouvreur, Francis-André Wollman, Rosalba Rothnangel, and Rick Webb for the provision of EM images included in the figures. JS, IR, BH, and HS thank the Australian Research Council for financial support (DP130100346 and DP160101018).

References

Abrahams JP, Leslie AG, Lutter R, Walker JE (1994) Structure at 2.8 A resolution of F1-ATPase from bovine heart mitochondria. Nature 370:621–628

Adrian M, Dubochet J, Lepault J, McDowall AW (1984) Cryo-electron microscopy of viruses. Nature 308:32–36

Ago H, Adachi H, Umena Y, Tashiro T, Kawakami K, Kamiya N, Tian L, Han G, Kuang T, Liu Z, Wang F, Zou H, Enami I, Miyano M, Shen J-R (2016) Novel features of eukaryotic photosystem II revealed by its crystal structure analysis from a red alga. J Biol Chem 291:5676–5687. doi:10.1074/jbc.M115.711689

Alber F, Förster F, Korkin D, Topf M, Sali A (2008) Integrating diverse data for structure determination of macromolecular assemblies. Annu Rev Biochem 77:443–477

Ali RA, Landsberg MJ, Knauth E, Morgan GP, Marsh BJ, Hankamer B (2012) A 3D image filter for parameter-free segmentation of macromolecular structures from electron tomograms. PLoS One 7:e33697

Allegretti M, Klusch N, Mills DJ, Vonck J, Kühlbrandt W, Davies KM (2015) Horizontal membrane-intrinsic α-helices in the stator a-subunit of an F-type ATP synthase. Nature 521:237–240

Allen JF, Bennett J, Steinback KE, Arntzen CJ (1981) Chloroplast protein phosphorylation couples plastoquinone redox state to distribution of excitation energy between photosystems. Nature 291:25–29

Alric J (2014) Redox and ATP control of photosynthetic cyclic electron flow in Chlamydomonas reinhardtii (II) involvement of the PGR5–PGRL1 pathway under anaerobic conditions. Biochem Biophys Acta 1897:825–834

Alric J, Lavergne J, Rappaport F (2010) Redox and ATP control of photosynthetic cyclic electron flow in Chlamydomonas reinhardtii (I) aerobic conditions. Biochim Biophys Acta 1797:44–51

Amunts A, Drory O, Nelson N (2007) The structure of a plant photosystem I supercomplex at 3.4 A resolution. Nature 447:58–63

Amunts A, Toporik H, Borovikova A, Nelson N (2010) Structure determination and improved model of plant photosystem I. J Biol Chem 285:3478–3486

Amunts A, Brown A, Bai X, Llácer JL, Ramakrishnan TH, Emsley P, Long F, Murshudov G, SHW S, Ramakrishnan V (2014) Structure of the yeast mitochondrial large ribosomal subunit. Science 343:1485–1489

Andoh Y, Yoshii N, Yamada A, Fujimoto K, Kojima H, Mizutani K, Nakagawa A, Nomoto A, Okazaki S (2014) All-atom molecular dynamics calculation study of entire poliovirus empty capsids in solution. J Chem Phys 141:1–11

Anthony KC, You C, Piehler J, Pomeranz Krummel DA (2014) High-affinity gold nanoparticle pin to label and localize histidine-tagged protein in macromolecular assemblies. Structure 22:628–635

Asano S, Fukuda Y, Beck F, Aufderheide A, Förster F, Danev R, Baumeister W (2015) A molecular census of 26. Science 347:439–443

Austin JR, Staehelin LA (2011) Three-dimensional architecture of grana and stroma thylakoids of higher plants as determined by electron tomography. Plant Physiol 155:1601–1611

Badger MR, Andrews TJ, Whitney SM, Ludwig M, Yellowlees DC, Leggat W, Price GD (1998) The diversity and coevolution of Rubisco, plastids, pyrenoids, and chloroplast-based CO_2-concentrating mechanisms in algae. Can J Bot 76:1052–1071

Baniulis D, Yamashita E, Zhang H, Hasan SS, Cramer WA (2008) Structure–function of the cytochrome b6f complex. Photochem Photobiol 84:1349–1358

Barber J, Chow WS (1979) A mechanism for controlling the stacking and unstacking of chloroplast thylakoid membranes. FEBS Lett 105:5–10

Bassi R, Soen SY, Frank G, Zuber H, Rochaix JD (1992) Characterization of chlorophyll a/b proteins of photosystem I from Chlamydomonas reinhardtii. J Biol Chem 267:25714–25721

Ben-Shem A, Frolow F, Nelson N (2003) Crystal structure of plant photosystem I. Nature 426:630–635

Berger O, Edholm O, Jahnig F (1997) Molecular dynamics simulations of a fluid bilayer of dipalmitoylphosphatidylcholine at full hydration, constant pressure, and constant temperature. Biophys J 72:2002–2013

Bergner SV, Scholz M, Trompelt K, Barth J, Gäbelein P, Steinbeck J, Xue H, Clowez S, Fucile G, Goldschmidt-Clermont M, Fufezan C, Hippler M (2015) State transition7-dependent phosphorylation is modulated by changing environmental conditions and its absence triggers remodeling of photosynthetic protein complexes. Plant Physiol 168(2):615–634. doi:10.1104/pp.15.00072

Bes MT, Parisini E, Inda LA, Peleato ML, Saraiva L (1999) Crystal structure determination at 1.4 Å resolution of ferredoxin from the green alga Chlorella fusca. Structure 7:1201–1211

Betzig E, Patterson GH, Sougrat R, Lindwasser OW, Olenych S, Bonifacino JS, Davidson MW, Lippincott-Schwartz J, Hess HF (2006) Imaging intracellular fluorescent proteins at nanometer resolution. Science 313:1642–1645

Bibby TS, Nield J, Barber J (2001) Iron deficiency induces the formation of an antenna ring around trimeric photosystem I in cyanobacteria. Nature 412:743–745

Biesiadka J, Loll B, Kern J, Irrgang K-D, Zouni A (2004) Crystal structure of cyanobacterial photosystem II at 3.2 Å resolution: a closer look at the Mn-cluster. Phys Chem Chem Phys 6:4733–4736

Binda C, Coda A, Aliverti A, Zanetti G, Mattevi A (1998) Structure of the mutant E92K of [2Fe-2S] ferredoxin I from Spinacia oleracea at 1.7 Å resolution. Acta Crystallogr D Biol Crystallogr 54:1353–1358

Boekema EJ, Dekker JP, van Heel MG, Rögner M, Saenger W, Witt I, Witt HT (1987) Evidence for a trimeric organization of the photosystem I complex from the thermophilic cyanobacterium Synechococcus sp. FEBS Lett 217:283–286

Bovi D, Narzi D, Guidoni L (2014) Magnetic interactions in the catalyst used by nature to split water: a DFT + U multiscale study on the Mn4CaO5 core in photosystem II. New J Phys 16:015020

Bowler MW, Montgomery MG, Leslie AGW, Walker JE (2007) Ground state structure of F1-ATPase from bovine heart mitochondria at 1.9 Å resolution. J Biol Chem 282:14238–14242

Boyer PD (1997) The ATP synthase - a splendid molecular machine. Annu Rev Biochem 66:717–749

Boynton JE, Gillham NW, Chabot JF (1972) Chloroplast ribosome deficient mutants in the green alga Chlamydomonas reinhardi and the question of chloroplast ribosome function. J Cell Sci 10:267–305

British Petroleum (2015) BP statistical review of world energy. June 2010:48

Brumfeld V, Charuvi D, Nevo R, Chuartzman S, Tsabari O, Ohad I, Shimoni E, Reich Z (2008) A note on three-dimensional models of higher-plant thylakoid networks. Plant Cell Online 20:2546–2549

Büchel C, Kühlbrandt W (2005) Structural differences in the inner part of photosystem II between higher plants and cyanobacteria. Photosynth Res 85:3–13

Canny J (1986) A computational approach to edge detection. IEEE 8:679–698

Carpenter EP, Beis K, Cameron AD, Iwata S (2008) Overcoming the challenges of membrane protein crystallography. Curr Opin Struct Biol 18:581–586

Castaño-Díez D, Kudryashev M, Arheit M, Stahlberg H (2012) Dynamo: a flexible, user-friendly development tool for subtomogram averaging of cryo-EM data in high-performance computing environments. J Struct Biol 178:139–151

Catarious DM, Baydush AH, Floyd CE (2006) Characterization of difference of Gaussian filters in the detection of mammographic regions. Med Phys 33:4104–4114

Central Intelligence Agency (2017) The world factbook. https://www.cia.gov/library/publications/the-world-factbook/geo. . .

Chari A, Haselbach D, Kirves J-M, Ohmer J, Paknia E, Fischer N, Ganichkin O, Möller V, Frye JJ, Petzold G, Jarvis M, Tietzel M, Grimm C, Peters J-M, Schulman BA, Tittmann K, Markl J, Fischer U, Stark H (2015) ProteoPlex: stability optimization of macromolecular complexes by sparse-matrix screening of chemical space. Nat Methods 12:859–865

Chen B-C, Legant WR, Wang K, Shao L, Milkie DE, Davidson MW, Janetopoulos C, Wu XS, Hammer JA, Liu Z, English BP, Mimori-Kiyosue Y, Romero DP, Ritter AT, Lippincott-Schwartz J, Fritz-Laylin L, Mullins RD, Mitchell DM, Bembenek JN, Reymann A-C, Bohme R, Grill SW, Wang JT, Seydoux G, Tulu US, Kiehart DP, Betzig E (2014) Lattice light-sheet microscopy: imaging molecules to embryos at high spatiotemporal resolution. Science 346:1257998

Chuartzman SG, Nevo R, Shimoni E, Charuvi D, Kiss V, Ohad I, Brumfeld V, Reich Z (2008) Thylakoid membrane remodeling during state transitions in Arabidopsis. Plant Cell 20:1029–1039

Cingolani G, Duncan TM (2011) Structure of the ATP synthase catalytic complex (F(1)) from Escherichia coli in an autoinhibited conformation. Nat Struct Mol Biol 18:701–707

Cope J, Gilbert S, Rayment I, Mastronarde D, Hoenger A (2011) Cryo-electron tomography of microtubule-kinesin motor complexes. J Struct Biol 170:257–265

Cortese K, Vicidomini G, Gagliani MC, Boccacci P, Diaspro A, Tacchetti C (2013) High data output method for 3-D correlative light-electron microscopy using ultrathin cryosections. In: Suosa AA, Kruhlak MJ (eds) Nanoimaging. Springer, New York, pp 417–438

Danev R, Baumeister W (2016) Cryo-EM single particle analysis with the Volta phase plate. Elife. doi:10.7554/eLife.13046.001

Danev R, Buijsse B, Khoshouei M, Plitzko JM, Baumeister W (2014) Volta potential phase plate for in-focus phase contrast transmission electron microscopy. Proc Natl Acad Sci U S A 111:15635–15640

Davies KM, Strauss M, Daum B, Kief JH, Osiewacz HD, Rycovska A, Zickermann V, Kuhlbrandt W (2011) Macromolecular organization of ATP synthase and complex I in whole mitochondria. Proc Natl Acad Sci 108:14121–14126

de Boer P, Hoogenboom JP, Giepmans BNG (2015) Correlated light and electron microscopy: ultrastructure lights up! Nat Methods 12:503–513

de Castro IF, Sanz-Sánchez L, Risco C (2014) Chap 3: Metallothioneins for correlative light and electron microscopy (pp 55–70). In: Thomas M-R, Paul V (eds) Correlative light and electron microscopy II, Methods in cell biology, vol 124. Academic Press, Cambridge, 452 pp. isbn:978-0128010754

Deisenhofer J, Epp O, Miki K, Huber R, Michel H (1985) Structure of the protein subunits in the photosynthetic reaction centre of Rhodopseudomonas viridis at 3A resolution. Nature 318:618–624

Delosme R, Olive J, Wollman F-A (1996) Changes in light energy distribution upon state transitions: an in vivo photoacoustic study of the wild type and photosynthesis mutants from Chlamydomonas reinhardtii. Biochim Biophys Acta 1273:150–158

Dickson VK, Silvester JA, Fearnley IM, AGW L, Walker JE (2006) On the structure of the stator of the mitochondrial ATP synthase. EMBO J 25:2911–2918

Dohnalkova AC, Kennedy DW, Mancuso J, Marshall MJ, Mainwaring PR, Fredrickson JK (2010) Characterization of pipe bomb fragments using optical microscopy and scanning electron microscopy. Microsc Microanal 16:1870–1871

Drop B, Webber-birungi M, Fusetti F, Kouril R, Kevin E, Boekema EJ, Croce R (2011) Photosystem I of Chlamydomonas reinhardtii contains nine light-harvesting complexes (Lhca) located on one side of the core. J Biol Chem 286:44878–44887

Drop B, Webber-Birungi M, Yadav SKN, Filipowicz-Szymanska A, Fusetti F, Boekema EJ, Croce R (2014a) Light-harvesting complex II (LHCII) and its supramolecular organization in Chlamydomonas reinhardtii. Biochim Biophys Acta 1837:63–72

Drop B, Yadav KNS, Boekema EJ, Croce R (2014b) Consequences of state transitions on the structural and functional organization of Photosystem I in the green alga Chlamydomonas reinhardtii. Plant J 78:181–191

Dubochet J, Adrian M, Chang J-J, Homo J-C, Lepault J, McDowall AW, Schultz P (1988) Cryo-electron microscopy of vitrified specimens. Q Rev Biophys 21:129–228

Engel GS, Engel GS, Calhoun TR, Calhoun TR, Read EL, Read EL, Ahn T-K, Ahn T-K, Mancal T, Mancal T, Cheng Y-C, Cheng Y-C, Blankenship RE, Blankenship RE, Fleming GR, Fleming GR (2007) Evidence for wavelike energy transfer through quantum coherence in photosynthetic systems. Nature 446:782–786

Engel BD, Schaffer M, Cuellar LK, Villa E, Plitzko JM, Baumeister W (2015) Native architecture of the Chlamydomonas chloroplast revealed by in situ cryo-electron tomography. Elife 2015:1–29

Ferreira KN, Iverson TM, Maghlaoui K, Barber J, Iwata S (2004) Architecture of the photosynthetic oxygen-evolving center. Science 303:1831–1838

Finazzi G (2005) The central role of the green alga Chlamydomonas reinhardtii in revealing the mechanism of state transitions. J Exp Bot 56:383–388

Fischer N, Neumann P, Konevega AL, Bock LV, Ficner R, Rodnina MV, Stark H (2015) Structure of the E. coli ribosome–EF-Tu complex at <3 Å resolution by Cs-corrected cryo-EM. Nature 520:567–570

Food and Agriculture Organisation (FAO) of the United Nations (2009) How to feed the world in 2050. 1–35

Ford RC, Holzenburg A (2014) Organization of protein complexes and a mechanism for grana formation in photosynthetic membranes as revealed by cryo-electron microscopy. Cryst Res Technol 49:637–644

Frangakis AS, Hegerl R (2001) Noise reduction in electron tomographic reconstructions using nonlinear anisotropic diffusion. J Struct Biol 135:239–250

Fukuyama K, Hase T, Matsumoto S, Tsukihara T, Katsube Y (1980) Structure of S. platensis [2Fe-2S] ferredoxin and evolution of the chloroplast-type ferredoxins. Nature 286:522–524

Gaietta G, Deerinck TJ, Adams SR, Bouwer J, Tour O, Laird DW, Sosinsky GE, Tsien RY, Ellisman MH (2002) Multicolor and electron microscopic imaging of connexin trafficking. Science 296:503–507

Gaietta GM, Giepmans BNG, Deerinck TJ, Smith WB, Ngan L, Llopis J, Adams SR, Tsien RY, Ellisman MH (2006) Golgi twins in late mitosis revealed by genetically encoded tags for live cell imaging and correlated electron microscopy. Proc Natl Acad Sci U S A 103:17777–17782

Galaz-Montoya JG, Flanagan J, Schmid MF, Ludtke SJ (2015) Single particle tomography in EMAN2. J Struct Biol 190:279–290

Garcia-Sanchez MI, Diaz-Quintana A, Gotor C, Jacquot JP, De la Rosa MA, Vega JM (2000) Homology predicted structure and functional interaction of ferredoxin from the eukaryotic alga Chlamydomonas reinhardtii with nitrite reductase and glutamate synthase. J Biol Inorg Chem 5:713–719

Germano M, Yakushevska AE, Keegstra W, van Gorkom HJ, Dekker JP, Boekema EJ (2002) Supramolecular organization of photosystem I and light-harvesting complex I in Chlamydomonas reinhardtii. FEBS Lett 525:121–125

Gibbons C, Montgomery MG, Leslie AG, Walker JE (2000) The structure of the central stalk in bovine F(1)-ATPase at 2.4 A resolution. Nat Struct Biol 7:1055–1061

Gold VAM, Ieva R, Walter A, Pfanner N, van der Laan M, Kühlbrandt W (2014) Visualizing active membrane protein complexes by electron cryotomography. Nat Commun 5:4129

Goodenough UW, Levine RP (1969) Chloroplast ultrastructure in mutant strains of Chlamydomonas reinhardi lacking components of the photosynthetic apparatus. Plant Physiol 44:990–1000

Goodenough U, Staehelin LA (1971) Structural differentiation of stacked and unstacked chloroplast membranes freeze-etch electron microscopy of wild-type and mutant strains of Chlamydomonas. J Cell Biol 48:594–619

Gregory JA, Topol AB, Doerner DZ, Mayfield S (2013) Alga-produced cholera toxin-Pfs25 fusion proteins as oral vaccines. Appl Environ Microbiol 79:3917–3925

Groth G, Pohl E (2001) The structure of the chloroplast F1-ATPase at 3.2 Å resolution. J Biol Chem 276:1345–1352

Guskov A, Kern J, Gabdulkhakov A, Broser M, Zouni A, Saenger W (2009) Cyanobacterial photosystem II at 2.9-A resolution and the role of quinones, lipids, channels and chloride. Nat Struct Mol Biol 16:334–342

Haehnel W, Ratajczak R, Robenek H (1989) Lateral distribution and diffusion of plastocyanin in chloroplast thylakoids. J Cell Biol 108:1397–1405

Hakulinen JK, Klyszejko AL, Hoffmann J, Eckhardt-strelau L, Brutschy B, Vonck J (2012) Structural study on the architecture of the bacterial ATP synthase F o motor. Proc Natl Acad Sci 109:2050–2056

Hasan SS, Cramer WA (2014) Internal lipid architecture of the hetero-oligomeric cytochrome b 6f complex. Structure 22:1008–1015

Hasan SS, Stofleth JT, Yamashita E, Cramer WA (2013) Lipid-induced conformational changes within the cytochrome b6f complex of oxygenic photosynthesis. Biochemistry 52:2649–2654

Hauer F, Gerle C, Fischer N, Oshima A, Shinzawa-Itoh K, Shimada S, Yokoyama K, Fujiyoshi Y, Stark H (2015) GraDeR: membrane protein complex preparation for single-particle cryo-EM. Structure 23:1769–1775

Heymann JB, Belnap DM (2007) Bsoft: image processing and molecular modeling for electron microscopy. J Struct Biol 157:3–18

Hippler M, Ratajczak R, Haehnel W (1989) Identification of the plastocyanin binding subunit of photosystem I. FEBS Lett 250:280–284

Hobe S, Förster R, Klingler J, Paulsen H (1995) N-proximal sequence motif in light-harvesting chlorophyll *a*/*b*-binding protein is essential for the trimerization of light-harvesting chlorophyll *a*/*b* complex. Biochemistry 34:10224–10228

Hoffmann C, Gaietta G, Zürn A, Adams SR, Terrillon S, Ellisman MH, Tsien RY, Lohse MJ (2010) Fluorescent labelling of tetracycteine-tagged proteins in intact cells. Nature 5:1666–1677

Hrabe T, Chen Y, Pfeffer S, Kuhn Cuellar L, Mangold AV, Förster F (2012) PyTom: a python-based toolbox for localization of macromolecules in cryo-electron tomograms and subtomogram analysis. J Struct Biol 178:177–188

Huang C, Wang ZQ, Lin HN, Brumbaugh EE, Li S (1994) Interconversion of bilayer phase transition temperatures between phosphatidylethanolamines and phosphatidylcholines. Biophys Biochem Acta 1189:7–12

Huisken J, Stainier DYR (2009) Selective plane illumination microscopy techniques in developmental biology. Development 136:1963–1975

Huisken J, Swoger J, Del Bene F, Wittbrodt J, Stelzer EHK (2004) Optical sectioning deep inside live embryos by selective plane illumination microscopy. Science 305:1007–1009

Intergovernmental Panel on Climate Change (2014) Climate change 2014: Synthesis Report. In: Core Writing Team Pachauri RK and Meyer LA (eds) Contribution of Working Groups I, II and III to the fifth assessment report of the Intergovernmental Panel on Climate Change. IPCC, Geneva

International Energy Agency (2010) World energy outlook. IEA, Paris

Ito Y, Ikeguchi M (2010) Structural fluctuation and concerted motions in F1-ATPase: a molecular dynamics study. J Comput Chem 31:2175–2185

Iwai M, Takahashi Y, Minagawa J (2008) Molecular remodeling of photosystem II during state transitions in Chlamydomonas reinhardtii. Plant Cell 20:2177–2189

Iwai M, Takizawa K, Tokutsu R, Okamuro A, Takahashi Y, Minagawa J (2010) Isolation of the elusive supercomplex that drives cyclic electron flow in photosynthesis. Nature 464:1210–1213

Jans F, Mignolet E, Houyoux P-A, Cardol P, Ghysels B, Cuiné S, Cournac L, Peltier G, Remacle C, Franck F (2008) A type II NAD(P)H dehydrogenase mediates light-independent

plastoquinone reduction in the chloroplast of Chlamydomonas. Proc Natl Acad Sci U S A 105:20546–20551
Jiang W, Hermolin J, Fillingame RH (2001) The preferred stoichiometry of c subunits in the rotary motor sector of Escherichia coli ATP synthase is 10. Proc Natl Acad Sci U S A 98:4966–4971
Johnson GN (2011) Physiology of PSI cyclic electron transport in higher plants. Biochim Biophys Acta 1807:384–389
Johnson UG, Porter KR (1968) Fine structure of cell division in Chlamydomonas reinhardi. Basal bodies and microtubules. J Cell Biol 38:403–425
Johnson MP, Vasilev C, Olsen JD, Hunter CN (2014) Nanodomains of cytochrome b_6f and photosystem II complexes in spinach grana thylakoid membranes. Plant Cell 26:3051–3061
Jordan P, Fromme P, Witt HT, Klukas O, Saenger W, Krauss N (2001) Three-dimensional structure of cyanobacterial photosystem I at 2.5 A resolution. Nature 411:909–917
Kabaleeswaran V, Puri N, Walker JE, Leslie AGW, Mueller DM (2006) Novel features of the rotary catalytic mechanism revealed in the structure of yeast F1 ATPase. EMBO J 25:5433–5442
Kamiya N, Shen J-R (2003) Crystal structure of oxygen-evolving photosystem II from Thermosynechococcus vulcanus at 3.7-A resolution. Proc Natl Acad Sci U S A 100:98–103
Kapla J, Stevensson B, Dahlberg M, Maliniak A (2012) Molecular dynamics simulations of membranes composed of glycolipids and phospholipids. J Phys Chem B 116:244–252
Kargul J, Nield J, Barber J (2003) Three-dimensional reconstruction of a light-harvesting complex I-photosystem I (LHCI-PSI) supercomplex from the green alga Chlamydomonas reinhardtii: insights into light harvesting for PSI. J Biol Chem 278:16135–16141
Kargul J, Turkina MV, Nield J, Benson S, Vener AV, Barber J (2005) Light-harvesting complex II protein CP29 binds to photosystem I of Chlamydomonas reinhardtii under state 2 conditions. FEBS J 272:4797–4806
Karplus PA, Daniels MJ, Herriott JR, Herriogir JONR (1991) Atomic structure of ferredoxin-NADP+ reductase: prototype for a structurally novel flavoenzyme family. Nature 251:60–66
Kass M, Witkin A, Terzopoulos D (1988) Snakes: active contour models. Int J Comput Vis 1:321–331
Kastner B, Fischer N, Golas MM, Sander B, Dube P, Boehringer D, Hartmuth K, Deckert J, Hauer F, Wolf E, Uchtenhagen H, Urlaub H, Herzog F, Peters JM, Poerschke D, Lührmann R, Stark H (2008) GraFix: sample preparation for single-particle electron cryomicroscopy. Nat Methods 5:53–55
Kerfeld CA, Anwar HP, Interrante R, Merchant S, Yeates TO (1995) The structure of chloroplast cytochrome c6 at 1.9 A resolution: evidence for functional oligomerization. J Mol Biol 250:627–647
Kern J, Alonso-Mori R, Tran R, Hattne J, Gildea RJ, Echols N, Gloeckner C, Hellmich J, Laksmono H, Sierra RG, Lassalle-Kaiser B, Koroidov S, Lampe A, Han G, Gul S, DiFiore D, Milathianaki D, Fry AR, Miahnahri A, Schafer DW, Messerschmidt M, Seibert MM, Koglin JE, Sokaras D, Weng T-C, Sellberg J, Latimer MJ, Grosse-Kunstleve RW, Zwart PH, White WE, Glatzel P, Adams PD, Bogan MJ, Williams GJ, Boutet S, Messinger J, Zouni A, Sauter NK, Yachandra VK, Bergmann U, Yano J (2013) Simultaneous femtosecond X-ray spectroscopy and diffraction of photosystem II at room temperature. Science 340:491–496
Kern J, Tran R, Alonso-Mori R, Koroidov S, Echols N, Hattne J, Ibrahim M, Gul S, Laksmono H, Sierra RG, Gildea RJ, Han G, Hellmich J, Lassalle-Kaiser B, Chatterjee R, Brewster AS, Stan CA, Glockner C, Lampe A, DiFiore D, Milathianaki D, Fry AR, Seibert MM, Koglin JE, Gallo E, Uhlig J, Sokaras D, Weng TC, Zwart PH, Skinner DE, Bogan MJ, Messerschmidt M, Glatzel P, Williams GJ, Boutet S, Adams PD, Zouni A, Messinger J, Sauter NK, Bergmann U, Yano J, Yachandra VK (2014) Taking snapshots of photosynthetic water oxidation using femtosecond X-ray diffraction and spectroscopy. Nat Commun 5:4371
Kirchhoff H, Lenhert S, Büchel C, Chi L, Nield J (2008) Probing the organization of photosystem II in photosynthetic membranes by atomic force microscopy. Biochemistry 47:431–440

Knoetzel J, Svendsen I, Simpson DJ (1992) Identification of the photosystem I antenna polypeptides in barley. Eur J Biochem 206:209–215
Kouřil R, Oostergetel GT, Boekema EJ (2011) Fine structure of granal thylakoid membrane organization using cryo electron tomography. Biochim Biophys Acta 1807:368–374
Kouril R, Strouhal O, Nosek L, Lenobel R, Chamrad I, Boekema EJ, Sebela M, Ilik P (2014) Structural characterization of a plant photosystem I and NAD(P)H dehydrogenase supercomplex. Plant J 77:568–576
Krogh A, Larsson B, von Heijne G, Sonnhammer ELL (2001) Predicting transmembrane protein topology with a hidden Markov model: application to complete genomes. J Mol Biol 305:567–580
Kudryashev M, Castaño-Díez D, Deluz C, Hassaine G, Grasso L, Graf-Meyer A, Vogel H, Stahlberg H (2016) The structure of the mouse serotonin 5-HT3 receptor in lipid vesicles. Structure 24:165–170
Kühlbrandt W (2014) The resolution revolution. Science 343:1443–1444
Kühlbrandt W, Wang DN, Fujiyoshi Y (1994) Atomic model of plant light-harvesting complex by electron crystallography. Nature 367:614–621
Kurisu G, Kusunoki M, Katoh E, Yamazaki T, Teshima K, Onda Y, Kimata-Ariga Y, Hase T (2001) Structure of the electron transfer complex between ferredoxin and ferredoxin-NADP(+) reductase. Nat Struct Biol 8:117–121
Kurisu G, Zhang H, Smith JL, Cramer WA (2003) Structure of the cytochrome b6f complex of oxygenic photosynthesis: tuning the cavity. Science 302:1009–1014
Lata S, Reichel A, Brock R, Tampé R, Piehler J (2005) High-affinity adaptors for switchable recognition of histidine-tagged proteins. J Am Chem Soc 127:10205–10215
Lemaire C, Wollman FA, Bennoun P (1988) Restoration of phototrophic growth in a mutant of Chlamydomonas reinhardtii in which the chloroplast atpB gene of the ATP synthase has a deletion: an example of mitochondria-dependent photosynthesis. Proc Natl Acad Sci U S A 85:1344–1348
Liao M, Cao E, Julius D, Cheng Y (2013) Structure of the TRPV1 ion channel determined by electron cryo-microscopy. Nature 504:107–112
Lin YS, Lin JH, Chang CC (2010) Molecular dynamics simulations of the rotary motor F0 under external electric fields across the membrane. Biophys J 98:1009–1017
Liss V, Barlag B, Nietschke M, Hensel M (2015) Self-labelling enzymes as universal tags for fluorescence microscopy, super-resolution microscopy and electron microscopy. Sci Rep 5:17740
Liu Z, Yan H, Wang K, Kuang T, Zhang J, Gui L, An X, Chang W (2004) Crystal structure of spinach major light-harvesting complex at 2.72 A resolution. Nature 428:287–292
Loll B, Kern J, Saenger W, Zouni A, Biesiadka J (2005) Towards complete cofactor arrangement in the 3.0 A resolution structure of photosystem II. Nature 438:1040–1044
Lučić V, Rigort A, Baumeister W (2013) Cryo-electron tomography: the challenge of doing structural biology in situ. J Cell Biol 202:407–419
Marrink SJ, Risselada HJ, Yefimov S, Tieleman DP, Vries AH De (2007) The MARTINI force field: coarse grained model for biomolecular simulations. J Phys Chem B 111: 7812–7824.
Marsh BJ, Mastronarde DN, Buttle KF, Howell KE, McIntosh JR (2001) Organellar relationships in the Golgi region of the pancreatic beta cell line, HIT-T15, visualized by high resolution electron tomography. Proc Natl Acad Sci U S A 98:2399–2406
Martell JD, Deerinck TJ, Sancak Y, Poulos TL, Mootha VK, Sosinsky GE, Ellisman MH, Ting AY (2012) Engineered ascorbate peroxidase as a genetically encoded reporter for electron microscopy. Nat Biotechnol 30:1143–1148
Mazor Y, Borovikova A, Nelson N (2015) The structure of plant photosystem I super-complex at 2.8 Å resolution. Elife 4:1–18
McCammon JA, Gelin BR, Karplus M (1977) Dynamics of folded proteins. Nature 267:585–590
McDonnel A, Staehelin LA (1980) Adhesion between liposomes mediated by the chlorophyll a/b light-harvesting complex isolated from chloroplast membranes. J Cell Biol 84:40–56

McDowall AW, Chang J-J, Freeman R, Lepault J, Walter A, Dubochet J (1983) Electron microscopy of frozen hydrated sections of vitreous ice and vitrified biological samples. J Microsc 131:1–9
Meier T, Polzer P, Diederichs K, Welte W, Dimroth P (2005) Structure of the rotor ring of F-type Na+-ATPase from Ilyobacter tartaricus. Science 308:659–662
Meimberg K, Fischer N, Rochaix JD, Mühlenhoff U (1999) Lys35 of PsaC is required for the efficient photoreduction of flavodoxin by photosystem I from Chlamydomonas reinhardtii. Eur J Biochem 263:137–144
Menz RI, Walker JE, Leslie AGW (2001) Structure of bovine mitochondrial F1-ATPase with nucleotide bound to all three catalytic sites: implications for the mechanism of rotary catalysis. Cell 106:331–341
Meyer M, Griffiths H (2013) Origins and diversity of eukaryotic CO_2-concentrating mechanisms: lessons for the future. J Exp Bot 64:769–786
Meyer Zu Tittingdorf JMW, Rexroth S, Schäfer E, Schlichting R, Giersch C, Dencher NA, Seelert H (2004) The stoichiometry of the chloroplast ATP synthase oligomer III in Chlamydomonas reinhardtii is not affected by the metabolic state. Biochim Biophys Acta 1659:92–99
Miller KR, Staehelin LA (1976) Analysis of the thylakoid outer surface. Coupling factor is limited to unstacked membrane regions. J Cell Biol 68:30–47
Minagawa J (2009) Light-harvesting proteins. In: The Chlamydomonas sourcebook, 2-vol set. Elsevier, Amsterdam, pp 503–539
Minagawa J, Han KC, Dohmae N, Takio K, Inoue Y (2001) Molecular characterization and gene expression of lhcb5 gene encoding CP26 in the light-harvesting complex II of Chlamydomonas reinhardtii. Plant Mol Biol 46:277–287
Mitome N, Suzuki T, Hayashi S, Yoshida M (2004) Thermophilic ATP synthase has a decamer c-ring: indication of noninteger 10:3 H+/ATP ratio and permissive elastic coupling. Proc Natl Acad Sci U S A 101:12159–12164
Moor H, Mühlethaler K (1963) Fine structure in frozen-etched yeast cells. J Cell Biol 17:609–628
Morphew MK, O'Toole ET, Page CL, Pagratis M, Meehl J, Giddings T, Gardner JM, Ackerson C, Jaspersen SL, Winey M, Hoenger A, Mcintosh JR (2015) Metallothionein as a clonable tag for protein localization by electron microscopy of cells. J Microsc 260:20–29
Mullineaux CW (2014) Co-existence of photosynthetic and respiratory activities in cyanobacterial thylakoid membranes. Biochim Biophys Acta 1837:503–511
Mullineaux CW, Kirchhoff H (2007) Using fluorescence recovery after photobleaching to measure lipid diffusion in membranes. In: Dopico AM (ed) Methods in membrane lipids. Humana, Totowa, NJ, pp 267–276
Murphy DB, Davidson MW (2012) Confocal laser scanning microscopy. In: Murphy DB, Davidson MW (eds) Fundamentals of light microscopy and electronic imaging. Wiley-Blackwell, New York, pp 265–305
Mussgnug JH, Wobbe L, Elles I, Claus C, Hamilton M, Fink A (2005) NAB1 is an RNA binding protein involved in the light-regulated differential expression of the light-harvesting antenna of Chlamydomonas reinhardtii. Plant Cell 17:3409–3421
Mussgnug JH, Thomas-Hall S, Rupprecht J, Foo A, Klassen V, McDowall A, Schenk PM, Kruse O, Hankamer B (2007) Engineering photosynthetic light capture: impacts on improved solar energy to biomass conversion. Plant Biotechnol J 5:802–814
Mustárdy L, Garab G (2003) Granum revisited. A three-dimensional model - where things fall into place. Trends Plant Sci 8:117–122
Nagayoshi M, Murase K, Fujino K, Uenishi Y, Kawamata M, Nakamura Y, Kitamura K, Higuchi I, Oku N, Hatazawa J (2005) Usefulness of noise adaptive non-linear gaussian filter in FDG-PET study. Ann Nucl Med 19:469–477
Nevo R, Charuvi D, Tsabari O, Reich Z (2012) Composition, architecture and dynamics of the photosynthetic apparatus in higher plants. Plant J 70:157–176
Nicastro D, Schwartz C, Pierson J, Gaudette R, Porter ME, McIntosh JR (2006) The molecular architecture of axonemes revealed by cryoelectron tomography. Science 313:944–948

Nield J, Kruse O, Ruprecht J, Da Fonseca P, Büchel C, Barber J (2000) Three-dimensional structure of Chlamydomonas reinhardtii and Synechococcus elongatus photosystem II complexes allows for comparison their oxygen-evolving complex organization. J Biol Chem 275:27940–27946

Ogata K, Yuki T, Hatakeyama M, Uchida W, Nakamura S (2013) All-atom molecular dynamics simulation of photosystem II embedded in thylakoid membrane. J Am Chem Soc 135:15670–15673

Olive J, Vallon O (1991) Structural organization of the thylakoid membrane: freeze-fracture and immunocytochemical analysis. J Electron Microsc Tech 374:360–374

Olive J, Wollman FA, Bennoun P, Recouvreur M (1981) Ultrastructure of thylakoid membranes in C. reinhardtii: evidence for variations in the partition coefficient of the light-harvesting complex-containing particles upon membrane fracture. Arch Biochem Biophys 208:456–467

Organisation for Economic Co-Operation and Development (OECD) (2012) OECD environmental outlook to 2050. OECD, Paris

Pan X, Li M, Wan T, Wang L, Jia C, Hou Z, Zhao X, Zhang J, Chang W (2011) Structural insights into energy regulation of light-harvesting complex CP29 from spinach. Nat Struct Mol Biol 18:309–315

Pantelic RS, Rothnagel R, Huang C-Y, Muller D, Woolford D, Landsberg MJ, McDowall A, Pailthorpe B, Young PR, Banks J, Hankamer B, Ericksson G (2006) The discriminative bilateral filter: an enhanced denoising filter for electron microscopy data. J Struct Biol 155:395–408

Pantelic RS, Ericksson G, Hamilton N, Hankamer B (2007) Bilateral edge filter: photometrically weighted, discontinuity based edge detection. J Struct Biol 160:93–102

Pantelic RS, Meyer JC, Kaiser U, Stahlberg H (2012) The application of graphene as a sample support in transmission electron microscopy. Solid State Commun 152:1375–1382

Phuthong W, Huang Z, Wittkopp TM, Sznee K, Heinnickel ML, Dekker JP, Frese RN, Prinz FB, Grossman AR (2015) The use of contact mode atomic force microscopy in aqueous medium for structural analysis of spinach photosynthetic complexes. Plant Physiol 169:1318–1332

Pogoryelov D, Yu JS, Meier T, Vonck J, Dimroth P, Muller DJ (2005) The c(15) ring of the Spirulina platensis F-ATP synthase: F-1/F-0 symmetry mismatch is not obligatory. EMBO Rep 6:1040–1044

Preiner J, Horner A, Karner A, Ollinger N, Siligan C, Pohl P, Hinterdorfer P (2015) High-speed AFM images of thermal motion provide stiffness map of interfacial membrane protein moieties. Nano Lett 15:759–763

Preiss L, Klyszejko AL, Hicks DB, Liu J, Fackelmayer OJ, Yildiz Ö, Krulwich TA, Meier T (2013) The c-ring stoichiometry of ATP synthase is adapted to cell physiological requirements of alkaliphilic Bacillus pseudofirmus OF4. Proc Natl Acad Sci U S A 110:7874–7879

Pribil M, Labs M, Leister D (2014) Structure and dynamics of thylakoids in land plants. J Exp Bot 65:1955–1972

Qin X, Suga M, Kuang T, Shen J-R (2015) Structural basis for energy transfer pathways in the plant PSI-LHCI supercomplex. Science 348:989–995

Redinbo MR, Cascio D, Choukair MK, Rice D, Merchant S, Yeates TO (1993) The 1.5-A crystal structure of plastocyanin from the green alga Chlamydomonas reinhardtii. Biochemistry 32:10560–10567

Rees DM, Leslie AGW, Walker JE (2009) The structure of the membrane extrinsic region of bovine ATP synthase. Proc Natl Acad Sci U S A 106:21597–21601

Renault L, Chou HT, Chiu PL, Hill RM, Zeng X, Gipson B, Zhang ZY, Cheng A, Unger V, Stahlberg H (2006) Milestones in electron crystallography. J Comput Aided Mol Des 20:519–527

Ringsmuth AK, Landsberg MJ, Hankamer B (2016) Can photosynthesis enable a global transition from fossil fuels to solar fuels, to mitigate climate change and fuel-supply limitations? Renew Sustain Energy Rev 62:134–163

Ruskin RS, Yu Z, Grigorieff N (2013) Quantitative characterization of electron detectors for transmission electron microscopy. J Struct Biol 184:385–393
Russo CJ, Passmore LA (2014) Electron microscopy: ultrastable gold substrates for electron cryomicroscopy. Science 346:1377–1380
Rust MJ, Bates M, Zhuang XW (2006) Sub-diffraction-limit imaging by stochastic optical reconstruction microscopy (STORM). Nat Methods 3:793–795
Sager R, Palade GE (1954) Chloroplast structure in green and yellow strains of Chlamydomonas. Exp Cell Res 7:584–588
Sager R, Palade GE (1957) Structure and development of the chloroplast in Chlamydomonas: I. The normal green cell. J Cell Biol 3:463–488
Sakurai I, Shen JR, Leng J, Ohashi S, Kobayashi M, Wada H (2006) Lipids in oxygen-evolving photosystem II complexes of cyanobacteria and higher plants. J Biochem 140:201–209
Scheller HV, Jensen PE, Haldrup A, Lunde C, Knoetzel J (2001) Role of subunits in eukaryotic photosystem I. Biochim Biophys Acta 1507:41–60
Schep DG, Zhao J, Rubinstein JL (2016) Models for the a subunits of the *Thermus thermophilus* V/A-ATPase and *Saccharomyces cerevisiae* V-ATPase enzymes by cryo-EM and evolutionary covariance. Proc Natl Acad Sci 113(12):3245–3250
Schötz FA (1972) Dreidimensionale, maßstabgetreue Rekonstruktion einer grünen Flagellatenzelle nach Elektronenmikroskopie von Serienschnitten. Planta 159:152–159
Scott KA, Bond PJ, Ivetac A, Chetwynd AP, Khalid S, Sansom MSP (2008) Coarse-grained MD simulations of membrane protein-bilayer self-assembly. Structure 16:621–630
Seelert H, Poetsch A, Dencher NA, Engel A, Stahlberg H, Müller DJ (2000) Proton-powered turbine of a plant motor. Nature 405:418–419
Sétif P (2001) Ferredoxin and flavodoxin reduction by photosystem I. Biochim Biophys Acta 1507:161–179
Sétif P, Fischer N, Lagoutte B, Bottin H, Rochaix JD (2002) The ferredoxin docking site of photosystem I. Biochim Biophys Acta 1555:204–209
Shaw DE, Maragakis P, Lindorff-Larsen K, Piana S, Dror RO, Eastwood MP, Bank JA, Jumper JM, Salmon JK, Shan Y, Wriggers W (2010) Atomic-level characterization of the structural dynamics of proteins. Science 330:341–346
Shimoni E, Rav-Hon O, Ohad I, Brumfeld V, Reich Z (2005) Three-dimensional organization of higher-plant chloroplast thylakoid membranes revealed by electron tomography. Plant Cell 17:2580–2586
Shroff H, Galbraith CG, Galbraith JA, White H, Gillette J, Olenych S, Davidson MW, Betzig E (2007) Dual-color superresolution imaging of genetically expressed probes within individual adhesion complexes. Proc Natl Acad Sci U S A 104:20308–20313
Shtengel G, Galbraith JA, Galbraith CG, Lippincott-Schwartz J, Gillette JM, Manley S, Sougrat R, Waterman CM, Kanchanawong P, Davidson MW, Fetter RD, Hess HF (2009) Interferometric fluorescent super-resolution microscopy resolves 3D cellular ultrastructure. Proc Natl Acad Sci U S A 106:3125–3130
Shu X, Lev-Ram V, Deerinck TJ, Qi Y, Ramko EB, Davidson MW, Jin Y, Ellisman MH, Tsien RY (2011) A genetically encoded tag for correlated light and electron microscopy of intact cells, tissues, and organisms. PLoS Biol 9
Staehelin LA (2003) Chloroplast structure: from chlorophyll granules to supra-molecular architecture of thylakoid membranes. Photosynth Res 76:185–196
Stahlberg H, Müller DJ, Suda K, Fotiadis D, Engel A, Meier T, Matthey U, Dimroth P (2001) Bacterial Na(+)-ATP synthase has an undecameric rotor. EMBO Rep 2:229–233
Standfuss J, Terwisscha van Scheltinga AC, Lamborghini M, Kühlbrandt W (2005) Mechanisms of photoprotection and nonphotochemical quenching in pea light-harvesting complex at 2.5 A resolution. EMBO J 24:919–928
Stephens DJ, Allan VJ (2003) Light microscopy techniques for live cell imaging. Science 300:82–86

Stock D, Leslie AGW, Walker JE (1999) Molecular architecture of the rotary motor in ATP synthase. Science 286:1700–1705
Stocker A, Keis S, Cook GM, Dimroth P (2005) Purification, crystallization, and properties of F1-ATPase complexes from the thermoalkaliphilic Bacillus sp. strain TA2.A1. J Struct Biol 152:140–145
Stoschek A, Hegerl R (1997) Denoising of electron tomographic reconstructions using multiscale transformations. J Struct Biol 120:257–265
Stroebel D, Choquet Y, Popot J-L, Picot D (2003) An atypical haem in the cytochrome b(6)f complex. Nature 426:413–418
Suga M, Akita F, Hirata K, Ueno G, Murakami H, Nakajima Y, Shimizu T, Yamashita K, Yamamoto M, Ago H, Shen J (2014) Native structure of photosystem II at 1.95 Å resolution viewed by femtosecond X-ray pulses. Nature 517:99–103
Tokutsu R, Kato N, Bui KH, Ishikawa T, Minagawa J (2012) Revisiting the supramolecular organization of photosystem II in Chlamydomonas reinhardtii. J Biol Chem 287:31574–31581
Tran M, Van C, Barrera DJ, Pettersson PL, Peinado CD, Bui J, Mayfield SP (2013) Production of unique immunotoxin cancer therapeutics in algal chloroplasts. Proc Natl Acad Sci U S A 110: E15–E22
Umena Y, Kawakami K, Shen J-R, Kamiya N (2011) Crystal structure of oxygen-evolving photsystem II at a resolution of 1.9 Å. Nature 473:55–60
United Nations (2015) World population prospects: the 2015 revision, Key findings & advances tables
Vallon O, Bulte L, Dainese P, Olive J, Bassi R, Wollman FAW (1991) Lateral redistribution of cytochrome b6/f complexes along thylakoid membranes upon state transitions. Proc Natl Acad Sci U S A 88:8262–8266
van der Heide P, Xu XP, Marsh BJ, Hanein D, Volkmann N (2007) Efficient automatic noise reduction of electron tomographic reconstructions based on iterative median filtering. J Struct Biol 158:196–204
Van Eerden FJ, De Jong DH, De Vries AH, Wassenaar TA, Marrink SJ (2015) Characterization of thylakoid lipid membranes from cyanobacteria and higher plants by molecular dynamics simulations. Biochim Biophys Acta 1848:1319–1330
Vasilev C, Brindley AA, Olsen JD, Saer RG, Beatty JT, Hunter CN (2014) Nano-mechanical mapping of the interactions between surface-bound RC-LH1-PufX core complexes and cytochrome c 2 attached to an AFM probe. Photosynth Res 120:169–180
Vassiliev S, Zaraiskaya T, Bruce D (2012) Exploring the energetics of water permeation in photosystem II by multiple steered molecular dynamics simulations. Biochim Biophys Acta 1817:1671–1678
Volkmann N (2002) A novel three-dimensional variant of the watershed transform for segmentation of electron density maps. J Struct Biol 138:123–129
Vollmar M, Schlieper D, Winn M, Büchner C, Groth G (2009) Structure of the c14 rotor ring of the proton translocating chloroplast ATP synthase. J Biol Chem 284:18228–18235
Vu TQ, Lam WY, Hatch EW, Lidke DS (2015) Quantum dots for quantitative imaging: from single molecules to tissue. Cell Tissue Res:71–86
Warshel A, Levitt M (1976) Theoretical studies of enzymic reactions: dielectric, electrostatic and steric stabilization of the carbonium ion in the reaction of lysozyme. J Mol Biol 103:227–249
Watanabe S, Punge A, Hollopeter G, Willig KI, Hobson RJ, Davis MW, Hell SW, Jorgensen EM (2011) Protein localization in electron micrographs using fluorescence nanoscopy. Nat Methods 8:80–84
Watt IN, Montgomery MG, Runswick MJ, Leslie AGW, Walker JE (2010) Bioenergetic cost of making an adenosine triphosphate molecule in animal mitochondria. Proc Natl Acad Sci U S A 107:16823–16827
Wei X, Su X, Cao P, Liu X, Chang W, Li M, Zhang X, Liu Z (2016) Structure of spinach photosystem II–LHCII supercomplex at 3.2 Å resolution. Nature 1:1–18
White SH (2016) Membrane proteins of known 3D structure. http://blanco.biomol.uci.edu/mpstruc/

Wollman FA, Olive J, Bennoun P, Recouvreur M (1980) Organization of the photosystem-II centers and their associated antennae in the thylakoid membranes - a comparative ultrastructural, biochemical, and biophysical study of Chlamydomonas wild-type and mutants lacking in photosystem-II reaction centers. J Cell Biol 87:728–735

Zhao C, Hellman LM, Zhan X, Bowman WS, Whiteheart SW, Fried MG (2010) Hexahistidine-tag-specific optical probes for analyses of proteins and their interactions. Anal Biochem 399:237–245

Zouni A, Witt HT, Kern J, Fromme P, Krauss N, Saenger W, Orth P (2001) Crystal structure of photosystem II from Synechococcus elongatus at 3.8 A resolution. Nature 409:739–743

Chlamydomonas: Triacylglycerol Accumulation

Mia Terashima

Abstract The unicellular microalga *Chlamydomonas reinhardtii* exhibits immense metabolic flexibility, adjusting to changes in the environment and nutrient availability. One metabolic response under stress conditions is the synthesis of the neutral lipid triacylglycerol (TAG), accumulating as intracellular lipid droplets in the cytosol and chloroplast. With increased industrial interest in microalgal production of biofuels, feed, food, and chemicals, research on lipid metabolism using *C. reinhardtii* as a model system has accelerated in recent years. Conditions in which *C. reinhardtii* accumulates TAG have been identified, with nitrogen starvation as one of the most commonly used methods for induction. Genome, transcriptome, proteome, and lipidome analyses have provided information on the pathways involved in TAG synthesis and degradation. These studies have demonstrated that although a multitude of stress conditions induce TAG accumulation, there are differential response and regulatory mechanisms occurring under various induction conditions. Studies utilizing mutants have further led to the identification of pathways and regulatory components contributing to TAG synthesis and degradation. TAG metabolism is a multifaceted process in *C. reinhardtii*, and induction of TAG accumulation is accompanied by major reorganization of metabolic pathways, adjustments of photosynthetic complexes, membrane lipid recycling, and changes in carbon partitioning.

1 Introduction

Intracellular polymers serving as energy reserves are found in organisms across the tree of life. Among these, synthesis and accumulation of the neutral lipid triacylglycerol (TAG) in the form of lipid droplets are widespread in eukaryotic cells and are also found in prokaryotes (Gao and Goodman 2015; Waltermann et al. 2007). The unicellular microalga *Chlamydomonas reinhardtii* (hereafter Chlamydomonas) is no exception and accumulates TAGs, especially under nutrient

M. Terashima (✉)
Institute of Low Temperature Science, Hokkaido University, Kita 19 Nishi 8, Kita-ku, Sapporo 060-0819, Japan
e-mail: m.terashima@lowtem.hokudai.ac.jp

M. Hippler (ed.), *Chlamydomonas: Biotechnology and Biomedicine*, Microbiology Monographs 31, DOI 10.1007/978-3-319-66360-9_8

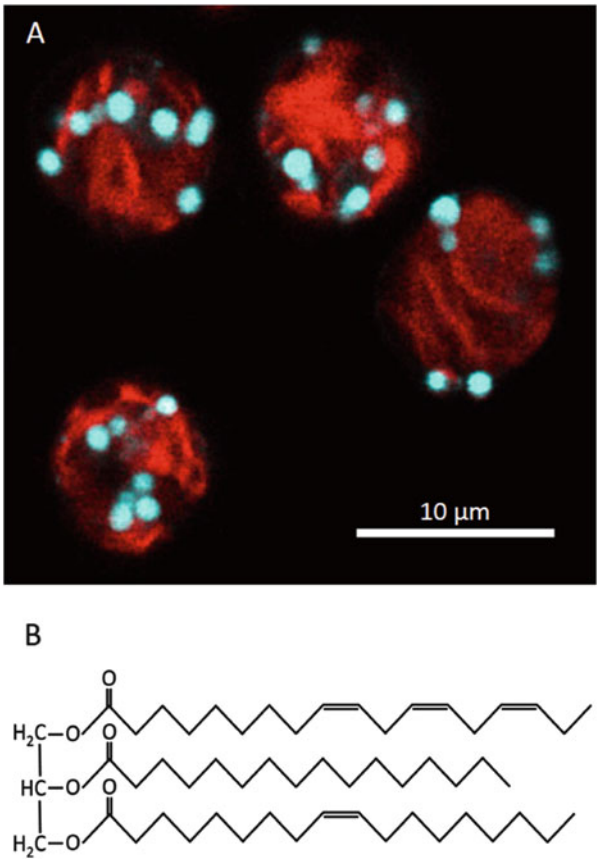

Fig. 1 *Chlamydomonas reinhardtii* accumulates triacylglycerol (TAG) in intracellular lipid droplets. (**a**) A false color image of Chlamydomonas cells after 4 days of nitrogen starvation and stained with nile red. *Cyan* represents fluorescence signal from nile red-stained lipid droplets, and *red* represents chlorophyll autofluorescence. Image was taken with a Leica SP5 confocal microscope using a 488 nm laser excitation and emission captured at 536–544 nm for nile red and 676–684 nm for chlorophyll. (**b**) An example of a triacylglycerol lipid species, TAG 18:3/16:0/18:1. Reference for protocol used for nile red staining and imaging: (Terashima et al. 2015)

deprivation or other environmental stress factors (Fig. 1a) (Merchant et al. 2012; Goold et al. 2015). Chlamydomonas has been studied in more detail compared to any other alga, resulting in the availability of molecular and genetic tools, annotated genome information, and an ever-increasing library of mapped mutants (Liu and Benning 2013; Blaby et al. 2014; Li et al. 2016b). For this reason, Chlamydomonas has become a model system to investigate microalgal lipid metabolism, and research in this field has particularly gained traction due to potential interest in the production of biofuels and high-grade lipids (Hu et al. 2008; Liu and Benning 2013; Goncalves et al. 2016).

TAG is a neutral lipid consisting of a glycerol backbone esterified with three fatty acid chains (Fig. 1b). TAGs allow for a considerable amount of metabolic energy to be stored due to its reduced and anhydrous nature. As TAGs are insoluble in water, they are also a suitable storage compound because they do not affect the aqueous substrate concentrations in the cells, allowing for storage of carbon compounds without affecting cellular metabolic flux (Flatt 1995). Additionally,

compared with free fatty acids, TAGs have low toxicity (Wältermann and Steinbüchel 2006).

Lipid droplets were once considered metabolically dormant storage organelles but have recently been recognized as important organelles for energy metabolism, playing a significant role in communication with other cellular organelles (Gao and Goodman 2015; Liu et al. 2013b). Therefore, understanding the physiological process and regulation of TAG accumulation merits investigation, both for basic science and for biotechnological applications.

2 Triacylglycerol Accumulation in Chlamydomonas

TAG accumulation in Chlamydomonas varies greatly depending on the strains and growth conditions. For wild type, 2 days of nitrogen starvation results in 2–15% dry weight TAG accumulation and 20–65% TAG accumulation reported for strains blocked in starch synthesis (Li et al. 2010a; Siaut et al. 2011; James et al. 2011). Numerous studies have been conducted to test different cultivation conditions of various wild-type and mutant strains. These types of growth tests and mutant characterizations in combination with omics analyses are beginning to reveal the complex metabolic pathways and regulation behind TAG accumulation in Chlamydomonas.

2.1 TAG Synthesis Is Triggered by Exposure to Stressful Growth Conditions

In Chlamydomonas, TAG accumulation is induced under stressful growth conditions. Among nutrient limitation stress, nitrogen starvation has the strongest induction of TAG synthesis, with TAG appearing in the form of lipid droplets already after 6 h following transfer to nitrogen-free, acetate-containing media (photoheterotrophic conditions), and increases exponentially up to 3 days, after which accumulation continues at a slower pace (Park et al. 2015; Siaut et al. 2011). TAG accumulation can be further enhanced under photoheterotrophic conditions by supplying the culture with extra acetate after 2 days of nitrogen starvation or even by growing cells in nitrogen-replete conditions but with extra acetate, effectively changing the carbon-to-nitrogen ratio in the media (Goodson et al. 2011; Goodenough et al. 2014; Fan et al. 2012). TAG synthesis also occurs under photoautotrophic nitrogen-depleted conditions but at a slower rate (Merchant et al. 2012; Davey et al. 2014). Additionally, when observed over a longer period, TAG initially accumulates over the first 2 days under photoautotrophic conditions but decreases rapidly back to baseline levels by day 6 (Schulz-Raffelt et al. 2016). However, another study found accumulation to steadily continue over 10 days

under photoautotrophic conditions with low nitrogen levels (tenfold lower than normal conditions) (Davey et al. 2014). Supplying minimal levels of nitrogen may sustain photoautotrophic TAG synthesis longer. Photosynthesis appears to be important for TAG synthesis, as TAG accumulation was significantly compromised under dark heterotrophic conditions and under photoheterotrophic conditions with photosynthesis blocked by the addition of a chemical inhibitor of photosystem II, 3-(3,4-dichlorophenyl)-1,1-dimethylurea (DCMU) (Fan et al. 2012).

Aside from nitrogen depletion, other growth conditions such as phosphate or sulfur deficiency, anaerobiosis, and salt or high light stress can induce TAG accumulation but to a lesser extent (Bajhaiya et al. 2016; Sato et al. 2014; Fan et al. 2011; Hemschemeier et al. 2013; Siaut et al. 2011). In nutrient-limiting conditions, TAG accumulation acts as a sink for carbon and photosynthetically generated reducing equivalents, a process that occurs over hours to days (Johnson and Alric 2013; Li et al. 2012b). There are also faster induction conditions that cause TAGs to accumulate already within an hour, such as heat stress and chemical treatments (Legeret et al. 2016; Kim et al. 2013, 2015). Heat stress and treatment with fungicide fenpropimorph, an inhibitor of sterol biosynthesis, induce chloroplast polar membrane lipids to be rapidly converted to TAGs (Legeret et al. 2016; Kim et al. 2015). Similarly, brefeldin A treatment causes ER stress, resulting in lipid droplet increase (Kim et al. 2013). Lipid droplets are believed to be in part synthesized in the ER, and disrupting vesicular transport in the ER by brefeldin A treatment may result in the accumulation of substrates of TAG synthesis, further enhancing TAG accumulation. Heat stress and chemical treatments that damage the cell can cause a rapid accumulation of unstable compounds such as unfolded proteins with exposed hydrophobic residues, and lipid droplets may provide a docking site for such unstable compounds and prevent further cellular damage (Kim et al. 2013; Welte 2007).

2.2 *TAG and Starch Are the Main Carbon Sinks in Chlamydomonas*

Under nitrogen starvation, growth is compromised with little cell density change observed after 24 h (Valledor et al. 2014; Park et al. 2015). Transcriptomic analyses after 48 h of nitrogen starvation indicate, as expected, that protein synthesis and glyoxylate and gluconeogenesis pathways are stalled and acetate is incorporated into fatty acids (Miller et al. 2010). Transcriptomics and proteomics starting from 0.5 to 24 h after switch to media without nitrogen show the metabolic transitioning leading to TAG accumulation (Park et al. 2015). Interestingly, glyoxylate cycle inhibition occurs very early on, resulting in a decrease of transcripts already 2 h and full protein reduction 24 h after switch to nitrogen-starved media. In contrast, gluconeogenesis is initially induced during the first couple of hours followed by reduction. TCA cycle transcripts were reduced during the first 24 h, but protein

levels remained stable. An enzyme of the TCA cycle, citrate synthase (CIS), had decreased transcripts after 2 days of nitrogen starvation and appears to affect TAG accumulation (Deng et al. 2013). RNA interference-based suppression of *CIS* gene expression led to increased TAG accumulation and overexpressing *CIS*-reduced cellular TAG levels, suggesting a link between TAG accumulation and cellular carbon flux via CIS. These data indicate that TAG accumulation is accompanied by major metabolic reorganization. In addition, proteomic analysis points to induction of ammonia uptake and assimilation enzymes and starch synthesis enzymes, while protein biosynthesis and amino acid degradation enzymes were decreased (Valledor et al. 2014). By storing excess carbon as starch and TAGs under nitrogen starvation, when nitrogen becomes readily available again, turnover of these stored fixed carbon reserves can allow for rapid synthesis of proteins for cell growth (Scott et al. 2010). As expected, lipid droplets formed during nitrogen starvation are rapidly consumed, with TAG content returning to basal levels within 2 days (Li et al. 2012a; Siaut et al. 2011).

Starch appears to be the initial carbon sink during nitrogen starvation, with rapid accumulation occurring during the first 24 h, while TAG accumulation is more delayed and lasts for several days (Siaut et al. 2011; Fan et al. 2012; Gardner et al. 2013; Krishnan et al. 2015). Accordingly, transcripts for enzymes involved in starch synthesis were induced already after 30 min following transfer to nitrogen-deprived medium (Park et al. 2015). Not surprisingly, mutants blocked in starch synthesis accumulate higher levels of TAG, and these "starchless" mutants are still among the highest TAG-accumulating strains in Chlamydomonas today, with high TAG content on a per-cell basis and by dry weight when measured during the early phase of TAG accumulation (~24 h) and during the later phases (24–96 h) (Ball et al. 1991; Zabawinski et al. 2001; Wang et al. 2009; Li et al. 2010b, a; Work et al. 2010; Goodson et al. 2011; Velmurugan et al. 2013). However, it is worth noting that various regularly used laboratory background strains of Chlamydomonas showed differing amounts of TAG accumulation, suggesting that a wide range of factors can affect carbon flux (Siaut et al. 2011). TAG accumulation is a multifaceted phenomenon with no single "on" and "off" switch, and comparison of mutants to its original background strain is crucial.

2.3 TAG Stems from Both Exogenous and Photosynthetically Fixed Carbon Sources

Fixed carbon via photosynthesis and acetate taken up from the media are both carbon sources for TAGs (Davey et al. 2014). Addition of exogenous lipids or fatty acids to the medium has also been reported to induce TAG accumulation (Grenier et al. 1991; Fan et al. 2011). Fatty acids that are esterified to the glycerol backbone to generate TAG are either synthesized de novo or derived from degraded membrane lipids (Liu and Benning 2013). Fatty acids are synthesized in the chloroplast

and get incorporated into TAGs either directly in the chloroplast or the free fatty acids are exported to the cytosol followed by import to the endoplasmic reticulum (ER) for TAG synthesis (Fan et al. 2011; Riekhof et al. 2005). Because changing the carbon-to-nitrogen ratio affects carbon flux in the cell, the highest TAG accumulation, albeit transient, has been achieved by adding external carbon sources, with increases observed both during photoheterotrophic conditions by additional acetate and during photoautotrophic conditions by induction in higher CO_2 levels (Goodson et al. 2011; Goodenough et al. 2014; Fan et al. 2012; Gardner et al. 2013; Goncalves et al. 2016).

3 TAG Synthesis: A Process Involving the Chloroplast and the ER

Microscopy images show lipid droplets in both the cytosol and the chloroplast, and TAG synthesis is thought to occur both in the ER and the chloroplast (Fan et al. 2011; Goodson et al. 2011). A complete set of genes predicted to be involved in TAG synthesis has been identified in the Chlamydomonas genome; however, most enzymes lack experimental evidence for subcellular localization (Riekhof et al. 2005; Merchant et al. 2012; Li-Beisson et al. 2015). Utilizing subcellular prediction programs, proteomic data, and comparison to higher plants have provided hypothesized localization of pathways involved in TAG biosynthesis (Tardif et al. 2012; Li-Beisson et al. 2015). A model for ER-localized and chloroplast TAG synthesis pathways is shown in Fig. 2. Under nitrogen starvation, the total amount of fatty acids increases, suggesting that a certain amount of TAGs are derived from de novo synthesis and not solely from membrane lipid recycling (Moellering and Benning 2010).

3.1 TAGs Are De Novo Synthesized or Generated via Membrane Lipid Recycling

For de novo synthesis, TAG is synthesized by the sequential acylation of glycerol-3-phosphate via the production of its precursor diacylglycerol (DAG), which also acts as a precursor for the synthesis of other membrane lipids (Riekhof et al. 2005; Li-Beisson et al. 2015). DAG is synthesized through three enzymatic steps from glycerol-3-phosphate (Fig. 2). Glycerol-3-phosphate is acylated at the sn-1 position by glycerol-3-phosphate acyltransferase (GPAT) followed by a second acylation at the sn-2 position by lysophosphatidic acid acyltransferase (LPAT). The phosphate group on the sn-3 position is removed by a phosphatidic acid phosphatase (PAP) to yield DAG. Next, DAG is converted to TAG by the esterification of the sn-3 position with an acyl group. Diacylglycerol acyltransferase (DGAT)

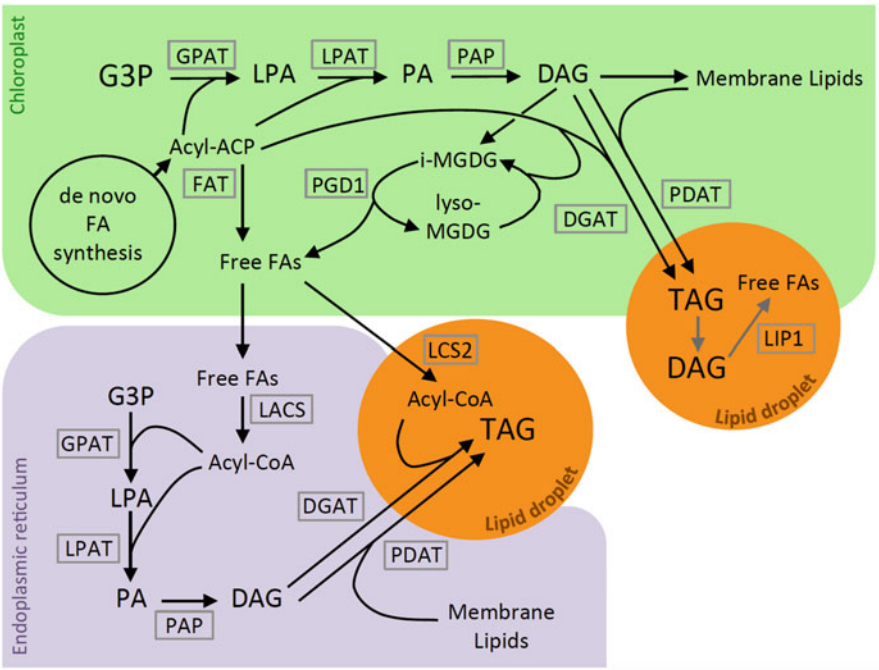

Fig. 2 Model for triacylglycerol (TAG) synthesis in *Chlamydomonas reinhardtii*. TAG is de novo synthesized via the acylation of glycerol-3-phosphate (G3P) with acyl chains derived from fatty acids synthesized in the chloroplast. Alternatively, acyl chains from membrane lipids are incorporated into TAGs. *ACP* acyl carrier protein, *DAG* diacylglycerol, *DGAT* diacylglycerol acyltransferase, *FA* fatty acid, *FAT* fatty acyl-ACP thioesterase, *GPAT* glycerol-3-phosphate acyltransferase, *i-MGDG* immature monogalactosyldiacylglycerol, *LACS* long-chain acyl-CoA synthetase, *LCS2* long-chain acyl-CoA synthetase 2, *LIP1* diacylglycerol lipase, *LPA* lysophosphatidic acid, *LPAT* lysophosphatidic acid acyltransferase, *PA* phosphatidic acid, *PAP* phosphatidic acid phosphatase, *PDAT* phospholipid:diacylglycerol acyltransferase, *PGD1* plastid galactoglycerolipid degradation 1. The localization of the enzymes should been seen as speculative, as experimental evidence for many are lacking or based on proteomic data, which does not rule out dual targeting (see text for details). Additionally, the mechanism of lipid transport between organelles is currently unknown, and the *arrows* are not indicative of any specific trafficking routes. *Green*, chloroplast; *purple*, endoplasmic reticulum; *orange*, lipid droplet. References for the figure: Riekhof et al. (2005), Moellering and Benning (2010), Nguyen et al. (2011), Fan et al. (2011), Goodson et al. (2011), Li et al. (2012a, b, 2016b), Boyle et al. (2012), Yoon et al. (2012), Liu and Benning (2013), Li-Beisson et al. (2015), Park et al. (2015), Goold et al. (2015), Goncalves et al. (2016)

catalyzes the reaction using acyl-CoA as a substrate (acyl-CoA-dependent TAG synthesis). Chlamydomonas has six genes encoding for DGAT (gene *DGAT1*, type I, and genes *DGTT1–DGTT5*, type II) (Miller et al. 2010). Heterologous complementation assays of Chlamydomonas DGTT in yeast mutants confirmed the functionality of DGTT1–DGTT3, but not DGTT4 (Hung et al. 2013). The reasons for so many isoforms of diacylglycerol transferases in Chlamydomonas

are unclear. However, recent research has shown distinct substrate specificities for each DGTT (Liu et al. 2016). DGTT1 favors unsaturated acyl-CoAs (especially polyunsaturated acyl-CoAs) and prefers shorter-chain acyl-CoAs. DGTT2 favors monounsaturated acyl-CoA, and DGTT3 prefers C16-containing acyl-CoA. Additionally, DGTT1 is partial for a DAG with C16 fatty acid in the sn-2 position, while DGTT2 and DGTT3 favor C18 at that position.

Aside from de novo synthesis, membrane lipids can be recycled directly into TAGs by replacing the head group with an acyl group or indirectly by transferring the acyl group from an acyl-lipid to DAG to generate TAG (Li-Beisson et al. 2015). The enzyme responsible for removing the head group from an acyl-lipid to yield DAG is currently unknown, although an abundant thylakoid membrane lipid monogalactosyldiacylglycerol (MGDG) appears to be the major contributing lipid source recycled to TAG via this mechanism (Legeret et al. 2016). Lipids that have been converted to DAG by removing the head group or de novo synthesized DAG can be subsequently acylated via an acyl-CoA-independent pathway by phospholipid:diacylglycerol acyltransferase (PDAT), which catalyzes the reaction using an acyl-lipid as an acyl donor (Fig. 2) (Boyle et al. 2012; Deng et al. 2012; La Russa et al. 2012; Hung et al. 2013). Chlamydomonas has one gene for PDAT, and in vitro assays revealed that it has a broad substrate specificity and can utilize phospholipids, galactolipids, DAG, and cholesteryl esters as acyl donors for TAG synthesis (Boyle et al. 2012; Yoon et al. 2012). Knockdown *pdat* lines accumulate higher levels of MGDG, sulfoquinovosyl diacylglycerol (SQDG), and phosphatidylglycerol (PG), suggesting that these lipids can act as substrates in vivo (Yoon et al. 2012).

As expected, nitrogen starvation RNA-seq resulted in the increase of three acyltransferases (*DGAT1*, *DGTT1*, *PDAT1*). *DGTT1* and *DGAT1* are also induced in other stress conditions (S, P, Zn, Fe) (Boyle et al. 2012; Hernandez-Torres et al. 2016). Knockdown lines for *DGTT1–DGTT3*, each with a single DGTT suppressed, resulted in a 20–35% decrease in TAG accumulation (Liu et al. 2016). Similarly, insertional mutants and artificial micro-RNA knockdown lines for *PDAT* showed up to 25% reduction in TAG accumulation (Boyle et al. 2012; Yoon et al. 2012). These knockdown line phenotypes indicate that both PDAT- and DGAT-dependent pathways contribute to TAG accumulation in Chlamydomonas.

Degradation of acyl-lipids by lipases also provides acyl chains for subsequent TAG generation. A galactoglycerolipid lipase, plastid galactoglycerolipid degradation 1 (PGD1), degrades immature MGDG, and the acyl chains are incorporated into TAG (Fig. 2) (Li et al. 2012b). Similarly, MGDG was found to be a source for fatty acids to generate TAG in a mutant *fdx5*, defective in a chloroplast ferredoxin (Yang et al. 2015). FDX5 was found to interact with two fatty acid desaturases important for the production of mature MGDG. In the *fdx5* knockout mutant, MGDG desaturation was compromised, and this immaturity likely promoted its degradation by lipases and subsequent incorporation into TAGs. Additionally, MGDG is likely not the sole recycled lipid as lipidomic analysis of cells accumulating TAGs in response to heat stress indicated that the sn-3 position of DAG is esterified from acyl groups derived from diacylglyceryl-trimethylhomoserine (DGTS) and phosphatidylethanolamine lipids (Legeret et al. 2016).

3.2 TAG Synthesis Requires Lipid Trafficking Across Organellar Membranes

TAG synthesis occurring outside of the chloroplast ("eukaryotic pathway") requires fatty acids to be transported out of the chloroplast where they were synthesized, a process that is not well understood (Riekhof et al. 2005; Li-Beisson et al. 2015; Li et al. 2016a). For the three enzymes synthesizing DAG from glycerol-3-phosphate, at least two isoforms exist for each enzyme, and based on protein localization prediction programs, it is highly plausible that DAG synthesis occurs in both the chloroplast and ER (Li-Beisson et al. 2015). Analysis of fatty acid components from TAGs revealed C16 fatty acids to be enriched at the sn-2 position, indicative of chloroplast-derived DAG precursor, as most extrachloroplastic membranes contain C18 fatty acids at this position (Fan et al. 2011). Furthermore, GPAT and PDAT have been identified in the chloroplast proteome, which points to a probable chloroplast localization of this pathway (Terashima et al. 2010, 2011; Yoon et al. 2012). Additionally, several proteins involved in DAG and TAG synthesis have been identified in the lipid proteome, suggesting parallel pathways occurring among various organelles (discussed in more detail in Sect. 6.2) (Moellering and Benning 2010; Nguyen et al. 2011).

Lipid precursors such as free fatty acids are likely imported into the ER from the chloroplast (Liu and Benning 2013). In *Arabidopsis thaliana*, several proteins have been identified that mediate fatty acid transport, which is thought to occur through membrane contact sites between the chloroplast and the ER (Block and Jouhet 2015). Components identified to play a role in fatty acid and lipid transport in higher plants, such as a transporter localized to the chloroplast inner envelope fatty acid export 1 (FAX1), lipid transfer proteins, and acyl-CoA binding proteins, have been identified in the Chlamydomonas genome but lack experimental evidence (Li et al. 2016a). The ATP-binding cassette (ABC) transporter that mediates lipid trafficking, consisting of trigalactosyldiacylglycerol proteins TGD1, TGD2, and TGD3, is localized to the inner envelope membrane of the chloroplast in higher plants (Benning 2009; Roston et al. 2012). The *TGD* genes are also present in Chlamydomonas, of which experimental evidence shows that the *TGD2* gene is necessary for phosphatidic acid trafficking from the ER to the chloroplast, indicating that lipid trafficking between these two organelles is not unidirectional (Warakanont et al. 2015).

Origins of fatty acids can be speculated based on the degree of saturation because fatty acids derived from de novo synthesis are more saturated than those derived from membrane lipids (Fan et al. 2011; Li et al. 2012b). During de novo TAG synthesis, the exported fatty acids are thought to be activated by long-chain acyl-CoA synthetase, resulting in acyl-CoA, allowing for incorporation during TAG synthesis (Li et al. 2016b). This conclusion is based on the presence of more unsaturated TAGs in a mutant in a long-chain acyl-CoA synthetase, *lcs2*, suggesting that in the absence of LCS2, production of TAGs from de novo

synthesized fatty acids is diminished, but not membrane-recycled TAGs. The *lcs2* mutant had 50% reduction in TAG abundance. Proteomic analysis localized LCS2 to the lipid droplets, which indicates direct synthesis of acyl-CoA from chloroplast-derived fatty acids on the surface of the lipid droplets (Moellering and Benning 2010). In addition to the export of fatty acids, membrane lipids must also be mobilized across organellar membranes so that they can be readily degraded and stored in the form of TAGs.

4 Regulation: Accumulation and Turnover of TAGs

Although the environmental stresses that stimulate TAG accumulation have been thoroughly documented, the regulation mechanisms that lead to the induction of TAG accumulation are not well understood. Transcriptomic studies have identified differentially expressed genes and pinpoint possible transcriptional regulators involved in a coordinated response of TAG accumulation (Miller et al. 2010; Boyle et al. 2012; Blaby et al. 2013; Lopez Garcia de Lomana et al. 2015; Schmollinger et al. 2014; Gargouri et al. 2015). Transcription factors are of particular interest because current induction conditions involve nutrient starvation, which ultimately limits cell growth and is not ideal for biofuel applications. Finding ways to turn on TAG accumulation while maintaining growth will maximize output and would have a major impact on biotechnological applications.

4.1 Transcription Factors Are Key Targets for Understanding TAG Synthesis Regulation

Comparison of transcriptome response between nitrogen, sulfur, and phosphorous starvation showed commonly up- or downregulated genes, but the majority of transcripts were differentially regulated between each of the stress conditions (Boyle et al. 2012; Schmollinger et al. 2014; Hernandez-Torres et al. 2016). Although various nutrient stresses can cause TAG accumulation, judging from the vastly different transcriptome responses between different nutrient starvation conditions, unique transcription factors may play a role in initiating TAG accumulation. mRNA of a putative transcription factor for TAG accumulation, *nitrogen response regulator 1* (*NRR1*), was found to be induced under nitrogen starvation (Boyle et al. 2012). NRR1 is presumed to be a transcription factor due to the presence of a *SQUAMOSA* promoter-binding protein domain at its N-terminus. *NRR1* has a similar transcript profile to *DGTT1* and ammonium transporter *AMT1D*, with induction observed within half an hour after transfer to media without nitrogen, and appears to be specific for nitrogen starvation. However, NRR1 is not the sole regulator for TAG accumulation under nitrogen starvation,

as the *nrr1* insertional mutant results in a 50% reduction of TAG accumulation. Additionally, several putative DNA-binding proteins were identified based on transcript accumulation under nitrogen starvation, and their low nitrogen content compared to the average of the proteome indicates easier protein induction under nitrogen limitation (Schmollinger et al. 2014). Overall, proteins high in nitrogen content were found to be reduced under nitrogen starvation, while proteins low in nitrogen were induced, indicating a survival strategy by cellular nitrogen redistribution. In another omics-based study, 70 putative transcription factors and transcriptional regulators were found to be co-regulated during nitrogen deprivation (Gargouri et al. 2015). Among them, the mRNA of the putative transcription factor *TAZ3* was induced over fivefold under nitrogen deficiency and showed a similar expression profile to *NRR1*.

Under phosphorous deficiency, *PSR1* was recently found to be a transcriptional regulator, where loss of function in the mutant *psr1* resulted in decreased starch and lipid accumulation (Bajhaiya et al. 2016). This further supports the notion of distinct response pathways for TAG induction under various conditions. These putative transcription factors showing transcript induction under nutrient-limiting conditions are targets for further studies to elucidate TAG accumulation response.

4.2 Putative Kinases Are Involved in TAG Accumulation

In addition to putative transcription factors and key enzymes in TAG synthesis and carbon partitioning, candidates for signaling pathways for sensing environmental stress and inducing starch and TAG accumulations have been identified (Park et al. 2015; Schmollinger et al. 2014). A mutant screen for strains with decreased TAG accumulation under sulfur deficiency led to the identification of *triacylglycerol accumulation regulator1* (*tar1*), which carried an insertion in a gene for a tyrosine phosphorylation-regulated kinase (Kajikawa et al. 2015). Diminished lipid accumulation in *tar1* was also observed in nitrogen starvation, and TAG accumulation could be restored to wild-type levels in the complemented strains, suggesting that TAR1 is a positive regulator for TAG accumulation under nitrogen and sulfur starvation, although its targets are currently unknown. Interestingly, *tar1* did not show the characteristic chlorotic phenotype accompanied by downregulation of photosynthesis that occurs during nitrogen starvation in the wild type and appears to be compensated by increasing chloroplast membrane lipid accumulation and genes involved in thylakoid maintenance, stress response, and viability.

Another kinase, which, unlike TAR1, appears to negatively regulate starch and TAG accumulation under photoautotrophy was recently identified (Schulz-Raffelt et al. 2016). This kinase is a dual-specificity tyrosine-phosphorylation-regulated kinase specific to plants (DYRKP), and a *dyrkp* mutant was initially identified as *starch degradation 1*, *std1*, due to higher intracellular starch reserves after nutrient resupply (Chochois et al. 2010). *Std1* accumulates increased starch and TAGs and maintains higher photosynthetic activity compared to the wild type under nitrogen-

starved photoautotrophic conditions (Schulz-Raffelt et al. 2016). Although the interaction partners of DYRKP are still unknown, DYRKP activity is necessary to inhibit starch and TAG accumulation under conditions of low cellular energy status, such as photoautotrophic conditions under low light.

4.3 *TAG Remobilization After the Return of Nitrogen Is a Rapid, Regulated Response*

On the flip side to TAG accumulation, when conditions become favorable for growth, the cells need to respond accordingly to degrade TAGs and resume growth. After nitrogen resupply in dark conditions, starch was found to be degraded initially, with 70% consumed within the first 20 h, followed by most of the TAGs being consumed during 20–24 h after nitrogen resupply along with the return of chlorophyll (Siaut et al. 2011). In general, numerous studies found lipid droplets to disappear within 36 h of nitrogen resupply (Cagnon et al. 2013; Li et al. 2012a; Valledor et al. 2014). Lipases act to hydrolyze TAGs for remobilization. In vitro analysis of PDAT, introduced earlier as an acyltransferase that synthesizes TAG (Sect. 3.1), revealed the enzyme to also act as a lipase that can degrade phospholipids, galactolipids, and TAGs to release free fatty acids (Yoon et al. 2012). However, judging from the induced *PDAT* transcripts under nitrogen starvation and the reduced accumulation of TAGs in *pdat* knockdown and mutant lines, PDAT is currently postulated to act as an acyltransferase rather than a lipase in vivo (Boyle et al. 2012; Yoon et al. 2012). Therefore, a lipase that uses TAG as a substrate and mediates TAG turnover in vivo has not yet been identified in Chlamydomonas, although transcriptomics and proteomics have identified candidate lipases (Miller et al. 2010; Goodenough et al. 2014; Nguyen et al. 2011). LIP1 lipase has been characterized in Chlamydomonas and was found to hydrolyze DAG, thereby assisting in TAG turnover by preventing DAG overaccumulation, but is unable to use TAG as a substrate (Li et al. 2012a).

In order to focus on TAG turnover, a mutant screen was performed to identify strain defect in mobilizing accumulated TAGs and initiating growth (i.e., exiting quiescence) even after 24 h following nitrogen resupply (Tsai et al. 2014). Eight mutants, named *compromised hydrolysis of triacylglycerols* (*cht*1–*cht*8), were isolated with *cht7* displaying the strongest phenotype, unable to mobilize TAGs, and resume growth under a variety of environmental signals, not just nitrogen resupply, although viability was not affected. *CHT7* encodes for a protein containing two cysteine-rich motifs, which could play a role in DNA binding, and GFP-tagged CHT7 complementation rescued the phenotype and localized the protein to the nucleus suggesting that CHT7 may act as a transcription factor required for quiescence exit (Tsai et al. 2014; Li et al. 2014).

5 Photosynthesis and TAG Accumulation

TAG accumulation is severely compromised in the dark, suggesting that photosynthesis is an important contributor for TAG synthesis (Fan et al. 2012). However, chlorosis is a signature phenotype of nitrogen starvation in Chlamydomonas, and, accordingly, photosynthetic efficiency decreases under nitrogen deprivation (Schmollinger et al. 2014). Chlorosis and downregulation of photosynthesis appear to be a mediated process and not just an inevitable result of nitrogen limitation, as the mutant *tar1* (see Sect. 4.2) does not turn chlorotic under nitrogen starvation and has high levels of photosynthetic activity compared to the wild type while maintaining similar viability. In Chlamydomonas wild-type cells, the accumulation of TAG and the concurrent decrease in chlorophyll and photosynthetic activity are closely linked response mechanisms, not just a passive consequence of stress.

5.1 Photosynthetic Electron Transport Chain Complexes Are Reduced Under Nitrogen Starvation

Upon nitrogen starvation, photosynthetic efficiency decreases due to reduction in light-harvesting complexes, photosystem I and II complexes, cytochrome b_6f, and ATP synthase, observed both in photoautotrophic and photoheterotrophic conditions (Plumley and Schmidt 1989; Peltier and Schmidt 1991; Schmollinger et al. 2014; Juergens et al. 2015). Interestingly, mitochondrial ATP synthase and cytochrome bc_1 complex and proteins of the TCA cycle are induced under photoheterotrophic conditions, which is also reflected by respiration rates remaining high compared to the drastic reduction of oxygen evolution (i.e., via photosynthesis) (Valledor et al. 2014; Schmollinger et al. 2014).

Downregulation of photosynthesis happens rapidly after the switch to nitrogen deficiency. Even after 6 h under nitrogen deprivation, CO_2 uptake was reduced, and after 24 h, linear electron flow decreased relative to cyclic electron flow (Juergens et al. 2015). Also, during the first few hours, transcripts, proteins, and pigments involved in non-photochemical quenching (NPQ), namely, photosystem II D1 subunit protein, subunit S transcript, LHCSR transcript, and zeaxanthin, are induced, although NPQ itself was not found to be elevated (Miller et al. 2010; Juergens et al. 2015). Components necessary for NPQ may be upregulated to prepare the cells for a sudden increase in light intensity, and the light intensity at 160 $\mu Em^{-2}\ S^{-1}$ used in the study by Juergens et al. may not have been enough to induce NPQ. A more in-depth analysis of the relationship between nutrient deprivation, TAG accumulation, and high light stress would be interesting. A gradual decrease in photosystem II was also observed under nitrogen starvation, which also resulted in photosynthetic hydrogen production after 3 days of nitrogen-deprived

photoheterotrophic conditions, although this effect was delayed compared to sulfur deprivation, which results in rapid degradation of photosystem II (Wykoff et al. 1998; Philipps et al. 2012).

As expected, under photoautotrophic conditions, TAG synthesis is much more linked to photosynthetic capacity. Acetyl-CoA is a key metabolite necessary for the synthesis of fatty acids, and multiple metabolic pathways can lead to its generation. Under photoautotrophic conditions, where acetate is not available to generate acetyl-CoA, the pyruvate dehydrogenase complex in the chloroplast is a major source of acetyl-CoA leading to TAG accumulation (Shtaida et al. 2014). Knockdown lines of the E1α subunit of the pyruvate dehydrogenase accumulate less TAGs compared to the wild type, only under photoautotrophic conditions.

5.2 TAG Accumulation Acts as Sink for Photosynthetically Generated Reducing Equivalents and Protects Against ROS Damage

The tight link between photosynthesis and TAG accumulation is further demonstrated through the analysis of the *pgd1* mutant (introduced in Sect. 3.1), which lacks a galactoglycerolipid lipase (Li et al. 2012b). TAG accumulation is compromised in this mutant, and this resulted in increased chlorosis and loss of viability after nitrogen deprivation, a phenotype that can be rescued by the addition of photosystem II inhibitor DCMU. This provided experimental evidence that TAG acts as an electron sink for the photosynthetic electron chain and compromising TAG accumulation, as seen in the PGD1 mutant, results in the generation of toxic reactive oxygen species. The observation that Chlamydomonas does not accumulate TAGs in the dark further indicates that TAG accumulation plays the role of sequestering photosynthetically derived reducing equivalents under nutrient starvation conditions, where other metabolic pathways cannot work fast enough to provide an outlet for these generated reducing powers.

6 Lipid Droplets: Morphology, Cellular Localization, and TAG Species

Lipid droplets consist of a TAG core surrounded by a polar lipid monolayer and associated proteins. Lipid droplets in Chlamydomonas are unique compared to their plant counterparts because substantial TAG synthesis appears to occur in the chloroplast, whereas TAG synthesis occurs in the ER in plants (Fan et al. 2011; Liu and Benning 2013). Although there are still many unknown aspects of lipid

droplet formation and its associated lipid species and proteins, lipidomic, proteomic, and microscopic analyses have revealed novel components of Chlamydomonas lipid droplets.

6.1 Lipid Droplets Contain a Wide Range of Lipid Species

The prominent polar lipids in Chlamydomonas lipid droplets are DGTS and digalactosyldiacylglycerol (DGDG), while phospholipids, which are primarily found in lipid droplets in yeast and animals, make up less than 25% of the polar lipids in lipid droplets in Chlamydomonas (Tsai et al. 2015). Interestingly, phosphatidylcholine, which is a major phospholipid found in plants and animals, is absent in Chlamydomonas (Yang et al. 2004). Instead, DGTS acts as the major polar lipid source for extrachloroplastic membranes in Chlamydomonas (Riekhof et al. 2005). On the lipid droplets, more than half of the polar lipids are galactolipids, such as DGDG, which are usually found in chloroplast membranes. However these lipid droplet-localized galactolipid species are more saturated, having increased abundance of 16:0 and 18:0 fatty acids compared to their chloroplast counterparts (Tsai et al. 2015). TAG profiling of nitrogen-starved Chlamydomonas identified 140 distinct species with most acyl groups consisting of 16- or 18-carbon chains (James et al. 2011; Liu et al. 2013a). Under nitrogen starvation and phosphate starvation, TAG species were particularly enriched with 16:0 and 18:1 fatty acids (Iwai et al. 2014). Aside from TAGs, the lipid droplet core contains some free fatty acids and carotenoids (Wang et al. 2009; Moellering and Benning 2010).

6.2 Lipid Droplet Proteome Consists of Structural and Metabolic Proteins

Proteomic analysis of lipid droplets identified a highly abundant protein, the major lipid droplet protein (MLDP) (Moellering and Benning 2010; Nguyen et al. 2011). MLDP is a green alga-specific 28 kDa protein, and suppression through RNAi resulted in larger lipid droplets, but without increase in total TAG accumulation per cell (Moellering and Benning 2010). In wild-type Chlamydomonas, MLDP abundance was shown to directly correlate with intracellular TAG abundance with localization to the lipid droplet surface (Tsai et al. 2014). In plants, oleosins are the main structural proteins present in the phospholipid monolayer that maintain lipid droplet integrity and prevent coalescence of the droplets (Huang 1992). MLDP is structurally not similar to oleosin, lacking a long hydrophobic polypeptide that inserts into the lipid droplet matrix to promote stable association. Furthermore, Chlamydomonas has a gene encoding for a protein similar to oleosin, but transcript

and protein levels were detected only in low amounts (Huang et al. 2013). Therefore, MLDP, instead of oleosin, appears to act as the key component for lipid droplets due to its sheer abundance and its ability to stabilize lipid droplet size by preventing coalescence (Tsai et al. 2015).

Aside from MLDP, other proteins are localized to the lipid droplets. Two independent proteomic studies identified 259 proteins and 248 proteins from lipid droplets isolated from nitrogen-starved photoheterotrophic and nitrogen-starved photoautotrophic cells, respectively (Moellering and Benning 2010; Nguyen et al. 2011). Among these, proteins involved in lipid metabolism include acyl-CoA synthetases (including LCS2 discussed earlier) and DGTS synthesis enzymes BTA1, GPAT, LPAT, and PDAT. The presence of BTA1 suggests direct synthesis of DGTS for the lipid monolayer of lipid droplets (Moellering and Benning 2010). The presence of key enzymes involved in TAG synthesis is indicative of TAG synthesis, in part, occurring directly at the lipid droplets. Interestingly, both proteomic studies did not identify DGAT, but a comparative study on the lipid droplet proteome versus other organellar proteomes must be conducted to determine the presence and localization of this protein. Furthermore, both studies isolated total lipid droplets from cell extracts, making localization of proteins between the chloroplast- and ER-derived lipid droplets difficult. Additionally, ER-chloroplast lipid trafficking proteins (TGD1–TGD3), discussed in more detail below, are also localized to the lipid droplets (Nguyen et al. 2011).

6.3 Biogenesis of Lipid Droplets Is an Elusive Process

Currently, not much is known about the biogenesis of lipid droplets. A widely used model for lipid droplet formation in non-photosynthetic eukaryotes, where lipid droplets accumulate exclusively in the cytosol, is via the accumulation of neutral lipid globules between leaflets of the ER membrane bilayer (Pol et al. 2014; Wilfling et al. 2014). These globules are thought to move laterally within the ER membrane, and as they increase in size, the bilayer leaflet separates and eventually forms a droplet. In yeast cells, lipid droplets still attached to the ER as well those detached have been observed (Jacquier et al. 2011; Wilfling et al. 2013). Electron microscopy images of Chlamydomonas cells also show close association of the cytoplasmic lipid droplets, usually around 1–2 μm in diameter, to the ER as well as the chloroplast outer membrane (Moellering and Benning 2010; Goodson et al. 2011). Chloroplast lipid droplets that are smaller (~60 nm) and often found attached to the thylakoid membranes are referred to as plastoglobules (Engel et al. 2015). Interestingly, a nitrogen-starved starchless mutant showed chloroplastic lipid droplets that are much larger than plastoglobules, suggesting that the plastoglobules could serve as a precursor for larger chloroplast lipid droplets (Goodson et al. 2011; Fan et al. 2011). Similarly, small lipid droplets (250–1000 nm) present under normal growth conditions could also act as a precursor for stress-induced cytoplasmic lipid droplets (Goodson et al. 2011).

7 Biotechnological Applications and Perspectives

Microalgae have been identified as a possible source for sustainable fuel, feed, food, and chemicals (Hu et al. 2008; Liu et al. 2012; Wijffels et al. 2013; Klok et al. 2014). Microalgae-based resources are not yet utilized at a global scale due to the high expense of cultivation, harvesting, and processing, especially when performed at a large scale (Slade and Bauen 2013). In the last decade, there has been an exponential increase in efforts to identify strains with altered TAG accumulation, especially in Chlamydomonas, in order to find clues in cultivation and genetic engineering strategies for biotechnological applications.

7.1 Mutants that Show Increased TAG Accumulation Has Been Identified

To date, only a handful of mutants relating to TAG metabolism have been characterized (for a list, refer to Goncalves et al. 2016). Many enzymes having a role in TAG metabolism or regulation have been identified by observing a decrease in TAG accumulation resulting from silencing or gene disruption via insertional mutagenesis, as seen for mutants in *pdat1*, *pgd1*, *nrr1*, and *tar1* discussed earlier (Boyle et al. 2012; Yoon et al. 2012; Li et al. 2012b; Kajikawa et al. 2015). Mutants with increased TAG accumulation have also been identified, with the starchless mutants being the most characterized (Li et al. 2010a; Wang et al. 2009; Work et al. 2010). Genetic engineering of strains with the aim of increasing TAG accumulation has had mixed outcomes. One clear target for increasing TAG accumulation is to overexpress DGAT, aiming to maximize DAG conversion to TAG. Individual overexpression of three type II DGATs (*DGTT1–DGTT3*) resulted in no changes in TAG accumulation when nitrogen-starved under photoheterotrophic conditions (La Russa et al. 2012). However, overexpression of *DGTT4* under the control of a promoter induced under phosphate starvation yielded increased TAG accumulation under photoheterotrophic conditions (Iwai et al. 2014). Overexpression of type II DGATs, *DGTT1* and *DGTT5*, was reported to show 27% and 48% increase in TAG accumulation, respectively (Deng et al. 2012).

7.2 Many Mutant Screens Have Been Developed with the Aim of Isolating Strains with Perturbed Lipid Content

Several mutant screens have been performed to isolate strains with altered TAG accumulation. To this end, lipophilic dyes such as nile red and BODIPY have been used as a readout for cellular TAG abundance (Greenspan et al. 1985; Moellering

and Benning 2010; Cirulis et al. 2012; Velmurugan et al. 2013). Various factors have to be addressed regarding fluorescence correlation with actual TAG accumulation, ensuring consistent dye penetration into the cells and choosing correct filters to separate chlorophyll autofluorescence from lipid dye fluorescence (Cagnon et al. 2013; Terashima et al. 2015). Arraying mutant strains in a 96-well format and screening for increased or diminished fluorescence signal can lead to the isolation of candidate mutants, which could be further analyzed by alternative methods to confirm the phenotype such as thin-layer chromatography or mass spectrometry (Li et al. 2012b; Yan et al. 2013). The mutant *pgd1* described earlier was isolated through this approach (Li et al. 2012b). Similarly, individual mutants in 96-well plate format have been analyzed by flow cytometry (Cagnon et al. 2013). Utilizing flow cytometry with cell sorting capabilities [i.e., fluorescence-activated cell sorting (FACS)] greatly increases the throughput of mutant analysis as 10,000 cells can be analyzed per second (Terashima et al. 2015). This allows for pooled cultivation, staining, and analysis, followed by individual mutant isolation after phenotype-based enrichment (Xie et al. 2014; Velmurugan et al. 2013; Terashima et al. 2015; Kajikawa et al. 2015). This approach has been successfully implemented in Chlamydomonas and in other microalgae as well (Montero et al. 2011; Doan and Obbard 2011, 2012; Manandhar-Shrestha and Hildebrand 2013).

Isolating a strain with altered lipid accumulation from a mutant pool generated via random insertional mutagenesis has been very successful. However, a major bottleneck has been in identifying the mutation site of a strain of interest. To address this issue, a large-scale mutant library with mapped insertion sites that cover much of the Chlamydomonas genome has been generated (Zhang et al. 2014; Li et al. 2016b). From a library of Chlamydomonas strains with mapped cassette insertion sites, hypothesis-driven characterization of a mutant can lead to subsequent identification of key components of TAG metabolism, as was the case for LCS2 discussed above (Li et al. 2016b). Furthermore, utilizing mutant pools with mapped insertion sites for high-throughput screening will be powerful as phenotypes can be matched to insertion sites rapidly.

8 Conclusions

An increased interest in microalgal TAG accumulation in the last decade has accelerated research in this field. Genome information has allowed prediction of pathways present in Chlamydomonas, and mutant analyses are revealing the enzymes contributing to TAG metabolism. Through numerous studies on transcriptomics, proteomics, and lipidomics, it has become clear that major metabolic shifts occur in Chlamydomonas under TAG-accumulating conditions, with TAG originating from both de novo synthesis and membrane recycling. The initiation of TAG synthesis and degradation appear to be controlled by transcription factors and kinases, involving a multitude of parallel and interconnected metabolic pathways. TAG is synthesized via a variety of carbon sources, and simply inhibiting

one component of TAG accumulation does not lead to complete inhibition of TAG synthesis. Although various stress conditions induce TAG accumulation, the response mechanisms are distinct with differential gene regulation observed that is unique to the applied stress.

While the main metabolic pathways in TAG metabolism are beginning to be elucidated, many aspects of the current model lack experimental evidence, especially regarding signaling cascades, the roles of various enzyme isoforms, protein localizations, lipid droplet biogenesis, and lipid trafficking mechanisms. The growing number of mapped mutants available to the research community will assist in elucidating TAG metabolism by identifying key genes or localizing proteins, such as by tagged protein complementation. Additionally, further understanding the link between TAG accumulation and photosynthesis will be of significance for industrial production of biofuels, food, feedstock, and high-grade oils in order to maximize sun energy capture into desirable products.

Acknowledgments I am grateful to Dr. Xiaobo Li for critical feedback and suggestions on the manuscript.

References

Bajhaiya AK, Dean AP, Driver T, Trivedi DK, Rattray NJ, Allwood JW, Goodacre R, Pittman JK (2016) High-throughput metabolic screening of microalgae genetic variation in response to nutrient limitation. Metabolomics 12(1):9. doi:10.1007/s11306-015-0878-4

Ball S, Marianne T, Dirick L, Fresnoy M, Delrue B, Decq A (1991) A Chlamydomonas-reinhardtii low-starch mutant is defective for 3-phosphoglycerate activation and orthophosphate inhibition of Adp-glucose pyrophosphorylase. Planta 185(1):17–26

Benning C (2009) Mechanisms of lipid transport involved in organelle biogenesis in plant cells. Annu Rev Cell Dev Biol 25:71–91. doi:10.1146/annurev.cellbio.042308.113414

Blaby IK, Glaesener AG, Mettler T, Fitz-Gibbon ST, Gallaher SD, Liu B, Boyle NR, Kropat J, Stitt M, Johnson S, Benning C, Pellegrini M, Casero D, Merchant SS (2013) Systems-level analysis of nitrogen starvation-induced modifications of carbon metabolism in a Chlamydomonas reinhardtii starchless mutant. Plant Cell 25(11):4305–4323. doi:10.1105/tpc.113.117580

Blaby IK, Blaby-Haas CE, Tourasse N, Hom EF, Lopez D, Aksoy M, Grossman A, Umen J, Dutcher S, Porter M, King S, Witman GB, Stanke M, Harris EH, Goodstein D, Grimwood J, Schmutz J, Vallon O, Merchant SS, Prochnik S (2014) The Chlamydomonas genome project: a decade on. Trends Plant Sci 19(10):672–680. doi:10.1016/j.tplants.2014.05.008

Block MA, Jouhet J (2015) Lipid trafficking at endoplasmic reticulum-chloroplast membrane contact sites. Curr Opin Cell Biol 35:21–29. doi:10.1016/j.ceb.2015.03.004

Boyle NR, Page MD, Liu B, Blaby IK, Casero D, Kropat J, Cokus SJ, Hong-Hermesdorf A, Shaw J, Karpowicz SJ, Gallaher SD, Johnson S, Benning C, Pellegrini M, Grossman A, Merchant SS (2012) Three acyltransferases and nitrogen-responsive regulator are implicated in nitrogen starvation-induced triacylglycerol accumulation in Chlamydomonas. J Biol Chem 287(19):15811–15825. doi:10.1074/jbc.M111.334052

Cagnon C, Mirabella B, Nguyen HM, Beyly-Adriano A, Bouvet S, Cuine S, Beisson F, Peltier G, Li-Beisson Y (2013) Development of a forward genetic screen to isolate oil mutants in the green microalga Chlamydomonas reinhardtii. Biotechnol Biofuels 6(1):178. doi:10.1186/1754-6834-6-178

Chochois V, Constans L, Dauvillee D, Beyly A, Soliveres M, Ball S, Peltier G, Cournac L (2010) Relationships between PSII-independent hydrogen bioproduction and starch metabolism as evidenced from isolation of starch catabolism mutants in the green alga Chlamydomonas reinhardtii. Int J Hydrog Energy 35(19):10731–10740. doi:10.1016/j.ijhydene.2010.03.052

Cirulis JT, Strasser BC, Scott JA, Ross GM (2012) Optimization of staining conditions for microalgae with three lipophilic dyes to reduce precipitation and fluorescence variability. Cytometry A 81(7):618–626. doi:10.1002/cyto.a.22066

Davey MP, Horst I, Duong GH, Tomsett EV, Litvinenko AC, Howe CJ, Smith AG (2014) Triacylglyceride production and autophagous responses in Chlamydomonas reinhardtii depend on resource allocation and carbon source. Eukaryot Cell 13(3):392–400. doi:10.1128/EC.00178-13

Deng XD, Gu B, Li YJ, Hu XW, Guo JC, Fei XW (2012) The roles of acyl-CoA: diacylglycerol acyltransferase 2 genes in the biosynthesis of triacylglycerols by the green algae Chlamydomonas reinhardtii. Mol Plant 5(4):945–947. doi:10.1093/mp/sss040

Deng X, Cai J, Fei X (2013) Effect of the expression and knockdown of citrate synthase gene on carbon flux during triacylglycerol biosynthesis by green algae Chlamydomonas reinhardtii. BMC Biochem 14:38. doi:10.1186/1471-2091-14-38

Doan TTY, Obbard JP (2011) Improved Nile Red staining of Nannochloropsis sp. J Appl Phycol 23(5):895–901. doi:10.1007/s10811-010-9608-5

Doan TTY, Obbard JP (2012) Enhanced intracellular lipid in Nannochloropsis sp via random mutagenesis and flow cytometric cell sorting. Algal Res Biomass Biofuels Bioprod 1(1):17–21. doi:10.1016/j.algal.2012.03.001

Engel BD, Schaffer M, Kuhn Cuellar L, Villa E, Plitzko JM, Baumeister W (2015) Native architecture of the Chlamydomonas chloroplast revealed by in situ cryo-electron tomography. Elife 4. doi:10.7554/eLife.04889

Fan J, Andre C, Xu C (2011) A chloroplast pathway for the de novo biosynthesis of triacylglycerol in Chlamydomonas reinhardtii. FEBS Lett 585(12):1985–1991. doi:10.1016/j.febslet.2011.05.018

Fan J, Yan C, Andre C, Shanklin J, Schwender J, Xu C (2012) Oil accumulation is controlled by carbon precursor supply for fatty acid synthesis in Chlamydomonas reinhardtii. Plant Cell Physiol 53(8):1380–1390. doi:10.1093/pcp/pcs082

Flatt JP (1995) Use and storage of carbohydrate and fat. Am J Clin Nutr 61(4):952s–959s

Gao Q, Goodman JM (2015) The lipid droplet-a well-connected organelle. Front Cell Dev Biol 3 (Aug):49. doi:10.3389/fcell.2015.00049

Gardner RD, Lohman E, Gerlach R, Cooksey KE, Peyton BM (2013) Comparison of CO(2) and bicarbonate as inorganic carbon sources for triacylglycerol and starch accumulation in Chlamydomonas reinhardtii. Biotechnol Bioeng 110(1):87–96. doi:10.1002/bit.24592

Gargouri M, Park JJ, Holguin FO, Kim MJ, Wang H, Deshpande RR, Shachar-Hill Y, Hicks LM, Gang DR (2015) Identification of regulatory network hubs that control lipid metabolism in Chlamydomonas reinhardtii. J Exp Bot 66(15):4551–4566. doi:10.1093/jxb/erv217

Goncalves EC, Wilkie AC, Kirst M, Rathinasabapathi B (2016) Metabolic regulation of triacylglycerol accumulation in the green algae: identification of potential targets for engineering to improve oil yield. Plant Biotechnol J:1–12. doi:10.1111/pbi.12523

Goodenough U, Blaby I, Casero D, Gallaher SD, Goodson C, Johnson S, Lee JH, Merchant SS, Pellegrini M, Roth R, Rusch J, Singh M, Umen JG, Weiss TL, Wulan T (2014) The path to triacylglyceride obesity in the sta6 strain of Chlamydomonas reinhardtii. Eukaryot Cell 13 (5):591–613. doi:10.1128/EC.00013-14

Goodson C, Roth R, Wang ZT, Goodenough U (2011) Structural correlates of cytoplasmic and chloroplast lipid body synthesis in Chlamydomonas reinhardtii and stimulation of lipid body production with acetate boost. Eukaryot Cell 10(12):1592–1606. doi:10.1128/EC.05242-11

Goold H, Beisson F, Peltier G, Li-Beisson Y (2015) Microalgal lipid droplets: composition, diversity, biogenesis and functions. Plant Cell Rep 34(4):545–555. doi:10.1007/s00299-014-1711-7

Greenspan P, Mayer EP, Fowler SD (1985) Nile red: a selective fluorescent stain for intracellular lipid droplets. J Cell Biol 100(3):965–973

Grenier G, Guyon D, Roche O, Dubertret G, Tremolieres A (1991) Modification of the membrane fatty-acid composition of Chlamydomonas-reinhardtii cultured in the presence of liposomes. Plant Physiol Biochem 29(5):429–440

Hemschemeier A, Casero D, Liu B, Benning C, Pellegrini M, Happe T, Merchant SS (2013) Copper response regulator1-dependent and -independent responses of the Chlamydomonas reinhardtii transcriptome to dark anoxia. Plant Cell 25(9):3186–3211. doi:10.1105/tpc.113.115741

Hernandez-Torres A, Zapata-Morales AL, Ochoa Alfaro AE, Soria-Guerra RE (2016) Identification of gene transcripts involved in lipid biosynthesis in Chlamydomonas reinhardtii under nitrogen, iron and sulfur deprivation. World J Microbiol Biotechnol 32(4):55. doi:10.1007/s11274-016-2008-5

Hu Q, Sommerfeld M, Jarvis E, Ghirardi M, Posewitz M, Seibert M, Darzins A (2008) Microalgal triacylglycerols as feedstocks for biofuel production: perspectives and advances. Plant J 54(4):621–639. doi:10.1111/j.1365-313X.2008.03492.x

Huang AHC (1992) Oil bodies and oleosins in seeds. Annu Rev Plant Physiol Plant Mol Biol 43:177–200

Huang NL, Huang MD, Chen TL, Huang AH (2013) Oleosin of subcellular lipid droplets evolved in green algae. Plant Physiol 161(4):1862–1874. doi:10.1104/pp.112.212514

Hung CH, Ho MY, Kanehara K, Nakamura Y (2013) Functional study of diacylglycerol acyltransferase type 2 family in Chlamydomonas reinhardtii. FEBS Lett 587(15):2364–2370. doi:10.1016/j.febslet.2013.06.002

Iwai M, Ikeda K, Shimojima M, Ohta H (2014) Enhancement of extraplastidic oil synthesis in Chlamydomonas reinhardtii using a type-2 diacylglycerol acyltransferase with a phosphorus starvation-inducible promoter. Plant Biotechnol J 12(6):808–819. doi:10.1111/pbi.12210

Jacquier N, Choudhary V, Mari M, Toulmay A, Reggiori F, Schneiter R (2011) Lipid droplets are functionally connected to the endoplasmic reticulum in Saccharomyces cerevisiae. J Cell Sci 124(Pt 14):2424–2437. doi:10.1242/jcs.076836

James GO, Hocart CH, Hillier W, Chen H, Kordbacheh F, Price GD, Djordjevic MA (2011) Fatty acid profiling of Chlamydomonas reinhardtii under nitrogen deprivation. Bioresour Technol 102(3):3343–3351. doi:10.1016/j.biortech.2010.11.051

Johnson X, Alric J (2013) Central carbon metabolism and electron transport in Chlamydomonas reinhardtii: metabolic constraints for carbon partitioning between oil and starch. Eukaryot Cell 12(6):776–793. doi:10.1128/EC.00318-12

Juergens MT, Deshpande RR, Lucker BF, Park JJ, Wang H, Gargouri M, Holguin FO, Disbrow B, Schaub T, Skepper JN, Kramer DM, Gang DR, Hicks LM, Shachar-Hill Y (2015) The regulation of photosynthetic structure and function during nitrogen deprivation in Chlamydomonas reinhardtii. Plant Physiol 167(2):558–573. doi:10.1104/pp.114.250530

Kajikawa M, Sawaragi Y, Shinkawa H, Yamano T, Ando A, Kato M, Hirono M, Sato N, Fukuzawa H (2015) Algal dual-specificity tyrosine phosphorylation-regulated kinase, triacylglycerol accumulation regulator1, regulates accumulation of triacylglycerol in nitrogen or sulfur deficiency. Plant Physiol 168(2):752–764. doi:10.1104/pp.15.00319

Kim S, Kim H, Ko D, Yamaoka Y, Otsuru M, Kawai-Yamada M, Ishikawa T, Oh HM, Nishida I, Li-Beisson Y, Lee Y (2013) Rapid induction of lipid droplets in Chlamydomonas reinhardtii and Chlorella vulgaris by Brefeldin A. PLoS One 8(12):e81978. doi:10.1371/journal.pone.0081978

Kim H, Jang S, Kim S, Yamaoka Y, Hong D, Song WY, Nishida I, Li-Beisson Y, Lee Y (2015) The small molecule fenpropimorph rapidly converts chloroplast membrane lipids to triacylglycerols in Chlamydomonas reinhardtii. Front Microbiol 6(February):54. doi:10.3389/fmicb.2015.00054

Klok AJ, Lamers PP, Martens DE, Draaisma RB, Wijffels RH (2014) Edible oils from microalgae: insights in TAG accumulation. Trends Biotechnol 32(10):521–528. doi:10.1016/j.tibtech.2014.07.004

Krishnan A, Kumaraswamy GK, Vinyard DJ, Gu H, Ananyev G, Posewitz MC, Dismukes GC (2015) Metabolic and photosynthetic consequences of blocking starch biosynthesis in the green alga Chlamydomonas reinhardtii sta6 mutant. Plant J 81(6):947–960. doi:10.1111/tpj.12783

La Russa M, Bogen C, Uhmeyer A, Doebbe A, Filippone E, Kruse O, Mussgnug JH (2012) Functional analysis of three type-2 DGAT homologue genes for triacylglycerol production in the green microalga Chlamydomonas reinhardtii. J Biotechnol 162(1):13–20. doi:10.1016/j.jbiotec.2012.04.006

Legeret B, Schulz-Raffelt M, Nguyen HM, Auroy P, Beisson F, Peltier G, Blanc G, Li-Beisson Y (2016) Lipidomic and transcriptomic analyses of Chlamydomonas reinhardtii under heat stress unveil a direct route for the conversion of membrane lipids into storage lipids. Plant Cell Environ 39(4):834–847. doi:10.1111/pce.12656

Li Y, Han D, Hu G, Dauvillee D, Sommerfeld M, Ball S, Hu Q (2010a) Chlamydomonas starchless mutant defective in ADP-glucose pyrophosphorylase hyper-accumulates triacylglycerol. Metab Eng 12(4):387–391. doi:10.1016/j.ymben.2010.02.002

Li Y, Han D, Hu G, Sommerfeld M, Hu Q (2010b) Inhibition of starch synthesis results in overproduction of lipids in Chlamydomonas reinhardtii. Biotechnol Bioeng 107(2):258–268. doi:10.1002/bit.22807

Li X, Benning C, Kuo MH (2012a) Rapid triacylglycerol turnover in Chlamydomonas reinhardtii requires a lipase with broad substrate specificity. Eukaryot Cell 11(12):1451–1462. doi:10.1128/EC.00268-12

Li X, Moellering ER, Liu B, Johnny C, Fedewa M, Sears BB, Kuo MH, Benning C (2012b) A galactoglycerolipid lipase is required for triacylglycerol accumulation and survival following nitrogen deprivation in Chlamydomonas reinhardtii. Plant Cell 24(11):4670–4686. doi:10.1105/tpc.112.105106

Li X, Umen JG, Jonikas MC (2014) Waking sleeping algal cells. Proc Natl Acad Sci U S A 111(44):15610–15611. doi:10.1073/pnas.1418295111

Li N, Xu C, Li-Beisson Y, Philippar K (2016a) Fatty acid and lipid transport in plant cells. Trends Plant Sci 21(2):145–158. doi:10.1016/j.tplants.2015.10.011

Li X, Zhang R, Patena W, Gang SS, Blum SR, Ivanova N, Yue R, Robertson JM, Lefebvre PA, Fitz-Gibbon ST, Grossman AR, Jonikas MC (2016b) An indexed, mapped mutant library enables reverse genetics studies of biological processes in Chlamydomonas reinhardtii. Plant Cell 28(2):367–387. doi:10.1105/tpc.15.00465

Li-Beisson Y, Beisson F, Riekhof W (2015) Metabolism of acyl-lipids in Chlamydomonas reinhardtii. Plant J 82(3):504–522. doi:10.1111/tpj.12787

Liu B, Benning C (2013) Lipid metabolism in microalgae distinguishes itself. Curr Opin Biotechnol 24(2):300–309. doi:10.1016/j.copbio.2012.08.008

Liu X, Clarens AF, Colosi LM (2012) Algae biodiesel has potential despite inconclusive results to date. Bioresour Technol 104:803–806. doi:10.1016/j.biortech.2011.10.077

Liu B, Vieler A, Li C, Jones AD, Benning C (2013a) Triacylglycerol profiling of microalgae Chlamydomonas reinhardtii and Nannochloropsis oceanica. Bioresour Technol 146:310–316. doi:10.1016/j.biortech.2013.07.088

Liu Y, Zhang C, Shen X, Zhang X, Cichello S, Guan H, Liu P (2013b) Microorganism lipid droplets and biofuel development. BMB Rep 46(12):575–581

Liu J, Han D, Yoon K, Hu Q, Li Y (2016) Characterization of type 2 diacylglycerol acyltransferases in Chlamydomonas reinhardtii reveals their distinct substrate specificities and functions in triacylglycerol biosynthesis. Plant J. doi:10.1111/tpj.13143

Lopez Garcia de Lomana A, Schauble S, Valenzuela J, Imam S, Carter W, Bilgin DD, Yohn CB, Turkarslan S, Reiss DJ, Orellana MV, Price ND, Baliga NS (2015) Transcriptional program for nitrogen starvation-induced lipid accumulation in Chlamydomonas reinhardtii. Biotechnol Biofuels 8:207. doi:10.1186/s13068-015-0391-z

Manandhar-Shrestha K, Hildebrand M (2013) Development of flow cytometric procedures for the efficient isolation of improved lipid accumulation mutants in a sp. microalga. J Appl Phycol 25:1643–1651. doi:10.1007/s10811-013-0021-8

Merchant SS, Kropat J, Liu B, Shaw J, Warakanont J (2012) TAG, you're it! Chlamydomonas as a reference organism for understanding algal triacylglycerol accumulation. Curr Opin Biotechnol 23(3):352–363. doi:10.1016/j.copbio.2011.12.001

Miller R, Wu G, Deshpande RR, Vieler A, Gartner K, Li X, Moellering ER, Zauner S, Cornish AJ, Liu B, Bullard B, Sears BB, Kuo MH, Hegg EL, Shachar-Hill Y, Shiu SH, Benning C (2010) Changes in transcript abundance in Chlamydomonas reinhardtii following nitrogen deprivation predict diversion of metabolism. Plant Physiol 154(4):1737–1752. doi:10.1104/pp.110.165159

Moellering ER, Benning C (2010) RNA interference silencing of a major lipid droplet protein affects lipid droplet size in Chlamydomonas reinhardtii. Eukaryot Cell 9(1):97–106. doi:10.1128/EC.00203-09

Montero MF, Aristizabal M, Reina GG (2011) Isolation of high-lipid content strains of the marine microalga Tetraselmis suecica for biodiesel production by flow cytometry and single-cell sorting. J Appl Phycol 23(6):1053–1057. doi:10.1007/s10811-010-9623-6

Nguyen HM, Baudet M, Cuine S, Adriano JM, Barthe D, Billon E, Bruley C, Beisson F, Peltier G, Ferro M, Li-Beisson Y (2011) Proteomic profiling of oil bodies isolated from the unicellular green microalga Chlamydomonas reinhardtii: with focus on proteins involved in lipid metabolism. Proteomics 11(21):4266–4273. doi:10.1002/pmic.201100114

Park JJ, Wang H, Gargouri M, Deshpande RR, Skepper JN, Holguin FO, Juergens MT, Shachar-Hill Y, Hicks LM, Gang DR (2015) The response of Chlamydomonas reinhardtii to nitrogen deprivation: a systems biology analysis. Plant J 81(4):611–624. doi:10.1111/tpj.12747

Peltier G, Schmidt GW (1991) Chlororespiration: an adaptation to nitrogen deficiency in Chlamydomonas reinhardtii. Proc Natl Acad Sci U S A 88(11):4791–4795

Philipps G, Happe T, Hemschemeier A (2012) Nitrogen deprivation results in photosynthetic hydrogen production in Chlamydomonas reinhardtii. Planta 235(4):729–745. doi:10.1007/s00425-011-1537-2

Plumley FG, Schmidt GW (1989) Nitrogen-dependent regulation of photosynthetic gene expression. Proc Natl Acad Sci U S A 86(8):2678–2682

Pol A, Gross SP, Parton RG (2014) Review: Biogenesis of the multifunctional lipid droplet: lipids, proteins, and sites. J Cell Biol 204(5):635–646. doi:10.1083/jcb.201311051

Riekhof WR, Sears BB, Benning C (2005) Annotation of genes involved in glycerolipid biosynthesis in Chlamydomonas reinhardtii: discovery of the betaine lipid synthase BTA1Cr. Eukaryot Cell 4(2):242–252. doi:10.1128/EC.4.2.242-252.2005

Roston RL, Gao J, Murcha MW, Whelan J, Benning C (2012) TGD1, -2, and -3 proteins involved in lipid trafficking form ATP-binding cassette (ABC) transporter with multiple substrate-binding proteins. J Biol Chem 287(25):21406–21415. doi:10.1074/jbc.M112.370213

Sato A, Matsumura R, Hoshino N, Tsuzuki M, Sato N (2014) Responsibility of regulatory gene expression and repressed protein synthesis for triacylglycerol accumulation on sulfur-starvation in Chlamydomonas reinhardtii. Front Plant Sci 5(Sept):444. doi:10.3389/fpls.2014.00444

Schmollinger S, Muhlhaus T, Boyle NR, Blaby IK, Casero D, Mettler T, Moseley JL, Kropat J, Sommer F, Strenkert D, Hemme D, Pellegrini M, Grossman AR, Stitt M, Schroda M, Merchant SS (2014) Nitrogen-sparing mechanisms in chlamydomonas affect the transcriptome, the proteome, and photosynthetic metabolism. Plant Cell 26(4):1410–1435. doi:10.1105/tpc.113.122523

Schulz-Raffelt M, Chochois V, Auroy P, Cuine S, Billon E, Dauvillee D, Li-Beisson Y, Peltier G (2016) Hyper-accumulation of starch and oil in a Chlamydomonas mutant affected in a plant-specific DYRK kinase. Biotechnol Biofuels 9:55. doi:10.1186/s13068-016-0469-2

Scott SA, Davey MP, Dennis JS, Horst I, Howe CJ, Lea-Smith DJ, Smith AG (2010) Biodiesel from algae: challenges and prospects. Curr Opin Biotechnol 21(3):277–286. doi:10.1016/j.copbio.2010.03.005

Shtaida N, Khozin-Goldberg I, Solovchenko A, Chekanov K, Didi-Cohen S, Leu S, Cohen Z, Boussiba S (2014) Downregulation of a putative plastid PDC E1alpha subunit impairs photosynthetic activity and triacylglycerol accumulation in nitrogen-starved photoautotrophic Chlamydomonas reinhardtii. J Exp Bot 65(22):6563–6576. doi:10.1093/jxb/eru374

Siaut M, Cuine S, Cagnon C, Fessler B, Nguyen M, Carrier P, Beyly A, Beisson F, Triantaphylides C, Li-Beisson Y, Peltier G (2011) Oil accumulation in the model green alga Chlamydomonas reinhardtii: characterization, variability between common laboratory strains and relationship with starch reserves. BMC Biotechnol 11(1):7. doi:10.1186/1472-6750-11-7

Slade R, Bauen A (2013) Micro-algae cultivation for biofuels: cost, energy balance, environmental impacts and future prospects. Biomass Bioenergy 53:29–38. doi:10.1016/j.biombioe.2012.12.019

Tardif M, Atteia A, Specht M, Cogne G, Rolland N, Brugiere S, Hippler M, Ferro M, Bruley C, Peltier G, Vallon O, Cournac L (2012) PredAlgo: a new subcellular localization prediction tool dedicated to green algae. Mol Biol Evol 29(12):3625–3639. doi:10.1093/molbev/mss178

Terashima M, Specht M, Naumann B, Hippler M (2010) Characterizing the anaerobic response of Chlamydomonas reinhardtii by quantitative proteomics. Mol Cell Proteomics 9(7):1514–1532. doi:10.1074/mcp.M900421-MCP200

Terashima M, Specht M, Hippler M (2011) The chloroplast proteome: a survey from the Chlamydomonas reinhardtii perspective with a focus on distinctive features. Curr Genet 57 (3):151–168. doi:10.1007/s00294-011-0339-1

Terashima M, Freeman ES, Jinkerson RE, Jonikas MC (2015) A fluorescence-activated cell sorting-based strategy for rapid isolation of high-lipid Chlamydomonas mutants. Plant J 81 (1):147–159. doi:10.1111/tpj.12682

Tsai CH, Warakanont J, Takeuchi T, Sears BB, Moellering ER, Benning C (2014) The protein compromised hydrolysis of triacylglycerols 7 (CHT7) acts as a repressor of cellular quiescence in Chlamydomonas. Proc Natl Acad Sci U S A 111(44):15833–15838. doi:10.1073/pnas.1414567111

Tsai CH, Zienkiewicz K, Amstutz CL, Brink BG, Warakanont J, Roston R, Benning C (2015) Dynamics of protein and polar lipid recruitment during lipid droplet assembly in Chlamydomonas reinhardtii. Plant J 83(4):650–660. doi:10.1111/tpj.12917

Valledor L, Furuhashi T, Recuenco-Munoz L, Wienkoop S, Weckwerth W (2014) System-level network analysis of nitrogen starvation and recovery in Chlamydomonas reinhardtii reveals potential new targets for increased lipid accumulation. Biotechnol Biofuels 7:171. doi:10.1186/s13068-014-0171-1

Velmurugan N, Sung M, Yim SS, Park MS, Yang JW, Jeong KJ (2013) Evaluation of intracellular lipid bodies in Chlamydomonas reinhardtii strains by flow cytometry. Bioresour Technol 138:30–37. doi:10.1016/j.biortech.2013.03.078

Wältermann M, Steinbüchel A (2006) Wax ester and triacylglycerol inclusions. In: Shively JM (ed) Inclusions in prokaryotes. Springer, Heidelberg, pp 137–166. doi:10.1007/7171_006/

Waltermann M, Stoveken T, Steinbuchel A (2007) Key enzymes for biosynthesis of neutral lipid storage compounds in prokaryotes: properties, function and occurrence of wax ester synthases/acyl-CoA: diacylglycerol acyltransferases. Biochimie 89(2):230–242. doi:10.1016/j.biochi.2006.07.013

Wang ZT, Ullrich N, Joo S, Waffenschmidt S, Goodenough U (2009) Algal lipid bodies: stress induction, purification, and biochemical characterization in wild-type and starchless Chlamydomonas reinhardtii. Eukaryot Cell 8(12):1856–1868. doi:10.1128/EC.00272-09

Warakanont J, Tsai CH, Michel EJ, Murphy GR 3rd, Hsueh PY, Roston RL, Sears BB, Benning C (2015) Chloroplast lipid transfer processes in Chlamydomonas reinhardtii involving a TRIGALACTOSYLDIACYLGLYCEROL 2 (TGD2) orthologue. Plant J 84(5):1005–1020. doi:10.1111/tpj.13060

Welte MA (2007) Proteins under new management: lipid droplets deliver. Trends Cell Biol 17 (8):363–369. doi:10.1016/j.tcb.2007.06.004

Wijffels RH, Kruse O, Hellingwerf KJ (2013) Potential of industrial biotechnology with cyanobacteria and eukaryotic microalgae. Curr Opin Biotechnol 24(3):405–413. doi:10.1016/j.copbio.2013.04.004

Wilfling F, Wang H, Haas JT, Krahmer N, Gould TJ, Uchida A, Cheng JX, Graham M, Christiano R, Frohlich F, Liu X, Buhman KK, Coleman RA, Bewersdorf J, Farese RV Jr, Walther TC (2013) Triacylglycerol synthesis enzymes mediate lipid droplet growth by relocalizing from the ER to lipid droplets. Dev Cell 24(4):384–399. doi:10.1016/j.devcel.2013.01.013

Wilfling F, Haas JT, Walther TC, Farese RV Jr (2014) Lipid droplet biogenesis. Curr Opin Cell Biol 29:39–45. doi:10.1016/j.ceb.2014.03.008

Work VH, Radakovits R, Jinkerson RE, Meuser JE, Elliott LG, Vinyard DJ, Laurens LM, Dismukes GC, Posewitz MC (2010) Increased lipid accumulation in the Chlamydomonas reinhardtii sta7-10 starchless isoamylase mutant and increased carbohydrate synthesis in complemented strains. Eukaryot Cell 9(8):1251–1261. doi:10.1128/EC.00075-10

Wykoff DD, Davies JP, Melis A, Grossman AR (1998) The regulation of photosynthetic electron transport during nutrient deprivation in Chlamydomonas reinhardtii. Plant Physiol 117 (1):129–139

Xie B, Stessman D, Hart JH, Dong H, Wang Y, Wright DA, Nikolau BJ, Spalding MH, Halverson LJ (2014) High-throughput fluorescence-activated cell sorting for lipid hyperaccumulating Chlamydomonas reinhardtii mutants. Plant Biotechnol J 12(7):872–882. doi:10.1111/pbi.12190

Yan C, Fan J, Xu C (2013) Chapter 5- Analysis of oil droplets in microalgae, Methods in cell biology, vol 116, 1st edn. Elsevier, Oxford, UK. doi:10.1016/B978-0-12-408051-5.00005-X

Yang W, Moroney JV, Moore TS (2004) Membrane lipid biosynthesis in Chlamydomonas reinhardtii: ethanolaminephosphotransferase is capable of synthesizing both phosphatidylcholine and phosphatidylethanolamine. Arch Biochem Biophys 430(2):198–209. doi:10.1016/j.abb.2004.07.016

Yang W, Wittkopp TM, Li X, Warakanont J, Dubini A, Catalanotti C, Kim RG, Nowack EC, Mackinder LC, Aksoy M, Page MD, D'Adamo S, Saroussi S, Heinnickel M, Johnson X, Richaud P, Alric J, Boehm M, Jonikas MC, Benning C, Merchant SS, Posewitz MC, Grossman AR (2015) Critical role of Chlamydomonas reinhardtii ferredoxin-5 in maintaining membrane structure and dark metabolism. Proc Natl Acad Sci U S A 112(48):14978–14983. doi:10.1073/pnas.1515240112

Yoon K, Han D, Li Y, Sommerfeld M, Hu Q (2012) Phospholipid:diacylglycerol acyltransferase is a multifunctional enzyme involved in membrane lipid turnover and degradation while synthesizing triacylglycerol in the unicellular green microalga Chlamydomonas reinhardtii. Plant Cell 24(9):3708–3724. doi:10.1105/tpc.112.100701

Zabawinski C, Van Den Koornhuyse N, D'Hulst C, Schlichting R, Giersch C, Delrue B, Lacroix JM, Preiss J, Ball S (2001) Starchless mutants of Chlamydomonas reinhardtii lack the small subunit of a heterotetrameric ADP-glucose pyrophosphorylase. J Bacteriol 183(3):1069–1077. doi:10.1128/JB.183.3.1069-1077.2001

Zhang R, Patena W, Armbruster U, Gang SS, Blum SR, Jonikas MC (2014) High-throughput genotyping of green algal mutants reveals random distribution of mutagenic insertion sites and endonucleolytic cleavage of transforming DNA. Plant Cell 26(4):1398–1409. doi:10.1105/tpc.114.124099